

Current Natural Sciences

Laurent BOURGOIS,
Rodolphe ANTONI
and Manon DELARUE

Radiation Problems: From Analytical to Monte-Carlo Solutions

Printed in France

EDP Sciences – ISBN(print): 978-2-7598-2461-8 – ISBN(ebook): 978-2-7598-2650-6
DOI: 10.1051/978-2-7598-2461-8

All rights relative to translation, adaptation and reproduction by any means whatsoever are reserved, worldwide. In accordance with the terms of paragraphs 2 and 3 of Article 41 of the French Act dated March 11, 1957, “copies or reproductions reserved strictly for private use and not intended for collective use” and, on the other hand, analyses and short quotations for example or illustrative purposes, are allowed. Otherwise, “any representation or reproduction – whether in full or in part – without the consent of the author or of his successors or assigns, is unlawful” (Article 40, paragraph 1). Any representation or reproduction, by any means whatsoever, will therefore be deemed an infringement of copyright punishable under Articles 425 and following of the French Penal Code.

© Science Press, EDP Sciences, 2021

Foreword

After a first book dealing with applied physics of external radiation exposure, the authors review the state-of-the-art in terms of dosimetric and radiation protection calculations through exercises related to practical applications in the covered fields.

For each problem, the book provides resolutions by means of analytical and semi-empirical formulas derived from nuclear physics theory and the latest research contributions. For some applications (cavity theory, absorbed dose calculation for protons, quantities and dimensioning calculations in the surroundings of X-ray generators...) the most recent data and calculation methods are among the tools used.

Moreover, in most of the applications/problems discussed, an inter-comparison with the numerical results obtained with a Monte-Carlo code is presented. Indeed, computational codes based on this approach are widely used in the radiation exposure field, given the reliability of the physical and dosimetric quantities' estimation they offer. Furthermore, the recent increase in performance and the democratization of computing means allow a practical use of these codes requiring significant computing resources. The MCNP code developed by the Los Alamos National Laboratory (LANL) has been considered for several years, as a reference in the field of numerical calculations for nuclear physics. It has been chosen in this book to provide "actual" values in order to test the accuracy of analytical or semi-empirical results. For each case study, the input file is fully provided, and their structure is detailed. Some of the complex geometries involved in the modeled radiological scenes are described, as well as the features used to generate, transport and track particles. On another note, emphasis is placed on the raw MCNP result normalization and on variance reduction techniques used to improve or allow the convergence of statistical estimators toward the end result. Although the aim of this book is not to replace the MCNP user's manual, it provides the necessary elements for the modeling, the simulation and the calculation of the desired quantities within the topics discussed. All MCNP simulations were performed by means of the

MCNP6 version 1.0. Note that the input files shown in this book are generally compatible with previous release of the MCNPX and MCNP5 code. The MCNP code is distributed by the RSICC (Radiation Safety Information Computational Center) and its use requires a personal license distributed by this center.

The interest of a dual resolution, analytical or semi-empirical and numerical, is diverse and meets the rigorousness required to carry out physical calculations. Firstly, the theoretical knowledge and the analytical approach which result from it allow to corroborate the numerical results obtained during the simulation. They can avoid using the calculation code as a “black box”, *i.e.*, without any real control over the physics options implemented. They also prevent the user from obtaining the desired result without having a tangible element to compare it to. Even if the analytical or semi-empirical result only provides, in some cases, a rough estimate of the quantities, it is still a gauge of the numerical value obtained or, at the very least, provides the orders of magnitude necessary to validate the chosen numerical method. In contrast, in the context of the radiological dimensioning of facilities, for example, the numerical simulation can make a contribution by refining the thicknesses of biological protection previously calculated with an analytical or semi-empirical model. It should also be added that, depending on the objective of the dosimetric or radiation protection calculation, and the accuracy of the result sought, the choice of an analytical or semi-empirical method may turn out to be sufficient. As a result, the subsequent cost of the engineering study will be limited compared with the study involving numerical simulations. Finally, it should be mentioned that in some cases, only one of the two approaches can be successful: the evaluation of the build-up factor is a relevant illustration of this case since it can only be achieved rigorously with a numerical simulation.

Three main topics, grouped in three chapters, are discussed in this book:

- Chapter 1: Calculation of radiometric and dosimetric quantities (fluence, kerma, dose and ambient dose equivalent).
- Chapter 2: Detection principles, detector response to reference physical quantities and operational dosimetric quantities.
- Chapter 3: Shielding and activation calculations for several types of facilities or devices (radioactive sources, X-ray generators, accelerators...).

An introduction to MCNP introduces basic notions and concepts to model a radiological scene with the MCNP (Monte-Carlo N-Particle) transport code. The block structure of a typical input file are discussed.

The first chapter starts with fluence calculations for simple and more complex geometries. Then, elementary dose equivalent calculations are carried out. These appear as simple applications of the MCNP code and enable the reader to become familiar with usual and classic functionalities of the code. The calculations of in-depth absorbed dose for β particles and protons are also proposed with a double resolution. Similarly, a study of dose and kerma profiles is undertaken for successive materials exposed to a photon field. Finally, a first collision kerma calculation for a neutron field is developed using both approaches, and a microdosimetric spectrum is drawn from the numerical simulation of a tissue-equivalent proportional counter.

The second chapter deals with detection principles, detector responses and calibration for applications related to radiation protection and ionizing radiation metrology. The detection and measurement of physical and dosimetric quantities for photons, neutrons, electrons, β particles and protons are addressed. The study of different types of reference detectors and absolute dosimeters are the subject of the applications discussed: ionization chamber, proportional counter, thermoluminescent dosimeters (LiF), extrapolation chamber, proton recoil telescope, time-of-flight measurement device, Bonner spheres spectrometer and calorimeter. In this chapter, special attention is paid to the evaluation of correction factors, which are of particular importance in the field of metrological measurements (*e.g.*, attenuation and scattering in a detector wall).

The last chapter is devoted to radiological shielding and activation. Different radiation source facilities (photons, neutrons or X-ray generators) are studied. In addition to analytical calculations, the convergence issues of the Monte-Carlo code, typical of radiation protection problems, are addressed and solved with variance reduction techniques. Finally, a complete application dedicated to an electron accelerator facility is proposed. It depicts the successive steps leading to the evaluation of the source term (Bremsstrahlung, photonuclear reactions), the shielding calculation process (primary and secondary barrier, skyshine), the air activation and accordingly the ozone concentration.

The book is intended to be didactic and each problem is treated independently. The reader can therefore study the applications of interest in the desired order. Nevertheless, it is recommended that the introduction and the first chapter be studied first, in order to understand and assimilate methods and techniques used for analytical and Monte-Carlo calculations of physical and dosimetric quantities.

Acknowledgments

Mehdi Ben Mosbah, Cédrine Bourgois, Nicolas Estre, Vincent Bottau, Emmanuel Payan, Katie Ioannidis and Alain Fausso.

Contents

Foreword	III
Acknowledgment	VII
Abstract	XI
An Introduction to MCNP	XXIII

CHAPTER 1

Calculation of Radiometric and Dosimetric Quantities (Fluence, Kerma, Dose and Ambient Dose Equivalent)	1
1.I Basic Calculations of the Fluence Rate for Sources of Different Geometric Shapes	1
1.II Basic Calculations of Ambient Dose Equivalent	10
1.III Dose and Kerma Calculation for Photons in a Medium Composed of Interfaces	16
1.IV Calculation of the Ambient Dose Equivalent Rate in a Uniformly Contaminated Pipe	26
1.V Calculation of the in-Depth Absorbed Dose for β Spectra	30
1.VI Calculation of the Absorbed Dose Profile to Water for 170 MeV Protons	41
1.VII Neutron Kerma Calculation and Microdosimetric Spectrum Reconstruction with a Tissue Equivalent Proportional Counter	53

CHAPTER 2

Detection Principles, Detector Response to Reference Physical Quantities and Operational Dosimetric Quantities.	71
2.I Gas-Filled Detector Operating in Ionization Chamber Mode for Photons and in Proportional Counter Mode for Neutrons	71
2.II Calibration of an Ionization Chamber with a ^{60}Co Source	83
2.III Calculation of a Dose Rate in a LiF Pellet	95
2.IV Measurement of the Operational Quantity $H'(0.07, 0^\circ)$ for a β Spectrum with an Extrapolation Chamber	103
2.V Fast Monoenergetic Neutron Energy and Fluence Measurements with a Proton Recoil Telescope	109
2.VI Fast Monoenergetic Neutron Time of Flight Energy Measurement	116

2.VII	Measurement of a Realistic Neutron Spectrum Using Bonner Spheres	121
2.VIII	Absorbed Dose Measurement in a Water Calorimeter for a 170 MeV Proton Beam Used in Proton Therapy	129
2.IX	Calibration of a Neutron Survey Meter with a ^{252}Cf Source	136
CHAPTER 3		
<hr/>		
	Shielding and Activation Calculations for Several Types of Facilities or Devices (Radioactive Sources, X-ray Generators, Accelerators...)	149
3.I	Shielding Calculation for an AmBe Neutron Source	149
3.II	Calculation of a ^{60}Co Photon Source Ambient Dose Equivalent Rate Behind a 4 m Water Shielding	154
3.III	Radiological Shielding for an X-ray Generator	164
3.IV	Evaluation of Ambient Dose Equivalent from Neutron Activation	176
3.V	Calculation of the Scattered Ambient Equivalent Dose Rate for an X-ray Generator Beam on a Water Phantom	187
3.VI	Calculation of Radiological Shielding for a 20 MeV Electron Accelerator with an X-ray Conversion Target	194
	References	229

Abstract

An Introduction to MCNP

This part introduces basic notions and concepts to model a radiological scene with the MCNP (Monte-Carlo N-Particle) transport code. The block structure of a typical input file are discussed. The elementary surfaces and geometries enabling the construction of cells are described and applied in simple examples. The other features such as particle characteristic (type, energy, flux,...), evaluated quantities, physics parameters and biasing, will be specifically addressed in applications developed throughout this book. Two case studies will be used to illustrate the different points addressed, as the explanations to create an MCNP input file will be detailed.

Chapter 1: Calculation of Radiometric and Dosimetric Quantities (Fluence, Kerma, Dose and Ambient Dose Equivalent)

1.1 Basic Calculations of the Fluence Rate for Sources of Different Geometric Shapes

We propose here to calculate the fluence rate for basic sources: point isotropic source, parallel beam, line source and disk-shaped source. For all of the cases, results of the analytical and numerical solutions will be compared.

Objectives:

- Application of the analytical formalism for fluence calculations.
- Fluence calculation for a point source (analytical and MCNP code).
- Fluence calculation for a parallel beam (analytical and MCNP code).
- Fluence calculation for a line (analytical and MCNP code).
- Fluence calculation for a disk (analytical and MCNP code).

1.II Basic Calculations of Ambient Dose Equivalent

Basic ambient dose equivalent rates for isotropic point sources are calculated for different radionuclides. For each case study, the analytical and numerical approaches are presented.

Objectives:

- Ambient dose equivalent rate calculations for isotropic point-sources.
- Application of the inverse-square law.
- Use of the ICRP “conversion coefficient for the ambient dose equivalent”.
- Numerical calculation of dose equivalent.
- Normalization of the MCNP results for multi-source problems.
- Definition of multiple sources in a MCNP file.

1.III Dose and Kerma Calculation for Photons in a Medium Composed of Interfaces

In this problem, dose and kerma curves, as a function of depth, are performed in a set of media.

Objectives:

- Analytical calculation of the kerma and the depth dose for photons.
- Calculation of kerma and dose at the interface between different materials.
- Numerical simulation of kerma and dose.
- Calculation of the Build-up factor in soft tissue.

1.IV Calculation of the Ambient Dose Equivalent Rate in a Uniformly Contaminated Pipe

For this application, the ambient dose equivalent rate within a pipe of which the inner wall is uniformly contaminated by several radionuclides is calculated. The close-form solution of this classic problem of external exposure is discussed below and compared to the numerical result.

Objectives:

- Application of the analytical form for the fluence and ambient dose equivalent.
- Analytical and numerical calculations of the ambient dose equivalent rate for a surface contamination.

1.V Calculation of the In-Depth Absorbed Dose for β Spectra

We propose to calculate the in-depth absorbed dose for β spectra in a water phantom, seen as tissue-equivalent. In a first section, semi-empirical and numerical models are detailed for calculation with a ^{90}Y point-source in contact with the inlet face of the phantom. In a second part are detailed the results of the first section which lead to obtaining the dose equivalent to extremities $H'(0.07)$ for this point-source. In the last section, calculations are achieved for a 50 cm^2 surface contamination for the same radionuclide.

Objectives:

- Semi-empirical calculation of the in-depth absorbed dose for β particles relying on two different models: a fairly simple one that approximates about a part of the maximum range of β particles and a complex accurate one that assesses the actual range.
- Numerical calculation of the absorbed in-depth dose for β spectra.
- Calculation of the absorbed dose with a 3D-mesh in MCNP.
- Semi-empirical and numerical calculations of a dose equivalent to extremities for a β point source.

1.VI Calculation of the Absorbed Dose Profile to Water for 170 MeV Protons

In this section, a calculation of the absorbed dose profile to water for 170 MeV protons is undertaken. The first part draws upon the 1997 work of Bortfield, to suggest an analytical formulation of the absorbed dose as a function of depth and to determine the resulting profile. The second part aims to describe the numerical simulation of the absorbed dose to water and compare the results with those obtained in the first part. The absorbed dose and then the directional dose equivalent under $70\ \mu\text{m}$ at a zero angle of incidence are determined analytically and numerically in the third part.

Objectives:

- Analytical calculation of the absorbed dose to water as a function of the depth for protons.
- Tracking of the different particles set in motion throughout nuclear interactions using MCNP.
- Creation of a mesh for the absorbed dose with MCNP.

- Determination of the mass stopping power at any point of a light ion range by means of the MCNP card “ft let”.
- Representation of a microdosimetric spectrum using the MCNP card “ft let”.
- Calculation of the operational quantity: directional dose equivalent under 70 μm for light ions.

1.VII Neutron Kerma Calculation and Microdosimetric Spectrum Reconstruction with a Tissue Equivalent Proportional Counter

In this problem, the “fluence – first collision kerma” factor for 13.9 MeV neutron is calculated for a low-pressure Tissue Equivalent Proportional Counter (TEPC). The value found is compared to the theoretical value. This factor is then compared to different values of the “fluence – mean organ dose” factor from ICRU (1998a), for the purpose of assessing its ability to estimate these macroscopic dosimetric quantities. The ability to assess the ambient dose equivalent, $H^*(10)$, from the neutron kerma is studied as well. Furthermore, a challenge of this problem is the reconstruction of microdosimetric spectra based on MCNP results. In a last step, the characteristic dosimetric quantities drawn from the MCNP spectra are compared to the reference values to judge the reliability of the proposed method.

Objectives:

- Analytical calculation of the first collision kerma for monoenergetic neutron.
- Study of microdosimetric spectrum and first collision kerma measurement technique with the standard spherical TEPC, *i.e.*, Rossi-type detector.
- Comparison of the first collision kerma with mean organ doses and evaluation of the ambient dose equivalent.
- Microdosimetric spectrum calculation with MCNP simulation using the “anti-coincidence pulse-height” card.
- Neutron mean quality factor calculation from a microdosimetric spectrum.

Chapter 2: Detection Principles, Detector Response to Reference Physical Quantities and Operational Dosimetric Quantities

2.I Gas-Filled Detector Operating in Ionization Chamber Mode for Photons and in Proportional Counter Mode for Neutrons

A gas-filled detector is successively operated in current mode (ionization chamber) for a photon field and in pulse mode (proportional counter) for a neutron field. This

application is aimed at evaluating separately dosimetric quantities with both operating modes. This problem highlights the possibility of determining different dosimetric quantities depending on the particle type and the operating mode.

Objectives:

- Establish if the chamber wall is tissue-equivalent.
- Determination of the cavity type according to the cavity theory.
- Calculation of the current in a small cavity.
- Evaluation of an operational quantity from a physical quantity measured by the ionization chamber in a photon field.
- Understand the associated electronic counting system, from the radiation interaction in the detector to the pulse counted and recorded, for a proportional counter exposed to a neutron field.
- Assessment of a protection dosimetric quantity from the fluence.
- Calculation of the neutron kerma in the detector wall.
- Numerical simulation of the energy response of a chamber.

2.II Calibration of an Ionization Chamber with a ^{60}Co Source

In this application, the calibration in terms of ambient dose equivalent, $H^*(10)$, for a radiation survey meter (ionizing chamber type) with a ^{60}Co source is studied. This calibration operation is processed in a secondary laboratory and requires a device for perfect measurement of air kerma. The first part is focused on the evaluation of the air kerma with a reference air-equivalent chamber (Sp01 type) in a metrology primary laboratory. In the second part, the calibration in terms of ambient dose equivalent is performed in a secondary laboratory. The third part is devoted to the study of the survey meter response to ^{241}Am gamma-rays. The main objective of this last part is to check if the deviation between measured and actual values of the operational quantity is within the limit recommended by standards.

Objectives:

- Understand the calibration process of a radiation protection device, from the primary laboratory to the operational use.
- Calculate the theoretical expression of the air kerma with an ionization chamber.
- Determine the energy response of a survey meter with MCNP.
- Assess a wall-scattering factor with MCNP.
- Assess the relevance of the calibration carried out, depending on the energy measured in a real situation.

2.III Calculation of a Dose Rate in a LiF Pellet

In the past few years, Haider *et al.* (1997) have improved Burlin intermediate cavity theory (association of a small cavity and a large cavity) mostly by taking into

account the electrons backscattered in the rear face of the chamber. In the first part, the new cavity theory is applied to evaluate the mean absorbed dose in a LiF pellet surrounded by aluminum (“buffer layer”). In this theory, this mean dose can be determined from the absorbed dose at a point under the aluminum inlet face of the detector with an analytical expression. In the second part, the analytical result is verified with MCNP simulations.

Objectives:

- Application of the new cavity theory.
- Calculation of the mean absorbed dose in a sensitive volume from the absorbed dose at a point under the aluminum inlet face of the detector.
- Dose calculation at an interface.
- Correction for photon scattering calculated with MCNP.

2.IV Measurement of the Operational Quantity $H'(0.07, 0^\circ)$ for a β Spectrum with an Extrapolation Chamber

In a first part, the directional dose equivalent at a zero angle of incidence, $H'(0.07, 0^\circ)$, is evaluated for a reference $^{90}\text{Sr}/^{90}\text{Y}$ source, using an extrapolation chamber, model 23392 PTW. This device is recommended by the ISO 6980 standard for the measurement of absorbed dose under $70\ \mu\text{m}$ of tissue, $D_t(0.07)$ for β radiation. For this chamber model, a micrometer screw on a piston enables to adjust the depth of the sensitive volume of the chamber. This feature allows to determine the slope of the ionization current *versus* the depth of the chamber. A check of the slope value with a numerical simulation is performed in a second part.

Objectives:

- Calculation of the dose at the entrance window for an extrapolation chamber.
- Calculation of the theoretical current generated in the sensitive volume using the energy deposition tally.

2.V Fast Monoenergetic Neutron Energy and Fluence Measurements with a Proton Recoil Telescope

This application is aimed at evaluating energy and fluence of monoenergetic neutrons with a proton recoil telescope. These neutrons emerge from a ^3H target impinged by a deuteron beam (150 keV) according to the reaction $^3\text{H}(d,n)^4\text{He}$. This method is highly recommended to carry out a reference measurement of the fluence and the energy of a fast neutron field for an external dosimetry purpose. In a next step, the ambient dose equivalent rate at the point at which the neutron beam interacts with the telescope radiator is inferred. A comparison between results drawn from theoretical and numerical methods is performed.

Objectives:

- Theoretical calculation of the energy of fast neutrons undergoing elastic scattering in an organic radiator and evaluation of the associated uncertainty.
- MCNP simulation of a proton recoil telescope.
- Calculation of a detector efficiency.
- Calculation of the energy resolution.

2. VI Fast Monoenergetic Neutron Time of Flight Energy Measurement

In this problem, the time of flight (ToF) technique is used to measure the energy of monoenergetic neutrons originating from the ${}^3\text{H}(p,n){}^3\text{He}$ reaction. In the first part, an analytical calculation of the ToF is detailed for the experimental data. In the second part, this calculation is done for a $d-d$ neutron spectrum simulated with MCNP.

Objectives:

- Theoretical calculation of the time-of-flight (ToF) and matching neutron energy.
- ToF technique with a coincident secondary particle.
- ToF uncertainty and energy resolution calculations.
- Calculation of the mean ToF with MCNP using a fusion spectrum.

2. VII Measurement of a Realistic Neutron Spectrum Using Bonner Spheres

In this application, we propose to determine the neutron fluence- and ambient dose equivalent- rates for three energy regions (thermal – epithermal – fast) by employing three Bonner spheres spectrometer (BSS). In the first part, the response of each Bonner sphere is simulated with MCNP for the three energy regions. In the second part, the neutron fluence is calculated for each energy range through the least squares method. Note that the multi Bonner spheres method is a reference to assess the overall fluence and the spectrum.

Objectives:

- Solving of an equation system through the least squares method.
- Study the principle of an unfolding algorithm to derive a spectrum from the signal provided by several detectors.
- Calculation of the matrix response of a BSS with MCNP.
- Study the principle of Bonner spheres to evaluate a reference neutron spectrum.
- Calculation of a mean “physical quantity-to-dosimetric quantity” conversion coefficient for an energy spectrum.

2.VIII Absorbed Dose Measurement in a Water Calorimeter for a 170 MeV Proton Beam Used in Proton Therapy

This application is aiming at measuring the absorbed dose deposited by a proton beam of 170 MeV maximum energy, for proton therapy. An proton box, corresponding to the Bragg curve plateau region in water, is scanned with an hermetic calorimeter. In the first part, the absorbed dose to water is evaluated from the thermistors temperature change. A subsidiary challenge will be to assess the fluence rate at the water phantom entrance face required for the proton beam to induce such a dose. In the second part, we will evaluate the charge measured by an Exradin T1 ionization chamber located at the reference measurement point for the same proton beam. Finally, in an independent third part, we will point out the difference in the holding time for the temperature variation, owing to the deposited dose, for both a graphite and a water calorimeter exposed to a ^{60}Co radiation field.

Objectives:

- Calculation of the absorbed dose from the temperature rise in a water calorimeter.
- Determination of the proton beam fluence as a function of the absorbed dose in depth.
- Study of the calibration process of an ionization chamber in air for the assessment of the proton dose to water.
- Evaluation of the holding time of the temperature variation in the calorimeter.

2.IX Calibration of a Neutron Survey Meter with a ^{252}Cf Source

This application is aimed at describing the calibration of a neutron survey meter. In the first section, the device is calibrated in terms of $\mu\text{Sv}\cdot\text{h}^{-1}/\text{c}\cdot\text{s}^{-1}$ with a ^{252}Cf source using the shadow cone method described in the ISO standard 8529-2 (ISO, 2000). The device is a spherical ^3He -filled proportional counter surrounded by a polyethylene layer, identical to the 8" Bonner sphere studied in the application 2.VII.

In the second section, the survey meter is used to measure a typical workplace neutron field, emitted by a PuF_4 solution considered as a point-like source. At the end, the reliability of the ^{252}Cf calibration is checked with respect to the deviation between the readout of the calibrated survey meter and the actual dose equivalent rate of the PuF_4 solution.

Objectives:

- Application of the shadow cone method described in the ISO 8529-2 standard.
- Calculation of the efficiency and energy response of a Bonner sphere using MCNP.
- Evaluation of a calibration coefficient for a proportional counter.
- Check of the calibration reliability depending on the characteristics of the workplace radiation field.

Chapter 3: Shielding and Activation Calculations for Several Types of Facilities or Devices (Radioactive Sources, X-ray Generators, Accelerators...)

3.I Shielding Calculation for an AmBe Neutron Source

In this application, the thickness of a polyethylene shielding is determined to ensure a dose equivalent of $2 \mu\text{Sv/h}$ at 1 m of a 60 GBq Am-Be source. The calculated thickness derives from a semi-empirical model, checked by a numerical simulation.

Objectives:

- Semi-empirical and numerical calculations of a shielding for a neutron source.
- Use of neutron transmission coefficient.
- Neutron spectrum implementation in MCNP.
- Numerical calculation of dose equivalents for a mixed particle field composed of neutrons and photons.

3.II Calculation of a ^{60}Co Photon Source Ambient Dose Equivalent Rate Behind a 4 m Water Shielding

In this problem, the ambient dose equivalent rate of a ^{60}Co photon source of 20 TBq is assessed behind a 4 m water shielding. The distance between the source and the calculation point is 4.2 m.

Objectives:

- Semi-empirical calculation of a Shielding thickness for a ^{60}Co source.
- Use of the build-up factor for photons.
- Numerical calculation of a very thick shielding.
- Use of a variance reduction technique for numerical calculations.

3.III Radiological Shielding for an X-ray Generator

The design of a radiological shielding for an X-ray generator is discussed in this problem. In the first part, a semi-empirical method is applied, and results are compared to a numerical approach in the second part.

Objectives:

- Semi-empirical calculation of a radiological shielding for an X-ray generator.
- Use of the transmission factor for an X-ray spectrum.
- Numerical simulation of an X-ray spectrum as a primary photon source.
- Application of a biasing technique to shielding calculations.

3.IV Evaluation of Ambient Dose Equivalent from Neutron Activation

The irradiation of a ^{59}Co sample with a monoenergetic neutron beam, resulting in the formation of ^{60}Co by activation is studied in this application. In a first part, the ^{60}Co activity is calculated analytically, as well as the resulting fluence and ambient dose equivalent rate at 1 m from the sample. In a second part, the same quantities are numerically evaluated and compared to that of the first part. The third part points out the possibility to assess fluence and dose equivalent rates for different irradiation scenarios and cooling steps, and therefore to perform the time profile of the external exposure.

Objectives:

- Analytical calculation of sample activation by neutrons, resulting fluence and ambient dose equivalent rates.
- Same as above with MCNP.
- MCNP calculations with the “act” card.
- Setting of an irradiation time profile with MCNP.
- Calculation of a prompt and delayed photon spectrum with MCNP during a continuous irradiation.
- Achievement of the time profile of the fluence rate for successive irradiation and cooling steps.

3.V Calculation of the Scattered Ambient Equivalent Dose Rate for an X-ray Generator Beam on a Water Phantom

In this application, the ambient dose equivalent rate resulting from the scattering of an X-ray generator beam on a water phantom is evaluated.

Objectives:

- The ambient equivalent dose rate for an X-ray scattering field.
- MCNP and semi-empirical models of the scattered radiation and its related ambient dose equivalent.
- Variance reduction techniques with use of the pseudo-particle and of the DXTRAN sphere.
- Single-step calculation of dosimetric quantities related to the bremsstrahlung radiation with MCNP.

3. VI Calculation of Radiological Shielding for a 20 MeV Electron Accelerator with an X-ray Conversion Target

This application presents recommendations and technical information related to the design of radiological shielding for a 20 MeV electron accelerator. The electron beam is fully stopped in a target of high-Z material (tungsten). Related issues of radiological exposure as air activation, skyshine and ozone production are also addressed.

Objectives:

- Complete study of source-terms for the irradiation facility (analytical and MCNP).
- Calculation of the ambient equivalent dose rate due to bremsstrahlung produced by the interaction of electrons in tungsten.
- Assessment of the photoneutron energy.
- Calculation of the ambient equivalent dose rate due to neutrons produced by photonuclear reactions.
- Calculation of the shielding around an electron accelerator with high-Z target.
- Calculation of the external exposure component due to skyshine.
- Numerical calculation of the saturation activity in the air accelerator room.
- Air activity evolution as a function of time with an air change rate.
- Calculation of ozone concentration arising from photon interaction with air molecules.

An Introduction to MCNP

This part introduces basic notions and concepts to model a radiological scene with the MCNP (Monte-Carlo N-Particle) transport code. The block structure of a typical input file is discussed. The elementary surfaces and geometries enabling the construction of cells are described and applied in simple examples. The other features, such as particle characteristics (type, energy, flux, etc.), evaluated quantities, physics parameters and biasing, will be specifically addressed in applications developed throughout this book.

Two case studies will be used to illustrate different points addressed, as explanations to create an MCNP input file will be detailed.

The first case is an isotropic point-like source of ^{60}Co located at positions $x = 51$ cm, $y = 2$ cm and $z = 3$ cm. We aim to assess the fluence in a water cube located in the air, 50 cm away from the source. The cube of 4 cm edge length is centered in the location $x = 1$ cm, $y = 2$ cm and $z = 3$ cm. In the second case, the configuration is inverted: the water cube becomes a ^{60}Co volumetric source and we intend to evaluate the fluence at the location of the source in the first case.

We must point out that this introduction offers only an elementary vision of the MCNP code formalism. It can be supplemented by the MCNP User's Manual (Pelowitz, 2013) completeness as well as the numerous specific documents provided by LANL: https://laws.lanl.gov/vhosts/mcnp.lanl.gov/references.shtml#mcnp6_refs.

(a) MCNP input file structure

The MCNP input file is written in ASCII format (text format, prepared for example with the “notepad” application for a Windows OS). The file is composed of three parts referred to as blocks, separated by a blank line. The first block encompasses the definition of the objects modeled in space, denoted as cells (3D geometry, materials and apparent densities). The second block contains the surfaces enabling to form the cells described in the first block. The third block states all the instructions necessary to generate, transport and track particles: the source, the type of particles, the physics parameters, the spatial and energy biasing, the calculation time, and the quantities to evaluate, so-called “tallies”. Note that the length of a line in the input file cannot exceed 80 characters, spaces included. If this

limitation is exceeded, adding a “&” character at the end of the line enables to link up with the next line.

(b) Units used in MCNP

For basic parameters, the units used are the length in cm, the energy in MeV, the time in shakes (10^{-8} s), the atom density in $\text{atoms}\cdot\text{b}^{-1}\cdot\text{cm}^{-1}$ (10^{24} $\text{atoms}\cdot\text{cm}^{-3}$), the mass density in $\text{g}\cdot\text{cm}^{-3}$, and the cross sections in barns.

(c) Block 2: Geometry specification

The volume of cells described in the 1st block is characterized by the intersection of elementary geometric objects. The latter are defined by elementary surfaces listed in table 1.

In the example illustrated in figure 1, the plan normal to x -axis, located at $x = 5$ cm, is a surface described by the instruction “px 5”. This surface is identified by a number at the beginning of the line, “10” in the case described below.

```
10 PX 5
```

A cylinder of radius 5 cm, of axis meeting $x = 2$ cm and $y = -1$ cm, parallel to the z -axis, indicated by the number 15, is also represented in figure 1. It is described by the following instruction:

```
15 C/Z 2 -1 5
```

Note that the cylinder is infinite along z -axis.

Since the release of MCNPX and MCNP5, closed surfaces, referred to as “macro-bodies”, are available. These pre-defined surfaces are, for instance, rectangular parallelepiped, spheres and finite cylinders. The macrobodies implemented in MCNP are described in table 2. It is possible to combine macrobodies with elementary surfaces presented in table 1.

Therefore, the cube used in both presented cases (cube centered at the position $x = 1$, $y = 2$ and $z = 3$ of 4 cm edge length) is defined by “rpp -1 3 0 4 1 5”, but it can also be described with the instruction “box -1 0 1 4 0 0 4 0 0 4”. This cube is displayed in figure 1 (in the xy plane). Generally, we will find out throughout this book that it is more convenient to use macrobodies instead of elementary surface. In most cases, macrobodies help avoid the description of a great number of surfaces necessary for cell definition.

A 45° inclined cylinder (in the xy plane) of 5 cm height and 1 cm radius whose lower base center is located at $(-2\ 2\ 0)$ is defined by the instruction “rcc -2 2 0 3.5355 3.5355 0 1”. The coordinates of the steering vector in the xy -plane stem from the hypotenuse projection, *i.e.*, $5/\sqrt{2} = 3.5355$.

(d) Block 1: Cell definition

The cells are described in the 1st block. To each of them are attached a cell number “ n ”, a material number “ m ” (defined in the 3rd block), a density “ ρ ” and a geometry “ s_i ” composed of surfaces listed in the 2nd block. A comment preceded by the character “\$” can be added at the end of each line.

```
n m p s1 s2 ... sn $ cell N
```

TAB. 1 – Elementary surfaces, available in the MCNP User’s Manual (Pelowitz, 2013).

Mnemonic	Type	Description	Equation	Card entries
P	Plane	General	$ax + by + cz - d = 0$	$a \ b \ c \ d$
PX		Normal to x -axis	$x - d = 0$	d
PY		Normal to y -axis	$y - d = 0$	d
PZ		Normal to z -axis	$z - d = 0$	d
SO	Sphere	Centered at the origin	$(x)^2 + (y)^2 + (z)^2 - R^2 = 0$	R
S		General	$(x - a)^2 + (y - b)^2 + (z - c)^2 - R^2 = 0$	$a \ b \ c \ R$
SX		Centered to x -axis	$(x - a)^2 + (y)^2 + (z)^2 - R^2 = 0$	$a \ R$
SY		Centered to y -axis	$(x)^2 + (y - b)^2 + (z)^2 - R^2 = 0$	$b \ R$
SZ		Centered to z -axis	$(x)^2 + (y)^2 + (z - c)^2 - R^2 = 0$	$c \ R$
C/X	Cylinder	Parallel to x -axis	$(y - b)^2 + (z - c)^2 - R^2 = 0$	$b \ c \ R$
C/Y		Parallel to y -axis	$(x - a)^2 + (z - c)^2 - R^2 = 0$	$a \ c \ R$
C/Z		Parallel to z -axis	$(x - a)^2 + (y - b)^2 - R^2 = 0$	$a \ b \ R$
CX		On x -axis	$(y)^2 + (z)^2 - R^2 = 0$	R
CY		On y -axis	$(x)^2 + (z)^2 - R^2 = 0$	R
CZ		On z -axis	$(x)^2 + (y)^2 - R^2 = 0$	R
K/X	Cone	Centered to x -axis	$\sqrt{(y - b)^2 + (z - c)^2} - t(x - a) = 0$	$a \ b \ c \ t^2 \pm 1$
K/Y		Centered to y -axis	$\sqrt{(x - a)^2 + (z - c)^2} - t(y - b) = 0$	$a \ b \ c \ t^2 \pm 1$
K/Z		Centered to z -axis	$\sqrt{(x - a)^2 + (y - b)^2} - t(z - c) = 0$	$a \ b \ c \ t^2 \pm 1$
KX		On x -axis	$\sqrt{(y)^2 + (z)^2} - t(x - a) = 0$	$a \ t^2 \pm 1$
KY		On y -axis	$\sqrt{(x)^2 + (z)^2} - t(y - b) = 0$	$b \ t^2 \pm 1$
KZ		On z -axis	$\sqrt{(x)^2 + (y)^2} - t(z - c) = 0$	$c \ t^2 \pm 1$

 ± 1 used only for 1-sheet cone

TAB. 1 – (continued).

Mnemonic	Type	Description	Equation	Card entries
SQ	Ellipsoid Hyperboloid paraboloid	Axis parallel to x , y Or z -axis	$E(x - a)^2 + F(y - b)^2 + G(z - c)^2 + 2H(x - a) + 2I(y - b) + 2J(z - c) + K = 0$	$E F G H I J$ $K a b c$
GQ	Cylinder, cone ellipsoid paraboloid hyperboloid	Axis are not parallel to x , y Or z -axis	$E(x)^2 + F(y)^2 + G(z)^2 + Hxy + Iyz + Jzx + Kx + Ly + Mz + N = 0$	$E F G H I J K$ $L M N$
TX	Ellipsoid or circular torus. Axis is parallel to x , y , z axis		$(x - a)^2/E^2 + \left(\sqrt{(y - b)^2 + (z - c)^2} - D\right)^2/F^2 - 1 = 0$	$a b c D E F$
TY			$(y - b)^2/E^2 + \left(\sqrt{(x - a)^2 + (z - c)^2} - D\right)^2/F^2 - 1 = 0$	$a b c D E F$
TZ			$(z - c)^2/E^2 + \left(\sqrt{(y - b)^2 + (x - a)^2} - D\right)^2/F^2 - 1 = 0$	$a b c D E F$

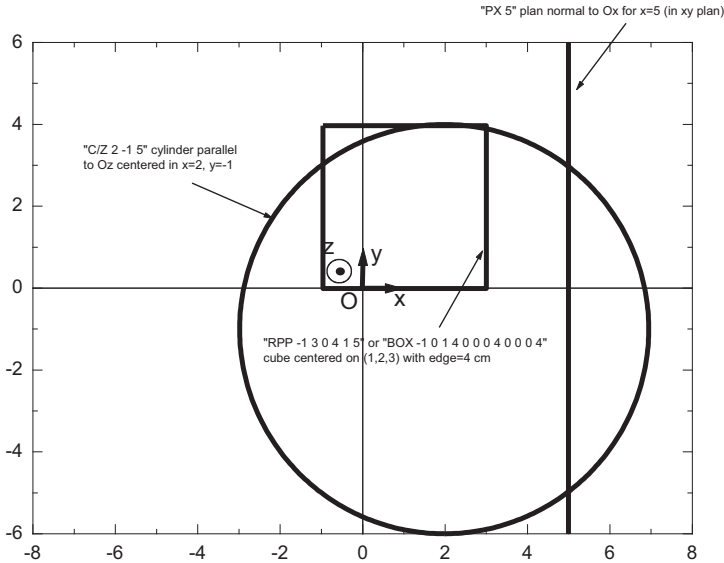


FIG. 1 – Examples of elementary surfaces (*xy* view).

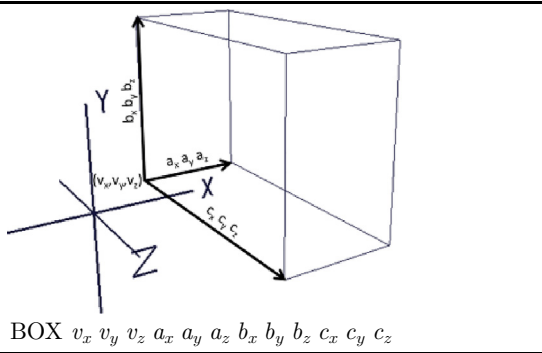
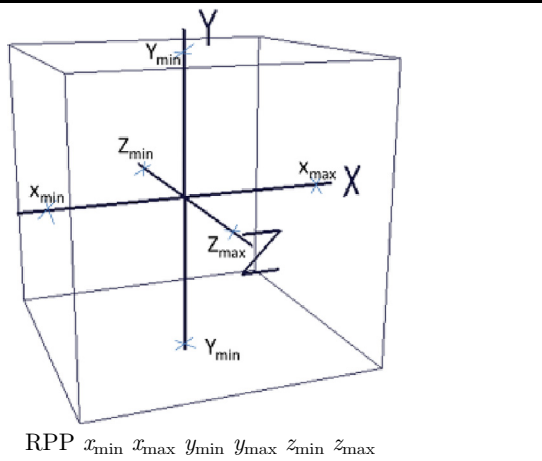
Special care has to be taken with the density: if ρ is negative, the density is expressed in g.cm^{-3} . Else, if ρ is positive, the unit is $(\text{atoms}).\text{b}^{-1}.\text{cm}^{-1}$.

A 3D geometry is designed with a mix of intersection and union of surfaces. To define spatial regions bounded by these surfaces, it is necessary to couple them with a sign. A “+” sign for a closed surface points the “region outside the surface” and a “-” sign indicates the “region inside the surface”. As to unclosed surfaces, every point where $f(x, y, z) > 0$ is located positively (+) with regard to the surface, and every point where $f(x, y, z) < 0$ is positioned negatively (-). Let us take the example of the flat surface “15”, normal to the x -axis and located at $x = 10$, *i.e.*, the plane defined by “15 px 10”. The region where $x > 10$ is denoted as “+”, and that where $x < 10$ corresponds to the “-” region. The shaded areas of figure 2 illustrate the spatial regions defined by the instructions “-15” or “+15”. By default, the absence of sign before a surface is interpreted as a “+” sign. The intersection and/or union operators are applied to several surfaces to define a volume.

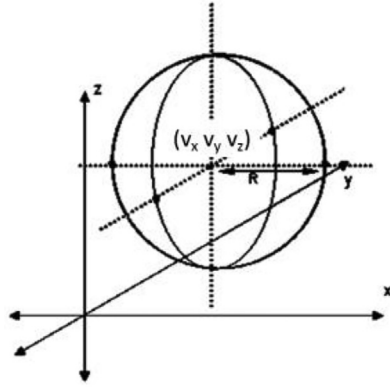
Surface intersections are stated with the logical ‘AND’ operator and unions with the ‘OR’ operator. In the code, these operators are, respectively, written as a blank space and a colon. For instance, the instruction “5 15” defines the region which is at the same time in the region “5” AND in the region “15”. On the other hand, “5:15” is used to point the region which is in the region “5” OR in the region “15”. To illustrate this concept, we consider two planes “15 px 10” and “5 py - 10”. The shaded area of figure 3a represents the region defined by the instruction “5 -15” and that of figure 3b that provided with “5:-15”.

Let us summarize this approach with the example of the 4 cm edge length cube centered at (1 2 3) used in both case studies. We intend to define the regions,

TAB. 2 – Definitions and input parameters for macrobodies.

Description	Mnemonic and sketch	Definition of entry
<p>Arbitrarily oriented orthogonal box</p>	 <p>BOX $v_x v_y v_z a_x a_y a_z b_x b_y b_z c_x c_y c_z$</p>	<p>$(v_x v_y v_z)$ The x, y, z coordinates of a corner of a box</p> <p>$a_x a_y a_z$ Vector of 1st side from the specified corner coordinates</p> <p>$b_x b_y b_z$ Vector of 2nd side from the specified corner coordinates</p> <p>$c_x c_y c_z$ Vector of 3rd side from the specified corner coordinates</p>
<p>Rectangular parallelepiped</p>	 <p>RPP $x_{min} x_{max} y_{min} y_{max} z_{min} z_{max}$</p>	<p>$x_{min} x_{max}$ Termini of box sides normal to the x-axis</p> <p>$y_{min} y_{max}$ Termini of box sides normal to the y-axis</p> <p>$z_{min} z_{max}$ Termini of box sides normal to the z-axis</p>

Sphere



SPH $v_x v_y v_z R$

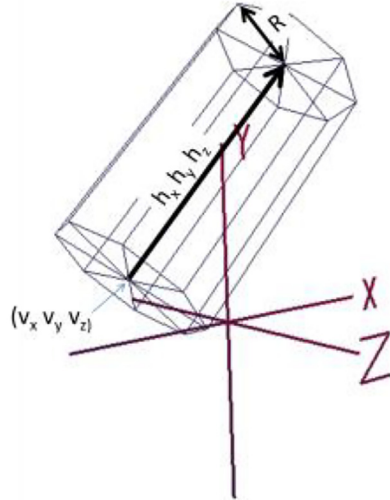
$(v_x v_y v_z)$

The x, y, z coordinates of the center of the sphere

R

Radius of the sphere

Right circular cylinder



RCC $v_x v_y v_z h_x h_y h_z R$

$(v_x v_y v_z)$

The x, y, z coordinates at the center of the base for the RCC

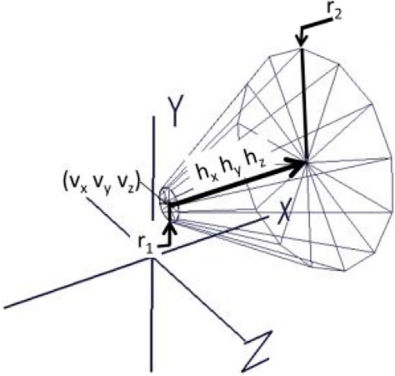
$h_x h_y h_z$

Right circular cylinder axis vector, which provides both the orientation and the height of the cylinder

R

Radius of the RCC

Tab. 2 – (continued).

Description	Mnemonic and sketch	Definition of entry
Truncated right-angle cone	 <p data-bbox="502 594 775 621">TRC $v_x v_y v_z h_x h_y h_z r_1 r_2$</p>	<p data-bbox="1021 305 1099 327">$v_x v_y v_z$</p> <p data-bbox="1199 305 1561 358">The x, y, z coordinates of the cone bottom</p> <p data-bbox="1021 370 1099 392">$h_x h_y h_z$</p> <p data-bbox="1284 370 1476 392">Axis height vector</p> <p data-bbox="1048 404 1071 426">r_1</p> <p data-bbox="1224 404 1536 426">Radius of the lower cone base</p> <p data-bbox="1048 438 1071 459">r_2</p> <p data-bbox="1184 438 1576 488">Radius of the upper cone base, where $r_1 < r_2$</p>

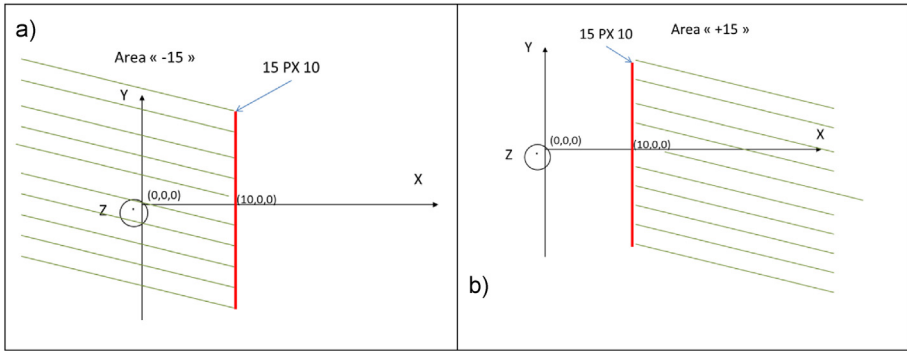


FIG. 2 – Illustration of the spatial region (shaded area) depending on the sign of the sign used with the flat surface. (a) “-” sign and (b) “+” sign.

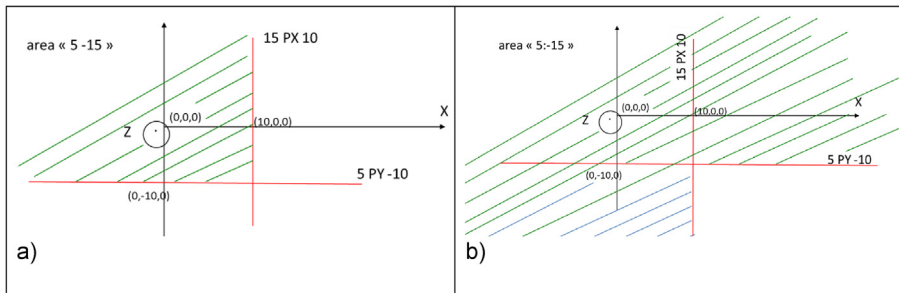


FIG. 3 – Regions from (a) the intersection of surfaces “5 -15”, (b) the union of surfaces “5:-15”.

respectively, inside and outside this cube. Basically, the cube is defined by its six faces. Inside block 2, these faces correspond to the following planes:

- 5 PX -1
- 10 PX 3
- 15 PY 0
- 20 PY 4
- 25 PZ 1
- 30 PZ 5

The inner region of the cube can be written as “5 -10 15 -20 25 -30” and the outer region as “-5:10:-15:20:-25:30”.

A more straightforward way to define the cube is from a RPP rectangular parallelepiped macrobody:

10 RPP -1 3 0 4 1 5

In this case, the inner region of the cube is written as “-10” and the outer region as “10”. Finally, a third way to define the same cube is to use the BOX macrobody:

```
10 BOX -1 0 1 4 0 0 0 4 0 0 0 4
```

The inside is described by the instruction “-10” and the outside by “10”.

(e) Block 3: Materials’ definition

The aim now is to assign a material and a density to the cell. The material has to be defined in the 3rd block beforehand. Each element composing the material is written as “ZZAAA.lib”, where Z is the atomic number and A is the mass number. The “.lib” extension refers to a particular cross section library (one can refer to J.L. Conlin (2017) for further explanation on the different libraries and their features). The part “.lib” can be omitted and by default, the code will work with the first library listed in the “xsdir” file of MCNP. For instance, the term “8016” defines oxygen-16 with its default library. When adding the extension “8016.80c”, the oxygen-16 is treated with the neutron cross sections available in the ENDF/B-VII.1 library, taken at $T = 293.6$ K. The extension “60c” in the term “8016.60c” would refer to neutron cross sections from a former library, ENDF/B-VI.0, at $T = 293.6$ K. If the simulation only carries out photon or electron transport, stable oxygen can be defined as “8000”, without adding an extension. It is important to note that for neutron transport, this format is not accepted and it is necessary to mention the atomic masses (AAA) to refer to a cross section library dedicated to neutrons.

A material is described by a succession of chemical elements, each associated with a weighting factor k : “ $Z_1Z_1A_1A_1A_1 k_1 Z_2Z_2A_2A_2A_2 k_2 \dots Z_nZ_nA_nA_nA_n k_n$ ” where Z_nZ_n is the atomic number of the element n , $A_nA_nA_n$ is its mass number and k_n is its mass fraction (if k_n is negative) or its atom fraction (if k_n is positive). In the case studies, if we consider material 8 to be water, it is defined through the instruction m8 and can be described by both of the following forms:

```
c -----
c WATER for gamma-ray or electron transport (by atom fraction)
c -----
M8 1000 2 8000 1 $ water
```

```
c -----
c WATER for gamma-ray or electron transport (by mass fraction)
c -----
M8 1000 -0.11190 8000 -0.88810 $ water
```

The text following the “c” characters is considered as a comment and is therefore not interpreted by the code. Note that lots of MCNP material definitions are provided in the reference McConn *et al.* (2011).

(f) Block 3: Particle transport definition

The types of particles transported in the simulation have to be specified in the 3rd block, within the “mode” card. The list of particles used in this book is provided in table 3.

TAB. 3 – Particle types and associated symbols in MCNP.

IPT	Type of particles	Symbol
1	Neutron	N
2	Photon	P
3	Electron	E
8	Positron	F
9	Proton	H
31	Deuteron	D
32	Triton	T
33	Helion (He-3)	S
34	Alpha (He-4)	A
37	Heavy ion*	#

*The “#” represents all possible heavy-ion types – in other words, any ion that is not one of the four light ions available in MCNP6.

For instance, setting the instruction “mode p” allows the transport of photons only, whereas the instruction “mode p n” enables the mixed transport of photons and neutrons.

(g) Block 3: Source definition

The particle source (type, energy, flux, emission geometry,...) is defined in the third block. The source is defined by entering the “sdef” card whose parameters are listed in table 4. The “default” column provides the default value or characteristics of parameters when the latter are not specified. For instance, when setting the “mode n”, the “sdef” card used alone would indicate a point-like source, located at the origin, isotropically emitting 14 MeV neutrons.

For example, an isotropic point-like source of 1 MeV photons at the location $x = 51$, $y = 2$ and $z = 3$ is stated as “sdef par = p erg = 1 pos = 51 2 3”. If a “sdef” parameter contains several inputs, one has to provide a distribution number (preceded by “d”). In this way, the source parameter can take several values sampled from the “si” distribution (source information), followed by a “sp” card (source probability), enabling to assign a probability to each of the source parameters. This can be illustrated with the energy definition of the ^{60}Co source considered in the two case studies proposed in this introduction. This radionuclide emits two photons of 1.17 MeV and 1.33 MeV, which will be listed in a “si” card. The 100% emission probability for each of these gamma rays will be specified in an associated “sp” card. The source of the first case is fully defined as follows:

```
SDEF par=p erg=d4 pos=51 2 3
si4 l 1.17 1.33
sp4 1 1
```

The parameter list of the “si” and “sp” cards are always correlated and written in an orderly manner. Particular attention has to be paid to match each of the “si” card input with its probability in the “sp” card. For the second case, the source is cubic

TAB. 4 – List of parameters for the “sdef” source definition card.

Variable	Meaning	Default
CEL	Cell	Determined from <i>XXX</i> , <i>YYY</i> , <i>ZZZ</i> and possibly <i>UUU</i> , <i>VVV</i> , <i>WWW</i>
SUR	Surface	0 (means cell source)
ERG	Energy	14 MeV
DIR	μ , the cosine of the angle between VEC and <i>UUU</i> , <i>VVV</i> , <i>WWW</i> The azimuthal angle is always sampled uniformly in $[0, 2\pi]$	Volume case: μ is sampled uniformly in $[-1.1]$ (isotropic). Surface case: $p(\mu) = 2\mu$ for $\mu [0, 1]$ (cosine distribution)
VEC	Reference vector for VEC	Volume case: required unless isotropic. Surface case: vector normal to the surface with sign determined by NRM
NRM	Sign of the surface normal	1
POS	Reference point for positioning sampling	0, 0, 0
RAD	Radial distance of the position from POS or AXS	0
EXT	Cell case: distance from POS along AXS Surface case: cosine of angle from AXS	0
AXS	Reference vector for EXT and RAD	Reference vector for EXT and RAD
<i>X</i>	<i>X</i> -coordinate of position	No <i>X</i>
<i>Y</i>	<i>Y</i> -coordinate of position	No <i>Y</i>
<i>Z</i>	<i>Z</i> -coordinate of position	No <i>Z</i>
CCC	Cookie-cutter cell	No cookie-cutter cell
ARA	Area of surface (required only for direct contributions to point detectors from a plane surface source)	None
WGT	Particle weight	1
EFF	Reference efficiency criterion for position sampling	0.01
PAR	Type of particle the source emits	Neutron if MODE N or N P or N P E; photon if MODE P; electron if MODE E

(4 cm edge length cube centered at (1, 2, 3)). If the cell “5” stands for the cube, the source can be written as:

```
SDEF cell=5 x=d1 y=d2 z=d3 erg=d4 par=p
si1 -1 3 $ x-range limits for source volume
sp1 0 1 $ uniform probability over y-range
si2 0 4 $ y-range limits for source volume
sp2 0 1 $ uniform probability over y-range
si3 1 5 $ x-range limits for source volume
sp3 0 1 $ uniform probability over x-range
si4 L 1.17 1.33 $ energy of each Co-60 photons
sp4 1 1 $ intensity of each Co-60 photons
```

(h) Block 3: Tally definition

Within the 3rd block, the assessed quantities are specified with statistical estimators called “tallies” in the MCNP code. These tallies are listed in table 5. Many of these are used in the applications of this book. For the second case, we are seeking the photon fluence at a point located 50 cm away from the cube center, *i.e.*, at the position (51 2 3). The tally is then defined by the instruction “F5:p 51 2 3 1”. For the first case, we want to evaluate the “mean” photon fluence in the cube, due to the point-like ⁶⁰Co source. If the cell 5 stands for the cube, the tally can be written as “F4:p 5”.

At this point, we have presented all the elements enabling to build the full input files necessary for the simulation of the two case studies presented.

TAB. 5 – Tally designators in MCNP.

Mnemonic	Tally type	Fn units	*Fn units
F1:pl	Current integrated over a surface	Particles	MeV
F2:pl	Fluence averaged over a surface	particles/cm ²	MeV/cm ²
F4:pl	Fluence averaged over a cell	particles/cm ²	MeV/cm ²
F5a:pl	Fluence at a point or ring detector	particles/cm ²	MeV/cm ²
F6:pl	Energy deposition averaged over a cell	MeV/g	jerks [‡] /g
+F6	Collision heating	MeV/g	n/a
F7:pl	Fission energy deposition in a cell	MeV/g	jerks/g
F8:pl	Energy distribution of pulses created in a detector by radiation	Pulses	MeV
+F8:pl	Charge deposition	Charges	n/a

[‡]1 jerks = 10⁹ J. 1 jerks/g = 10¹² Gy.

(i) Input file for the first case

The first case is a ^{60}Co isotropic point-like source located at the position (51 2 3). We want to evaluate the photon fluence at 50 cm from the source, in a 4 cm side water cube centered in (1 2 3).

```

Case 1
c block 1 cells
5 8 -1 5 -10 15 -20 25 -30 $ inside cube material 8 d=1 g/cm3
10 2 -1.3e-3 -40 (-5:10:-15:20:-25:30) $ air mat 2 d=1.3e-3 g/cm3 around the cube
999 0 40 $ outside void

c block 2 geometry
5 PX -1
10 PX 3
15 PY 0
20 PY 4
25 PZ 1
30 PZ 5
40 SO 100 $ sphere centered on (0,0,0) R=100 cm

c block 3 the rest
SDEF par=p erg=d4 pos 51 2 3
si4 L 1.17 1.33
sp4 1 1
m2 6000 -.000124 7000 -.755258 8000 -.23 18000 -.0128 $ air
m8 1000 2 8000 1 $ water
mode p
imp:p 1 1 0 $ transport in cell 5 and cell 10 no transport in cell 999
ctme 10 $ time of the calculation
F4:p 5 $ fluence in the cube - cell 5

```

Generally, the first line of an input file contains the title. It is the only case when it is not mandatory to add “c” as a first line character to indicate a comment.

Note that an infinite cell made of vacuum, where the particle transport is not enabled, has been defined beyond the sphere. Without this cell providing a matter-vacuum boundary, the particles would be continuously transported. This would cause an infinite routine and a calculation break in the code. Vacuum is indicated by setting the instruction 0 instead of the material number and density (refer to cell 999).

(j) Input file for the second case

The second case is about a cubic ^{60}Co source filled with water. The cube has the same dimensions as in the first case. We want to estimate the fluence at a point located at 50 cm from this source.


```

Case 2
c block 1 cells
5 8 -1 5 -10 15 -20 25 -30 $ inside cube material 8 d=1 g/cm3
10 2 -1.3e-3 -40 # 5 $ air d=1.3e-3 g/cm3 around the cube
999 0 40 $ outside void

c block 2 geometry
5 PX -1
10 PX 3
15 PY 0
20 PY 4
25 PZ 1
30 PZ 5
40 SO 100 $ sphere centered on (0,0,0) R=100 cm

c block 3 the rest
SDEF cell=5 x=d1 y=d2 z=d3 erg=d4 par=p
si1 -1 3 $ x-range limits for source volume
sp1 0 1 $ uniform probability over y-range
si2 0 4 $ y-range limits for source volume
sp2 0 1 $ uniform probability over y-range
si3 1 5 $ x-range limits for source volume
sp3 0 1 $ uniform probability over x-range
si4 L 1.17 1.33 $ energy of each Co-60 photons
sp4 1 1 $ intensity of each Co-60 photons
m2 6000 -.000124 7000 -.755258 8000 -.23 18000 -.0128 $ air
m8 1000 2 8000 1 $ water
mode p
imp:p 1 1 0 $ transport in cell 5 and cell 10 no transport in cell 999
ctme 10 $ time of the calculation
F5:p 51 2 3 .1 $ fluence at 50 cm of the center of the cube (in x-axis)

```

In cell 10 parameters, the instruction “#5” provokes the cell 5 exclusion. Thus, writing `-40 #5` enables to define the inside of the sphere 40 while excluding the geometry defined in the cell 5, *i.e.*, the cube.

Note that, in this case, “`10 2 -1.3e -3 -40 # 5`” is equivalent to “`10 2 -1.3e -3 -40 (-5:10:-15:20:-25:30)`”.

The VisEd software can be used to visualize the files in a two dimension frame. This software is provided in the MCNP package. For Windows OS, the free software “Xming” (<https://sourceforge.net/projects/xming/>) can also be employed.

These simple cases allow understanding the general structure of MCNP input files. More complex cases, as well as output file analysis and result normalization will be discussed throughout this book.

Chapter 1

Calculation of Radiometric and Dosimetric Quantities (Fluence, Kerma, Dose and Ambient Dose Equivalent)

1.I Basic Calculations of the Fluence Rate for Sources of Different Geometric Shapes

Abstract:

We propose here to calculate the fluence rate for basic sources: point isotropic source, parallel beam, line source and disk-shaped source. Each source emits a same flux of 10^6 particles per second. For all of the cases investigated here, the results of the analytical and numerical solutions will be compared.

Objectives:

- Application of the analytical formalism for fluence calculations.
- Fluence calculation for a point source (analytical and MCNP code).
- Fluence calculation for a parallel beam (analytical and MCNP code).
- Fluence calculation for a line (analytical and MCNP code).
- Fluence calculation for a disk (analytical and MCNP code).

These trivial and classic applications of external radiation are covered with the aim of getting acquainted with the MCNP result normalization in the convenient units.

- (a) Fluence calculation within one meter of an isotropic source

The fluence rate within a distance d of one meter of an isotropic source emitting a flux $\dot{N} = 10^6$ (particles).s⁻¹ is obtained with the following form:

$$\dot{\Phi} = \frac{\dot{N}}{4\pi d^2} = \frac{10^6}{4\pi \times 100^2} = 7.96 \text{ s}^{-1} \text{ cm}^{-2}$$

Concerning the MCNP simulation, an ASCII format input file has to be built, the latter will be interpreted by the code. This file is composed of three parts referred to as blocks throughout this book. Two blocks are separated by a blank line. Block 1 contains the cell definition. A cell is defined by a volume resulting in a composition of surfaces specified in Block 2, plus a density and a material. As the case study is simple, the particle transport will be conducted into the vacuum. Thus, there is no need to define a material or a density. This assumption is set out inside the input file [1.1.1](#) below, using the instruction “10 0 -15” composed of:

- the cell number, “10”, in which the particle transport takes place,
- a zero-material, “0”, to specify a vacuum region (no interaction in this case),
- the “-15” parameter, with a minus sign to indicate that the transport will occur within the surface “15” defined in Block 2.

Block 2 is a list of the surfaces enabling the cell definition in Block 1. Generally speaking, the region of space for the radiation transport is defined by a sphere surrounding the simulated case. Particles reaching the sphere boundary are “killed” and their “history” is interrupted. Without this feature, particles would be transported *ad libitum*, causing an infinite tracking of their “history” which will end up in a “fatal error” after ten infinite tracks (“10 particles got lost” in the output file). In order to model this radiation transport sphere, the instruction “15 so 200” stands for:

- the surface number, “15” enabling to model the cell number “10” of Block 1,
- the surface type, “so”, corresponding to an origin centered sphere,
- the “200” cm radius of the sphere.

It is necessary to refer to the chapter “an introduction to MCNP” to get an overview of surfaces for use in the code.

Finally, Block 3 defines the type of particles generated and transported. For the studied case, the “mode p” instruction indicates a photon transport. This block is also used to describe the radiation source. The instruction “sdef par = p erg = 1 pos = 0 0 0” defines a 1 MeV (“erg = 1”) photon source (“par = p”) emitted at the origin of the coordinate system (“pos = 0 0 0”). The calculation features are specified using the tallies. In this case, the “f5” card refers to a type 5 tally for the fluence at a point. For this estimator, a small sphere of exclusion is required with the radius set in the 4th entry of the tally. The radius is 0.1 cm in the example below. This parameter avoids a singularity risk in the fluence calculation (*cf.* Antoni and Bourgois, [2017a](#)). In our case, the instruction “f5:p 0 0 100 0.1” estimates the photon fluence at the point “0,0,100”. It is also worth mentioning that in Block 3, the physics options are set for generating and transporting particles. These options are mainly handled by the “phys” card, to which we shall refer in some of the following applications. The entire input file is given below:

```

Fluence calculation for a point source
c block 1 cells definition
10 0 -15 $ cell 10, inside the sphere 15: transport
20 0 15 $ cell 20, outside the sphere 15: no transport

C block 2 geometry definition
15 S0 200 $ sphere "15" radius 200 cm at the origin point (0,0,0)

C block 3 source definition, physics parameters, results, material
imp:p 1 0 $ transport in cell 10 no transport in cell 20
mode p $ only photons are transported
sdef par=p erg=1 pos= 0 0 0 $ photons isotropic source of 1 MeV
f5:p 0 0 100 .1 $ fluence calculation at the point (0,0,100)
stop F5 .000001 $ calculation stops when tally f5 error is equal to .000001

```

File 1.I.1

The result obtained for f5 tally is given in the output file as below:

	tally	5			
nps	mean	error	vov	slope	fom
1000	7.9577E-06	0.0000	0.0000	10.0	1.0E+30

This result provides the fluence per photon emitted by the virtual source; this value is

$\Phi/N = 7.96 \times 10^{-6} \text{ cm}^{-2}(\gamma)^{-1}$. For a flux of $\dot{N}(\gamma).\text{s}^{-1}$, the resulting fluence rate is:

$$\dot{\Phi} = \left(\frac{\Phi}{N}\right)\dot{N} = 7.96 \times 10^{-6} \times 10^6 = 7.96 \text{ s}^{-1}.\text{cm}^{-2}$$

We infer that the fluence rates obtained with both methods are identical. Although the studied case is fairly simple, it points out from the outset the need for an ad-hoc normalization of the estimator raw results to obtain the latter in the convenient units.

(b) Fluence calculation for a parallel beam

For a beam of circular cross-section of radius 5 cm, with a flux $\dot{N} = 10^6 (\gamma).\text{s}^{-1}$, the fluence rate is:

$$\dot{\Phi} = \frac{\dot{N}}{S} = \frac{10^6}{\pi \times 5^2} = 1.27 \times 10^4 \text{ s}^{-1}.\text{cm}^{-2}$$

When using the MCNP code with this type of source, the fluence per source particle can be simulated by means of the fluence averaged over a cell, which corresponds to a type 4 tally. The type 5 tally previously used is not appropriate in this case of a parallel beam. Inside the input file presented hereinafter, the fluence is calculated within a spherical void cell of 0.1 cm radius, located in the beam. As for the source definition through the “sdef” card, the “vec” card indicates the particle beam direction along z axis, *i.e.*, “vec 0 0 1”. The “dir” card sets the beam width around the direction-vector “vec” according to “dir cos(θ)”. Thus, by setting “dir 1”, the beam is parallel since $\theta = 0$. The “rad” card indicates the beam cross section radius described in “s11” and the “axs” card sets the direction of the emission surface. If the cards “vec”, “dir” and “axs” are omitted, the default emission is isotropic as in the file 1.I.1. of the previous application. Figure 1.I.1 exhibits the different directions. The MCNP file for the parallel beam is the following:

```
Fluence calculation for a parallel beam
10 0 -10 15 $ region for transport
15 0 -15 $ scoring calculation cell
20 0 10 $ outside the transport region

10 SO 200
15 SZ 100 .1 $ calculation sphere (centered on z-axis) for z=100 and r=0.1

imp:p 1 1 0 $ transport in cells 10 15, no transport in cell 20
mode p
c sdef for a // beal in oz radius 5 cm
sdef par=P pos 0 0 -10 axs 0 0 1 ext 0 rad=d1 vec 0 0 1 dir 1 erg 1
S11 0 5
spl -21 1
f4:p 15 $ means of the average fluence inside cell 15
stop F4 .003
```

File 1.I.2

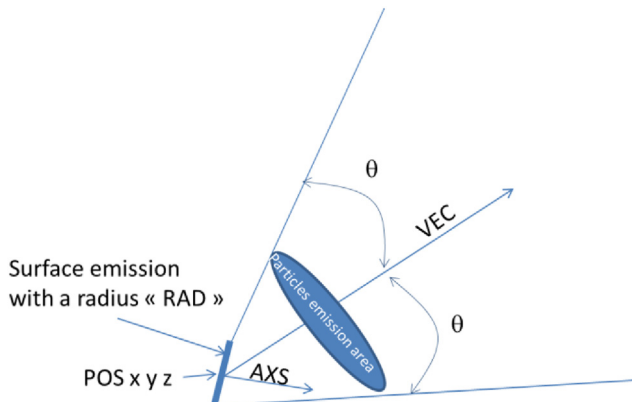


FIG. 1.I.1 – Definition of the “sdef” parameters for an anisotropic source.

Tally 4 result of the output file is:

		tally	4		
nps	mean	error	vov	slope	fom
313560279	1.2731E-02	0.0030	0.0000	10.0	12889

This result corresponds to the mean fluence per photon emitted by the virtual source; this value is $\bar{\Phi}/N = 1.27 \times 10^{-2} \text{ cm}^{-2}(\gamma)^{-1}$. For a $10^6 (\gamma).s^{-1}$ flux, the fluence rate is:

$$\dot{\Phi} = \left(\frac{\bar{\Phi}}{N}\right)\dot{N} = 1.27 \times 10^{-2} \times 10^6 = 1.27 \times 10^4 \text{ s}^{-1}\text{cm}^{-2}$$

Here also the results obtained with both methods are identical.

(c) Fluence calculation for a line

A linear source of length L emitting a total flux \dot{N} homogeneously is considered. Figure 1.1.2 represents the geometry as well as the variables used for the calculation.

First of all, the flux per unit length n_L shall be defined:

$$n_L = \frac{\dot{N}}{L}$$

By dividing the linear source into infinitesimal elements of length dl , each of these elements can be considered as point-like source from the observer. The flux emitted by each one of these subsequent elements is equal to $n_L dl$ and the differential fluence at a distance ρ takes the form:

$$d\Phi = \frac{n_L}{4\pi\rho^2} dl \tag{1}$$

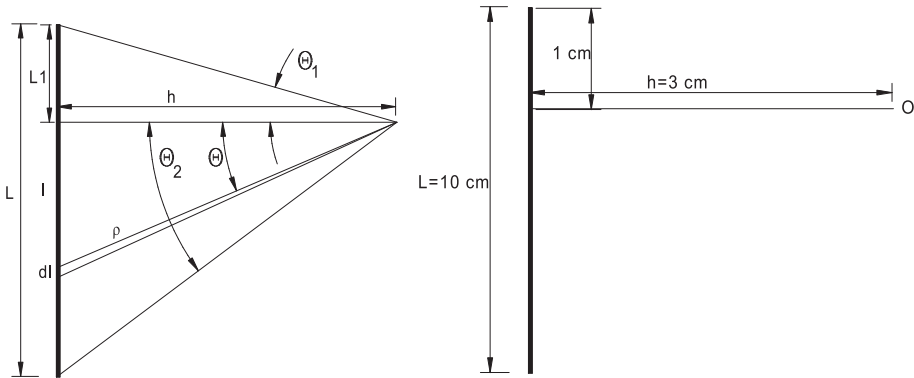


FIG. 1.1.2 – Geometry used for calculating the fluence of a line.

then distance ρ is expressed as a function of distance h and angle θ shown in figure 1.I.2:

$$h \tan\theta = l \xleftrightarrow{\text{by deriving}} h \frac{d\theta}{\cos^2\theta} = dl \text{ and } \rho = \frac{h}{\cos\theta}$$

ρ and dl are replaced in equation (1) by expressions found just above:

$$d\Phi = \frac{n_L \left(\frac{h}{\cos^2\theta} \right)}{4\pi \left(\frac{h}{\cos\theta} \right)^2} d\theta = \frac{n_L}{4\pi h} d\theta$$

Afterwards, the differential fluence is integrated over the line:

$$\dot{\Phi} = \int_L d\dot{\Phi} = \frac{n_L}{4\pi h} \int_{-\theta_1}^{\theta_2} d\theta = \frac{\dot{N}}{4\pi L h} \left[\arctan\left(\frac{L_1}{h}\right) + \arctan\left(\frac{L-L_1}{h}\right) \right]$$

With dimensions given in figure 1.I.2, the calculated fluence rate at the observer (point O) is:

$$\dot{\Phi} = \frac{10^6}{4\pi \times 10 \times 3} \left(\arctan\left(\frac{1}{3}\right) + \arctan\left(\frac{9}{3}\right) \right) = 4.17 \times 10^3 \text{ s}^{-1} \text{ cm}^{-2}$$

Note that the arc tangent function angles must be expressed in radians (SI unit). Concerning the numerical simulation, the fluence is estimated using type 5 tally located at the observer. In file 1.I.3. below, the linear source is set up with “sdef” parameters, like a cylinder along z axis, with a zero radius, *i.e.* “rad = 0”, and with a height set in the “ext” parameter.

```
fluence calculation for a line source
10 0 -10
20 0 10

10 SO 30

imp:p 1 0
mode p
SDEF par=p pos=0 0 0 axs=0 0 1 ext=d1 rad=0 erg=1
SI1 -9 1 $ line from z=-9 to z=1
SP1 -21 0
f5:p 3 0 0 .1
stop F5 .0001
```


The output file provides the following result:

nps	mean	tally error	5 vov	slope	fom
49152000	4.1665E-03	0.0000	0.0000	10.0	1.0E+30

As a result, the fluence per photon emitted by the virtual source is $\Phi/N = 4.17 \times 10^{-3} \text{ cm}^{-2}(\gamma)^{-1}$. For a flux of $10^6 (\gamma).s^{-1}$ the corresponding fluence rate is:

$$\dot{\Phi} = \left(\frac{\Phi}{N}\right)\dot{N} = 4.17 \times 10^{-3} \times 10^6 = 4.17 \times 10^3 \text{ s}^{-1} \text{ cm}^{-2}$$

Once again both results are identical.

(d) Fluence calculation for a disk

This application gives the fluence at distance D from a disk of radius R , with a uniform contamination, emitting a flux of \dot{N} particles per second in the whole space. Figure 1.I.3 shows the details of the considered geometry.

In the first place, a surface flux n_s is defined as follows:

$$n_s = \frac{\dot{N}}{S} = \frac{\dot{N}}{\pi R^2}$$

When dividing the disk into infinitesimal elements of surface dS , each of them can be considered as point-like source to the observer. The flux emitted by each of these elements is equal to $n_s dS$. Therefore, for a point source emitting a total flux $n_s dS$, the differential fluence at distance ρ is equal to:

$$d\phi = \frac{n_s}{4\pi\rho^2} dS$$

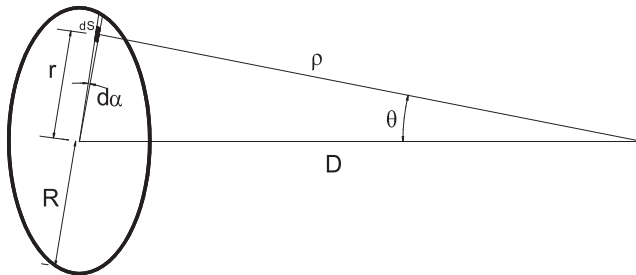


FIG. 1.I.3 – Geometry used for calculating the fluence of a disk.

The total fluence of the disk is achieved by integrating the differential fluence over the whole surface of the source:

$$\dot{\phi} = \iint_S \frac{n_s}{4\pi\rho^2} dS \quad (2)$$

The three following equations are derived from the geometry and the variables presented in figure 1.1.3:

$$dS = r dr d\alpha \quad (3)$$

$$\rho = \frac{D}{\cos\theta} \quad (4)$$

$$D \tan\theta = r \quad (5)$$

Differential form of equation (5) is written as:

$$\frac{D}{\cos^2\theta} d\theta = dr \quad (6)$$

Substituting expressions (3), (4) and (6) in integral (2) leads to:

$$\begin{aligned} \dot{\Phi} &= \frac{n}{4\pi} \iint_S r \left(\frac{D}{\cos\theta} \right)^{-2} d\alpha dr = \frac{n}{4\pi} \iint_S \left[D \tan\theta \left(\frac{D}{\cos^2\theta} \right) \right] \left(\frac{D}{\cos\theta} \right)^{-2} d\alpha d\theta \\ &\Leftrightarrow \dot{\Phi} = \frac{n}{4\pi} \int_0^{2\pi} d\alpha \times \int_0^{\arctan(\frac{R}{D})} \tan\theta d\theta = \frac{n}{2} [-\ln|\cos\theta|]_0^{\arctan(\frac{R}{D})} \end{aligned}$$

Finally:

$$\dot{\Phi} = \frac{N}{2\pi R^2} \left(-\ln \left| \cos \left(\arctan \left(\frac{R}{D} \right) \right) \right| \right)$$

The following trigonometrical relationship simplifies the above expression:

$$\arctan\theta = \arccos\left(\frac{1}{\sqrt{1+\theta^2}}\right)$$

Thus, a closed-form solution of the fluence rate at the observer is:

$$\dot{\Phi} = \frac{\dot{N}}{2\pi R^2} \left[-\ln \left(\frac{1}{\sqrt{1 + \left(\frac{R}{D}\right)^2}} \right) \right] = \frac{\dot{N}}{4\pi R^2} \ln \left| 1 + \left(\frac{R}{D} \right)^2 \right|$$

By setting $R = 5$ cm and $D = 3$ cm for the numerical application, we get:

$$\dot{\Phi} = \frac{\dot{N}}{4\pi R^2} \ln \left| 1 + \left(\frac{R}{D} \right)^2 \right| = \frac{1 \times 10^6}{4\pi 5^2} \ln \left| 1 + \left(\frac{5}{3} \right)^2 \right| = 4231 \text{ cm}^{-2} \text{ s}^{-1}$$

As for the numerical simulation, the fluence is estimated by type 5 tally. In the following file, the disc-shaped source is defined by means of the “rad” parameter in the “sdef” card:

```
Fluence calculation for a disk
10 0 -10
20 0 10

10 SO 30

imp:p 1 0
mode p
SDEF POS=0 0 0 AXS=0 0 1 EXT=0 RAD=d1 PAR=p ERG=1
SI1 0 5 $ disk radius between 0 and 5 cm
SP1 -21 1 $ radial sampling weighting: r^1 for disk source
f5:p 0 0 3 .1
stop F5 .0001
```

File 1.I.4

The result is given below:

nps	mean	tally error	vov	5 slope	fom
16384000	4.2314E-03	0.0000	0.0000	10.0	1.0E+30

Tally 5 result provides the value of the fluence per photon emitted by the source; this value is $\Phi/N = 4.23 \times 10^{-3} \text{ cm}^{-2}(\gamma)^{-1}$. For a flux of $10^6 (\gamma).s^{-1}$ the fluence rate is:

$$\dot{\Phi} = \left(\frac{\Phi}{N} \right) \dot{N} = 4.23 \times 10^{-3} \times 10^6 = 4.23 \times 10^3 \text{ s}^{-1} \text{ cm}^{-2}$$

Both results are also the same.

1.II Basic Calculations of Ambient Dose Equivalent

Abstract:

Basic ambient dose equivalent rates for isotropic point sources are calculated for different radionuclides. For each case study, the analytical and numerical approaches are presented.

Objectives:

- Ambient dose equivalent rate calculations for isotropic point-sources.
- Application of the inverse-square law.
- Use of the ICRP “conversion coefficient for the ambient dose equivalent”.
- Numerical calculation of dose equivalent.
- Normalization of the MCNP results for multi-source problems.
- Definition of multiple sources in a MCNP file.

The approaches detailed hereunder, enabling to evaluate operational quantities for external exposure in a given radiological context, constitute a basic knowledge in radiation protection calculations.

Part 1: Ambient Dose Equivalent rate at 1 m and 30 cm from a 10 GBq ^{22}Na Point-Source

(a) Analytical calculation

The ambient dose equivalent rate at any point of space can be obtained by multiplying the fluence rate $\dot{\Phi}$ and the “fluence-to-ambient dose equivalent” conversion coefficient h_{Φ} :

$$\dot{H} = h_{\Phi} \dot{\Phi}$$

The fluence rate is given in $\text{cm}^{-2}.\text{s}^{-1}$ and the conversion coefficient, h_{Φ} , in $\text{Sv}.\text{cm}^2$. For an isotropic source of activity A emitting particles with different probabilities Γ_E associated with their energy, the ambient dose equivalent rate at a distance ρ (in cm) is formally expressed as:

$$\dot{H} = \sum_E h_{\Phi,E} \dot{\Phi}_E = \sum_E h_{\Phi,E} \left(\frac{\dot{N}_E}{4\pi\rho^2} \right) = \sum_E h_{\Phi,E} \left(\frac{A\Gamma_E}{4\pi\rho^2} \right) = \frac{A}{4\pi\rho^2} \sum_E h_{\Phi,E} \Gamma_E \quad (1)$$

^{22}Na radioactive decay emits two photons with energies and emission intensities: 511 keV at 180% and 1274 keV at 99.94%. The photon emission spectrum of this radionuclide is drawn from the web link “<http://www.nucleide.org/Laraweb/>”. The “fluence-to-ambient dose equivalent” conversion coefficients, $h_{\Phi}^*(10)$, are taken from the ICRP (1996) publication (see figure 1.II.1).

The values of this coefficient are obtained for both energies from figure 1.II.1. We get $h_{\Phi}^*(10)_{511} = 3 \text{ pSv}.\text{cm}^2$ and $h_{\Phi}^*(10)_{1274} = 6.2 \text{ pSv}.\text{cm}^2$. Therefore, for a 10 GBq point-source at 1 m:

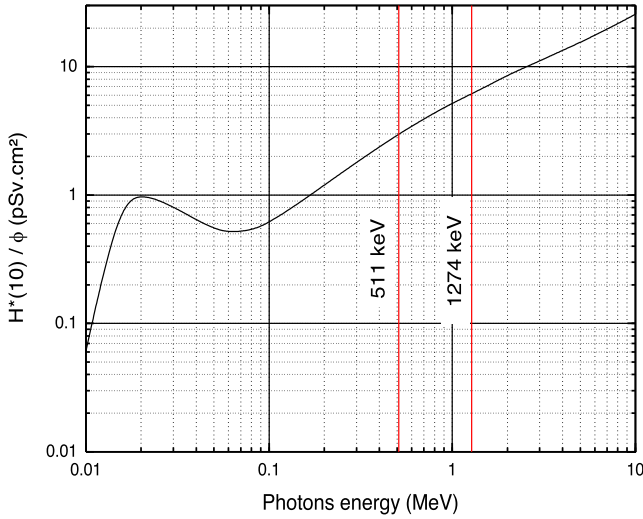


FIG. 1.II.1 – ICRP (1996) “fluence-to-ambient dose equivalent” conversion coefficient.

$$\dot{H}^*(10)_{1\text{m}} = \dot{H}^*(10)_{511} + \dot{H}^*(10)_{1274} = \frac{A}{4\pi d^2} (\Gamma_{511} h_{\Phi}^*(10)_{511} + \Gamma_{1274} h_{\Phi}^*(10)_{1274})$$

Thus:

$$\dot{H}^*(10)_{1\text{m}} = \frac{10 \times 10^9}{4\pi \times 100^2} (1.8 \times 3 \times 10^{-12} + 0.9994 \times 6.2 \times 10^{-12}) = 9.2 \cdot 10^{-7} \text{ Sv} \cdot \text{s}^{-1}$$

The result given in a usual unit ($\text{mSv} \cdot \text{h}^{-1}$) is:

$$\dot{H}^*(10)_{1\text{m}} = 3600 \times 1000 \times 9.2 \cdot 10^{-7} = 3.3 \text{ mSv} \cdot \text{h}^{-1}$$

For an isotropic point-source responsible for ambient dose equivalent rate \dot{H}_1 at distance d_1 , the ambient dose equivalent rate \dot{H}_2 at distance d_2 obeys the inverse-square law:

$$\frac{\dot{H}_2}{\dot{H}_1} = \left(\frac{d_1}{d_2} \right)^2$$

Note that both distances d_1 and d_2 must be expressed with the same unit. At 30 cm, it becomes:

$$\dot{H}^*(10)_{30\text{cm}} = \dot{H}^*(10)_{1\text{m}} \left(\frac{d_{1\text{m}}}{d_{30\text{cm}}} \right)^2 = 3.3 \times \left(\frac{1}{0.3} \right)^2 = 36.7 \text{ mSv} \cdot \text{h}^{-1}$$

It is recalled that the inverse-square law holds only for point-sources or point-like objects. An object can be considered as a point-source when its distance to the observer is roughly equal to 5 times its largest dimension.

(b) Numerical calculation

The ambient dose equivalent is calculated with the point detector tally (F5). In order to convert the calculated fluence into an ambient dose equivalent, one needs to multiply the tally result by “fluence-to-ambient dose equivalent” conversion coefficients, in accordance with formula (1). This can be done by implementing dose energy “de” and dose function “df” cards in the MCNP input file. The “de” card contains discrete energies and the “df” card provides the values of the conversion factors $h_{\Phi}^*(10)$ for each energy of the “de” card. The “df” values are written in the file with the same unit as that of ICRP (1996), in pSv.cm². The weighted result obtained is an ambient equivalent dose per photon emitted by the virtual source, $H^*(10)/N$. The F5 and F15 estimators below give, respectively, the equivalent dose at 1 m and at 30 cm from the source.

Since the particles are transported in the air, the parameters “1 5 -0.00129 -100” represent a cell “1”, filled with air. Air is characterized by material “5” described in Block 3 by the “m5” card and by the density 0.00129 g/cm³ noted “-0.00129”. The minus sign of the latter indicates a unit in g.cm⁻³; whereas a positive sign would stand for “(atoms)/barn-cm”. The last entry, “-100”, points the inside of surface “100”.

In Block 3, the source is specified by the instruction “sdef pos = 0 0 0 par = p erg = d1” in which the parameter “erg = d1” refers to the photon energies of distribution 1. This distribution described by “si1 1 0.511 1.274”, simulates, with parameter “l”, a discrete source of photons of 0.511 and 1.274 MeV. The “sp1” card coupled with “si1” holds for the intensity of photons at each energy, namely 1.8 and 0.9994.

```

**** Calculation for a Na-22 point source ****
C block 1
c cell block
1 5 -0.00129 -100 $ transport area cell; material 1 (air) density 0.00129
10 0 100          $ vacuum

C block 2
c geometry block
100 SO 200 $ 200 cm radius sphere defining the scoring zone

C block 3
c source, materials and results definition block
imp:p 1 0 $ transport in cell 1, no transport in cell 10
mode p
sdef pos=0 0 0 par=p erg=d1
SI1 L .511 1.274 $ Na-22 energies
SP1 1.8 .9994    $ Na-22 emission intensities

```

```

ctme 1 $ 1 min calculation time
F5:p 0 100 0 .1 $ fluence at 1 meter
F15:p 0 0 30 .1 $ fluence at 30 cm
c Energies (MeV) for H*(10)/phi coefficients
DE5 .01 .015 .02 .03 .04 .05 .06 .08 .1 .15 .2 .3 .4 .5 .6 &
.8 1 1.5 2 3 4 5 6 8 10
c H*(10)/phi pSv.cm2 photons coefficients, ICRP 1996
DF5 0.061 .83 1.05 .81 .64 .55 .51 .53 .61 .89 1.2 1.8 2.38 2.93 3.44 &
4.38 5.2 6.9 8.6 11.1 13.4 15.5 17.6 21.6 25.6
DE15 .01 .015 .02 .03 .04 .05 .06 .08 .1 .15 .2 .3 .4 .5 .6 &
.8 1 1.5 2 3 4 5 6 8 10
DF15 0.061 .83 1.05 .81 .64 .55 .51 .53 .61 .89 1.2 1.8 2.38 2.93 3.44 &
4.38 5.2 6.9 8.6 11.1 13.4 15.5 17.6 21.6 25.6
M5 1000 -1.0 7000 -78.0 8000 -21.0 $ air
    
```

File 1.II.1

The tally results in the output file are:

tally 5					tally 15				
nps	mean	error	vov	slope fom	mean	error	vov	slope fom	
14262217	3.2728E-05	0.0002	0.0561	2.6 3.4E+07	3.6408E-04	0.0001	0.0010	3.0 8.5E+07	

The values at 1 m and 30 cm are, respectively: $3.27 \times 10^{-5} \text{ pSv} \cdot (\gamma)^{-1}$ and $3.64 \times 10^{-4} \text{ pSv} \cdot (\gamma)^{-1}$. The normalization operated to format the results differs from the analytical approach. In this case, a total flux of particles is considered, by summing up the emission intensity of each energy.

$$\dot{H}^*(10) = \left(\frac{H^*(10)}{N} \right) \dot{N} = \left(\frac{H^*(10)}{N} \right) A \sum_E \Gamma_E$$

$H^*(10)/N$ is the value computed by MCNP given in $\text{pSv} \cdot (\gamma)^{-1}$. For a 10 GBq activity of ^{22}Na , the total flux obtained is:

$$\dot{N} = A \sum_E \Gamma_E = 10 \times 10^9 \times (1.8 + 0.9994) = 2.8 \times 10^{10} (\gamma) \cdot \text{s}^{-1}$$

Ambient dose equivalent rates, given in $\text{mSv} \cdot \text{h}^{-1}$, at 30 cm and 1 m are:

$$\dot{H}^*(10)_{1\text{m}} = 3.27 \times 10^{-5} \times 2.8 \times 10^{10} \times 10^{-12} \times 3600 \times 1000 = 3.3 \text{ mSv} \cdot \text{h}^{-1}$$

$$\dot{H}^*(10)_{30\text{cm}} = 3.64 \times 10^{-4} \times 2.8 \times 10^{10} \times 10^{-12} \times 3600 \times 1000 = 36.7 \text{ mSv} \cdot \text{h}^{-1}$$

The factor $10^{-12} \times 3600 \times 1000$ converts the results from pSv.s⁻¹ to mSv.h⁻¹. We infer that analytical and numerical results are similar.

Part 2: Ambient Dose Equivalent Rate for Two Point-Sources: 10 GBq of ²²Na at 1 m and 1 GBq of ⁶⁰Co at 30 cm

(a) Analytical calculation

In part 1, a ²²Na point-source of 10 GBq gave an ambient dose equivalent rate of 3.3 mSv.h⁻¹ at one meter. For usual sources, simple equations allow direct access to the operational quantity at a given distance, as a function of the source activity. For instance, Antoni and Bourgois (2017a) give 0.351 mSv.h⁻¹ at one meter from a ⁶⁰Co point source of 1 GBq. At 30 cm, it follows:

$$\dot{H}^*(10)_{30\text{ cm}} = \dot{H}^*(10)_{1\text{ m}} \left(\frac{d_{1\text{ m}}}{d_{30\text{ cm}}} \right)^2 = 0.351 \times \left(\frac{1}{0.3} \right)^2 = 3.9 \text{ mSv.h}^{-1}$$

Also, the ambient dose equivalent for two point-sources located at different distances from the observer is:

$$\dot{H}^*(10) = 3.3 + 3.9 = 7.2 \text{ mSv.h}^{-1}$$

(b) Numerical calculation

The different locations of the point-sources need a specific source definition in the “sdef” card. The location is identified depending on the energy of the source by means of the parameter “pos = ferg”. Furthermore, the multi-source case requires a specific parametrization for the launching probability of a given energy. This probability is handled by associating the “si1” and “sp1” cards in the file suggested below. It is necessary to associate to each energy a probability corresponding to the ratio of the number of particles emitted to the total flux. Generally, for k point sources, the total flux can be formally expressed as follows:

$$\dot{N} = \sum_k \dot{N}_k = \sum_k \left(A_k \sum_E \Gamma_{k,E} \right)$$

with A_k the respective activity of each source and $\Gamma_{E,k}$ the emission intensity of each source for energy E . The total flux for this application is:

$$\dot{N} = A_{\text{Na}} \times (\Gamma_{0.51} + \Gamma_{1.27}) + A_{\text{Co}} \times (\Gamma_{1.17} + \Gamma_{1.33})$$

With values, we get:

$$\dot{N} = 10 \times 10^9 \times (1.8 + 0.9994) + 10^9 \times (1 + 1) = 3 \times 10^{10} (\gamma).\text{s}^{-1}$$

Then, ratio r_E of the number of photons emitted to the total flux is built for each energy E . The number of photons emitted is calculated by multiplying the activity by the emission intensity of energy line E . The ratio is given by:

$$r_{k,E} = \frac{N_{k,E}}{\dot{N}} = \frac{A_k \Gamma_{k,E}}{\dot{N}}$$

For instance, the ratio for the 511 keV line of ^{22}Na is:

$$r_{\text{Na},0.51} = \frac{N_{\text{Na},0.51}}{\dot{N}} = \frac{10 \times 10^9 \times 1.8}{3 \times 10^{10}} = 0.6$$

In similar fashion, ratios for other energies are: $r_{\text{Na},1.27} = 0.333$, $r_{\text{Co},1.17} = 0.033$ and $r_{\text{Co},1.33} = 0.033$. These ratios appear in the set of parameters of the “sp1” card in the following file:

```
Dose rate for 2 point sources; Na-22 at 1 m and Co-60 at 30 cm
C block 1
1 1 -0.00129 -100 $ transport area cell
10 0 100          $ outside vacuum

C block 2
100 SO 200

C block 3
imp:p 1 0
mode p
sdef pos=ferg d2 par=p erg=d1
SI1 L .511 1.274 1.17 1.33 $ Na-22 et Co-60 emission lines
SP1 .6 .3333333333 .0333333333 .0333333333 $ flux ratio for each energy
DS2 S 3 3 6 6 $ position number; function of energy
SI3 L 0 0 0 $ position of both Na-22 energies
SP3 1
SI6 L 0 0 70 $ position of both Co-60 energies
SP6 1
ctme 10
F5:p 0 0 100 .1 $ fluence at 1 meter
c energies (MeV) for H*(10)/phi coefficients
DE5 .01 .015 .02 .03 .04 .05 .06 .08 .1 .15 .2 .3 .4 .5 .6 &
.8 1 1.5 2 3 4 5 6 8 10
c H*(10)/phi pSv.cm2 ICRP 74 coefficients for photons
DF5 0.061 .83 1.05 .81 .64 .55 .51 .53 .61 .89 1.2 1.8 2.38 2.93 3.44 &
4.38 5.2 6.9 8.6 11.1 13.4 15.5 17.6 21.6 25.6
M1 1000 -1.0 7000 -78.0 8000 -21.0 $ air
```

The output results are:

nps	mean	tally error	5 vov	slope	fom
35832630	6.6302E-05	0.0003	0.0002	2.9	945146

Tally 5 result is an ambient dose equivalent per photon emitted by the two virtual sources: $H^*(10)/N = 6.63 \times 10^{-5} \text{ pSv}(\gamma)^{-1}$. Finally, the numerical ambient dose equivalent rate is:

$$\begin{aligned} \dot{H}^*(10) &= \left(\frac{H^*(10)}{N} \right) \dot{N} = 6.63 \times 10^{-5} \times 3 \times 10^{10} \times 10^{-12} \times 3600 \\ &= 7.2 \times 10^{-3} \text{ Sv.h}^{-1} (7.2 \text{ mSv.h}^{-1}) \end{aligned}$$

Once again, analytical and numerical results are the same.

1.III Dose and Kerma Calculation for Photons in a Medium Composed of Interfaces

Abstract:

In this problem, dose and kerma curves, as a function of depth, are performed in a set of media. We assume that a parallel beam of 2 MeV photons with a 2 cm section radius irradiates a solid cylinder of the same section radius. This cylinder is successively filled with a 2 cm layer of soft tissue, 1 cm layer of titanium and 2 cm layer of soft tissue. An overview of this multi-layer cylinder is displayed in figure 1.III.1.

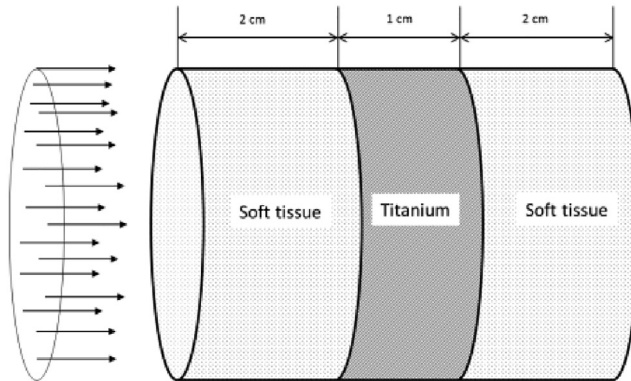


FIG. 1.III.1 – Multi-layer cylinder for calculation.

Objectives:

- Analytical calculation of the kerma and the depth dose for photons.
- Calculation of kerma and dose at the interface between different materials.
- Numerical simulation of kerma and dose.
- Calculation of the build-up factor in soft tissue.

Part 1: Semi-Empirical Calculation of the Dose Profile

Hereafter, steps to describe theoretically the kerma and the absorbed dose profiles in successive materials are described.

(a) Kerma calculation at the cylinder entrance ($x = 0$)

For photons of energy E_i (MeV) with a fluence Φ_i (cm^{-2}), the collision kerma (Gy) has the form:

$$K^{\text{col}} = 1.602 \times 10^{-10} \sum_i \left(\frac{\mu_{\text{en}}}{\rho} \right)_{ii} \Phi_i E_i$$

with $(\mu_{\text{en}}/\rho)_i$ the mass absorption coefficient at a given energy, expressed in $\text{cm}^{-2} \cdot \text{g}$, in material i . The coefficient 1.602×10^{-10} converts $\text{MeV} \cdot \text{g}^{-1}$ into Gy. Assuming a single energy, the kerma at the entrance of the cylinder is:

$$K^{\text{col}}(0) = 1.602 \times 10^{-10} \left(\frac{\mu_{\text{en}}}{\rho} \right) \Phi(0) E_\gamma \quad (1)$$

The fluence in the parallel beam for 1 emitted photon, at the inlet face of the cylinder is:

$$\Phi(0) = \frac{N}{S} = \frac{1}{\pi R^2} = \frac{1}{\pi \times 2^2} = 7.96 \times 10^{-2} (\gamma) \cdot \text{cm}^{-2}$$

The mass absorption coefficients (μ_{en}/ρ) are available in several references. In the present case, data are drawn from the website: “<https://www.nist.gov/pml/x-ray-mass-attenuation-coefficients>”. For soft tissue and 2 MeV photons, this coefficient is $2.582 \times 10^{-2} \text{ cm}^2 \cdot \text{g}^{-1}$. Using the above equation (1), we get:

$$K^{\text{col}}(0) = 1.602 \times 10^{-10} \times 2.582 \times 10^{-2} \times 7.96 \times 10^{-2} \times 2 = 6.59 \times 10^{-13} \text{ Gy}$$

(b) Kerma calculation in a 2 cm layer of soft tissue

At depth d inside the first slice of soft tissue, the incoming photon fluence is attenuated and the collision kerma becomes:

$$K^{\text{col}}(d) = K^{\text{col}}(0) \exp \left(- \left(\frac{\mu}{\rho} \right)_{\text{soft tissue}} \rho_{\text{soft tissue}} d \right) \quad (2)$$

The value of the mass attenuation coefficient $(\mu/\rho)_{\text{tm}}$ at 2 MeV is $4.895 \times 10^{-2} \text{ g.cm}^{-2}$. The kerma for a 2 cm thickness is:

$$K^{\text{col}}(2) = 6.59 \times 10^{-13} \exp(-4.895 \times 10^{-2} \times 1 \times 2) = 6 \times 10^{-13} \text{ Gy}$$

Actually, equation (2) yields an approximate solution. For the considered energy, photons mainly interact through Compton effect in matter, increasing the fluence as the depth rises. A more accurate method entails including in the above expression a “build-up” factor $B(\mu x, E)$, taking into account this increase as opposed to the attenuation phenomenon. Thus, expression (2) takes the form:

$$K^{\text{col}}(x) = B(\mu x, E) K^{\text{col}}(0) \exp\left(-\left(\frac{\mu}{\rho}\right) \rho x\right) \quad (3)$$

The build-up factor $B(\mu x, E)$ depends on the number of mean free paths “ μx ”, on the photon energy as well as on the considered geometry. There is no theoretical formula providing this coefficient but only empirical expressions such as that of Berger discussed in § 3.II. Its value can also be assessed more precisely by performing a Monte Carlo simulation. However, for photons in soft tissues at the considered energy, this coefficient is almost 1. That is why we assume this factor set to 1 in the further analytical calculations.

(c) Kerma ratio at the interface

At the interface between the soft tissue and the titanium front entrance, the kerma ratio equates to the ratio of the mass absorption coefficients at the considered energy and we get:

$$\frac{K_{\text{Ti}}^{\text{col}}(2)}{K_{\text{soft tissue}}^{\text{col}}(2)} = \left(\frac{\mu_{\text{en}}}{\rho}\right)_{\text{soft tissue}}^{\text{Ti}} = \frac{2.166 \times 10^{-2}}{2.582 \times 10^{-2}} = 0.839$$

An inverted ratio can be considered at the next interface, at 3 cm depth.

(d) Electronic equilibrium condition and dose calculation

Except for electronic equilibrium conditions, the dose calculation is complex and there is no analytical approach to evaluate it. Only a Monte Carlo simulation allows estimating the dose shape in the region between the beginning of a new medium and the depth from which the electronic equilibrium holds. From this depth, the absorbed dose is strictly equal to the collision kerma.

$$D(x) = K^{\text{col}}(x)$$

Electronic equilibrium conditions are verified for a depth at least equal to the range of the most energetic electrons set in motion by photons, in the considered material. At 2 MeV, Compton effect is prevailing. Thus, the range of the most energetic Compton electrons must be determined; this maximum energy $T_{c \text{ max}}$ holds the following equation:

$$T_{c\max} \approx \frac{4E_\gamma^2}{4E_\gamma + 1} = \frac{4 \times 2^2}{4 \times 2^2 + 1} = 1.78 \text{ MeV}$$

For 1.78 MeV, the CSDA (*Continuous Slowing Down Approximation*) range in soft tissue is 0.8516 g.cm^{-2} (*i.e.* 0.8516 cm for 1 g.cm^{-3}) and 1.15 g.cm^{-2} in titanium (*i.e.* 0.255 cm). Data derived from the website “<https://physics.nist.gov/PhysRefData/Star/Text/ESTAR.html>”. Therefore, for a depth x larger than 0.85 cm in soft tissue and larger than 0.255 cm in titanium, it can be assumed that $D(x) = K^{\text{col}}(x)$.

(e) Dose ratio at the interface

As a first approximation, the mean energy of secondary electrons set in motion inside a material can be determined based on primary photons according to:

$$\bar{T}_{e^-} = \frac{\left(\frac{\mu_{\text{tr}}}{\rho}\right)}{\left(\frac{\mu}{\rho}\right)} E_\gamma$$

For this calculation, one can consider that the mass absorption coefficient is almost equal to the mass transfer coefficient ($\mu_{\text{tr}} \cong \mu_{\text{en}}$) the mean energy transferred to secondary electrons is entirely locally imparted with no fraction converted into bremsstrahlung. The mean energy in soft tissue and in titanium is respectively:

$$\begin{aligned} [\bar{T}_{e^-}]_{\text{tm}} &= \frac{2.582 \times 10^{-2}}{4.893 \times 10^{-2}} \times 2 = 1.05 \text{ MeV} \\ \text{and } [\bar{T}_{e^-}]_{\text{Ti}} &= \frac{2.166 \times 10^{-2}}{4.18 \times 10^{-2}} \times 2 = 1.04 \text{ MeV} \end{aligned}$$

The absorbed doses ratio at the interface is given by the ratio of the mean stopping power in both materials. Stopping power values are chosen for the secondary electrons mean energy previously calculated:

$$\frac{D_{\text{Ti}}(2)}{D_{\text{tm}}(2)} = \left(\frac{\bar{S}}{\rho}\right)_{\text{tm}}^{\text{Ti}} = \frac{1.37}{1.843} = 0.74$$

Although the theoretical approach is quite convenient, the numerical simulation requires a special care concerning the understanding of algorithms and parameters governing the electron transport in the Monte-Carlo code (Antoni and Bourgois, 2017b).

Part 2: Numerical Solving with MCNP

The MCNP simulation of the absorbed dose requires a mixed transportation of photons and electrons throughout the same run, which implies a “mode e p” instruction in the input file. The absorbed dose is calculated by means of a type 8 tally on electrons, *i.e.*, “*F8:e”. The kerma evaluation is done using a type 6 tally on photons, *i.e.*, “*F6:p”. In order to obtain the depth distributions, the absorbed dose

and kerma calculations are performed in successive cylindrical cells of low thickness ($\Delta x = 0.01$ cm).

The electron processing in MCNP is highly depending on the transport algorithm chosen and on the implemented parameters (see Antoni and Bourgois, 2017b). Indeed, several path sampling algorithms are available for electrons. For the case study, the default MCNP 6.1 algorithm “detailed electron energy – loss straggling logic” is enabled. For earlier versions than MCNP 5, *e.g.*, versions X and 4, it is advisable to use the “ITS” algorithm triggered by the “dbcn” physics card, by setting the 18th entry to 1. Furthermore, it is worth setting up the number of transportation substeps, by means of the “estep” card, according to the following estimation:

$$\text{ESTEP} = 10 \frac{L_s}{\rho} (h)^{-1}$$

where L_s stands for the step length corresponding to the default value of label “estep” of table 85 in the output file for MCNP6 and that of label “drange” in the previous MCNP versions. These values are, respectively, 8.51×10^{-2} g.cm⁻² and 1.103×10^{-1} g.cm⁻² for soft tissue and for titanium. As titanium density is 4.51, the number of substeps to set up for each material is:

$$\text{ESTEP}_{\text{st}} = 10 \times (8.51 \times 10^{-2}/1) \times (0.01)^{-1} = 85$$

$$\text{ESTEP}_{\text{Ti}} = 10 \times (1.103 \times 10^{-1}/4.51) \times (0.01)^{-1} = 22$$

The values obtained are implemented at the end of the lines dedicated to the materials’ definition (refer to m1 and m2 in the provided file). The MCNP model used is shown in figure 1.III.2. The full input file is provided at the end of the problem solution.

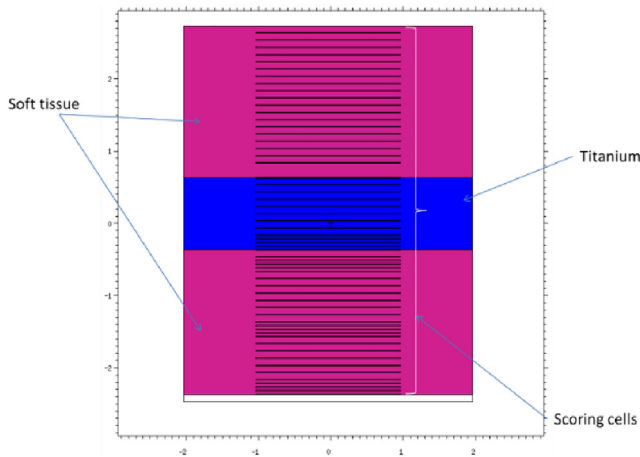


FIG. 1.III.2 – Model used in MCNP for the kerma and absorbed dose profiles.

The *F6 tally results correspond to a “mean kerma” in the cell of thickness Δx , per source photon. They are denoted as $\bar{K}_{\Delta x}$ in what follows. In the output file, mean kerma unit is jerk.s.g^{-1} with 1 jerk = 10^9 J. In order to get Gy unit, the results have to be weighted by a factor 10^{12} :

$$K^{\text{col}}(x) = 10^{12} \times \bar{K}_{\Delta x} \quad \forall x \in \Delta x$$

The type *F8 tally results provide the total energy $\varepsilon_{t,\Delta x}$, in MeV, imparted in the cell of thickness Δx per source photon. Thus, for an absorbed dose in Gy for a photon, in a cell of a given thickness Δx , we use the following normalization:

$$D(x)_{\Delta x} = 1.602 \times 10^{-13} \left(\frac{\varepsilon_{t,\Delta x}}{m} \right) \quad \forall x \in \Delta x$$

with $m = \rho V$ the mass of the cell expressed in kg. The titanium mass is:

$$m_{\text{Ti}} = \rho V = \frac{\rho \pi r^2 h}{1000} = \frac{4.51 \times \pi \times 1^2 \times 0.01}{1000} = 1.41 \times 10^{-4} \text{ kg}$$

In a similar fashion, for the soft tissue mass, the cell mass is 3.14×10^{-5} kg. A benchmark between theoretical calculations and numerical simulations is summarized in table 1.III.1. All the results are given for 1 source photon.

Figure 1.III.3 exhibits simulated kerma and absorbed dose profiles as a function of depth for the irradiated cylinder. In both layers of soft tissue, it is noteworthy that the dose gradually increases until it reaches the kerma and then it is superimposed on the decreasing curve of the kerma. The junction of kerma and dose profiles occurs at the depth holding electronic equilibrium conditions. However, same conclusion cannot be drawn for titanium because of the representation scale and the low depth at which these conditions hold true.

Overall, this profile shape depicts the fact that the electronic equilibrium depends on the type of material crossed by incident photons. Furthermore, it is worth noting that the increase in the simulated absorbed dose is almost exponential near the entrance face of titanium. This effect is not handled in the theoretical approach and is owing to the backscattering of secondary electrons set in motion in the previous layer of soft tissue. This finding is hugely significant when a high

TAB. 1.III.1 – Overview of the theoretical and numerical values for the absorbed dose and kerma.

	Theoretical	Numerical
$K^{\text{col}}(0)$	6.59×10^{-13} Gy	6.66×10^{-13} Gy
x for $D = K$ inside tissues	$x > 0.85$ cm	$x > 0.80$ cm
x for $D = K$ inside titanium	$x > 0.255$ cm	$x > 0.220$ cm
$K^{\text{col}}(2)$	6.0×10^{-13} Gy	6.4×10^{-13} Gy
	without $B(\mu x, E)$	with $B(\mu x, E)$
$K_{\text{Ti}}^{\text{col}}(2)/K_{\text{tm}}^{\text{col}}(2)$	0.84	0.85
$D_{\text{Ti}}(2)/D_{\text{tm}}(2)$	0.74	0.83

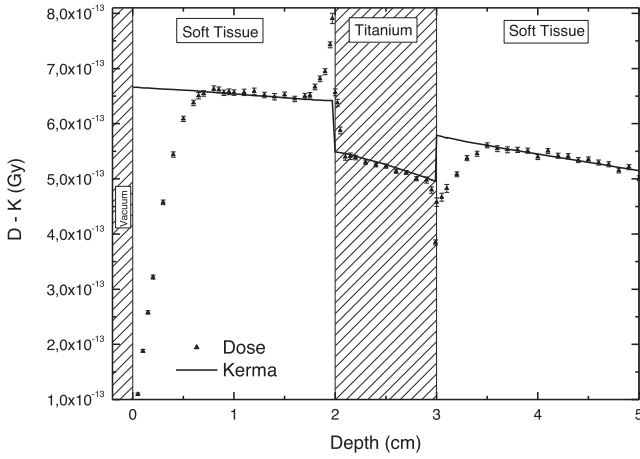


FIG. 1.III.3 – Kerma and dose profiles inside the irradiated cylinder, as a function of depth.

Z medium is located after a lower Z medium. This dose bump at the interface is handled by the new cavity model (see § 2.III about the LiF). This phenomenon can have a broad impact in radiotherapy, especially when human tissues of different densities follow one another in the irradiated area. Finally, the build-up factor in tissues can be calculated according to formula (3), by replacing the values found with numerical simulation.

$$B = \frac{K^{\text{col}}(2)}{K^{\text{col}}(0)} \exp\left(\left(\frac{\mu}{\rho}\right) \rho x\right) = \frac{6.4 \times 10^{-13}}{6.66 \times 10^{-13}} \exp(-4.895 \times 10^{-2} \times 1 \times 2) = 1.06$$

This factor is close to 1 and can be neglected for rough radioprotection calculations. However, for the metrology field of ionizing radiation, it has to be considered to better match reference measurements (refer to § 2.II and § 2.III).

Full input file:

```
Dose - Kerma calculation
C cell block
10 1 -1 -10 $ tissues: material 1 density -1
15 1 -1 -15
20 1 -1 -20
25 1 -1 -25
30 1 -1 -30
40 1 -1 -40
50 1 -1 -50
60 1 -1 -60
70 1 -1 -70
80 1 -1 -80
90 1 -1 -90
95 1 -1 -95
```


100	1	-1	-100	
105	1	-1	-105	
110	1	-1	-110	
120	1	-1	-120	
130	1	-1	-130	
140	1	-1	-140	
150	1	-1	-150	
160	1	-1	-160	
170	1	-1	-170	
180	1	-1	-180	
185	1	-1	-185	
190	1	-1	-190	
195	1	-1	-195	
200	1	-1	-200	
205	1	-1	-205	\$ end for tissues
210	2	-4.51	-210	\$ titanium: material 2 density 4.51
215	2	-4.51	-215	
220	2	-4.51	-220	
225	2	-4.51	-225	
230	2	-4.51	-230	
240	2	-4.51	-240	
250	2	-4.51	-250	
260	2	-4.51	-260	
270	2	-4.51	-270	
280	2	-4.51	-280	
290	2	-4.51	-290	
300	2	-4.51	-300	
310	2	-4.51	-310	\$ end for titanium
320	1	-1	-320	\$ tissues
330	1	-1	-330	
340	1	-1	-340	
350	1	-1	-350	
360	1	-1	-360	
370	1	-1	-370	
380	1	-1	-380	
390	1	-1	-390	
400	1	-1	-400	
410	1	-1	-410	
420	1	-1	-420	
430	1	-1	-430	
440	1	-1	-440	
450	1	-1	-450	
460	1	-1	-460	
470	1	-1	-470	
480	1	-1	-480	
490	1	-1	-490	
500	1	-1	-500	

```

510 1 -1 -510 $ end for tissues
520 1 -1 -520 10 15 20 25 30 40 50 60 70 80 90 100 110 &
95 105 120 130 140 150 160 170 180 185 190 195 200 205
535 2 -4.51 -535 210 215 220 225 230 240 250 &
260 270 280 290 300 310
530 1 -1 530 320 330 340 350 360 370 &
380 390 400 410 420 430 440 450 460 470 480 490 500 510 &
525 0 -525
550 0 520 530 535 525

```

C geometry block

```

10 RCC 0 0 0 0 0 0.01 1
15 RCC 0 0 .05 0 0 0.01 1
20 RCC 0 0 0.1 0 0 0.01 1
25 RCC 0 0 0.15 0 0 0.01 1
30 RCC 0 0 0.2 0 0 0.01 1
40 RCC 0 0 0.3 0 0 0.01 1
50 RCC 0 0 0.4 0 0 0.01 1
60 RCC 0 0 0.5 0 0 0.01 1
70 RCC 0 0 0.6 0 0 0.01 1
80 RCC 0 0 0.7 0 0 0.01 1
90 RCC 0 0 0.8 0 0 0.01 1
95 RCC 0 0 0.85 0 0 0.01 1
100 RCC 0 0 0.9 0 0 0.01 1
105 RCC 0 0 0.95 0 0 0.01 1
110 RCC 0 0 1 0 0 0.01 1
120 RCC 0 0 1.1 0 0 0.01 1
130 RCC 0 0 1.2 0 0 0.01 1
140 RCC 0 0 1.3 0 0 0.01 1
150 RCC 0 0 1.4 0 0 0.01 1
160 RCC 0 0 1.5 0 0 0.01 1
170 RCC 0 0 1.6 0 0 0.01 1
180 RCC 0 0 1.7 0 0 0.01 1
185 RCC 0 0 1.75 0 0 0.01 1
190 RCC 0 0 1.8 0 0 0.01 1
195 RCC 0 0 1.85 0 0 0.01 1
200 RCC 0 0 1.9 0 0 0.01 1
205 RCC 0 0 1.99 0 0 0.01 1
210 RCC 0 0 2 0 0 0.01 1
215 RCC 0 0 2.05 0 0 0.01 1
220 RCC 0 0 2.1 0 0 0.01 1
225 RCC 0 0 2.15 0 0 0.01 1
230 RCC 0 0 2.2 0 0 0.01 1
240 RCC 0 0 2.3 0 0 0.01 1
250 RCC 0 0 2.4 0 0 0.01 1
260 RCC 0 0 2.5 0 0 0.01 1
270 RCC 0 0 2.6 0 0 0.01 1
280 RCC 0 0 2.7 0 0 0.01 1
290 RCC 0 0 2.8 0 0 0.01 1

```



```

DBCN 17j 2 3j
stop F8 .005
c print 85 for the estep value
print 85

```

File 1.III.1

1.IV Calculation of the Ambient Dose Equivalent Rate in a Uniformly Contaminated Pipe

Abstract:

For this application, the ambient equivalent dose rate within a pipe of which the inner wall is uniformly contaminated by several radionuclides is calculated. The close-form solution of this classic problem of external exposure is discussed below and compared to the numerical result.

Objectives:

- Application of the analytical form for the fluence and ambient equivalent dose.
- Analytical and numerical calculations of the ambient equivalent dose rate for a surface contamination.

Characteristics:

The inner wall of the pipe is uniformly contaminated with ^{60}Co (30% of the total activity) and ^{137}Cs (70% of the total activity). The total activity of the two contaminants is 1 GBq. Observer O is located along the axis of the cylinder at a distance $L_1 = 5$ m of one of its bases. The radius and the length of the cylinder are, respectively, $R = 1.5$ m and $H = 15$ m (see figure 1.IV.1). In what follows, the ambient equivalent dose rate at the observer is calculated.

The analytical and numerical solutions of this classical problem are highly based on those detailed in § 1.I about the disk-shaped source.

Part 1: Analytical Calculation

The surface flux related to the internal contamination of the cylinder is the ratio between the total flux and the surface of the cylinder:

$$n_s = \frac{\dot{N}_\gamma}{S} = \frac{\dot{N}_\gamma}{2\pi RH}$$

By dividing the inner surface of the pipe into tiny units of area dS , each of them is considered as a point-like object from the observer. The flux emitted by each

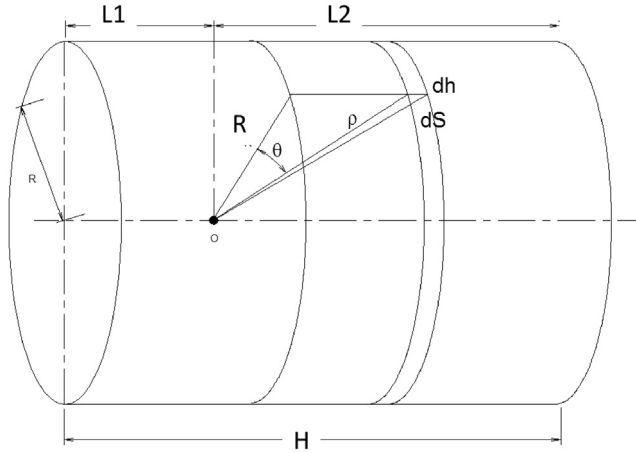


FIG. 1.IV.1 – Uniformly contaminated cylinder, with an observer located inside.

subsequent element is $n_s dS$. Therefore, for a point source emitting a flux $n_s dS$, the differential fluence at a distance ρ is:

$$d\dot{\Phi} = \frac{n_s}{4\pi\rho^2} dS$$

The total fluence of the inner wall is obtained by solving the double integral of the differential fluence over the whole surface of the source:

$$\Phi = \iint_s \frac{n_s}{4\pi\rho^2} dS \tag{1}$$

Considering R as a constant, the unit of area can be expressed as a function of an infinitesimal variation of the variable h :

$$dS = 2\pi R dh$$

The differential element dh and the distance ρ is expanding in terms of the variables R and θ :

$$R \tan \theta = h \stackrel{\text{by deriving}}{\iff} \frac{R}{\cos^2 \theta} d\theta = dh \tag{2}$$

$$\rho = \frac{R}{\cos \theta} \tag{3}$$

By substituting expressions (2) and (3) in form (1), it follows:

$$d\dot{\Phi} = \frac{n_s 2\pi R}{4\pi\rho^2} dh = \frac{n_s 2\pi R}{4\pi \left(\frac{R}{\cos \theta}\right)^2} \left(\frac{R}{\cos^2 \theta} d\theta\right) = \frac{n_s}{2} d\theta$$

The integral of $d\Phi$ over the whole pipe gives:

$$\dot{\Phi} = \frac{n_s}{2} \int_{\theta_{\min}}^{\theta_{\max}} d\theta = \frac{\dot{N}_\gamma}{4\pi RH} \left(\arctan\left(\frac{L_2}{R}\right) + \arctan\left(\frac{L_1}{R}\right) \right)$$

with the angular bounds:

$$\theta_{\min} = -\arctan\left(\frac{L_1}{R}\right) \text{ and } \theta_{\max} = \arctan\left(\frac{L_2}{R}\right)$$

^{60}Co emits two photons of 1.17 and 1.33 MeV with 100% emission intensity for each of the two. ^{137}Cs emits a 662 keV photon of 85% intensity. For a 1 GBq activity split into 30% of ^{60}Co and 70% of ^{137}Cs , the total flux is:

$$\dot{N}_t = \dot{N}_{\text{Co}} + \dot{N}_{\text{Cs}} = 1 \times 10^9 \times ((0.3 \times 2) + (0.7 \times 0.85)) = 1.195 \times 10^9 (\gamma) \cdot \text{s}^{-1}$$

The resulting total fluence rate at the observer within the pipe is:

$$\dot{\Phi}_t = \frac{1.195 \times 10^9}{4\pi \times 150 \times 1500} \left(\arctan\left(\frac{10}{1.5}\right) + \arctan\left(\frac{5}{1.5}\right) \right) = 1142 (\gamma) \text{s}^{-1} \text{cm}^{-2}$$

Note that the $\arctan\theta$ term is expressed in radians (SI unit). For this case study, the ambient equivalent dose rate is expanded as follows:

$$\dot{H}^*(10) = \frac{A}{4\pi RH} \left(\arctan\left(\frac{L_2}{R}\right) + \arctan\left(\frac{L_1}{R}\right) \right) \sum_k (\%)_k \sum_E \Gamma_{k,E} h_{\Phi}^*(10)_E$$

where the term $(\%)_k$ represents the part of the total activity from contaminant k and $\Gamma_{k,E}$ stands for the intensity of the emission line E . For the ambient equivalent dose rate, it is necessary to determine prior the “fluence – ambient equivalent dose” conversion factors at the energy of photons emitted by both contaminants, given by the ICRP (1996) (see section 1.II). These factors are $h_{\Phi}^*(10)_{0.662} = 3.75 \text{ pSv} \cdot \text{cm}^2$, $h_{\Phi}^*(10)_{1.17} = 5.9 \text{ pSv} \cdot \text{cm}^2$ and $h_{\Phi}^*(10)_{1.33} = 6.35 \text{ pSv} \cdot \text{cm}^2$ and lead to the ambient equivalent dose rate below:

$$\dot{H}^*(10) = 1 \times 10^{-12} \times 3600 \times \left[\frac{1 \times 10^9}{4\pi \times 150 \times 1500} \right] \times \left(\arctan\left(\frac{10}{1.5}\right) + \arctan\left(\frac{5}{1.5}\right) \right) \times ((0.7 \times 3.75 \times 0.85) + (0.3 \times 5.9 \times 1) + (0.3 \times 6.35 \times 1))$$

$$\dot{H}^*(10) = 2 \times 10^{-5} \text{ Sv} \cdot \text{h}^{-1} (20 \mu\text{Sv} \cdot \text{h}^{-1})$$

Part 2: Numerical Calculation

For this problem, the numerical modelling requires a non-trivial source definition. A well-suited method consists in simulating an envelope of 0.1 mm thickness, covering the surface of the pipe, for the internal contamination. In the input file below, the line “si2 150 150.01” related to the “rad” card of the “sdef”, handles this

surface definition. For the probability of the starting energy for the multi-lines emission, ratio r_E of the number of photons emitted to the total flux is drawn up, in similar manner as in application 1.II. This ratio for contaminant k and energy E , is the total activity A multiplied by terms $(\%)_k$ and $\Gamma_{k,E}$:

$$r_{k,E} = \frac{N_{k,E}}{\dot{N}_t} = A \frac{(\%)_k \Gamma_{k,E}}{\dot{N}_t}$$

Therefore, for the ^{137}Cs energy, this ratio is:

$$r_{0.662} = \frac{N_{0.662}}{\dot{N}_t} = \frac{1 \times 10^9 \times 0.7 \times 0.85}{1.195 \times 10^9} = 0.497$$

For the 30% of ^{60}Co and the two emission lines, ratios are:

$$r_{1.17} = r_{1.33} = \frac{N_{1.17}}{\dot{N}_t} = \frac{1 \times 10^9 \times 0.3 \times 1}{1.195 \times 10^9} = 0.251$$

These ratios are then set in the “sp1” card for the definition of the “erg” card, related to the probability of the starting energy of photons. Tallies 5 and 15 provide, respectively, the fluence per emitted photon (Φ/N_γ) and the ambient equivalent dose per emitted photon to the observer ($H^*(10)/N_\gamma$).

```
Ambient equivalent dose rate in a uniformly contaminated pipe
c cell block
10 1 -1.3e-3 -10    $ inside pipe air
20 1 -1.3e-3 -15 10 $ source
30 0 15            $ outside pipe

10 RCC -500 0 0 1500 0 0 150 $ interior of the pipe
15 RCC -500 0 0 1500 0 0 150.01 $ pipe wall

imp:p 1 1 0
M1 7014 .781 8016 .212 7015 .007 $ air
mode p
SDEF pos 0 0 0 cel 20 par=p erg=d1 rad D2 ext D3 axs 1 0 0
SI1 L 1.17 1.33 .662 $ discrete energy (MeV) of Co-60 and Cs-137
SP1 .251 .251 .497 $ intensity per energy
SI2 150 150.01 $ source wall
SP2 -21 1
SI3 -500 1000 $ source in length from -L1 (500) to L2 (1000)
SP3 -21 0
F5:p 0 0 0 .1 $ photons fluence at 0, see figure
F15:p 0 0 0 .1 $ photons equivalent dose at 0
c fluence-to-equivalent dose conversion coefficient
c DE: energy
DE15 0.01 0.015 0.02 0.03 0.04 0.05 0.06 0.08 0.1 0.15 0.2 0.3 0.4 &
0.5 0.6 0.8 1 1.5 2 3 4 5 6 8 10
```

```

c DF: H*(10)/phi pSv.cm2 from IRCP 74
DF15 7.2 3.19 1.81 0.9 0.62 0.5 0.47 0.49 0.58 0.85 1.15 1.8 2.38 &
2.93 3.44 4.38 5.2 6.9 8.6 11.1 13.4 15.5 17.6 21.6 25.6
stop F15 .002

```

File 1.IV.1

Below, the results after the computation are displayed:

tally				5	tally				15	
nps	mean	error	vov	slope	fom	mean	error	vov	slope	fom
576000	9.5303E-07	0.0020	0.0615	2.6	4959383	4.6431E-06	0.0020	0.1094	2.5	5086648

Thus, the fluence rate derived from the photon flux analytically calculated in the previous section is:

$$\dot{\Phi} = \left(\frac{\Phi}{N_\gamma} \right) \dot{N}_\gamma = 9.53 \times 10^{-7} \times 1.19 \times 10^9 = 1139 (\gamma).s^{-1}.cm^{-2}$$

The equivalent dose ambient rate is:

$$\begin{aligned} \dot{H}^*(10) &= \left(\frac{H^*(10)}{N_\gamma} \right) \dot{N}_\gamma = 4.64 \times 10^{-6} \times 1 \times 10^{-12} \times 1.19 \times 10^9 \times 3600 \\ &= 2.10^{-5} Sv.h^{-1} (20 \mu Sv.h^{-1}) \end{aligned}$$

The results found for these quantities are consistent with those determined analytically in the previous section.

1.V Calculation of the in-Depth Absorbed Dose for β Spectra

Abstract:

This problem proposes to calculate the in-depth absorbed dose for β spectra in a water phantom, seen as tissue-equivalent. In a first section, semi-empirical and numerical models are detailed for calculation with a ^{90}Y point-source in contact with the inlet face of the phantom. In a second part are detailed the results of the first section which lead to obtaining dose equivalent to extremities $H'(0.07)$ for this point-source. In the last section, calculations are achieved for a 50 cm^2 surface contamination for the same radionuclide.

Objectives:

- Semi-empirical calculation of the in-depth absorbed dose for β particles relying on two different models: a fairly simple one that approximates about a part of the maximum range of β particles and a complex accurate one that assesses the actual range.
- Numerical calculation of the absorbed in-depth dose for β spectra.
- Calculation of the absorbed dose with a 3D-mesh in MCNP.
- Semi-empirical and numerical calculations of a dose equivalent to extremities for a β point source.

The β -delivered in-depth absorbed dose calculation is commonly approximated by a simple semi-empirical formula function of the particle fluence. The limited assumptions of this approach only lead to a rough estimation of the absorbed dose profile as a function of the thickness of material crossed through. In what follows, we propose a semi-empirical approach from Cross (1997), which makes it possible to fit well this profile for a point and disk-shaped source.

Part 1: Absorbed Dose Profile for a Point Source

(a) Simplified semi-empirical model

In most of literature devoted to external dosimetry, the simplified expression of the absorbed dose at depth x related to a point source emitting a β spectrum is the following:

$$D_{\beta}(x) = \left(\frac{\bar{S}}{\rho}\right)_{\text{col}} \Phi_{\beta}(x)$$

with (\bar{S}/ρ) the mass stopping power for the mean energy of the original β spectrum. Although crossing the material changes the electron energy spectrum, this approach implies a constant mean energy along the range, therefore constituting a bias on the result reliability. Also, the absorbed dose calculated by the equation of this model varies in depth only as a function of the β fluence. According to this simplified model, the fluence undergoes attenuation described by a single decreasing exponential on the whole range as written below:

$$D_{\beta}(x) = \left(\frac{\bar{S}}{\rho}\right)_{\text{col}} \Phi_{\beta}(x) \exp(-vx); \text{ for water } v = \frac{18.6}{(\beta E_{\text{max}} - 0.036)^{1.37}}$$

with $\Phi_{\beta}(x)$ the β fluence at depth x and v the attenuation coefficient of the β fluence. Thus, for a point source in contact with the phantom, the absorbed dose per incident β at depth x can be expressed as follows:

$$D_{\beta}(x) = \left(\frac{\bar{S}}{\rho}\right)_{\text{col}} \frac{1}{4\pi x^2} \exp(-vx)$$

For ^{90}Y , the maximum energy of the original spectrum is $E_{\beta_{\text{max}}} = 2.28$ MeV (data drawn from RADAR, The Radiation Dose Assessment Resource,

<http://www.doseinfo-radar.com/>) and the attenuation coefficient ν is equal to (Loevinger *et al.*, 1956):

$$\nu = \frac{18.6}{(2.28 - 0.036)^{1.37}} = 6.15 \text{ cm}^2 \cdot \text{g}^{-1}$$

The mean mass stopping power (\bar{S}/ρ) for ^{90}Y is about $2 \text{ MeVg}^{-1}\text{cm}^2$ (ESTAR NIST tables). When weighting by the coefficient allowing the conversion from $\text{MeV}\cdot\text{Kg}^{-1}$ to Gy, *i.e.*, $1.602 \times 10^{-10} \text{ Gy}\cdot\text{MeV}^{-1}\cdot\text{Kg}$, the simplified expression of the dose, per β emitted by the source, under thickness x of water is equal to:

$$D_{\beta}(x) = \frac{2.55 \times 10^{-11}}{x^2} \exp(-6.15x) \quad (1)$$

We recall that the absorbed dose profile described by this standard model is approximate, owing to both simplifying assumptions mentioned above (see figure 1.V.2).

(b) Cross semi-empirical model

Cross (1997) suggested semi-empirical expressions corresponding to different range intervals for a β point source in a semi-infinite medium. These expressions lead to a well fit of the absorbed dose profile on the whole range. They are given hereinafter, for three depth intervals.

$$D_{\beta}(x) = \begin{cases} \frac{k}{(\nu x)^2} [c - \nu x \exp(1 - (\frac{\nu x}{c})) + \nu x \exp(1 - \nu x) - a] & \text{if } x \leq \frac{c}{\nu} \\ \frac{k}{(\nu x)^2} [\nu x \exp(1 - \nu x) - a] & \text{if } \frac{c}{\nu} < x < R_p \\ 0 & \text{if } x > R_p \end{cases} \quad (2)$$

The attenuation coefficient ν , given in cm^2g^{-1} , depends on the material crossed through. For water, it can be expressed as a function of the maximum energy of the β spectrum as follows:

$$\nu = 17.24(E_{\beta\text{max}})^f \quad \text{with } f = -1.401 + 0.1186 \ln(E_{\beta\text{max}})$$

The c parameter depends on the β maximum energy, the spectrum shape, depending on whether it is a classic Maxwellian spectrum or a multi-component spectrum, and finally on the particle type, *i.e.*, electron or positron:

$$c = \begin{cases} 1.349 - 0.416 \ln(E_{\beta\text{max}}) & \text{simple spectrum} \\ 1.637 - 0.496 \ln(E_{\beta\text{max}}) & \text{multi - component spectrum} \\ 1.135 - 0.1086 \ln(E_{\beta\text{max}}) - 0.086(\ln(E_{\beta\text{max}}))^2 & \text{positrons} \end{cases}$$

The practical range R_p to describe the validity interval of expressions (2) derives from the maximum range R_{max} of β particles in the considered material according to:

$$R = 0.74 R_{\text{max}}$$

The latter is used to write the a parameter of the two first expressions of (2):

$$a = \nu R_p \exp(1 - \nu R_p)$$

The dose factor k , in Gy, is expressed as a function of the initial mean energy of the β spectrum and an empirical parameter α by means of the following expression:

$$k = 1.602 \times 10^{-10} \left(\frac{v^3 \bar{E}_\beta \alpha}{4\pi\rho} \right)$$

The α parameter is obtained from the v , c and R_p parameters with the following formula:

$$\alpha = \left[3c^2 - (c^2 - 1)\exp(1) - \left(1 + vR_p + v^2R_p^2 \right) \exp(1 - vR_p) \right]^{-1}$$

For ^{90}Y , the mean energy is calculated from the histogram spectrum given in figure 1.V.1 (data from RADAR) as the following weighted average:

$$\bar{E}_\beta = \frac{\sum_i E_i N(E_i)}{\sum_i N(E_i)} = 0.93 \text{ MeV}$$

Note that this mean energy is almost equal to the third of the maximum energy, which corresponds to the theoretical and classic fraction for a Maxwellian spectrum. For water, parameter c and attenuation coefficient v are:

$$c = 1.349 - 0.416 \ln(2.28) = 1.006$$

$$f = -1.401 + 0.1186 \ln(2.28) = -1.303 \Rightarrow v = 17.24 \times (2.28)^{-1.303} = 5.9 \text{ cm}^2 \cdot \text{g}^{-1}$$

For the calculation of the maximum range of electrons, the empirical expressions of Katz and Penfold (1952) can be used:

$$R_{\max} = 0.412 (E_{\beta_{\max}})^n \text{ with } n = 1.265 - 0.0954 \ln(E_{\beta_{\max}})$$

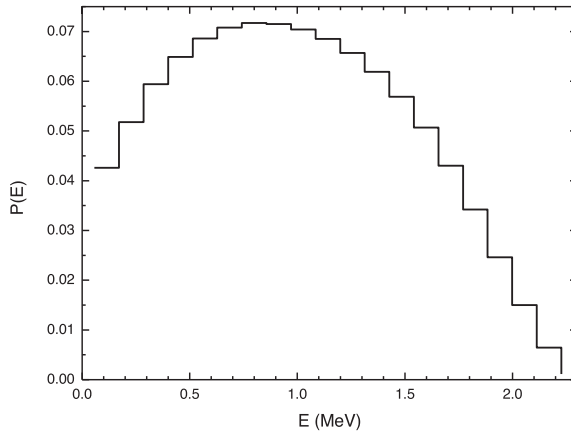


FIG. 1.V.1 – β spectrum of ^{90}Y (data from RADAR).

Therefore, for ^{90}Y it follows:

$$n = 1.265 - 0.0954 \ln(2.28) = 1.19 \Rightarrow R_{\max} = 0.412 \times (2.28)^{1.19} = 1.094 \text{ g.cm}^{-2}$$

With water density, it corresponds to a depth of 1.094 cm.

The practical range R_p obtained with this maximum range is:

$$R_p = 0.74 \times 1.094 = 0.81 \text{ cm}$$

Then, it becomes:

$$a = 5.9 \times 0.87 \times \exp(1 - (5.9 \times 0.81)) = 0.11$$

$$\alpha = \left[3 \times (1.006)^2 - \left((1.006)^2 - 1 \right) \exp(1) - (1 + (5.9 \times 0.8) + (5.9^2 \times 0.8^2)) \exp(1 - 5.9 \times 0.8) \right]^{-1} = 0.426$$

The dose factor k is equal to:

$$k = 1.602 \times 10^{-10} \left(\frac{5.9^3 \times 0.93 \times 0.426}{4\pi \times 1} \right) = 1.04 \text{ nGy}$$

Finally, the absorbed dose in nGy per source β of ^{90}Y for each of the three depth intervals is:

$$D_\beta(x) = \begin{cases} \frac{1.04}{(5.9x)^2} \left[1.006 - 5.9x \exp\left(1 - \left(\frac{5.9x}{1.006}\right)\right) + 5.9x \exp(1 - (5.9x)) - 0.11 \right] & \text{if } x \leq 0.17 \\ \frac{1.04}{(5.9x)^2} \left[5.9x \exp(1 - (5.9x)) - 0.11 \right] & \text{if } 0.17 < x < 0.8 \\ 0 & \text{if } x > 0.8 \end{cases} \quad (3)$$

These expressions lead to a dose profile, normalized per source β , displayed in figure 1.V.2. In this figure, the profile from expression (1) of the simplified approach is also plotted.

Figure 1.V.2 reveals a good agreement between the simplified and the cross models roughly beyond 5% of the maximum range R_{\max} while a shift in curves occurs above. At 80% of R_{\max} the Cross profile drops abruptly to reach the practical range R_p while the simplified model curve decreases linearly to run into R_{\max} .

(c) Numerical calculation

In this section, we propose to assess the absorbed dose profile using a 3D mesh grid. This calculation is developed with a *rectangular mesh-tally* as shown in figure 1.V.3. The “cora” card handles the x coordinates, “corb” the y coordinates and “corc” the z coordinates.

In each voxel, it is then possible to calculate the energy deposit using the “pedep” card. The result of each voxel is provided in MeV.cm^{-3} . In the problem, the absorbed

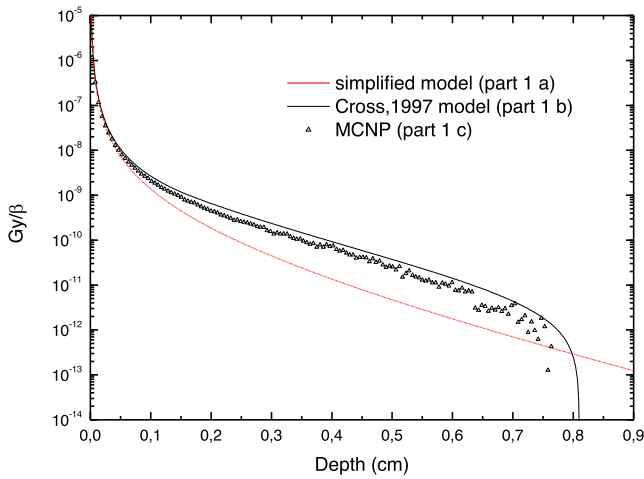


FIG. 1.V.2 – Absorbed dose profile for β of ^{90}Y , from simplified and Cross models and numerical calculation.

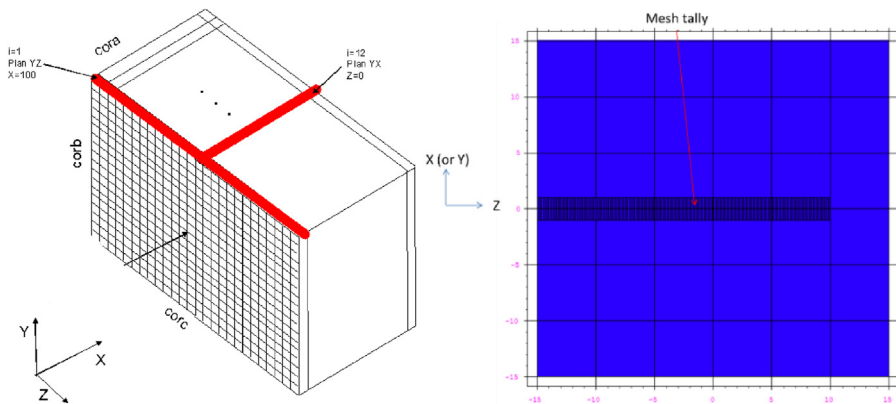


FIG. 1.V.3 – (left) Mesh size for the problem, (right) Sketch of general parameters for a rectangular mesh-tally.

dose is assessed in a sequence of 200 virtual cells of $50\ \mu\text{m}$ by $50\ \mu\text{m}$, filling a 1.2 cm long rectangular parallelepiped. The depth of 1.2 cm is substantially equal to the maximum range of the β spectrum. The central axis of the mesh grid passes through the point source and is perpendicular to the inlet face of the phantom. The ^{90}Y spectrum is described in the following file by the “*si2*” and “*sp2*” cards.

```

beta dose
c cell block
10 1 -1 -10 $ water cube
30 0          -30 10 $ scoring cell
40 0 30

10 RPP -6 6 -6 6 -15 -12 $ water
30 RPP -20 20 -20 20 -20 20 $ outside water

imp:e 1 1 0
mode e
sdef par=e pos 0 0 -15 erg d2
c Y90 spectrum
# SI2 SP2
0 0
0.0571  4.26E-02
0.1713  5.18E-02
0.2855  5.94E-02
0.3997  6.49E-02
0.5139  6.86E-02
0.6281  7.08E-02
0.7423  7.17E-02
0.8565  7.15E-02
0.9707  7.04E-02
1.0849  6.85E-02
1.1991  6.57E-02
1.3133  6.19E-02
1.4275  5.69E-02
1.5417  5.07E-02
1.6559  4.30E-02
1.7701  3.42E-02
1.8843  2.46E-02
1.9985  1.50E-02
2.1127  6.43E-03
2.2269  1.13E-03
tmesh
RMESH1:e pedep
coral -.005 .005 $ one cell 50x50 µm in x
corbl -.005 .005 $ one cell 50x50 µm in y
corcl -15 200i -13.8 $ 200 cells in z
endmd
M1 1000 2 8000 1
ctme 200

```

File 1.V.1

The $\text{MeV}\cdot\text{cm}^{-3}$ unit corresponds to $\text{MeV}\cdot\text{g}^{-1}$ at the water density. The results have to be weighted by the coefficient enabling the conversion from $\text{MeV}\cdot\text{g}^{-1}$ to Gy, *i.e.*, $1.602 \times 10^{-10} \text{ Gy}\cdot\text{MeV}^{-1}\cdot\text{g}$. The profiles defined from MCNP and drawn from

the semi-empirical expressions (2) are plotted in figure 1.V.2b. One can note a quasi-overlay of the two curves, confirming the accuracy of the Cross semi-empirical model, 1997 (see figure 1.V.2).

Part 2: Calculation of the Dose Equivalent to the Extremities $H'(0.07)$ for the Point-Source

The Cross semi-empirical model allows calculating the dose equivalent to the extremities $H'(0.07)$ for a β point source in contact with the skin. We get this quantity by multiplying the absorbed dose under $70 \mu\text{m}$ by the quality factor Q equal to 1 for electron:

$$H'(0.07) = Q D_{\beta}(0.07) = D_{\beta}(0.07)$$

For this calculation, as $x < c/v$ since $0.07 < 0.17$, the first expression of (3) is used:

$$\begin{aligned} H'(0.07) &= \frac{1.04}{(5.9 \times 0.007)^2} \left[1.006 - (5.9 \times 0.007) \exp\left(1 - \left(\frac{5.9 \times 0.007}{1.006}\right)\right) \right. \\ &\quad \left. + (5.9 \times 0.007) \exp(1 - (5.9 \times 0.007)) - 0.11 \right] \\ &= 0.547 \mu\text{Sv} \cdot (\beta)^{-1} \end{aligned}$$

With MCNP, the calculation providing this result is done using the energy deposit estimator “*F8” in a quasi-point sphere located at a depth of $70 \mu\text{m}$ after the inlet face of the water phantom (refer to cell 20 in the following input file).

```
beta dose
c cell block
10 1 -1 -10 20 $ water cube
20 1 -1 -20 $ scoring cell
30 0          -30 10
40 0 30

10 RPP -6 6 -6 6 0 3
20 SZ 0.007 .001
30 RPP -6 6 -6 6 -.001 3.0001

imp:e 1 1 1 0
mode e
sdef par=e pos 0 0 0 erg d2
c Y90 spectrum
# SI2 SP2
0 0
0.0571 4.26E-02
0.1713 5.18E-02
0.2855 5.94E-02
```

```

.
.
1.9985  1.50E-02
2.1127  6.43E-03
2.2269  1.13E-03
*F8:e 20
M1 1000 2 8000 1
stop F8 .001

```

File 1.V.2

The mean energy $\bar{\epsilon}$ deposited in the sphere, per β is given by the tally result of the output file:

*F8 = 1.412×10^{-5} MeV with a relative uncertainty of 0.1%. It is convenient to divide it by the sphere mass, m_{sph} , in order to yield a mean absorbed dose in the sphere:

$$H'(0.07) = D_{\beta}(0.07) = \frac{\bar{\epsilon}}{m_{\text{sph}}} = \frac{\bar{\epsilon}}{\rho V_{\text{sph}}} = \frac{\bar{\epsilon}}{\rho(4/3)\pi r^3}$$

By multiplying the previous result by a factor 1.602×10^{-13} , the conversion of MeV to J and the g to kg is made. The final normalized result is:

$$H'(0.07) = 1.602 \times 10^{-13} \times \frac{1.412 \times 10^{-5}}{1 \times (4/3) \times \pi \times (0.001)^3 \times 10^{-3}} = 0.534 \mu\text{Sv} \cdot (\beta)^{-1}$$

As a result, the semi-empirical model and MCNP are consistent and differ only with a small deviation of 2.4%.

Part 3: Absorbed Dose Profile for a Surface Contamination

We propose in this third part to assess the absorbed dose profile inside the water phantom for a skin surface contamination.

(a) Semi-empirical calculation (Bourgeois, 2011)

We assume that the surface contamination of 50 cm^2 is uniformly distributed on the skin and can be simulated by a disk-shaped source of radius $r_d = 4 \text{ cm}$. Figure 1.V.4 displays the calculation geometry with variables used.

With the Point-Kernel method, the absorbed dose at depth x is calculated with the following dual integral:

$$D_s(x) = \iint_S D_{\beta}(\rho) dS = 2\pi \int_x^{R_{\text{max}}} \rho D_{\beta}(\rho) d\rho$$

where $D_{\beta}(\rho)$ corresponds to expression (2) of the absorbed dose for a point-source,

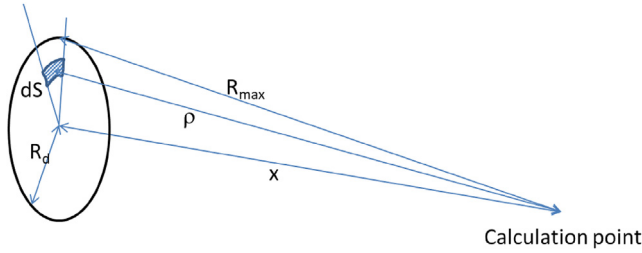


FIG. 1.V.4 – Geometry used for the calculation of the depth dose due to a surface contamination of the skin.

the dual integral calculation provides the absorbed dose for the three range intervals. For practical purposes, the result is expressed hereafter as Gy per β emitted per cm^2 of the source:

$$D_s(x) = \begin{cases} \frac{2\pi k}{v^2} \left[c(1 - \exp(1 - \frac{vx}{c}) - \ln(\frac{vx}{c})) \right. \\ \quad \left. + \exp(1 - vx) - \exp(1 - vR) - a \ln(\frac{R}{x}) \right] & \text{if } x \leq \frac{c}{v} \\ \frac{2\pi k}{v^2} \left[\exp(1 - vx) - \exp(1 - vR) - a \ln(\frac{R}{x}) \right] & \text{if } \frac{c}{v} < x < R \\ 0 & \text{if } x > R \end{cases} \quad (4)$$

The parameters and coefficients used in (4) are identical to those described in the first section for ^{90}Y .

(b) Numerical calculation

The absorbed dose profile is simulated in similar fashion as for the point-source with a disk-shaped source. This source is defined with a uniform radial sampling scheme from 0 to 4 cm, specified with the “*si1*” in Block 3.

```
Beta dose disk-shaped source
c cell block
10 1 -1 -10
30 0          -30 10
40 0 30

10 RPP -6 6 -6 6 -15 -12
30 RPP -20 20 -20 20 -20 20

imp:e 1 1 0
mode e
sdef par=e pos 0 0 -15 axs 0 0 1 ext 0 rad=d1 erg d2
Si1 0 4 $ S=50 cm2
sp1 -21 1
c Y90 spectrum
# SI2 SP2
```

```

0 0
0.0571 4.26E-02
0.1713 5.18E-02
0.2855 5.94E-02
.
.
1.9985 1.50E-02
2.1127 6.43E-03
2.2269 1.13E-03
tmesh
RMESH1:e pedep
coral -.5 .5
corbl -.5 .5
corcl -15 200i -13.9
endmd
M1 1000 2 8000 1
ctme 1000

```

File 1.V.3

As well as for the point source, it is convenient to multiply the results by $1.602 \times 10^{-10} \text{ GyMeV}^{-1}\text{Kg}$. Figure 1.V.5 shows the absorbed dose profiles as a function of depth overall for the numerical calculation and semi-empirical expression (4). As specified above, on this graph, the absorbed dose is normalized in Gy per β emitted per cm^2 of the source.

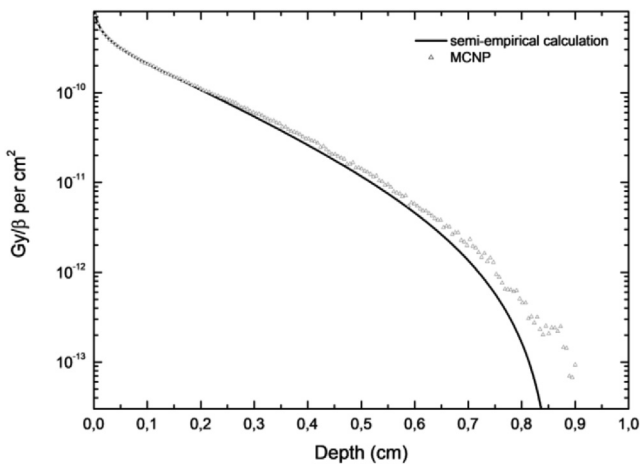


FIG. 1.V.5 – Absorbed dose profiles as a function of depth for the β surface contamination, for the numerical simulation and the Cross semi-empirical expression.

Up to half the β maximum range, a slight overestimation is observed with the numerical calculation. Above, the Cross model exhibits a significantly inflected profile compared to the MCNP calculation.

1.VI Calculation of the Absorbed Dose Profile to Water for 170 MeV Protons

Abstract:

In this section, a calculation of the absorbed dose profile to water for 170 MeV protons is undertaken. Such energy is typically used for treatments by proton therapy. The first part draws upon the 1997 work of Bortfeld, to suggest an analytical formulation of the absorbed dose as a function of depth and to determine the resulting profile.

The second part aims to describe the numerical simulation of the absorbed dose to water and to compare the results with those obtained in the first part.

The absorbed dose and then the directional equivalent dose under $70 \mu\text{m}$ at a zero angle of incidence are determined analytically and numerically in the third part.

Objectives:

- Analytical calculation of the absorbed dose to water as a function of the depth for protons.
- Tracking of the different particles set in motion throughout nuclear interactions using MCNP.
- Creation of a mesh for the absorbed dose with MCNP.
- Determination of the mass stopping power at any point of a light ion range by means of the MCNP card “ft let”.
- Representation of a microdosimetric spectrum using the MCNP card “ft let”.
- Calculation of the operational quantity: directional equivalent dose under $70 \mu\text{m}$ for light ions.

Part 1: Analytical Calculation of the Absorbed Dose to Water as a Function of Depth

(a) Expression of the absorbed dose per unit fluence as a function of depth

Unlike for the electrons, a new dosimetric quantity must be defined when considering protons. It takes into account nuclear interactions of protons in the medium as well as coulomb interactions. This quantity is referred to as the “terma” and translates the total energy release per unit mass at depth z . It is expressed in terms of $\Phi(z)$, the protons fluence at depth z and $E(z)$, the proton energy at depth z , as:

$$T(z) = -\frac{1}{\rho} \left[\Phi(z) \frac{dE(z)}{dz} + \frac{1}{\rho} \frac{d\Phi(z)}{dz} E(z) \right]$$

The left term represents the energy loss by coulomb interaction. It is interesting to note that this term can be compared with $\Phi(z)(S/\rho)_z$, where $(S/\rho)_z$ is the mass stopping power of protons at z . The right term describes the released energy during inelastic nuclear interactions of protons at the same point. It is necessarily expressed as a function of the protons fluence decrease at depth z , given by $d\Phi(z)/dz$. If we consider γ to be the locally absorbed fraction of the released energy during these nuclear interactions, then the absorbed dose at z can be estimated by:

$$\left| \widehat{D}(z) \right| = \left(\frac{S}{\rho} \right)_z \Phi(z) + \gamma \frac{1}{\rho} \frac{d\Phi(z)}{dz} E(z) \quad (1)$$

Typically, 60% of this energy is locally deposited (Berger, 1993). Also, for further calculations we will assume that $\gamma = 0.6$. An empirical formula enables to determine the proton range in water:

$$R_0 = \alpha E_0^p \quad (2)$$

with $\alpha \approx 2.2 \times 10^{-3}$, $p \approx 1.77$ (ICRU, 1993) and E_0 expressed in MeV. It is possible to write $(S/\rho)_z$ in expression (1) as a function of R_0 and z from the expression of range (2). This semi-empirical approach overcomes the fact that the integration of the Bethe-Block formula is not solvable. Similarly, for the right term, Lee *et al.* (1993), suggested a proportional relationship between $\Phi(z)$ and the quantities R_0 and z . However, it should be borne in mind that the energy absorbed in the medium at a given depth z is not flat but obeys a gaussian distribution. This is even more significant at the Bragg maximum, of which the widening explains the values calculated with expression (2) beyond the range R_0 . To improve the dose evaluation, one has to convolve the dose estimation given by (1) with a gaussian distribution with a standard deviation σ :

$$D(z) = \frac{1}{\sqrt{2\pi}\sigma} \int_{-\infty}^{R_0} \widehat{D}(z) \exp \left[-\frac{(z-\bar{z})^2}{2\sigma^2} \right] d\bar{z} \quad (3)$$

The solution for this integral is not trivial and it is only used in the depth interval $R_0 - 10\sigma \leq z \leq R_0 + 5\sigma$. Figure 1.VI.1 shows the change made by this convolution for 150 MeV protons.

Below $R_0 - 10\sigma$, the effect of the convolution with the gaussian distribution is tenuous and the development of the dose approximation $\widehat{D}(z)$ as a function of R_0 and z is reasonable. Thus, the dose depending on the depth can be calculated as following:

$$\begin{cases} \widehat{D}(z) & \text{for } z < R_0 - 10\sigma \\ D(z) & \text{for } R_0 - 10\sigma \leq z \leq R_0 + 5\sigma \end{cases}$$

Expressions (4) and (5) below correspond to semi-empirical relations with several constant terms (Bortfeld, 1997). Inside the two expressions in square brackets, the left term stands for the fraction related to coulomb scattering and the right term expresses the fraction associated with inelastic nuclear reactions.

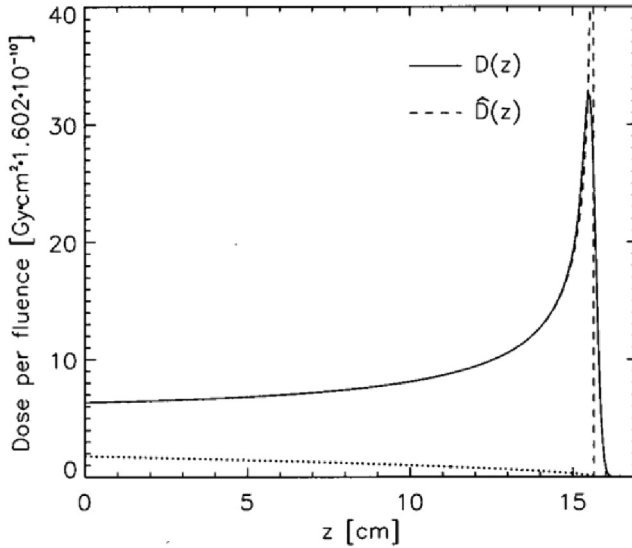


FIG. 1.VI.1 – Bragg curves with and without a gaussian distribution for 150 MeV protons in water. The dashed oblique line in the lower part of the graph represents the contribution to the dose due to the fraction of protons undergoing interaction, according to Bortfeld (1997).

$$\widehat{D}(z) = \frac{\Phi_0}{1 + 0.012R_0} \left[17.93(R_0 - z)^{-0.435} + \left(0.444 + \frac{31.7\epsilon}{R_0} \right) (R_0 - z)^{0.565} \right] \quad (4)$$

$$D(z) = \Phi_0 \frac{\sigma^{0.565}}{1 + 0.012R_0} \exp\left(-\frac{(R_0 - z)^2}{4\sigma^2}\right) \left[\frac{11.26}{\sigma} \mathcal{D}_{-0.565}\left(-\frac{R_0 - z}{\sigma}\right) + \left(0.157 + \frac{11.26\epsilon}{R_0} \right) \mathcal{D}_{-1.565}\left(-\frac{R_0 - z}{\sigma}\right) \right] \quad (5)$$

In these expressions, the parameter ϵ corresponds to the fraction of the initial fluence which is not at the 170 MeV energy. Practically, protons beams cannot be totally monoenergetic; there is a beam component at lower energies. This factor takes into account this effect not exceeding ten percent. For the problem we study herein, the beam is considered ideal. As a consequence, this factor will be set to zero in further calculations. The standard deviation σ is estimated as a function of the range R_0 by:

$$\sigma \approx 0.012R_0^{0.935}$$

The terms $\mathcal{D}_n(z)$ represent the Weber–Hermite functions and make it possible to perform the following series expansion (Lee, 1993):

$$\mathcal{D}_n(z) = \exp\left(-\frac{z^2}{4}\right) [a_0 A_0 + z a_1 A_1] \quad (6)$$

with

$$a_o = (2^{\frac{n}{2}}) \frac{\sqrt{\pi}}{\Gamma(\frac{1}{2} - \frac{n}{2})}; \quad a_1 = \left(-2^{\frac{n+1}{2}}\right) \frac{\sqrt{\pi}}{\Gamma(-\frac{n}{2})};$$

$$A_0 = 1 + \sum_{k=1}^{\infty} (-1)^k \frac{n(n-2)\dots(n-2k+2)}{(2k)!} z^{2k};$$

$$A_1 = 1 + \sum_{k=1}^{\infty} (-1)^k \frac{(n-1)(n-3)\dots(n-2k+1)}{(2k+1)!} z^{2k}$$

The values of a_o and a_1 do not depend on z and are equal to $a_o = 1.230$ and $a_1 = -0.647$ for $\mathcal{D}_{-0.565}$; and $a_o = 1.145$ and $a_1 = -1.230$ for $\mathcal{D}_{-1.565}$. This series expansion is not trivial and converges toward the correct result with two decimal places, when the expansion is made up to 10th order. Some software like LabVIEW can compute the Weber–Hermite functions.

Calculation of the absorbed dose per unit fluence at the Bragg maximum and at 15 cm depth.

The calculation of the dose at the Bragg maximum in the case $z = R_0$ is greatly simplified since expression (6) becomes $D_n(z) = [a_0]_n$. Thus thanks to (5), $D(R_0)$ can be written as follows:

$$D(R_0) = \Phi_0 \frac{\sigma^{0.565}}{1 + 0.012R_0} \left[\frac{11.26}{\sigma} [a_0]_{-0.565} + 0.157[a_0]_{-1.565} \right]$$

When weighting by the factor 0.1602, the result is obtained in nGy and for an absorbed dose per unit fluence (nGy.cm²) the above formula becomes:

$$\frac{D(R_0)}{\Phi_0} = 0.1602 \times \frac{\sigma^{0.565}}{1 + 0.012R_0} \left[\frac{11.26}{\sigma} [a_0]_{-0.565} + 0.157[a_0]_{-1.565} \right]$$

The range in water for 170 MeV protons and the standard deviation of the Gaussian distribution are given by:

$$R_0 = 2.2 \times 10^{-3} \times (170)^{1.77} = 19.51 \text{ cm} \quad \text{and} \quad \sigma \approx 0.012 \times (19.51)^{0.935} = 0.193 \text{ cm}$$

Therefore, the two dose components at the Bragg maximum can be obtained. The component related to coulomb scattering (c) and the one associated to nuclear reactions (r) are, respectively:

$$\left(\frac{D(R_0)}{\Phi_0} \right)_c = 0.1602 \times \frac{(0.193)^{0.565}}{1 + (0.012 \times 19.51)} \times \left(\frac{11.26}{0.193} \times 1.230 \right) = 3.68 \text{ nGy.cm}^2$$

$$\left(\frac{D(R_0)}{\Phi_0} \right)_r = 0.1602 \times \frac{(0.193)^{0.565}}{1 + (0.012 \times 19.51)} \times (0.157 \times 1.145) = 0.01 \text{ nGy.cm}^2$$

Then the value of the total dose per unit fluence at the Bragg maximum is $(D(R_0)/\Phi_0) = 3.69 \text{ nGy.cm}^2$. It can be noted that the fraction related to nuclear reactions at this depth is relatively low (0.27%). More generally, this component keeps on fading as the proton energy decreases. This is due to nuclear reactions cross sections and threshold levels of some of them (see figure 1.VI.1). The application of formula (4) is easier; it can be used for $z < R_0 - 10\sigma$, in other words up to 17.6 cm.

Hereinafter, it is proposed to calculate the dose per unit fluence at 15 cm depth.

$$\frac{\widehat{D}(15)}{\Phi_0} = \frac{0.1602}{1 + 0.012 \times 19.51} \left[17.93 \times (19.51 - 15)^{-0.435} + (0.444) \times (19.51 - 15)^{0.565} \right]$$

$$= 1.34 \text{ nGy.cm}^2$$

The dose profile obtained with this calculation using expressions (4) and (5) is shown in figure 1.VI.3.

Part 2: Calculation of the Dose Profile Per Unit Fluence Using MCNP

In this part, we intend to use MCNP to calculate the deposited dose in depth in a water phantom measuring $30 \times 30 \times 30 \text{ cm}^3$, by a parallel 170 MeV proton beam of section radius equal to 5 cm. This calculation is done with a spatial mesh of the absorbed dose using the “MESH tally” feature of MCNP (*cf.* 1.V part 2). For this purpose, the proton beam is considered to be along the Oz axis and the water phantom is divided into 200 cells to a depth of 25 cm. As for the x and z axes they are cut into 2 cm bins. The 7th entry of the neutron physics card “phys:n” is set to 1 to enable the generation and the transport of recoil protons on hydrogen and of light ions from nuclear reactions such as (n,p) or (n,α) , caused by secondary neutrons. The same setting is put on the proton physics card “phys:h” to enable the generation and tracking of light ions from nuclear reactions like (p,d) , (p,α) , etc. The MCNP input file is given below:

```
proton dose
c cell definition
10 1 -1 -10
30 0 -30 10
40 0 30

10 RPP -15 15 -15 15 -15 15
30 RPP -20 20 -20 20 -20 20

imp:n,h,d,t,s,a,# 1 1 0
c transport of: neutrons n, protons h, deuterons d, tritons t, helions s
c alpha a, heavy ions #
mode n h d t s a #
```

```
sdef par=h pos 0 0 -16 axs 0 0 1 ext 0 rad=d1 vec 0 0 1 dir 1 erg 170
Si1 0 5
spl -21 1
c 7th entry (coilf) of PHYS set to 1:
c light-ion recoil turned on
PHYS:N 200 0 0 J J J 1 -1 J J J 0 0
phys:h 200 0 -1 J 0 J 1 J J J 0 0 j j
c cut enter 2 =0 to reduce the cut energy to 1e-3 MeV for d t s a a,d HI
c cut enter 3 and 4 =0 for analog capture
cut:n,h,d,t,s,a,# j 0 0 0 j
tmesh
c proton
RMESH1:h pedep
cora1 -1 1
corb1 -1 1
corc1 -15 200i 10
c alpha
RMESH11:a pedep
cora11 -1 1
corb11 -1 1
corc11 -15 200i 10
c neutron
RMESH21:n pedep
cora21 -1 1
corb21 -1 1
corc21 -15 200i 10
c heavy ion
RMESH31:# pedep
cora31 -1 1
corb31 -1 1
corc31 -15 200i 10
c deuton
RMESH41:d pedep
cora41 -1 1
corb41 -1 1
c triton
RMESH51:t pedep
cora51 -1 1
corb51 -1 1
c helion
RMESH61:s pedep
cora61 -1 1
corb61 -1 1
RMESH3
Cora3 -1 1
Corb3 -1 1
```



```

Corc3 -15 200i 10
endmd
M1 1001 2 8016 1 $ water
ctme 1000

```

File 1.VI.1

The type 1 mesh (from “rmesh1” to “rmesh61”) related to the keyword “pedep” makes it possible to estimate the deposited energy per unit volume, for different types of primary and secondary charged particles. That is to say “rmesh1” for protons, “rmesh11” for alpha particles, “rmesh21” for heavy ions, “rmesh31” for neutrons, “rmesh41” for deuterons, “rmesh51” for tritons and “rmesh61” for helions. The type 3 mesh (“rmesh3”) enables to calculate the total energy deposited per unit volume.

When the input file is executed, a “mdata” file is created in addition to the standard output file. It is a binary file that must be converted to an ASCII format thanks to, for example, the “gridconv.exe” application supplied with the MNCP package. The sequence of operations to be executed for the conversion is replicated in the command prompt shown in figure 1.VI.2.

Then the file (here bragg_p) can be directly read or used by 3D visualization post-processing applications such as VISED for instance. The results are given in $\text{MeV}\cdot\text{cm}^{-3}$, which corresponds for water to $\text{MeV}\cdot\text{g}^{-1}$. Thus, it is convenient to multiply the results by the factor $1.602 \times 10^{-19} \times 10^6 \times 10^3$ to obtain the results in Gy; next these are divided by the protons fluence for a standardization in $\text{Gy}\cdot\text{cm}^2$. In our case, a beam of parallel protons, which of radius section is 5 cm, is considered. Therefore, the fluence per incident proton is $\Phi = 1 / [\pi \cdot (5)^2] \text{cm}^{-2}$.

```

mcnp6
C:\logiciel_calcul\mcnp6\cas_mcnp\gridconv
Enter the type of data file: mdata or mctal.
<default=mdata>:
#
Enter name of input file. <default=mdata>:
#
mdata
Is this a binary data file? y/n
<default=yes>:
#
Do you wish to create a text file? y/n
(This file is portable to any system.
<default=no>):
#
y
What do you want to name your file?
<default=mdata>:
#
bragg_p
Do you wish to continue? y/n
<default=no>:
#
n
Do you wish to work with another data file. y/n ?
Type yes(y) or no(n) or hit return to exit.
#
C:\logiciel_calcul\mcnp6\cas_mcnp>

```

FIG. 1.VI.2 – Conversion method of the MCNP output file “mdata” to ASCII format.

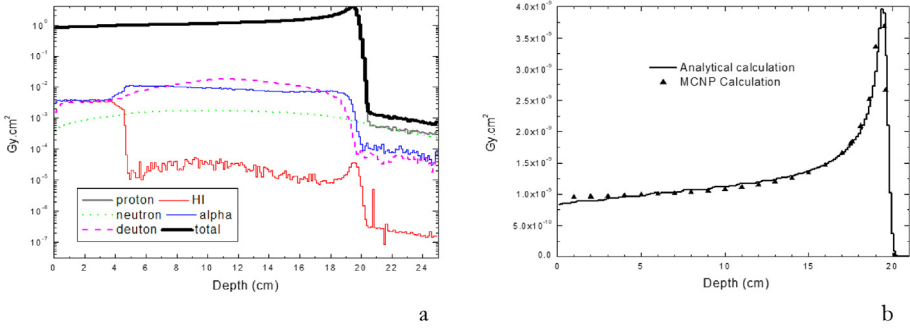


FIG. 1.VI.3 – (a) Total absorbed dose profiles per unit fluence and components of heavy charged particles, calculated with MCNP, (b) solid line: total dose profile per unit fluence calculated with MCNP and in triangles the one calculated analytically with equations (3) and (4).

The dose profiles per unit fluence for the total result and for each component of heavy charged particles are presented in figure 1.VI.3a. It can be noted that beyond the Bragg maximum, *i.e.*, from 20 cm depth, a weak dose component remains due to neutrons (approximately 4 decades smaller than the Bragg maximum). Those neutrons come essentially from (p,xn) reactions on oxygen, nitrogen and carbon nuclei. In turn, the neutrons are responsible for elastic scattering (n,n) essentially on hydrogen with secondary protons set in motion and inelastic reactions (n,p) , and more marginally (n,α) . These contributions can be seen on the curves “protons” and “alpha” beyond the Bragg maximum.

Figure 1.VI.3b shows the total dose profiles per unit fluence obtained with the semi-empirical expressions (4) and (5) and with the MCNP code. One can notice that the two profiles are practically superimposed. The range calculated with expression (2) is 19.5 cm and the one obtained with the spatial mesh for the absorbed dose is between 19.2 cm and 19.4 cm. For calculated values of dose at 15 cm and at the range, the values obtained with the MCNP code are, respectively, 1.37 (0.085%) nGy.cm² and 3.95 (0.0724%) nGy.cm²; the difference between the values obtained with the semi-empirical method and with MCNP are, respectively, -2.2% and -6.6%.

Part 3: Calculation of the Absorbed Dose and of the Directional Equivalent Dose under 70 μm at a Zero Angle of Incidence

(a) Analytical calculation of the absorbed dose under 70 μm

If the depth is way smaller than the range ($z \ll R_0$), the impact of z becomes negligible compared to R_0 and expression (4) of the absorbed dose can be summed up as:

$$\widehat{D}(z \ll R_0) = \frac{\Phi_0}{1 + 0.012R_0} \left[17.93(R_0)^{-0.435} + \left(0.444 + \frac{31.7\epsilon}{R_0} \right) (R_0)^{0.565} \right] \quad (7)$$

Thus, when considering an ideal ($\epsilon = 0$) and parallel protons beam, the absorbed dose to water under $70 \mu\text{m}$, per unit fluence can be estimated as follows:

$$\frac{\widehat{D}(70 \mu\text{m})}{\Phi_0} = \frac{0.1602}{1 + 0.012 \times 19.51} \left[17.93 \times (19.51)^{-0.435} + (0.444) \times (19.51)^{0.565} \right]$$

$$= 0.95 \text{ nGy.cm}^2$$

(b) Numerical calculation of the absorbed dose under $70 \mu\text{m}$

In MCNP, the calculation that allows to get the value of the dose under $70 \mu\text{m}$ $D'(0.07)$, is provided using the energy deposition tally *F8. The deposited energy is estimated inside a quasi-point cylinder of entrance surface 1 cm^2 located at $65 \mu\text{m}$ depth and $10 \mu\text{m}$ in regard to the entrance face of the water phantom, which results in a mean depth of $70 \mu\text{m}$ (see cell 15 in the input file presented below). The section radius of the modeled protons beam is 1.5 cm .

```

Proton dose
C cell block
10    1   -1   -10 15 $ water
15    1   -1   -15  $ calculation cell
520   1   -1    10  $ outside

C geometry block
10    RCC    0    0   -1e-10 0    0    30    2
15    RCC    0    0    6.5e-3 0    0    1e-3   .5642

mode h
imp:h 1 1 0
sdef par=h pos 0 0 0 axs 0 0 1 ext 0 rad=d1 vec 0 0 1 dir 1 erg 170
phys:h 200 0 -1 J 0 J 1 J J J 0 0 j j
Si1 0 1.5
spl -21 1
M1 1001 2 8016 1 $ water
*F8:h 15
ctme 1200

```

File 1.V1.2

The mean energy $\bar{\epsilon}$ deposited in cell 15, per proton emitted by the source, is given by the tally result $*F8 = 8.12 \times 10^{-4} \text{ MeV}$. It is convenient to divide this result by the cylinder mass m in order to obtain the absorbed dose in this cell.

$$D'(0.07) = 1.602 \times 10^{-13} \left(\frac{\bar{\epsilon}}{m} \right)$$

The factor 1.602×10^{-13} stands for the J/MeV conversion. The mass of the cell used for the calculation is given by:

$$m = \rho V = \rho Sh = 1 \times 1 \times 1 \times 10^{-3} = 1 \times 10^{-3} \text{ g} \quad (1 \times 10^{-6} \text{ kg})$$

Moreover, the dose has to be standardized with respect to the protons fluence in the beam, which leads to the following ratio:

$$\begin{aligned} \frac{D'(0.07)}{\Phi_0} &= \frac{D'(0.07)}{1/\pi r^2} = \pi r^2 \times 1.602 \times 10^{-13} \left(\frac{\bar{\epsilon}}{m} \right) \\ &= \pi \times 1.5^2 \times 1.602 \times 10^{-13} \left(\frac{8.12 \times 10^{-4}}{10^{-6}} \right) \\ &= 9.2 \times 10^{-10} \text{ Gy.cm}^2 (0.92 \text{ nGy.cm}^2) \end{aligned}$$

A shallow but significant discrepancy of 3% can be noted between the results obtained with the two approaches, considering that the uncertainty on the result of the MCNP estimation is about $\pm 1.2\%$.

(c) Calculation of the directional equivalent dose under 0.07 mm at a zero angle of incidence $H'(0.07, 0^\circ)$

The directional equivalent dose under 0.07 mm at a zero angle of incidence can be obtained from the absorbed dose under $70 \mu\text{m}$ by weighting it by the mean quality factor for protons under $70 \mu\text{m}$.

$$H'(0.07) = \bar{Q} \times D'(0.07)$$

The mean quality factor \bar{Q} depends on the mean Linear Energy Transfer (LET), noted \bar{L} according to the following relationship:

$$\bar{Q} = \begin{cases} 1 & \text{for } \bar{L} < 10 \text{ keV} \cdot \mu\text{m}^{-1} \\ 0.32\bar{L} - 2.2 & \text{for } 10 \leq \bar{L} \leq 100 \text{ keV} \cdot \mu\text{m}^{-1} \\ 300/\sqrt{\bar{L}} & \text{for } \bar{L} > 100 \text{ keV} \cdot \mu\text{m}^{-1} \end{cases}$$

The mean LET in cell 15 can be evaluated thanks to the “FT LET” card of MCNP. This feature allows to calculate the charged particle fluence as a function of the LET, that is to say as a function of the energy absorbed in the cell per unit distance covered. This function is associated with a F4 tally for protons in the considered cell. For a LET spectrum to be established it is necessary to add an “E4” card with an energy binning. LET are provided by MCNP with the common unit of the linear stopping power: $\text{MeV} \cdot \text{cm}^{-1}$; one will keep in mind to multiply all the results by 1/10 to obtain results in $\text{keV} \cdot \mu\text{m}^{-1}$. It can be noted that these spectra divided into $\text{keV} \cdot \mu\text{m}^{-1}$ can also be regarded as linear energy spectrum or microdosimetric spectrum (see the exercise with the Rossi proportional counter). For an exhaustive calculation taking into account all moving charged particles, first it is necessary to transport them all; this instruction is given using the “mode” card which enables the tracking of neutrons “n”, protons “h”, deuterons “d”, tritons “t”, helions “s”, alpha particles “a” and heavy ions “#” such as residual nuclei set in

motion at the end of nuclear reactions. These residual ions are created, transported and tracked by setting to “1” the 7th entry of the proton physics card “phys:h”. Similarly, recoil protons originating from elastic scattering reactions of secondary neutrons coming from (p, xn) reactions can be tracked as long as the 7th entry of the neutron physics card is set to “1”. Without the proper setting of these physics cards, the reactions actually happen, causing the annihilation of the incident proton or a decrease in the proton energy, but neither the secondary charged particles, nor the residual nuclei would be tracked. As a result, the corresponding component in the LET spectrum would be zero. Inside the following MCNP input file 1.V1.3, the “F4” tally allows to obtain the complete LET spectrum; and the tally from “F14” to “F34” enable to get the partial LET spectra for each of the component corresponding to the different charged particles set in motion.

```

Spectrum in LET
C cell block
10 1 -1 -10 15 20 $ water
15 1 -1 -15 $ scoring cell calculation at 70 μm
520 1 -1 10 $ outside

C geometry block
10 RCC 0 0 -1e -10 0 0 30 2
15 RCC 0 0 6.5e-3 0 0 1e-3 .5642

imp:n,h,d,t,s,a,# 1 1 1 0
mode n h d t s a #
sdef par=h pos 0 0 0 axs 0 0 1 ext 0 rad=d1 vec 0 0 1 dir 1 erg 170
phys:h 10000 10000 -1 J 0 J 1 J J J 0 0 j j
PHYS:N 10000 10000 0 J J J 1 -1 J J J 0 0
cut:n,h,d,t,s,a,# j 0 0 0 j
Si1 0 1.5
spl -21 1
M1 1001 2 8016 1 $ water
FC4 all
F4:h,d,t,s,a,# 15
FT4 LET
FC14 H
F14:h 15
FT14 LET
FC24 a
F24:a 15
FT24 LET
FC34 HI
F34:# 15
FT34 LET

```

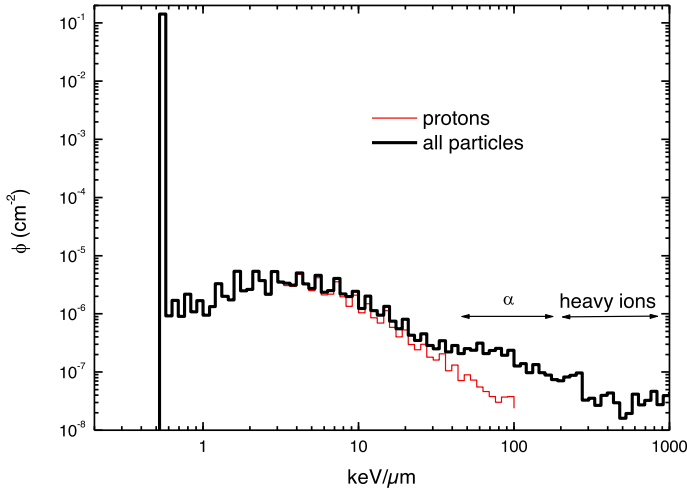


FIG. 1.VI.4 – Fluence spectrum of charged particles as a function of the LET, calculated with MCNP inside a micro-cylinder of water.

Hereinafter figure 1.VI.4 gives a representation of the fluence spectrum of charged particles as a function of the LET in $\text{keV} \cdot \mu\text{m}^{-1}$, for protons going through cell 15.

A peak for the weakest LET of the spectrum can be noticed, it is located around $0.5 \text{ keV} \cdot \mu\text{m}^{-1}$. There is also a continuum beyond this peak, for which the occurrences are marginal, which extends up to $1000 \text{ keV} \cdot \mu\text{m}^{-1}$. The peak corresponds to 170 MeV protons, which, considering their energy, deposit very low energy in water, explaining a low LET. Up to several tens of $\text{keV} \cdot \mu\text{m}^{-1}$, the continuum corresponds essentially to protons undergoing elastic scattering on the nuclei constituting water molecules (Rutherford scattering). In this LET range, the continuum is also sustained by recoil protons originating from the elastic scattering of neutrons produced by (p, xn) reactions. Beyond $10 \text{ keV} \cdot \mu\text{m}^{-1}$, the continuum is mainly due to α particles from (p, α) capture reactions and to residual heavy ions in motion. It can be recalled that at the beginning of the track, approximately 20% of the energy deposited in the medium is the result of nuclear reactions.

The mean LET under $70 \mu\text{m}$ of water can be obtained from the histogram spectrum per LET bin according to the following weighted arithmetic mean:

$$\bar{L}(70 \mu\text{m}) = \frac{\sum L_i \times \Phi_i}{\sum \Phi_i} = 0.53 \text{ keV} \cdot \mu\text{m}^{-1}$$

Since $\bar{L}(70 \mu\text{m}) < 10$, we have $\bar{Q} = 1$ which means a directional equivalent dose equal to:

$$\frac{H'(0.07)}{\Phi_0} = \frac{D'(0.07) \times \bar{Q}}{\Phi_0} = 9.2 \times 10^{-10} \text{ Sv} \cdot \text{cm}^2$$

It can be noted that a similar calculation at the Bragg maximum would have led to a mean LET larger of approximately $5 \text{ keV} \cdot \mu\text{m}^{-1}$, due to the proton velocity decrease at this length of the track. Moreover, this technique for the determination of the mean LET can provide access to the linear stopping power or mass stopping power at any point of the track of a charged particle. This way, the usual formula of the absorbed dose for charged particles (without Bremsstrahlung) can fairly be used:

$$\bar{L}(z)_{\text{MCNP}} \Rightarrow \left(\frac{S}{\rho}\right)_z \Rightarrow D(z) = \left(\frac{S}{\rho}\right)_z \Phi(z)$$

It is recalled that for the simplified application of this formula for the absorbed dose, the mass stopping power is considered constant all over the range, which constitutes a bias regarding the obtention of the true value.

1.VII Neutron Kerma Calculation and Microdosimetric Spectrum Reconstruction with a Tissue Equivalent Proportional Counter

Abstract:

In this problem, the “fluence – first collision kerma” factor for 13.9 MeV neutron is calculated for a low-pressure Tissue Equivalent Proportional Counter (TEPC). The value found is compared to the theoretical value. This factor is then compared to different values of the “fluence – mean organ dose” factor from ICRU (1998a), for the purpose of assessing its ability to estimate these macroscopic dosimetric quantities. The ability to assess the ambient dose equivalent, $H^*(10)$, from the neutron kerma is studied as well. Furthermore, a challenge of this problem is the reconstruction of microdosimetric spectra based on MCNP results. In a last step, the characteristic dosimetric quantities drawn from the MCNP spectra are compared to the reference values to judge the reliability of the proposed method.

Objectives:

- Analytical calculation of the first collision kerma for monoenergetic neutron.
- Study of microdosimetric spectrum and first collision kerma measurement technique with the standard spherical TEPC, *i.e.*, Rossi-type detector.
- Comparison of the first collision kerma with mean organ doses and evaluation of the ambient dose equivalent.
- Microdosimetric spectrum calculation with MCNP simulation using the “anti-coincidence pulse-height” card.
- Neutron mean quality factor calculation from a microdosimetric spectrum.

For this problem, the standard TEPC, *i.e.*, Rossi-type detector is considered. It is designed with a spherical Proportional Counter of 1.27 cm inner diameter for which the outer shell is composed of A150 tissue-equivalent plastic mainly made of C

(77.5% by weight), H (10.1%), O (5.2%), N (3.5%), with a wall thickness of 2.54 mm. Note that the wall is thick enough to maintain charged particle equilibrium during neutron irradiation. The inner cavity is filled with a low-pressure propane-based tissue-equivalent gas mixture ($P_m = 7.4$ kPa) of density $\rho_m = 1.064 \times 10^{-3} \text{ g.cm}^{-3}$ TPN. Therefore, with these parameters, it becomes a mass thickness of:

$$\begin{aligned} m_s &= d\rho_m \left(\frac{P_m}{P_{\text{atm}}} \right) = 1.27 \times 1.064 \times 10^{-3} \times \left(\frac{7.4 \times 10^{-2}}{1.013} \right) \\ &= 9.87 \times 10^{-5} \text{ g.cm}^{-2} \cong 1 \times 10^{-4} \text{ g.cm}^{-2} \end{aligned}$$

A $10^{-4} \text{ g.cm}^{-2}$ mass thickness corresponds to a tissue-equivalent thickness of $1 \mu\text{m}$ for 1 g.cm^{-3} tissue density that corresponds to the order of magnitude of the cell size and enables the microdosimetric spectrum measurement.

Experimentally, the 13.9 MeV neutron field is obtained with a Van de Graff accelerator *via* the ${}^3\text{H}(d,n){}^4\text{He}$ reaction. The counter is located at 30 cm from the conversion target and its calibration is done with an Am-Be α source. The set of parameters needed to calculate the “fluence – first collision kerma” conversion coefficient are the following:

- The ratio of the alpha energy imparted on the mean chord of the sphere ($\bar{l} = \frac{2}{3}d$) is $\frac{1}{\rho}(\Delta\varepsilon_\alpha/\bar{l}) = 1277 \text{ MeV.g}^{-1}\text{cm}^2$ ICRU (1983).
- The mass stopping power ratio for secondary charged particles, between the counter wall and the gas, set in motion by neutrons in the wall is equal to $(\bar{S}/\rho)_g^w = 1$.
- The average ionization energy of Am-Be alpha particles is $W_\alpha = 28 \text{ eV}$ (Thomas and Burke, 1985).
- The ratio of mean ionizing energy in propane gas for neutron by α from AmBe is $W_n/W_\alpha = 1$.
- The neutron fluence, per unit charge of the accelerator beam, is $(\Phi/q) = 1.33 \times 10^4 \text{ cm}^{-2}\mu\text{C}^{-1}$ at 30 cm from the target; the accelerator operates at an intensity $I = 10 \mu\text{A}$ (Menzel *et al.*, 1984).
- The current measured in the chamber during the pulse is $i = 2.75 \times 10^{-2} \text{ pA}$.

Part 1: Calculation of the “Fluence – First Collision Kerma” Conversion Coefficient and of the Measured Signal

For this issue, we considered the Bragg–Gray classic formula for narrow cavities, which links the measured dose through wall thickness, D_t , and the total charge q_t created inside the cavity:

$$D_t = \left(\frac{q_t}{m_g} \right) \left(\frac{W_g}{e} \right) \left(\frac{\bar{S}}{\rho} \right)_g^w \quad (1)$$

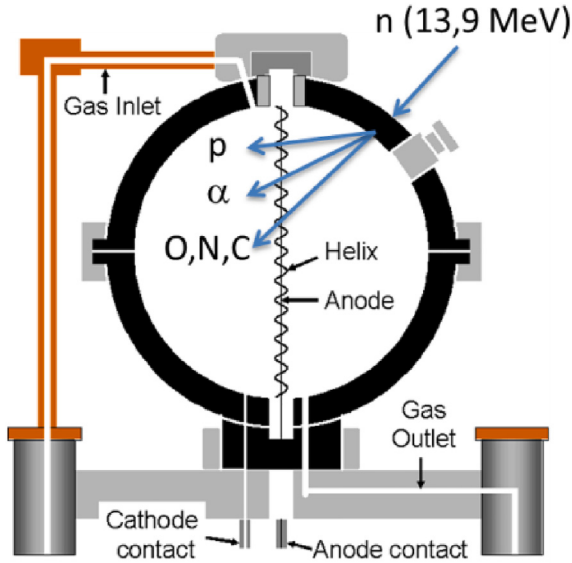


FIG. 1.VII.1 – Rossi-type TEPC for a neutron field microdosimetric spectrum measurement (adapted from Oak Ridge Associated Universities).

This formula is going to be adapted to a proportional counter with an amplification gain g . The total charge corresponds to the integral of the whole spectrum of charge q , related to the counting of each single event that allows proportional counter mode.

$$q_t = \int_0^{\infty} q n(q) dq$$

The collected charge q from ionizations is directly connected to the energy imparted ε for each single event. A broad lineal energy spectrum can then be drawn up since the corresponding lineal energy for each single event is given by ratio of energy imparted by the mean chord $y = \varepsilon/\bar{l}$. The mean chord is here given by $\bar{l} = 2d/3$ where d stands for the equivalent tissue diameter of $1 \mu\text{m}$. By including the integral of the collected charges spectrum, equation (1) becomes:

$$D_t = \frac{1}{g} \left[\frac{\int_0^{\infty} qn(q) dq}{m_g} \right] \left(\frac{\overline{W}_g}{e} \right) \left(\frac{\overline{S}}{\rho} \right)_g^W \quad (2)$$

where $n(q)$ is the charge distribution in the acquisition channels. The integral over the whole charge provides the total charge. Then, there is a direct relationship between the charge distribution and the microdosimetric spectrum $n(q) \propto d(y)$. At this point, it is necessary to complete an energy calibration in order to match the

collected charge q to the energy imparted transferred by secondary charged particles. The energy calibration is realized by means of an Am-Be α source. Let $\Delta\varepsilon_x$ be the energy transferred by an Am-Be α particle in the cavity. If the latter is responsible for a q_x charge ionization, it is then possible to express lineal energy y as a function of these two parameters (we assume that the gain is identical regardless of the charged particle):

$$y = \frac{\varepsilon}{l} = \left(\frac{1}{g}\right) \frac{q(\overline{W_g})_n}{e\bar{l}} \quad \text{and} \quad \Delta E_x = \left(\frac{1}{g}\right) \frac{q_x(\overline{W_g})_x}{e} \Rightarrow y = \left(\frac{q}{q_x} \frac{(\overline{W_g})_n}{(\overline{W_g})_x}\right) \left(\frac{\Delta\varepsilon_x}{\bar{l}}\right) \quad (3)$$

Expression (3) of y allows the completion of the microdosimetric spectrum drawn in figure 1.VII.2 and commented hereafter. The absorbed dose can also be expressed as a function of the mean value of the considered energy frequency distribution $\bar{\varepsilon}_f$ and of the mean lineal energy \bar{y}_f :

$$D = \frac{\bar{\varepsilon}_f N}{m} = \frac{\bar{\varepsilon}_f N}{\rho V} = \frac{\bar{\varepsilon}_f N}{\rho \frac{4}{3}\pi(\frac{d}{2})^3} = \frac{\bar{\varepsilon}_f}{(\frac{2d}{3})} \frac{4N}{\rho\pi d^2} = \left(\frac{\bar{\varepsilon}_f}{\bar{l}}\right) \frac{4N}{\rho\pi d^2} = \bar{y}_f \frac{4N}{\rho\pi d^2} \quad (4)$$

N is the number of times the mean energy is imparted. Thus, with equations (3) and (4), and by assuming the dose equal to the kerma since equilibrium conditions of secondary charged particles in the detector wall are held, equation (2) becomes:

$$K_n = \frac{4}{\rho\pi d^2} \left[\frac{\int_0^\infty qn(q) dq}{q_x} \right] \frac{(\overline{W_g})_n}{(\overline{W_g})_x} \left(\frac{\bar{S}}{\rho}\right)_g^W \left(\frac{\Delta\varepsilon_x}{\bar{l}}\right) \quad (5)$$

This equation can be written in terms of kerma rate as a function of the measured current. By matching the different units, equation (6) provides the first collision kerma rate in $\mu\text{Gy}\cdot\text{s}^{-1}$:

$$\dot{K}_n = 6.38 \times 10^{-4} \frac{i}{\rho\pi d^2 q_x} \frac{(\overline{W_g})_n}{(\overline{W_g})_x} \left(\frac{\bar{S}}{\rho}\right)_g^W \left(\frac{\Delta\varepsilon_x}{\bar{l}}\right) \quad (6)$$

All parameters of equation (6) are available except charge q_x . To obtain this quantity, the ratio of the energy imparted by alpha particles on the average chord of the sphere is used to firstly evaluate the deposited energy $\Delta\varepsilon_x$. We assume the stopping power to be constant along the short distance covered, which allows to consider a constant amount of charges created for such an energy deposit:

$$\begin{aligned} \frac{1}{\rho} \left(\frac{\Delta\varepsilon_x}{\frac{2}{3}d}\right) &= 1277 \text{ MeVg}^{-1}\text{cm}^2 \iff \Delta E_x = 1277 \times \frac{2}{3}\rho d = 1277 \times \frac{2}{3} \times 10^{-4} \\ &= 85.13 \text{ keV} \end{aligned}$$

$$q_x = \frac{\Delta E_x}{W_\alpha} e = \frac{85130}{28} \times 1.6 \times 10^{-19} = 4.86 \times 10^{-16} \text{ C}$$

The first collision kerma rate is:

$$\dot{K}_n = 6.38 \times 10^{-4} \times \frac{2.75 \times 10^{-14}}{\pi \times (1.27)^2 \times 4.86 \times 10^{-16}} \times 1 \times 1 \times 1277 = 9.11 \mu\text{Gy.s}^{-1} \quad (7)$$

To determine the conversion coefficient, the fluence rate at 30 cm from the target is first evaluated:

$$\dot{\Phi} = \left(\frac{\Phi}{q}\right) I = 1.33 \times 10^4 \times 10 = 1.33 \times 10^5 \text{ (n).cm}^{-2}.\text{s}^{-1}$$

For the “fluence – first collision kerma” conversion coefficient, also denoted as “kerma factor”, we get:

$$\left(\frac{K_n}{\Phi}\right)_{13,9} = \frac{9.11 \times 10^{-6}}{1.33 \times 10^5} = 6.84 \times 10^{-11} \text{ Gy.cm}^2 = 68.4 \text{ pGy.cm}^2$$

Figure 1.VII.2 represents the microdosimetric spectrum as a function of lineal energy, reconstructed after acquisition and processing of the signal measured in the TEPC. The y -axis is expressed here in $yd(y)K_n/\Phi$ with cm^2ss unit. The integral of $yd(y)$ over the whole spectrum is normalized to 1 and the total area under the curve provides the conversion factor K_n/Φ .

The main peak centered at $10 \text{ keV}.\mu\text{m}^{-1}$ of lineal energy relates to recoil protons from elastic scattering (n,n) on hydrogen, and to a more marginal extent to protons from (n,p) reactions. It extends up to a lineal energy of about $150 \text{ keV}.\mu\text{m}^{-1}$,

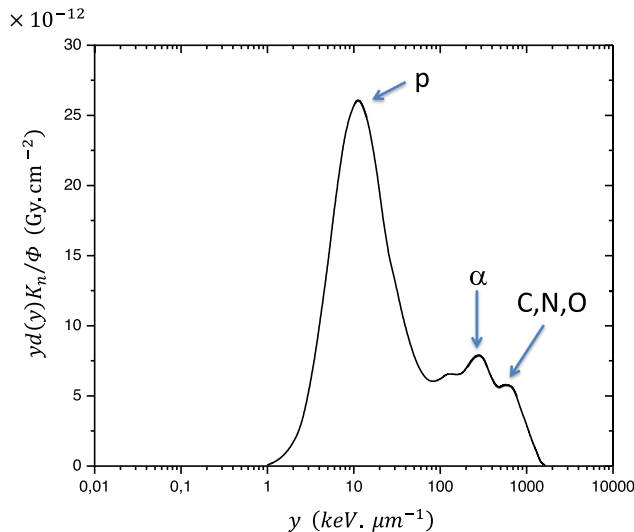


FIG. 1.VII.2 – Microdosimetric spectrum measured with a Rossi counter (from Menzel *et al.*, 1984).

described in the literature as “p-edge”. This value is reached for incident neutron energies higher than 100 keV. In fact, from 100 keV, if the whole recoil proton energy is transferred to the cavity gas, an event of lineal energy $y = 100/(2/3) = 150 \text{ keV} \cdot \mu\text{m}^{-1}$ will be counted. For incident energies higher than 100 keV, this cut-off value of the lineal energy cannot be exceeded since the mean recoil protons energy is higher, and the mean stopping power in the gas is lower. This leads to an energy deposit less than or equal to 100 keV. From this observation, we can explain that from 100 keV, for an increasing energy, the maximum lineal energy of the proton peak decreases: it is equal to $10 \text{ keV} \cdot \mu\text{m}^{-1}$ for 13.9 MeV neutrons and $100 \text{ keV} \cdot \mu\text{m}^{-1}$ for 1 MeV neutrons. For the 13.9 MeV neutron spectrum measured, the second peak observed at $380 \text{ keV} \cdot \mu\text{m}^{-1}$ relates to alpha particles from (n, α) reactions and from $(n, n'3\alpha)$ reaction on ^{12}C . It is referred to as “ α -edge”. The last bump on the right of the spectrum concerns heavy recoil ions from elastic scattering on carbon, oxygen and nitrogen. In order to obtain the measured signal \dot{S} in $(\text{c}) \cdot \text{cm}^2$, an estimation of the TEPC efficiency as a function of the neutron energy is derived from the empirical formula of Nunomiya *et al.* (2002):

$$\varepsilon_d = 0.045(E_n)^{0.9} = 0.045 \times (13.9)^{0.9} = 0.48$$

This gives the following measured signal during irradiation:

$$\dot{S} = \varepsilon_d \dot{\Phi} = 0.48 \times 1.33 \times 10^5 = 6.4 \times 10^4 (\text{c}) \cdot \text{s}^{-1}$$

Part 2: Kerma Factor Theoretical Calculation and Comparison with Operational and Protection Quantities

In this part, the first collision kerma factor will be calculated theoretically. Then, it will be compared to that obtained “experimentally” in the previous part.

(a) Kerma factor theoretical calculation

The mass repartition of chemical constituents of tissue used for calculations is: 72.9% of oxygen, 12.3% of carbon, 10.2% of hydrogen and 3.5% of nitrogen. Cross-sections and heats of reactions likely to occur in the energy transfer process for the 4 chemical elements, for a 13.9 MeV neutron energy, are listed in table 1.VII.1 (from the website “<http://www.nndc.bnl.gov/exfor/endf02.jsp>”). It is worth to note that the $(n, n'3\alpha)$ exotic inelastic reaction on ^{12}C is responsible for half the partial kerma related to carbon.

The general formula of the first collision kerma is defined for an interaction on a depth lower or equal to the free path of neutrons in the crossed medium. Beyond this path, scattering phenomena, opposed to neutron attenuation, can become significant. This is the reason why the first collision kerma is the only dosimetric quantity that can be calculated analytically for neutrons. Under the shallow depth where the first collision kerma is calculated, we assume the secondary charged particles’ equilibrium is held and kerma is equivalent to dose. Its general, the expression for a single chemical element is the following:

TAB. 1.VII.1 – Cross-sections and Q value for nuclear reactions of 13.9 MeV neutrons with tissue components.

<i>Oxygen</i>		
Reaction	σ (barn)	Q (MeV)
(n,n)	0.993	0
(n,p)	0.045	-9.638
(n,α)	0.138	-2.215
(n,n')	0.306	-6.05
<i>Nitrogen</i>		
Reaction	σ (barn)	Q (MeV)
(n,n)	0.932	0
(n,p)	0.054	0.625
(n,α)	0.062	-0.175
<i>Carbon</i>		
Reaction	σ (barn)	Q (MeV)
(n,n)	0.803	0
(n,α)	0.064	-5.70
$(n,n'3\alpha)$	0.300	-7.79
<i>Hydrogen</i>		
Reaction	σ (barn)	Q
(n,n)	0.687	0

$$K_n = \frac{\Phi}{\rho} N \sum_i \sigma_i(\bar{e}_{tr})_i$$

with N the atomic density in cm^3 of the considered element, σ_i the cross-section of reaction i on this element and $(\bar{e}_{tr})_i$ the mean energy transferred to secondary charged particles following this reaction. For a mix of chemical elements with weight fractions w_c and with a kerma expressed in Gy, this equation becomes:

$$K_n = 1.6 \times 10^{-10} \eta_A \Phi \sum_c \frac{w_c}{A_c} \sum_i \sigma_{c,i}(\bar{e}_{tr})_{c,i}$$

with η_A the Avogadro constant and A_c the molar mass of constituent c . Factor 1.6×10^{-10} enables the conversion from $\text{MeV}\cdot\text{g}^{-1}$ to Gy. Thus, the kerma factor can be written as:

$$\frac{K_n}{\Phi} = 9.63 \times 10^{13} \sum_c \frac{w_c}{A_c} \sum_i \sigma_{c,i}(\bar{e}_{tr})_{c,i} \tag{8}$$

Kerma factors, in reference ICRU (2000), for energies between 25 and 150 MeV, are calculated with this theoretical approach (ICRU, 2000). The calculations resulting from equations (8) are detailed for the kerma factor fraction related to

oxygen (oxygen partial kerma). At the considered neutron energy, four reactions can occur:

- (n,n) elastic scattering reaction

For this reaction, the mean transferred energy is the mean energy of the recoil proton given by the following equation:

$$\bar{\epsilon}_{\text{tr}} = \frac{2A}{(A+1)^2} E_n$$

Thus, this reaction contribution to the kerma factor is:

$$\begin{aligned} \left(\frac{K_n}{\Phi}\right)_{(n,n)}^O &= 9.63 \times 10^{13} \times \frac{0.729}{16} \times 0.993 \times 10^{-24} \times \frac{2 \times 16}{(16+1)^2} \times 13.9 \\ &= 6.71 \times 10^{-12} \text{ Gy.cm}^2 \end{aligned}$$

- (n,p) reaction

The energy transferred to the secondary proton and to the recoil nucleus is the sum of the neutron energy and the nuclear reaction Q -value:

$$\bar{\epsilon}_{\text{tr}} = E_n + Q$$

Thus, this reaction contribution to the kerma factor is:

$$\begin{aligned} \left(\frac{K_n}{\Phi}\right)_{(n,p)}^O &= 9.63 \times 10^{13} \times \frac{0.729}{16} \times 0.045 \times 10^{-24} \times (13.9 - 9.6) \\ &= 8.49 \times 10^{-13} \text{ Gy.cm}^2 \end{aligned}$$

- (n,α) reaction

Same principle as the previous reaction. Therefore, this reaction contribution to the kerma factor is:

$$\begin{aligned} \left(\frac{K_n}{\Phi}\right)_{(n,\alpha)}^O &= 9.63 \times 10^{13} \times \frac{0.729}{16} \times 0.138 \times 10^{-24} \times (13.9 - 2.2) \\ &= 7.08 \times 10^{-12} \text{ Gy.cm}^2 \end{aligned}$$

- (n,n') inelastic scattering reaction

The energy transferred to the recoil nucleus is given by the following expression (Ritts *et al.*, 1969):

$$\bar{\epsilon}_{\text{tr}} = \frac{2AE_n}{(A+1)^2} \left[1 + \frac{|Q|(A+1)}{2AE_n} \right]$$

This reaction contribution to the kerma factor is:

$$\begin{aligned} \left(\frac{K_n}{\Phi}\right)_{(n,n')}^O &= 9.63 \times 10^{13} \times \frac{0.729}{16} \times 0.306 \times 10^{-24} \times \frac{2 \times 16 \times 13.9}{(16+1)^2} \\ &\times \left[1 + \frac{6.05 \times (16+1)}{2 \times 16 \times 13.9}\right] \\ &= 2.54 \times 10^{-12} \text{ Gy.cm}^2 \end{aligned}$$

Thus, the contribution to the first collision kerma of reactions occurring on oxygen is:

$$\left(\frac{K_n}{\Phi}\right)^O = \sum_i \left(\frac{K_n}{\Phi}\right)_i^O = 1.72 \times 10^{-11} \text{ Gy.cm}^2$$

Partial kerma for each chemical element as well as total kerma are summarized in the table 1.VII.2.

TAB. 1.VII.2 – Partial kerma of each chemical element and total kerma, calculated theoretically.

	H	O	C	N	Total
$\left(\frac{K_n}{\Phi}\right)_{13.9}$	4.69×10^{-11}	1.72×10^{-11}	3.044×10^{-12}	7.81×10^{-13}	6.79×10^{-11}

Elastic scattering on hydrogen and oxygen as well as (n,α) reactions on oxygen account for most of the transferred energy. The total result of 67.9 pGy.cm^2 is substantially equal to that found previously.

- (b) Comparison of the kerma factor with the “fluence – mean organ dose” from ICRU (1998a) and evaluation of the ambient dose equivalent

The quality factor, $Q^*(10)$, for 13.9 MeV neutrons is 7.1 (Leuthold *et al.*, 1992). The latter is obtained *via* a quality factor average over all primary and secondary particles, under 10 mm of ICRU sphere in tissue-equivalent. “Fluence – mean organ dose” conversion coefficients (in pGy.cm^2) for breasts and marrow, the “fluence – effective dose” conversion coefficients (in pSv.cm^2) for antero-posterior geometry come from ICRP (2010); “fluence – ambient dose equivalent” conversion coefficients come from ICRP (1996). They are listed in table 1.VII.3.

TAB. 1.VII.3 – “Fluence – mean organ dose” conversion coefficients for breasts and marrow, “fluence – effective dose” and “fluence – ambient dose equivalent”.

$\left(\frac{D_T}{\Phi}\right)_{\text{bre}}$	$\left(\frac{D_T}{\Phi}\right)_{\text{mar}}$	$\left(\frac{E}{\Phi}\right)$	$\left(\frac{H^*(10)}{\Phi}\right)$
78.5	52.9	495	520

Note that the kerma factor ranges between the mean dose to breasts and the mean marrow dose at the considered energy. Breasts location, at the front of human body, facilitates multiple scattering, therefore increasing the mean dose in contrast with the neutron kerma. Conversely, marrow is located deep inside bones, therefore easing the neutron attenuation and leading to an overestimation of the mean dose by the neutron kerma.

The “fluence – ambient dose equivalent” conversion coefficient can be assessed from the kerma factor. This assessment can be made with the assumption that the kerma matches the absorbed dose at 10 mm deep within the ICRU sphere, $D^*(10)$. As shown in figure 1.VII.3, for 13.9 MeV, this assumption holds true since from about 100 keV and for increasing energies, the kerma and $D^*(10)$ curves are superimposed.

This assessment is accurate since it almost yields the “fluence – ambient dose equivalent” conversion factor of table 1.VII.3:

$$\left(\frac{\widehat{H}^*(10)}{\Phi}\right) = \left(\frac{K_n}{\Phi}\right) Q^*(10) = 67.9 \times 7.1 = 482 \text{ pSv.cm}^2 \cong \left(\frac{H^*(10)}{\Phi}\right)$$

The relative deviation between assessed and actual values of $H^*(10)/\Phi$ is -7% .

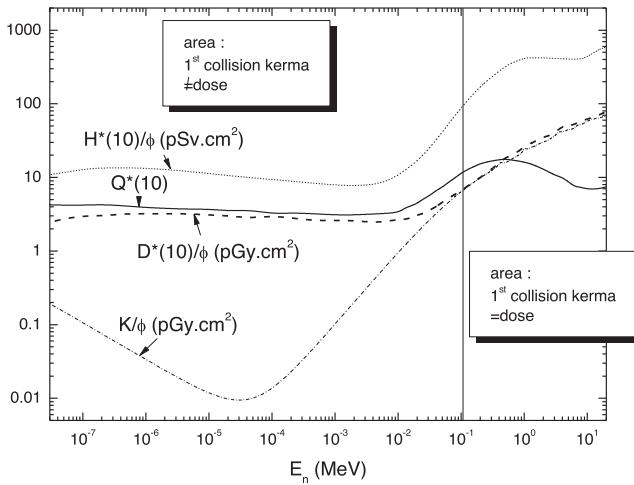


FIG. 1.VII.3 – Dosimetric quantities as a function of neutron energy (from Antoni and Bourgois, 2017a).

Part 3: Modeling the First Collision Kerma, the Ambient Dose Equivalent and the Microdosimetric Spectrum (Antoni and Bourgois, 2019)

In this section, we propose to determine the dose and the ambient dose equivalent in the Rossi counter from the simulated microdosimetric spectrum. The numerical model derives from that displayed in figure 1.VII.1. The counter is exposed to a 13.9 MeV parallel neutron beam of section 1 cm radius, *i.e.*, a fluence $\Phi = 1/\pi r^2 = 1/\pi$. Compositions of tissue equivalent A150 plastic and tissue equivalent propane are presented in table 1.VII.4 (from McConnell Jr. *et al.*, 2011). The density of tissue equivalent propane is $1.064 \times 10^{-3} \text{ g.cm}^{-3}$ at $1.013 \times 10^5 \text{ Pa}$. Thus, for a 7400 Pa pressure, it amounts $1.064 \times 10^{-3} \times 7400/1.013 \times 10^5 = 7.77 \times 10^{-5} \text{ g.cm}^{-3}$.

TABLE 1.VII.4 – A150 plastic (density 1.127 g.cm^{-3}) and tissue equivalent propane (density $1.064 \times 10^{-3} \text{ g.cm}^{-3}$ TPN) compositions.

Component	Mass fraction
A150 plastic	
H	0.101327
C	0.775501
N	0.035057
O	0.052316
F	0.017422
Ca	0.018378
Propane	
H	0.101869
C	0.456179
N	0.035172
O	0.406780

- (a) Use of the “anticoincidence” card for the lineal energy spectrum of secondary particles set in motion in the wall

The lineal energy distribution for each secondary heavy charged particle is estimated using a F6 tally type for energy deposit coupled to a pulse height tally F8 for each heavy charged particle specie (Fawaz, 2014). An coincidence pulse height card, *i.e.*, “ft8 phl”, is added to the F8 tally for counting single-event of energy imparted in gas arising from specific nuclear reaction in the cavity wall. For example, the following instructions are set to determine the occurrence number of the elastic scattering reaction (n,n) on hydrogen. It also accounts for the more marginal (n,p) reaction on other nuclei since the F6 tally followed by the “h” parameter, standing for protons, records only interactions producing secondary protons. In addition, an energy spectra card, *i.e.*, “e8”, enables the energy distribution of lineal energy counts

in the gas. For setting up this card, 185 logarithmic lineal energy bins are defined to ensure about 50 equal subdivisions per decade between 0.6 and 3030 keV. μm^{-1} . In the command lines hereafter, this card provides the lineal energy spectrum for protons.

```
F6:H 10
F8:N 10
E8 0 13.9E-12 0.00040 183LOG 2.02
FT8 PHL 1 6 1 0
```

Setting all ions in the F6 tally yields the total energy spectrum for all secondary charged particles produced. Tallies F66 and F68 of the full input file enable this feature. F_i8 tallies providing energy spectra in the sensitive volume for each nuclear reaction type occurring in the wall are given in table 1.VII.5.

TAB. 1.VII.5 – Reactions tracked in the MCNP simulation and corresponding tallies.

Reaction	Tally
(n,p)	F8
(n,α)	F28
$(n,{}^3\text{He})$	F58
(n,d)	F48
Heavy recoil ions	F18
All reactions	F68

(b) Characterization of the microdosimetric spectrum from MCNP results

MCNP results for each F8 tally are given in the output file in a column format listing the “F8_{*i*}” result for each energy bin ε_i . For example, the table below describes how the results for the F68 reaction are set out in the output file, according to the 185 energy bins specified in the “e8” card.

E (MeV)	F68 (pulses)
ε_1	F68 ₁
ε_2	F68 ₂
...	...
ε_i	F68 _{<i>i</i>}
...	...
ε_{185}	F68 ₁₈₅

As $y = \varepsilon/\bar{l}$ with $\bar{l} = 2d/3$ and $d = 1 \mu\text{m}$, the lineal energy is obtained with MCNP, depending on the energy ε_i , in MeV, for each group, as follows:

$$y_i = \left(\frac{1000}{2/3}\right) \varepsilon_i = 1500 \varepsilon_i$$

The number of pulses in y_i channel is equal to $n_i = F68_i$ and the total number of all pulses is given by the sum of all n_i . For each y_i , the frequency distribution is obtained *via*:

$$f(y_i) = \frac{n_i}{\sum n_i} = \frac{F68_i}{\sum_{i=1}^{i=185} F68_i}$$

The $f(y)$ function integral is normalized to 1. Two microdosimetric quantities can be drawn from the frequency distribution: the mean frequency energy \bar{y}_f , and the mean lineal energy \bar{y}_D , in $\text{keV} \cdot \mu\text{m}^{-1}$. Quantitatively, the mean frequency energy stands for the most frequent lineal energy measured by the TEPC, whereas the mean lineal energy corresponds to the lineal energy contributing the most, in average, to the absorbed dose delivered in the TEPC cavity by the radiation field. This latter can be roughly regarded as the mean stopping power of secondary particles set in motion.

$$\bar{y}_f = \int_0^\infty y f(y) dy \quad \bar{y}_D = \frac{\int_0^\infty y^2 f(y) dy}{\bar{y}_f}$$

For the value histogram of 185 bins, these theoretical expressions can be written as follows:

$$\bar{y}_f = \sum_{i=1}^{i=n} y_i f(y_i) = 1500 \times \frac{\sum_{i=1}^{i=185} \varepsilon_i n_i}{\sum_{i=1}^{i=185} n_i} = 12.3 \text{ keV} \cdot \mu\text{m}^{-1}$$

$$\bar{y}_D = \frac{\sum_{i=1}^{i=n} y_i^2 f(y_i)}{\sum_{i=1}^{i=n} y_i f(y_i)} = 1500 \times \frac{\sum_{i=1}^{i=185} \varepsilon_i^2 n_i}{\sum_{i=1}^{i=185} \varepsilon_i n_i} = 111 \text{ keV} \cdot \mu\text{m}^{-1}$$

The uncertainties associated to both quantities derive from the statistical uncertainties σ_i of tally F8 result for the i^{th} lineal energy according to:

$$\sigma(\bar{y}_f) = \bar{y}_f \left[\left(\frac{\sqrt{\sum_i (\varepsilon_i \sigma_i)^2}}{\sum_i \varepsilon_i n_i} \right)^2 + \left(\frac{\sqrt{\sum_i \sigma_i^2}}{\sum_i n_i} \right)^2 \right]^{1/2};$$

$$\sigma(\bar{y}_D) = \bar{y}_D \left[\left(\frac{\sqrt{\sum_i (\varepsilon_i^2 \sigma_i)^2}}{\sum_i \varepsilon_i^2 n_i} \right)^2 + \left(\frac{\sqrt{\sum_i (\varepsilon_i \sigma_i)^2}}{\sum_i \varepsilon_i n_i} \right)^2 \right]^{1/2}$$

To build the lineal energy spectrum, the total absorbed dose fraction per occurrence in the bin y is defined according to equation (9).

$$d(y) = \frac{yf(y)}{\bar{y}_f} \quad (9)$$

It is convenient to plot this dose fraction in a semi-logarithmic scale (x -axis in log scale). By assuming that the integral over the whole spectrum provides the dose:

$$d(y) = \frac{dD}{dy} \Rightarrow d(y) = \frac{dD}{d(\ln y)} \Leftrightarrow yd(y) = \frac{dD}{dy}$$

Therefore, for the $yd(y)$ plot, MCNP results are processed as follows:

$$y_i d(y_i) = \frac{y_i f(y_i)}{\sum_{i=1}^{i=n} y_i f(y_i)} \left(\frac{1}{\Delta \ln y_i} \right) \Leftrightarrow y_i d(y_i) = \frac{\varepsilon_i n_i}{\sum_{i=1}^{185} \varepsilon_i n_i} \left(\frac{1}{\ln(\varepsilon_i/\varepsilon_{i-1})} \right)$$

(c) Physics instructions in Block 3 and two-step calculation method with MCNP

The kerma factor calculation has to be carried out in two steps in order to evaluate all secondary charged particles components of the microdosimetric spectrum. The first calculation refers to the evaluation of the partial kerma related to protons and alpha particles, and the second refers to the partial kerma related to heavy nuclei: O, C and N. In fact, at the considered energy, the alpha production from capture reactions is only partially taken into account by the default physical model of intranuclear cascade implemented in MCNP, namely CEM03.03. In a first file, the intranuclear cascade model CEM03.03 is replaced by INCL4/ABLA models, *i.e.*, “LCA 8 J 2 1”, which leads to a more precise alpha particles production rate, notably thanks to the compound nucleus evaporation process described by the ABLA model. This first file also enables to determine the component attributed to recoil protons and (n,p) reaction. However, this replacement does not allow the generation of heavy recoil nuclei during elastic scatterings. It is then necessary to write a second file with the default model CEM03.03 to obtain this component. Instructions to include in the two input files are the following:

```
TEPC Rossi chamber
10 1 -7.77E-05 -10 $ internal cavity
20 2 -1.127 -20 10 $ wall
30 0 -30 20
40 0 30

10 so 0.635
20 so 0.889
30 so 2

imp:n 1 1 1 0
imp:h,a 1 1 0 0
mode n h a
act fission=none nonfiss=a
```

```

sdef par=n pos 0 0 -1.5 axs 0 0 1 ext 0 rad=d1 vec 0 0 1 dir 1 erg 13.9
Si1 0 1
spl -21 1
m1 1001 -.103 6000.00a -.569 7014.00a -.035 8016.00a -.293 HSTEP 30
mx1:h 1001.70h 6012.70h 7014.70h 8016.70h
mx1:n model model model model
M2 1001 -0.1011327 6000.00a -0.775501 7014.00a -0.035057 &
8016.00a -0.052316 9019.00a -0.017422 20000.00a -0.018378
mx2:h 1001.70h 6012.70h 7014.70h 8016.70h j 20040.70h
mx2:n model model model model model model
PHYS:N 20 20 0 J J J 1 -1 J J J 0 0 $ 7th entry set to 1
PHYS:H 20 20 -1 J 0 J 1 J J J 0 0 0 .917
phys:a 20 3j 0 5j 0 0 0 .917
LCA 8J 2 1 $ ABLA model
cut:n j 0 0 0 j
cut:h,a j 1E-3 0 0 j
CTME 600
C ++++++ PROTON Energy Deposition ++++++
F6:H 10
F8:N 10
E8 0 1.39E-11 0.0004 183LOG 2.02
FT8 PHL 1 6 1 0
C ++++++ ALPHA Energy Deposition ++++++
F26:A 10
F28:N 10
E28 0 1.39E-11 0.0004 183LOG 2.02
FT28 PHL 1 26 1 0
C ++++++ ALL NUCLEI Energy Deposition ++++++
c F66:h,a,# 10
F66:h,a 10
F68:N 10
E68 0 1.39E-11 0.0004 183LOG 2.02
FT68 PHL 1 66 1 0

```

The transport mode is set with neutrons “n”, protons “h” and alpha particles “a”, *i.e.*, “mode n h a”. The 7th parameter of the “phys:n” card and “phys:p” is set to 1 to ensure the generation and transport of recoil and (*n,p*) protons as well as recoil heavy ions. The second entry, “emcnf”, of the “phys:n” card is set to “20” and “wc1” and “wc2” parameters to 0 in the energy card “cut” for neutrons, protons and alpha particles, in order for the transport to be treated as “analog” below 20 MeV. For neutron transport, models are used *via* the “model” card. Endf70prot (“0.70 h”) and tendl17 libraries are invoked, respectively, for protons and alpha particle transport. The second entry of the “cut: h,a” is set at 1 keV to transport all particles above this energy. The intranuclear cascade model INCL4/ABLA implementation is done by

adding the “lca” physics card with its 9th entry, *i.e.*, “icem”, set to “2”. Eventually, the “act” activation card is added with the instruction “act fission = none non-fiss = a” for the delayed alpha particles emission. A particular attention has to be drawn on the fact that the MCNP code carries out the charged particles transport with a class I algorithm. The low inner diameter of the detector cavity imposes to set an appropriate number of substeps for the transport, by means of the “hstep” card. This card works like the “estep” card used for electron transport. The reader can refer to § 1.III part 2 to understand the calculation method for the number of substeps. For the alpha particle transport, the tendl library has been implemented and used. Indeed, no α library is originally implemented in MCNP (a model is used). To implement a library, such as tendl, one needs to download it from the website https://tendl.web.psi.ch/tendl_2017/tendl2017.html, and copy it into the following directory: \mncp6\MCNP_DATA\xdata. Then, one has to add the lines in the “xsdir_mcnp6.” file.

Parameters of the second file stay almost the same as previously, with this time a transport mode implemented for neutrons “n” and heavy ions “#”, *i.e.*, “mode n #”. A “cut:#” card is added, with its first entry set to “1” and “wc1” and “wc2” parameters fixed at 0, for an analog transport of heavy ions above 1 keV. The command line of the “lca” card is removed to restore the default intranuclear cascade model, CEM03.03., as well as the production and transport of heavy nuclei during the code execution. The new or changing instruction lines enabling to evaluate the heavy ion components are given below:

Change inside Block 3:

```

imp:h,# 1 1 0 0
mode n h #
phys:# 20 3j 1 5j 0 0 0 .917
c LCA 8J 2 1
cut:n j 0 0 0 j
cut:h,# j 1e-3 0 0 j
C ++++++ HEAVY RECOIL NUCLEI Energy Deposition ++++++
F16:# 10
F18:N 10
E18 0 1.39E-11 0.0004 183LOG 2.02
FT18 PHL 1 16 1 0

```

(d) Microdosimetric spectrum and partial kerma of each component

The left graph of figure 1.VII.4 displays the microdosimetric spectrum $yd(y)$ as a function of lineal energy for 13.9 MeV neutrons, obtained with the two-steps numerical calculation and with experimental measurement. The right graph of the figure states the different components of the microdosimetric spectrum, protons, alpha particles and heavy ions, obtained thanks to the *Anticoincidence pulse-height* feature of the MCNP code.

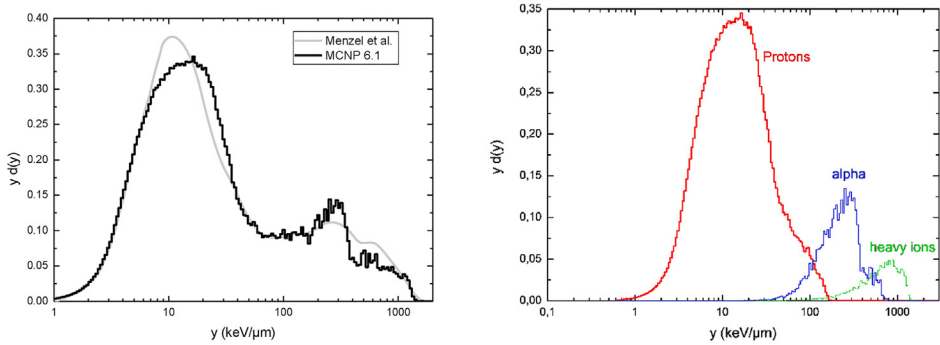


FIG. 1.VII.4 – (left) Microdosimetric spectrum obtained by numerical simulation and experimentally, for 13.9 MeV neutrons, (right) components of the simulated spectrum, *i.e.* protons, alpha and heavy ions set in motion in the TEPC wall.

The partial kerma distribution, calculated with MCNP, for each type of charged particle set in motion is: 79.5% for protons, 15.2% for alpha particles and 5.3% for heavy recoil ions. The theoretical distribution, calculated by means of expression (2), leads to: 78.9% for protons, 11.4% for alpha particles and 9.7% for heavy ions. It is worth noticing that the principal component, related to secondary protons, is roughly the same as that obtained theoretically. By contrast, the MCNP simulation slightly overestimates the alpha contribution while underestimating a bit that of heavy ions.

(e) Kerma factor calculation

In order to calculate the dose, and subsequently the first collision kerma in the wall, both equal in gas since $(\bar{S}/\rho)_g^W = 1$, the following formatting is operated:

$$\frac{K_n}{\Phi} = 1.6 \times 10^{-13} \left(\frac{\bar{l}}{\Phi m_g} \right) \sum_{i=1}^{i=n} y_i n_i = \frac{1.6 \times 10^{-10}}{\Phi m_g} \sum_{i=1}^{i=185} \varepsilon_i n_i$$

The gas mass m_g in the cavity is directly available in a specific section of the MCNP output file. The uncertainty associated to this calculation is given by:

$$\sigma \left(\frac{K}{\Phi} \right) = \frac{1.6 \times 10^{-10}}{\Phi \rho V} \left[\sum_i (\varepsilon_i \sigma_i)^2 \right]^{1/2}$$

The overall calculation leads to a kerma factor 69.7 ± 0.2 pGy.cm² for a computing time of 1000 min. This value is very close to that obtained experimentally: 6.84 pGy.cm² and that obtained by theoretical calculation: 67.9 pGy.cm², which validates the proposed numerical approach. The frequency mean lineal energy and the dose mean lineal energy are respectively $\bar{y}_f = 11.4 \pm 0.1$ keV.μm⁻¹ and

$\bar{y}_D = 87.7 \pm 1.1 \text{ keV} \cdot \mu\text{m}^{-1}$; these values are consistent with those found in the literature.

(f) Calculation of the mean quality factor from the microdosimetric spectrum

The mean quality factor can be assessed with the lineal energy distribution of the absorbed dose $d(y)$ for a given neutron energy:

$$\bar{Q} = \frac{\int_0^\infty Q(y) d(y) dy}{\int_0^\infty d(y) dy}$$

By substituting $d(y)$ by expression (9), the mean quality factor can be expressed as:

$$\bar{Q} = \frac{\int_0^\infty Q(y) y f(y) dy}{\int_0^\infty y f(y) dy}$$

From the MCNP results, this ratio is:

$$\bar{Q} = \frac{\sum_{i=1}^{i=n} Q(y_i) y_i f(y_i)}{\sum_{i=1}^{i=n} y_i f(y_i)} = \frac{\sum_{i=1}^{i=185} Q(y_i) \varepsilon_i n_i}{\sum_{i=1}^{i=185} \varepsilon_i n_i}$$

with, according to ICRU (1986), $Q(y_i)$ expressed with the following formula:

$$Q(y_i) = \frac{a}{y_i} [1 - \exp(-by_i^2 - cy_i^3)]$$

with parameters:

$$\begin{cases} a = 5510 \text{ keV} \cdot \mu\text{m}^{-1} \\ b = 5 \times 10^{-5} \text{ keV}^{-2} \cdot \mu\text{m}^2 \\ c = 2 \times 10^{-7} \text{ keV}^{-3} \cdot \mu\text{m}^3 \end{cases}$$

By performing the overall calculation, we finally obtain a mean quality factor $\bar{Q} = 8.8$ that suffers a significant deviation of 24% with the reference value $Q^*(10) = 7.1$. This deviation can be partially imputed to multiple scatterings occurring 10 mm deep in the ICRU sphere, that cannot be taken into account in the neutron measurement context with the TEPC. By assessing the “fluence – ambient dose equivalent” conversion coefficient similarly as in the previous part, *i.e.*, from the first collision kerma and the quality factor, we get:

$$\left(\frac{\hat{H}^*(10)}{\Phi} \right) = \left(\frac{K_n}{\Phi} \right)_{13.9} \bar{Q} = 67.9 \times 8.8 = 597 \text{ pSv} \cdot \text{cm}^2$$

We infer a deviation of 15% with the reference value (520 pSv.cm²), mainly due to the misevaluation of the $Q^*(10)$ quality factor.

Chapter 2

Detection Principles, Detector Response to Reference Physical Quantities and Operational Dosimetric Quantities

2.I Gas-Filled Detector Operating in Ionization Chamber Mode for Photons and in Proportional Counter Mode for Neutrons

Abstract:

A gas-filled detector is successively operated in current mode (ionization chamber) for a photon field (figure 2.I.1) and in pulse mode (proportional counter) for a neutron field (figure 2.I.1). This application is aimed at evaluating separately dosimetric quantities with both operating modes. This problem highlights the possibility of determining different dosimetric quantities depending on the particle type and the operating mode.

Objectives:

- Establish if the chamber wall is tissue-equivalent.
- Determination of the cavity type according to the cavity theory.
- Calculation of the current in a small cavity.
- Evaluation of an operational quantity from a physical quantity measured by the ionization chamber in a photon field.
- Understand the associated electronic counting system, from the radiation interaction in the detector to the pulse counted and recorded, for a proportional counter exposed to a neutron field.
- Assessment of a protection dosimetric quantity from the fluence.
- Calculation of the neutron kerma in the detector wall.
- Numerical simulation of the energy response of a chamber.

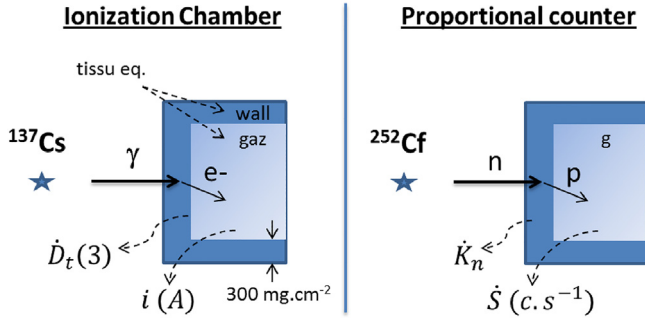


FIG. 2.I.1 – Detector operating in ionization chamber- or proportional counter-mode respectively for a photon or a neutron field.

Part 1: Ionization Chamber in a Photon Field

A chamber with a cylindrical gaseous cavity of 8 cm length and 4.5 cm radius (*i.e.*, a volume of 500 cm^3) is considered. The filling gas is a tissue-equivalent ($\rho = 5.2 \times 10^{-3} \text{ g.cm}^{-3}$ and $W_g = 26 \text{ eV}$). The wall is composed of a mixture of polyethylene $(\text{CH}_2)_n$ and magnesium fluoride (MgF_2) with a surface mass of 300 mg.cm^{-2} . This detector operating in current mode is exposed to the photon field described below:

- ^{137}Cs point-source encapsulated in 1 mm of steel.
- $A = 3.7 \times 10^{10} \text{ Bq}$.
- $E_\gamma = 662 \text{ keV}$.
- $\Gamma_\gamma = 0.85$.
- “Air kerma – ambient dose equivalent under 3 mm” conversion coefficient at 662 keV: $(H'(3.0^\circ)/K_a) = 1.184 \text{ Sv.Gy}^{-1}$ (from Behrens, 2017).

The source is placed in the air at 40 cm from the entrance face of the detector. Data used in this problem at 662 keV are given in table 2.I.1 (drawn from the website: <https://www.nist.gov/pml/x-ray-mass-attenuation-coefficients>).

TAB. 2.I.1 – Mass energy-absorption coefficients, mass attenuation coefficients, molar masses and densities.

Element	H	C	F	Mg	Soft tissue	Steel	Air
$\left(\frac{\mu_{\text{en}}}{\rho}\right) (\text{cm}^2 \text{g}^{-1})$	0.0583	0.0294	0.0288	0.0291	0.0324		0.0294
Molar mass (g.mol^{-1})	1	12	19	24			
$\left(\frac{\mu}{\rho}\right) (\text{cm}^2 \text{g}^{-1})$					0.0853	0.0737	0.0774
$\rho (\text{g.cm}^{-3})$					1	8	1.3×10^{-3}

(a) Calculation of the polyethylene mass fraction for a tissue-equivalent wall

At a given energy, the necessary condition for a wall to be considered as tissue-equivalent is that the mass energy-absorption coefficient of its material (m) is equal to that of tissue (t):

$$\left(\frac{\mu_{\text{en}}}{\rho}\right)_{662}^t = \left(\frac{\mu_{\text{en}}}{\rho}\right)_{662}^m$$

The mass energy-absorption coefficients of CH_2 and MgF_2 are separately deduced using the following additivity formula for the i elements composing the material with weight fractions w_i :

$$\left(\frac{\mu_{\text{en}}}{\rho}\right) = \sum_i w_i \left(\frac{\mu_{\text{en}}}{\rho}\right)^i$$

The calculation for CH_2 yields:

$$\begin{aligned} \left(\frac{\mu_{\text{en}}}{\rho}\right)^{\text{CH}_2} &= \frac{2}{14} \left(\frac{\mu_{\text{en}}}{\rho}\right)^{\text{H}} + \frac{12}{14} \left(\frac{\mu_{\text{en}}}{\rho}\right)^{\text{C}} = \frac{2}{14} \times 0.0583 + \frac{12}{14} \times 0.0294 \\ &= 0.0335 \text{ cm}^2 \cdot \text{g}^{-1} \end{aligned}$$

In a similar manner for MgF_2 , it becomes:

$$\left(\frac{\mu_{\text{en}}}{\rho}\right)^{\text{MgF}_2} = 0.0289 \text{ cm}^2 \cdot \text{g}^{-1}$$

Finally, fractions by weight must be solutions of the system hereafter:

$$\begin{cases} w_{\text{CH}_2} \left(\frac{\mu_{\text{en}}}{\rho}\right)^{\text{CH}_2} + w_{\text{MgF}_2} \left(\frac{\mu_{\text{en}}}{\rho}\right)^{\text{MgF}_2} = \left(\frac{\mu_{\text{en}}}{\rho}\right)^t \\ w_{\text{CH}_2} + w_{\text{MgF}_2} = 100\% \end{cases}$$

Solving the set of equations provides the following fractions: $w_{\text{CH}_2} = 76.1\%$ and $w_{\text{MgF}_2} = 23.9\%$.

(b) Calculation of the collision kerma rate in air at the entrance surface of the detector

The collision kerma rate in air as a function of the fluence rate $\dot{\Phi}$ at the calculation point is derived from the expression below. Note that a normalization factor has been applied to get the result in $\text{mGy} \cdot \text{h}^{-1}$.

$$\dot{K}_a^{\text{col}} = 5.76 \times 10^{-4} \left(\frac{\mu_{\text{en}}}{\rho}\right)^a \dot{\Phi} E_\gamma$$

This formula can be expressed against the source activity A and the various transmissions of materials located between the source and the calculation point, *i.e.*, steel and air:

$$\dot{K}_a^{\text{col}} = 5.76 \times 10^{-4} \left(\frac{\mu_{\text{en}}}{\rho} \right)^a E_\gamma \frac{A\Gamma_\gamma}{4\pi d^2} \exp\left(-\left(\frac{\mu}{\rho}\right)^s \rho_s x_s\right) \exp\left(-\left(\frac{\mu}{\rho}\right)^a \rho_a x_a\right) \quad (1)$$

The numerical application provides:

$$\begin{aligned} \dot{K}_a^{\text{col}} &= 5.76 \times 10^{-4} \times 0.0294 \times 0.667 \times \frac{3.7 \times 10^{10} \times 0.85}{4\pi \times 40^2} \times \exp(-0.0737 \times 8 \times 0.1) \\ &\times \exp(-0.0774 \times 1.3 \cdot 10^{-3} \times 39.9) = 16.6 \text{ mGy} \cdot \text{h}^{-1} \end{aligned}$$

(c) Calculation of the absorbed dose under the wall of mass surface $300 \text{ mg} \cdot \text{cm}^{-2}$

Firstly, we have to check if the electronic equilibrium holds true in the cavity wall, under a depth corresponding to the range of the most energetic secondary electrons set in motion in the wall. For photons of 662 keV, Compton scattering effect is prominent. The maximum energy of Compton electrons is given by the following formula:

$$E_{C_{\text{max}}} = \frac{4E_\gamma^2}{4E_\gamma + 1} = \frac{4 \times (0.667)^2}{(4 \times 0.667) + 1} = 0.48 \text{ MeV}$$

The range of electrons in the wall at this given energy is evaluated using the formula of Katz and Penfold (1952):

$$\begin{aligned} R &= 412 \times (0.48)^n \quad \text{with} \quad n = 1.265 - 0.0954 \ln(0.48) \quad (2) \\ &=> R = 154.6 \text{ mg} \cdot \text{cm}^{-2} \end{aligned}$$

This range is smaller than the $300 \text{ mg} \cdot \text{cm}^{-2}$ mass surface of the wall. Therefore, the electronic equilibrium can be assumed and the collision kerma rate is very close to the dose rate at this point.

$$\dot{D}_t(3) \cong \dot{K}_t^{\text{col}}(3) = \dot{K}_a^{\text{col}} \left(\frac{\mu_{\text{en}}}{\rho} \right)_a^t \exp\left(-\left(\frac{\mu}{\rho}\right)^t \rho_t x_t\right)$$

$$\dot{D}_t(3) = 16.6 \times \frac{0.0324}{0.0294} \times \exp(-0.0853 \times 300 \times 10^{-3}) = 17.8 \text{ mGy} \cdot \text{h}^{-1}$$

(d) Type of cavity at which the chamber operates

To determine the type of cavity at which the chamber operates (either large or small), we have to evaluate the range of secondary electrons in the gas filling the cavity, which are set in motion in the wall. Since the medium has a low Z and the energy of secondary electrons is quite low, we can assume that $(\mu_{tr})_t \cong (\mu_{en})_t$. Thus, the mean energy of secondary electrons is calculated as follows:

$$\bar{T}_{e^-} = \frac{\left(\frac{\mu_{tr}}{\rho}\right)^t}{\left(\frac{\mu}{\rho}\right)^t} E_\gamma = \frac{0.0324}{0.0853} \times 662 = 251.4 \text{ keV} \quad (3)$$

Note that this mean energy can be seen as an upper limit. The mean energy of electrons crossing the wall, indeed, is lower since they experience Coulomb scattering in the cavity wall. Otherwise, Attix (2007) recommends choosing $\bar{T}_{e^-}/2$ whereas an MCNP calculation shows that, for ^{60}Co , the mean energy is rather close to $2\bar{T}_{e^-}/3$. In this application, we use the conservative assumption of the whole mean energy \bar{T}_{e^-} . The range of electrons in the gas at this energy is derived from the Katz and Penfold formula:

$$R = 51.9 \text{ mg.cm}^{-2} \Rightarrow R = \frac{51.9 \times 10^{-3}}{1.5 \times 10^{-3}} = 34.6 \text{ cm}$$

This range is compared to the mean chord of the chamber provided by the Cauchy theorem:

$$\bar{l} = \frac{4V}{S} = \frac{4\pi r^2 h}{2\pi r h} = 2r = 9 \text{ cm}$$

As a result, the range of electrons is 3.8 times longer than the mean chord of the chamber. Moreover, we can assume that the fluence of primary photons and secondary electrons do not change when entering the gas cavity. Thus, this cavity fulfils the required Bragg–Gray conditions to be considered of “small” type.

(e) Calculation of the current generated in the chamber

For a small cavity, the relationship between the current arising in the cavity gas and the dose rate under the wall of mass surface 300 mg.cm^{-2} is derived from the following expression:

$$\dot{D}_t(3) = 3.6 \times 10^9 \frac{\bar{W}_g}{\rho_g V_g} \left(\frac{\bar{S}}{\rho}\right)_i^t$$

Since the gas is considered as tissue-equivalent, $(\bar{S}/\rho)_g^t = 1$ and the chamber current is:

$$i = \dot{D}_t(3) \frac{\rho_g V_g}{3.6 \times 10^9 \bar{W}_g} \left(\frac{\bar{S}}{\rho}\right)_t^g = 17.8 \times \frac{5.2 \times 10^{-3} \times 500}{3.6 \times 10^9 \times 26} = 4.9 \times 10^{-10} \text{ A}$$

- (f) Evaluation of the directional dose equivalent under 3 mm at 0° from the dose under the wall of mass surface 300 mg.cm^{-2} ; comparison with the value obtained from the air kerma

We assume that the measurement of $\dot{D}_t(3)$ with this chamber is quite close to the dose measurement under 3 mm of ICRU sphere. Then, the directional dose equivalent under 3 mm at 0° is assessed by weighting $\dot{D}_t(3)$ with the quality factor $Q = 1 \text{ Sv.Gy}^{-1}$.

$$\hat{H}'(3.0^\circ) = \dot{D}_t(3)Q = 17.8 \text{ mSv.h}^{-1}$$

The value of this operational quantity is drawn from the air kerma:

$$\dot{H}'(3.0^\circ) = \dot{K}_a^{\text{col}} \left(\frac{H'(3.0^\circ)}{K_a} \right) = 16.6 \times 1.184 = 19.6 \text{ mSv.h}^{-1}$$

There is a deviation under 10% when comparing the assessed value with the actual value obtained from the air kerma:

$$\frac{\Delta H'}{H'} = \frac{17.8 - 19.6}{19.6} \times 100 = -9.2\%$$

Part 2: Proportional Counter in a Neutron Field

In this second part, we consider the same chamber as before, operating as a proportional counter for pulse measurement (figure 2.I.2). The counter is exposed to the neutron field described below:

- ^{252}Cf point-source at 40 cm from the wall.
- Neutron yield: $\dot{N} = 7.2 \times 10^8 \text{ (n).s}^{-1}$ in 4π sr.
- Mean energy: 2.4 MeV.

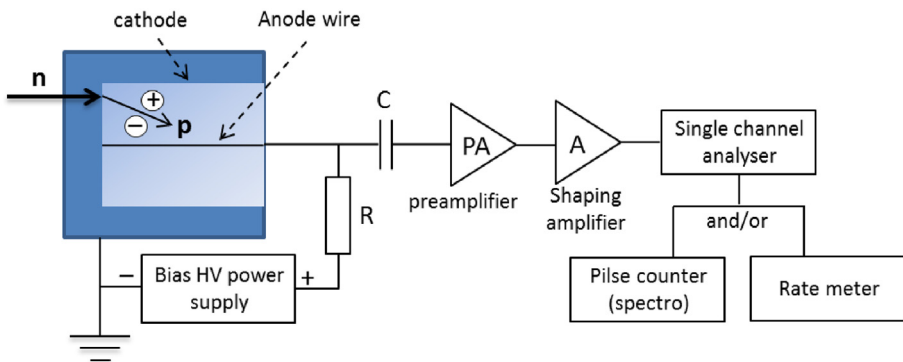


FIG. 2.I.2 – Typical bloc diagram of the counting electronics associated with the proportional counter in pulse mode.

- “Fluence – ambient dose equivalent” conversion coefficient for ^{252}Cf , $H^*(10)/\Phi = 385 \text{ pSv.cm}^2$ (Antoni and Bourgois, 2017a).

A charge-sensitive preamplifier of time constant RC small compared with the charge collection time integrates the collected charge. This limits the amplitude of the pulse and maintains higher count rates. Characteristics of the detector operated in pulse mode are the following (Ravazzani *et al.*, 2006):

Characteristics of the chamber:

- Anode radius: $a = 2.5 \times 10^{-3} \text{ cm}$.
- Cathode radius: $b = 1.22 \text{ cm}$.
- Gas pressure: $p = 4 \text{ atm}$.
- Detection efficiency: $\varepsilon_d = 0.1 \text{ (c).cm}^2$.

Operating mode and electronic properties of the gas:

- Bias high-voltage: $V = 1430 \text{ V}$.
- Potential difference through which an electron moves between successive ionizing events: $\delta V = 34.5 \text{ V}$.
- Minimum value of the electric field below which multiplication cannot occur: $K = (E/p)_{\min} = 10^4 \text{ V.cm}^{-1}.\text{atm}^{-1}$.
- Fano factor: $F = 0.2$.
- Polya distribution parameter: $b_p = 0.7$.
- Electron drift time: $T_{\text{el}} = 1 \mu\text{s}$.
- Positive ion drift time: $T_{\text{ion}} = 1 \text{ ms}$.

Characteristics of the counting electronics:

- Capacitance of the RC integrator: $C = 3.4 \text{ pF}$.
- Amplification factor: $A = 80$.
- Discrimination threshold in total counting: $V_{\text{th}} = 2 \text{ V}$.

For the following calculations, the air neutron attenuation as well as the scattered radiation are omitted. Moreover, we assume the fluence to be constant over all the sensitive volume of the detector. Other useful data are given hereafter.

Dosimetric data are in tables 2.1.2 and 2.1.3.

Radiation weighting factors for neutron as a function of energy are drawn from ICRP (2007).

$$W_R = \begin{cases} 2.5 + 18.2 \exp\left[-(\ln(E_n))^2/6\right] & E_n < 1 \text{ MeV} \\ 5 + 17 \exp\left[-(\ln(2E_n))^2/6\right] & 1 \text{ MeV} < E_n < 50 \text{ MeV} \\ 2.5 + 3.25 \exp\left[-(\ln(0.04E_n))^2/6\right] & E_n > 50 \text{ MeV} \end{cases}$$

In this application, nuclear reactions are restricted to elastic scattering on the hydrogen of the detector cavity wall.

TAB. 2.I.2 – “Fluence – mean dose to the organ” conversion coefficients for anteroposterior geometry, from ICRP (2010).

Tissue or organ	$\frac{\bar{D}_T}{\Phi}$ en pGy.cm ²
Bladder	26.5
Bone marrow (red)	17.4
Bone surface	21.2
Breast	42.8
Colon	24.6
Gonads	34.7
Liver	20.2
Lung	23.5
Oesophagus	21.2
Remainder	21.1
Skin	26.8
Stomach	24.3
Thyroid	37.8
Brain	15.4
Salivary glands	23.6

TAB. 2.I.3 – Tissue weighing factors for several organs, taken from ICRP (2007).

Tissue or organ	Weighting factor W_T	Tissue or organ	Weighting factor W_T
Gonads	0.08	Liver	0.04
Bone marrow (red)	0.12	Oesophagus	0.04
Colon	0.12	Thyroid	0.04
Lung	0.12	Skin	0.01
Stomach	0.12	Bone surface	0.01
Bladder	0.04	Salivary glands	0.01
Breast	0.12	Brain	0.01
Remainder	0.12		

(a) Calculation of the first collision kerma rate

The general formula of the first collision kerma is defined for an interaction at a depth smaller than or equal to the first mean free path of neutrons in the crossed medium. It is the only dosimetric quantity that can be calculated analytically for neutrons owing to the issue of assessing the fluence beyond the first mean free path. Its expression for a single chemical element is the following:

$$K_n = \frac{\Phi}{\rho} N \sum_i \sigma_i \bar{\epsilon}_{tr,i}$$

with N the atom density (in cm⁻³) of the chemical element, σ_i the cross section of reaction i and $(\bar{\epsilon}_{tr})_i$ the mean energy transferred to secondary charged particles

originating from this reaction. For a mixture of various materials, denoted by m , of mass fractions w_m , the formula of the kerma, expressed in $\text{mGy}\cdot\text{h}^{-1}$, is written as:

$$\dot{K}_n = 5.76 \times 10^{-4} \eta_A \dot{\Phi} \sum_m \frac{w_m}{A_m} \sum_c n_{m,c} \sum_i \sigma_{m,c,i} \bar{\epsilon}_{\text{tr},m,c,i}$$

where η_A is the Avogadro constant, A_m is the molar mass of material m and $n_{m,c}$ is the number of atoms of a chemical element c composing the material. In this application, only scattering on hydrogen of the CH_2 compound accounts for kerma calculation. Accordingly, $(\bar{\epsilon}_{\text{tr}})_{(n,n)} = E_n/2$, and the expression presented above is reduced to:

$$\dot{K}_n = 5.76 \times 10^{-4} \eta_A \left(\frac{\dot{N}}{4\pi d^2} \right) w_{\text{CH}_2} \frac{n_{\text{H}}}{A_{\text{CH}_2}} \sigma_{(n,n)} \frac{E_n}{2}$$

The cross section of the elastic scattering on hydrogen is derived from the empirical formula of Gammel (1973), expressed against the neutron energy (in MeV):

$$\sigma_{(n,n)}(E_n) = \frac{5.063 \pi}{1 + 7.412 E_n + 0.1105 (E_n)^2} + \frac{0.8652 \pi}{1 + 0.2427 E_n + 0.0028 (E_n)^2}$$

The cross section at 2.4 MeV is:

$$\begin{aligned} \sigma_{(n,n)}(2.4) &= \frac{5.063\pi}{1 + (7.412 \times 2.4) + 0.1105 \times (2.4)^2} + \frac{0.8652\pi}{1 + (0.2427 \times 2.4) + 0.0028 \times (2.4)^2} \\ &= 2.52 \text{ barns} \end{aligned}$$

Thus, the first collision kerma rate in the cavity wall is:

$$\begin{aligned} \dot{K}_n &= 5.76 \times 10^{-4} \times 6.02 \times 10^{23} \times \frac{7.2 \times 10^8}{4\pi \times 40^2} \times 0.716 \times \frac{2}{14} \times 2.52 \times 10^{-24} \times \frac{2.4}{2} \\ &= 3.9 \text{ mGy}\cdot\text{h}^{-1} \end{aligned}$$

- (b) Assessment of the total charge collected for a pulse and its associated uncertainty

For this calculation, wall effects are neglected and the assumption is made that all the mean energy transferred in a collision with hydrogen is deposited within the cavity. The charge resulting from the deposit of the entire energy of the recoil proton is:

$$q = g \frac{(\bar{\epsilon}_{\text{tr}})_{(n,n)}}{W_g} e \quad (4)$$

The gain value, when no space charge effect occurs, is derived from the formula of Diethorn (1956):

$$\ln g = \frac{V}{\ln(a/b)} \frac{\ln 2}{\delta V} \left[\ln \left(\frac{V}{p a \ln(a/b)} \right) - \ln K \right]$$

In this case study, the gain is:

$$\Leftrightarrow g = \exp \left[\frac{1430}{\ln(1.22/2.5 \times 10^{-3})} \times \frac{\ln 2}{34.5} \right. \\ \left. \times \left[\ln \left(\frac{1430}{4 \times 2.5 \times 10^{-3} \times \ln(1.22/2.5 \times 10^{-3})} \right) - \ln 10^4 \right] \right] = 50$$

Thus, the maximum pulse height reaches:

$$q = 50 \times \frac{2.4 \times 10^6}{2} \times \frac{1.6 \times 10^{-19}}{26} = 3.69 \times 10^{-13} \text{ C}$$

The relative uncertainty of the charge is calculated from expression (4). Let $n_o = (\bar{\epsilon}_{\text{tr}})_{(n,n)}/\bar{W}_g$ be the original number of ion pairs created. Then, the propagation law allows to write:

$$\left(\frac{\sigma_q}{q} \right)^2 = \left(\frac{\sigma_{n_o}}{n_o} \right)^2 + \left(\frac{\sigma_g}{g} \right)^2$$

It is shown that the relative uncertainty can be expressed as the ratio below (Knoll, 1989):

$$\left(\frac{\sigma_q}{q} \right)^2 = \frac{(F + b_p)}{n_o} = \frac{\bar{W}_g(F + b_p)}{(\bar{\epsilon}_{\text{tr}})_{(n,n)}}$$

Therefore, the relative uncertainty for the charge is:

$$\frac{\sigma_q}{q} = \sqrt{\frac{26 \times (0.2 + 0.5)}{1.2 \times 10^6}} \cong 4 \times 10^{-3}$$

The charge with its uncertainty is finally: $3.69 \times 10^{-13} \pm 0.01 \times 10^{-13} \text{ C}$.

(c) Determination of the pulse height matching the maximum charge collected

Most of the collected charge is produced by positive secondary ions, created in the zone where avalanches form, drifting toward the cathode within a time $T_{\text{ion}} = 1 \text{ ms}$. T_{ion} can be considered as the total charge collection time. Indeed, only a small fraction of the collected charge is due to electrons drifting toward the anode within a very short time $T_{\text{el}} = 1 \mu\text{s}$. However, in order to limit the pulse duration and thus, to increase the count rate, a small time constant RC ($\sim 10 \mu\text{s}$) is chosen at the charge preamplifier. Accordingly, the pulse rise time stops at T_{el} (see figure 2.I.3).

The signal voltage is given by the following expression (Knoll, 1989):

$$V(t) = \frac{q}{C} \frac{1}{2 \ln(b/a)} \left\{ \ln \left[a^2 + (b^2 - a^2) \frac{t}{T_{\text{ion}}} \right] - \ln(a^2) \right\}$$

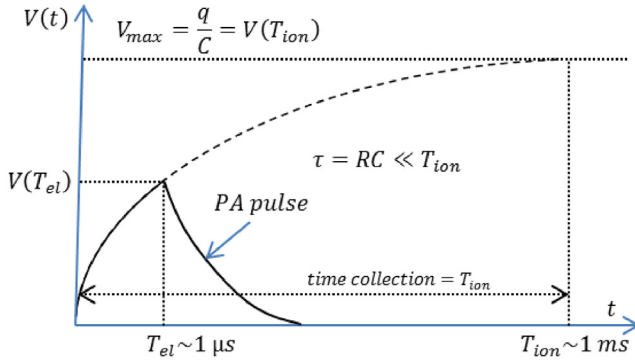


FIG. 2.I.3 – Proportional counter charge collection process.

When $t = T_{ion}$, the amplitude reaches a maximum:

$$\begin{aligned}
 V_m \pm \sigma_{V_m} &= \frac{q}{C} \pm \left(\frac{\sigma_Q}{Q} \right) \frac{q}{C} = \frac{3.69 \times 10^{-13}}{3.4 \times 10^{-12}} \pm \frac{7.38 \times 10^{-11}}{3.4 \times 10^{-12}} \times 4 \times 10^{-3} \\
 &= 108.5 \pm 0.4 \text{ mV}
 \end{aligned}$$

- (d) Determination of the pulse height for a time constant RC setting the pulse height for a rise time equal to the electron drift time

With the RC integrator, the pulse rise time is limited to $t = T_{el}$. Accordingly, the pulse is generated with the following voltage:

$$\begin{aligned}
 V(T_{el}) &= 108.5 \times \frac{1}{2 \ln(1.22/2.5 \times 10^{-3})} \left\{ \ln \left[(2.5 \times 10^{-3})^2 \right. \right. \\
 &\quad \left. \left. + \left(1.22^2 - (2.5 \times 10^{-3})^2 \right) \frac{10^{-6}}{10^{-3}} \right] - \ln \left((2.5 \times 10^{-3})^2 \right) \right\} = 48 \text{ mV}
 \end{aligned}$$

Along with its uncertainty: $V(T_{el}) \pm \sigma_{V(T_{el})} = 48 \pm 0.2 \text{ mV}$.

Finally, with an amplification factor of 80 at the amplifier output, the height V_a of the pulse following a gaussian distribution is:

$$V_a \pm \sigma_{V_a} = A V(T_{el}) \pm A \sigma_{V(T_{el})} = 80 \times 0.048 \pm 80 \times 2.10^{-3} = 3.84 \pm 0.16 \text{ V}$$

This value can be processed in two ways, depending on the purpose:

- *Spectroscopy*: in a multichannel analyzer, a single-channel analyzer compares V_a to a higher level and to a lower level (discrimination process) and sends a logic pulse (TTL type) in the matching channel. In this case, 3.84 V would ideally correspond to a pulse in the 1.2 MeV preliminarily energy calibrated channel.

- *Total counting*: the pulse height V_a is compared to a low amplitude threshold V_{th} in order to spur signal due to background noise, gamma radiation, etc. If the value is higher than the threshold, a logic pulse is generated and counted.
- (e) Evaluation of the energy resolution of the chamber and assessment of the count rate

The energy calibration matches the 3.84 V channel with a 1.2 MeV energy. The energy resolution corresponding to the full width at half maximum of the peak following a gaussian distribution is:

$$FWHM = 2.355 \left(\frac{\sigma_{V_a}}{V_a} \right) (\bar{e}_{tr})_{(n,n)} = 11.3 \text{ keV}$$

Practically, the resolution is determined by the electronic counting system and particularly by the discrimination ability of the single-channel pulse height analyzer. By assuming that all pulse heights are identical (*i.e.*, energy transferred entirely in the gas and absence of wall effect), as $V_a \pm \sigma_{V_a} > V_{th}$, in total counting mode, the measured signal corresponds to the efficiency multiplied by the initial neutron fluence:

$$\dot{S} = \varepsilon_d \dot{\Phi} = \varepsilon_d \frac{\dot{N}}{4\pi d^2} = 0.1 \times \frac{7.2 \times 10^8}{4\pi \times 40^2} = 3.6 \times 10^3 \text{ (c).s}^{-1}$$

- (f) Evaluation and comparison of the effective dose rate and the ambient dose equivalent at the detector location

The effective dose rate can be evaluated according to the expression below:

$$\dot{E} = \sum_T W_T \dot{H}_T = \sum_T W_T \sum_R W_R \dot{\Phi} \left(\frac{\bar{D}_T}{\Phi} \right)$$

With the fluence rate:

$$\dot{\Phi} = \frac{7.2 \times 10^8}{4\pi \times (40^2)} = 3.6 \times 10^4 \text{ (n) cm}^{-2}\text{s}^{-1}$$

The radiation weighting factor for neutrons of 2.4 MeV mean energy is:

$$W_R = 5 + 17 \exp \left[-(\ln(2 \times 2.4))^2 / 6 \right] = 16.2$$

Table 2.I.4 gives the details to achieve the final result.

Summing the right column components provides the effective dose rate: $\dot{E} = 55.5 \text{ mSv.h}^{-1}$. Note that the first collision kerma rate evaluated previously at 3.9 mGy.h^{-1} is close to all values of \dot{D}_T stated in the first column of table 2.I.4. For some organs, the kerma is higher than the values found (case of internal organs such as the colon) and for others, the kerma is lower (case of external organs like breast).

TAB. 2.I.4 – Results of mean- and equivalent- doses to organs.

	\dot{D}_T (mGy.h ⁻¹)	\dot{H}_T (mSv.h ⁻¹)	$W_T \dot{H}_T$ (mSv.h ⁻¹)
Bladder	3.43	55.91	2.24
Bone marrow (red)	2.26	36.71	4.41
Bone surface	2.75	44.73	0.45
Breast	5.55	90.30	10.84
Colon	3.19	51.90	6.23
Gonads	4.50	73.21	5.86
Liver	2.62	42.62	1.70
Lung	3.05	49.58	5.95
Oesophagus	2.75	44.73	1.79
Remainder	2.73	44.52	5.34
Skin	3.47	56.54	0.57
Stomach	3.15	51.27	6.15
Thyroid	4.90	79.75	3.19
Brain	2.00	32.49	0.32

The first case highlights the neutron fluence attenuation and the second case brings to the fore neutron scattering in tissues. The ambient dose equivalent rate is:

$$\dot{H}^*(10) = \left(\frac{H^*(10)}{\Phi} \right) \dot{\Phi} = 385 \times 10^{-12} \times 3.6 \times 10^4 = 1.386 \times 10^{-5} \text{ Sv.s}^{-1}$$

$$\dot{H}^*(10) = 1.386 \times 10^{-5} \times 3600 = 0.0499 \text{ Sv.h}^{-1} \approx 50 \text{ mSv.h}^{-1}$$

The protection quantity is smaller than the operational quantity: $\dot{H}^*(10) < \dot{E}$.

We must point out that this observation goes against the feature of the operational quantity to slightly overestimate the protection quantity. However, in general, for more realistic neutron fields of workplace, having for most a mean energy around a hundred keV, the protection quantity is overestimated compared to the operational quantity.

2.II Calibration of an Ionization Chamber with a ⁶⁰Co Source

Abstract:

In this application, the calibration in term of ambient dose equivalent, $H^*(10)$, for a radiation survey meter (ionization chamber type) with a ⁶⁰Co source is studied. This calibration operation is processed in a secondary laboratory and requires a device for perfect measurement of air kerma.

The first part is focused on the evaluation of the air kerma with a reference air-equivalent chamber (Sp01 type) in a metrology primary laboratory. In the second part, the calibration in terms of ambient dose equivalent is performed in a secondary laboratory. The third part is devoted to the study of the survey meter response to ^{241}Am gamma rays. The main objective of this last part is to check if the deviation between measured and actual values of the operational quantity is within the limit recommended by standards.

Objectives:

- Understand the calibration process of a radiation protection device, from the primary laboratory to the operational use.
- Calculate the theoretical expression of the air kerma with an ionization chamber.
- Determine the energy response of a survey meter with MCNP.
- Assess a wall-scattering factor with MCNP.
- Assess the relevance of the calibration carried out, depending on the energy measured in a real situation.

Characteristics:

The detector used as an absolute dosimeter for the air kerma measurement is a Sp01 type air-equivalent spherical ionization chamber with the following characteristics:

- Wall: 3 mm of graphite (C) density $\rho_c = 1.847 \text{ g.cm}^{-3}$.
- Inner radius of the cavity: 1.2 cm.
- Effective volume: 7.215 cm^3 .
- Filling gas: dry air density $\rho_a = 1.293 \times 10^{-3} \text{ g.cm}^{-3}$.
- When the source is located at 1 m, the Sp01 chamber measures a current $i = 2 \times 10^{-12} \text{ A}$.

This absolute dosimeter is only employed in the primary laboratory. For the second part, the main characteristics of the cylindrical ionization chamber (Babyline 81 type) are:

- Dry air-filled cylinder of 10 cm length and 8 cm diameter.
- Entrance window surface mass: 1000 mg.cm^{-2} .
- Entrance window material: tissue equivalent (H 10%, C 61%, F 18% and Mg 11%) density $\rho_t = 1.12 \text{ g.cm}^{-3}$.
- Electronic equilibrium is established for 1.25 MeV gamma rays.
- Calibration factor provided by the manufacturer: $N_1 = \dot{D}_t(10)/i = 2.08 \times 10^{11} \text{ mGy.h}^{-1}.\text{A}^{-1}$.
- For ^{60}Co .
- Source-detector distance: 1 m.

The other necessary data are:

- Mean fraction of the secondary electrons kinetic energy lost and released as photon radiation in air (Allisy *et al.*, 2006): $\bar{g} = 0.0032$.
- Mean ionization energy of dry air: $\bar{W} = 33.97 \text{ eV}$.

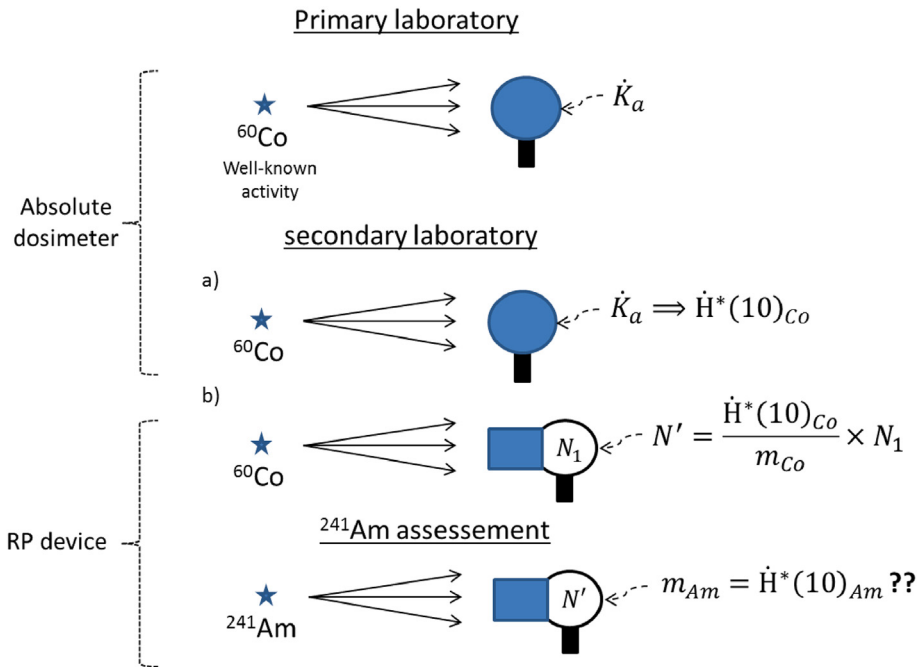


FIG. 2.II.1 – Calibration process of a radiation protection device: from the primary laboratory to the field measurement.

N.B.: all results are given with 3 digits after the decimal point, in accordance with typical conditions of the metrological measurement.

Part 1: Calculation of the Kerma Rate in Air Measured in the Sp01 Chamber at 1 m from the Source

The first step of the calibration is processed in the primary laboratory and consists in measuring with the reference chamber, *i.e.*, an absolute dosimeter, the air kerma at 1 m from a primary source of ^{60}Co (figure 2.II.2).

(a) Air-equivalence property of the wall for 1.25 MeV gamma rays

Table 2.II.1 shows that mass energy-absorption coefficients of carbon and air are identical for 1.25 MeV photons. This implies that for both materials, the transfer of a part of energy from incoming photons to secondary electrons is, in average, the same for the air and for the chamber wall.

$$\left(\frac{\mu_{\text{en}}}{\rho}\right)_{1.25}^a = \left(\frac{\mu_{\text{en}}}{\rho}\right)_{1.25}^c \tag{1}$$

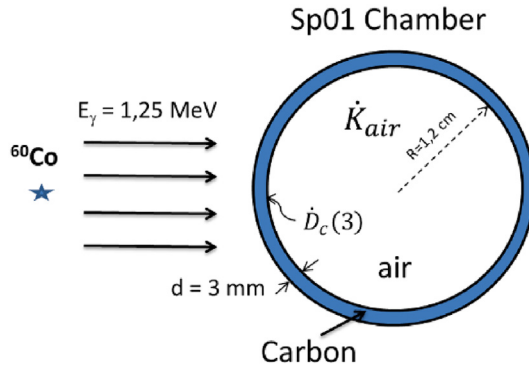


FIG. 2.II.2 – Sketch of the Sp01 reference chamber for the measurement of the air kerma.

TAB. 2.II.1 – Mass energy-absorption coefficients, mass attenuation coefficients and mass stopping powers (from NIST).

	$\left(\frac{\mu_{en}}{\rho}\right)^a$	$\left(\frac{\mu}{\rho}\right)^c$	$\left(\frac{\mu_{en}}{\rho}\right)^c$	$\left(\frac{\mu_{en}}{\rho}\right)^t$	$\left(\frac{\mu}{\rho}\right)^t$	$\left(\frac{\bar{S}}{\rho}\right)^a$	$\left(\frac{\bar{S}}{\rho}\right)^c$
$E_\gamma = 1.25 \text{ MeV}$	0.0267	0.0569	0.0267	0.0293	0.0626		
$\bar{T}_{e^-} = 586 \text{ keV}$						1.757	1.736

- (b) Checking of electronic equilibrium condition in the wall and of Bragg–Gray conditions in the chamber for source photons

Compton scattering is predominant at this energy. The maximum energy of scattered electrons is:

$$E_{C \max} = \frac{4E_\gamma^2}{4E_\gamma + 1} = \frac{4 \times (1.25)^2}{(4 \times 1.25) + 1} = 1.041 \text{ MeV}$$

Using the formula of Katz and Penfold (1952) enables to evaluate the range of electrons in carbon at this energy, in surface mass units:

$$R = 412 \times (1.041)^n \quad \text{with} \quad n = 1.265 - 0.0954 \ln(1.041) \quad (2)$$

$$\Rightarrow R = 433 \text{ mg.cm}^{-2}$$

It corresponds to the following range:

$$R = \frac{433 \times 10^{-3} \text{ g.cm}^{-2}}{1.847 \text{ g.cm}^{-3}} = 0.23 \text{ cm}$$

This value is smaller than the 3 mm wall thickness under which the measurement dose is performed in the Sp01 chamber. Accordingly, the electronic equilibrium is established at this depth for the given photon energy.

The first condition of the Bragg–Gray theory is that the photon fluence rate is the same everywhere inside the chamber, which can be assumed in this case. The second condition is that the secondary electron fluence rate is not modified by the presence of the gaseous cavity. To check if this assumption holds true, we have to assess the mean energy of secondary electrons set in motion by gamma rays in the wall. For this calculation, we assume that the mass energy-absorption coefficient is approximately equal to the mass energy-transfer coefficient for carbon composing the wall, *i.e.*, $(\mu_{tr})_c \cong (\mu_{en})_c$.

$$\bar{T}_{e^-} = \frac{\left(\frac{\mu_{tr}}{\rho}\right)_c}{\left(\frac{\mu}{\rho}\right)_c^{1.25}} E_\gamma = \frac{0.0267}{0.0569} \times 1.25 = 0.586 \text{ MeV} \quad (3)$$

Applying the formula of Katz and Penfold for air and secondary electrons of the energy calculated above leads to:

$$R = \frac{191 \times 10^{-3} \text{ g.cm}^{-2}}{1.293 \times 10^{-3} \text{ g.cm}^{-3}} = 147 \text{ cm}$$

This range is far beyond the 2.4 cm diameter of the chamber. This enables to confirm that the chamber fulfils the conditions for operating in small cavity mode.

(c) Calculation of the air kerma rate using the expression of the dose in a small cavity

The dose rate under the wall thickness for this small cavity is expressed as:

$$\dot{D}_C(3) = 3.6 \times 10^9 \frac{\bar{W}}{\rho_a V_a} \left(\frac{\bar{S}}{\rho}\right)_a^c \quad (4)$$

Since the electronic equilibrium condition holds true in carbon, the dose rate under the wall thickness is very close to the collision kerma rate at this point. Given the assumption of a constant secondary electron fluence and because of the low energy loss of secondary electrons in the gaseous cavity, we can infer that electronic equilibrium is also held in the air filling the cavity. Accordingly, the dose rate in the air of the cavity is equal to the collision kerma rate (\dot{K}^{col}) .

$$\dot{D}_c(3) = \dot{K}_c^{\text{col}}(3) = \left(\frac{\bar{\mu}_{en}}{\rho}\right)_c \dot{\Psi}_c \quad \text{and} \quad \dot{D}_{\text{air}} = \dot{K}_a^{\text{col}} = \left(\frac{\bar{\mu}_{en}}{\rho}\right)_a \dot{\Psi}_a$$

where $\dot{\Psi}$ stands for the fluence rate of primary photons, *i.e.*, the product $\dot{\Phi} \times E_\gamma$. This rate is considered as a constant in the wall and in the gas filling the cavity, so $\dot{\Psi}_c = \dot{\Psi}_a$. Then, by combining the above expressions, it becomes:

$$\dot{K}_a^{\text{col}} = \left(\frac{\bar{\mu}_{\text{en}}}{\rho} \right)_c^a \dot{D}_C(3) \quad (5)$$

However, the total kerma is the sum of (\dot{K}_a^{col}) , the collision kerma and of (\dot{K}_a^{rad}) , the kerma due to different radiation emitting processes (bremsstrahlung, in-flight annihilation and fluorescence for a small fraction). The fraction of the mean energy transferred to secondary electrons and then released as photon radiation is given by the factor $\bar{g} = \dot{K}_a^{\text{rad}} / \dot{K}_a$. Accordingly, we can address the following expression:

$$\dot{K}_a = \dot{K}_a^{\text{col}} + \dot{K}_a^{\text{rad}} \Rightarrow \dot{K}_a^{\text{col}} = \dot{K}_a \left(1 - \frac{\dot{K}_a^{\text{rad}}}{\dot{K}_a} \right) \Rightarrow \dot{K}_a = \frac{\dot{K}_a^{\text{col}}}{(1 - \bar{g})} \quad (6)$$

Finally, with expressions (1), (2) and (3), comes formula (4) of the air kerma inside the gaseous cavity of the chamber.

$$\dot{K}_{\text{air}} = 3.6 \times 10^9 \ i \frac{\bar{W}}{\rho_a V_a} \left(\frac{\bar{S}}{\rho} \right)_a^c \left(\frac{\bar{\mu}_{\text{en}}}{\rho} \right)_c^a \left(\frac{1}{1 - \bar{g}} \right) \prod_i k_i \quad (7)$$

The k_i terms are corrective factors taking into account several phenomena:

- Attenuation and scattering in the wall.
- Charge recombination.
- The polarity of the high voltage.
- The correction of the capacitance of the capacitor related to the charge measurement.
- The radial and axial non-uniformity of the fluence in the gaseous volume in contrast to the kerma measurement at a given point.

In this case study, only the first correction, attenuation and scattering in the wall, is addressed. Other correction factors differ from 1 starting from the 4th digit after the decimal point.

$$\prod_i k_i \approx k_{\text{wall}} = k_{\text{sc}} \exp \left(\left(\frac{\mu}{\rho} \right)_c^a \rho_c d \right)$$

The exponential term reflects the attenuation of photons through the carbon wall. Factor k_{sc} represents the build-up factor of the photon fluence, related to scattering in the wall. The latter can only be obtained with a Monte-Carlo calculation. In order to evaluate the wall total correction factor k_{wall} , a parallel beam of 1.25 MeV photons directed toward a 3 mm thick graphite cylinder is simulated with MCNP. The scattering and attenuation components are separately assessed. To that extent, the mean fluence and its energy distribution are calculated in an empty

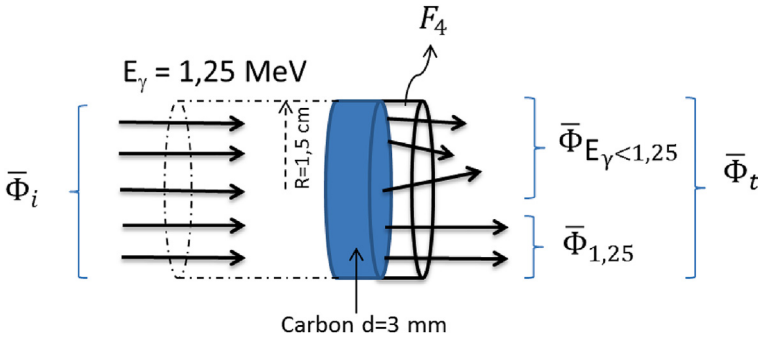


FIG. 2.II.3 – Principle of the MCNP calculation to assess the attenuation and scattering components of the k_{wall} factor.

cylinder of same axis and radius as the graphite cylinder, placed just behind the graphite wall (see figure 2.II.3).

Calculations are performed using the estimator of the mean fluence in a cell, *i.e.*, a F4 tally. The fluence energy distribution is derived from the “e4” card coupled to the tally. The corresponding input file 2.II.1 is presented below.

```

Build up calculation
c cell block
10 1 -1.847 -10 $ material 1: carbon; density 1.847
15 0 -15      $ scoring calculation cell
20 0 -20
30 0 20 10 15

10 RCC 0 0 0 0 0 .3 1.5 $ carbon
15 RCC 0 0 .3 0 0 .0001 1.5 $ scoring calculation cell
20 RCC 0 0 -.1 0 0 .1 1.5

mode p
imp:p 1 1 1 0
sdef par=p pos 0 0 -.05 axs 0 0 1 ext 0 rad=d1 vec 0 0 1 dir 1 erg 1.25
Si1 0 1.5
sp1 -21 1
M1 6000 1
F4:p 15
E4 0 100i 1.25
ctme 3000
    
```

File 2.II.1

The total result of tally F4 is 0.1425 cm^{-2} and represents the total mean fluence in the empty cylinder behind the wall ($\bar{\Phi}_t$). The fluence related to the last energy bin of the “e4” card is 0.1371 cm^{-2} and corresponds to the fluence of 1.25 MeV uncollided photons, going straightaway in the empty cylinder ($\bar{\Phi}_{1.25}$). The wall coefficient k_{wall} is

calculated as the ratio of the fluence at the entrance face of the graphite cylinder (Φ_i) and the total mean fluence in the empty cylinder. The fluence Φ_i is normalized per source photon and is calculated as the inverse of the beam section area.

$$\bar{\Phi}_i = \frac{1}{\pi \times (1.5)^2} = 0.1415 \text{ cm}^{-2} \Rightarrow k_{\text{wall}} = \frac{\bar{\Phi}_i}{\bar{\Phi}_t} = \frac{0.1415}{0.1425} = 0.993$$

The ratio of the fluence at the entrance face of the graphite cylinder (Φ_i) and the mean fluence of 1.25 MeV photons in the empty cylinder (result of the F4 tally in the last energy bin) provides the component related to attenuation (uncollided photon flux).

$$\frac{\bar{\Phi}_i}{\bar{\Phi}_{1.25}} = \frac{0.1415}{0.1371} = 1.032 \approx \exp\left(\left(\frac{\mu}{\rho}\right)^c \rho_c d\right)$$

The exact calculation of the exponential term leads to a theoretical result of 1.032 for the attenuation. Finally, we can derive the scattering coefficient in the wall, k_{sc} :

$$k_{\text{sc}} = \frac{k_{\text{wall}}}{\exp\left(\left(\frac{\mu}{\rho}\right)^c \rho_c d\right)} = \frac{\bar{\Phi}_{1.25}}{\bar{\Phi}_t} = \frac{0.1371}{0.1425} = 0.962$$

For the ratio of mass stopping powers, \bar{S}/ρ , of carbon and air, we take the values related to the mean energy of secondary electrons set in motion in the wall: $\bar{T}_{e^-} = 586 \text{ keV}$. This ratio is 0.988, very close to 1, which enables to verify an additional condition required for the dosimeter to be considered as ‘‘absolute’’.

Note that some authors, *e.g.*, Attix, recommend to take the mass stopping power values corresponding to $\bar{T}_{e^-}/2$. This recommendation relies on a better representation of the energy spectrum of the secondary electrons in the wall, the latter undergoing collisions before entering the gas of the cavity. An MCNP simulation indicates that the mean energy of the outgoing electrons of the wall is more around $2/3 \bar{T}_{e^-} = 483 \text{ keV}$.

The mass energy-absorption coefficient values, in expression (7), have to be taken at the mean energy of photons crossing the detector. However, very few initial photons are scattered in the wall, and to a lesser extent in the gaseous cavity. Thus, we can consider the mass energy-absorption coefficients at the energy of source photons, *i.e.*, 1.25 MeV. The calculation provides:

$$\begin{aligned} \dot{K}_a &= 3.6 \times 10^9 \times 2 \times 10^{-12} \times \frac{33.97}{1.293 \times 10^{-3} \times 7.215} \times 0.988 \times 1 \times \left(\frac{1}{1-0.0032}\right) \times 0.992 \\ \dot{K}_a &= 25.778 \text{ mGy.h}^{-1} \end{aligned}$$

Part 2: Calculation of the Babyline 81 Calibration Factor with the ^{60}Co Source

In this second part, the calibration factor of the ambient dose equivalent is assessed for a cylindrical ionization chamber (Babyline 81 type). This calibration process is

conducted in a secondary laboratory. The first step consists in replicating the primary laboratory conditions of the measurement with the reference chamber: the Sp01 chamber is located at 1 m from a ^{60}Co point source. The same source as that used in the previous part is considered. This leads to an identical measurement of the air kerma, *i.e.*, $\dot{K}_a = 25.778 \text{ mGy.h}^{-1}$. The next step is a calibration operation to associate an ambient dose equivalent rate with the air kerma rate at the same location (see figure 2.II.1).

(a) Ambient dose equivalent rate evaluation at the measurement point

The ambient dose equivalent rate is the multiplication of the air kerma rate by the “air kerma – ambient dose equivalent” conversion coefficient:

$$\dot{H}^*(10) = \dot{K}_a \left(\frac{H^*}{K_a} \right)_{1.25} = 25.778 \times 1.16 = 29.90 \text{ mSv.h}^{-1}$$

The detector to calibrate is placed at the same position as the reference chamber, *i.e.*, at 1 m from the source. First of all, we have to assess the absorbed dose rate under 10 mm of tissue, which is the expected objective of this detector.

(b) Calculation of the absorbed dose rate under the depth of the detector wall

In the first place, we have to evaluate the photon fluence rate at 1 m from the source. This value is derived from the theoretical expression of the collision kerma rate at this point:

$$\dot{K}_a = 5.76 \times 10^{-4} \dot{\Phi} \left(\frac{\mu_{\text{en}}}{\rho} \right)_{1.25}^a \left(\frac{1}{1-\bar{g}} \right) E_\gamma \Rightarrow \dot{\Phi} = \frac{\dot{K}_a(1-\bar{g})}{5.76 \times 10^{-4} E_\gamma \left(\frac{\mu_{\text{en}}}{\rho} \right)_{1.25}^a}$$

$$\dot{\Phi} = \frac{25.778 \times (1 - 0.0032)}{5.76 \times 10^{-4} \times 1.25 \times 0.0267} = 1.336 \times 10^6 (\gamma) \cdot \text{cm}^{-2} \cdot \text{s}^{-1}$$

Since the electronic equilibrium condition holds true under 10 mm for 1.25 MeV gamma-rays, the dose rate under 10 mm of tissue, *i.e.*, under the 1000 mg.cm $^{-2}$ surface mass of the entrance window, is theoretically obtained as follows:

$$\dot{D}_t(10) = \dot{K}_t^{\text{col}}(10) = 5.76 \times 10^{-4} \frac{\dot{\Phi}}{k_{\text{wall}}} E_\gamma \left(\frac{\mu_{\text{en}}}{\rho} \right)_{1.25}^t$$

where k_{wall} is the product of the inverse of the transmission by the scattering coefficient k_{sc} in the tissue-equivalent wall.

$$k_{\text{wall}} = k_{\text{sc}} \exp \left(\left(\frac{\mu}{\rho} \right)_{1.25}^t \rho_t d \right)$$

A numerical simulation can only precisely evaluate the scattering coefficient. A similar MCNP calculation to that accomplished for the Sp01 absolute dosimeter provides $k_{\text{sc}} = 0.926$. The dose rate under the wall thickness is:

$$\dot{D}_t(10) = \frac{5.76 \times 10^{-4} \times 1.336 \times 10^6 \times 0.0293 \times 1.25}{0.926 \times \exp(0.0626 \times 1.12 \times 1)} = 28.37 \text{ mGy.h}^{-1}$$

This rate is very close from the ambient dose equivalent rate, accounting the 1 Sv.Gy⁻¹ quality factor. Hence, we can deduce that:

$$\dot{H}^*(10) \approx \dot{D}_t(10) Q$$

This finding confirms the feature that, for gamma-rays in this energy range, this type of chamber is well-suited to estimate the ambient dose equivalent, without prior calibration.

(c) Calculation of the calibration coefficient specific to the detector

For an accurate $\dot{H}^*(10)$ calibration of the device, we define a new calibration coefficient $N' = N_1 N_2$ with

$$N_2 = \frac{\dot{H}^*(10)}{\dot{D}_t(10)} = \frac{29.90}{28.37} = 1.054 \text{ Sv.Gy}^{-1}$$

$$\Rightarrow N' = N_1 N_2 = 2.08 \times 10^{11} \times 1.054 = 2.19 \times 10^{11} \text{ mSv.h}^{-1}.\text{A}^{-1}$$

In what follows, we propose to evaluate the ambient dose equivalent rate with this Babyline, calibrated with the N' coefficient, for a ²⁴¹Am source.

Part 3: Calculation of the Babyline 81 Response for a ²⁴¹Am Source

In this part, the source is defined with 60 keV photons of 100% intensity and the same fluence at the entrance face of the detector than that calculated for the ⁶⁰Co source. Although the range of 60 keV photons in air is 0.8 cm, much less than the chamber dimensions, the principle of large cavity or the Burlin intermediate cavity theory cannot be used. The attenuation of 60 keV photons in 10 cm of air is, indeed, too high and the assumption of a quasi-constant photon field in the sensitive volume cannot hold. Accordingly, for this step, a Monte-Carlo simulation is mandatory to evaluate, for the same fluence, the ratio of the absorbed dose in the gas for the ⁶⁰Co source and for the ²⁴¹Am source.

For this simulation, the chamber of the previous part is modeled and same conditions apply. The detector is described within a vacuum sphere and its entrance face is exposed to a parallel beam of photons of cross section radius 15 cm. A calculation with the statistical estimator of the total energy deposit, *i.e.*, *F8 tally, is performed to assess the energy imparted to the gas by photons, ε_t , in order to deduce the mean absorbed dose in the sensitive volume. The input file for the 1.25 MeV photons of ⁶⁰Co is shown below:

```

Babyline 81
c cell block
10 1 -1.293e-3 -10
20 2 -1.12      -20 10
30 0           -30 20
40 0           30

10 RCC 0 -5      0 0 10      0 4
20 RCC 0 -5.893 0 0 11.786 0 4.893
30 SO 100

mode e p
imp:p 1 1 1 0
imp:e 1 1 0 0
sdef par=p pos 0 0 -5 axs 0 0 1 ext 0 rad=d1 vec 0 0 1 dir 1 erg 1.25
Si1 0 15
spl -21 1
*F8:e 10
c Air
M1 006000 -0.000124 $ C
    007000 -0.755268 $ N
    008000 -0.231781 $ O
    018000 -0.012827 $ Ar
c tissue equivalent
M2 1000 -.1 6000 -.61 9000 -.18 12000 -.11
ctme 500
    
```

File 2.II.2

For the ²⁴¹Am source, one has to replace the “erg 1.25” energy card of the source definition by “erg 0.06”. The results for the energy deposit in the chamber per source photon, ϵ_t , are 28.1 eV for ⁶⁰Co and 1.6 eV for ²⁴¹Am. The “fluence – absorbed dose in the gaseous volume” conversion coefficient derives as follows:

$$\frac{D_g}{\dot{\Phi}} = 1.602 \times 10^{-19} \left(\frac{\epsilon_t}{\rho_{\text{air}} V_{\text{air}} \dot{\Phi}} \right)$$

For a flux of 1 gamma per second, the fluence rate is $\dot{\Phi} = 1/(\pi \times 15^2) = 1.415 \times 10^{-3} (\gamma) \cdot \text{cm}^{-2} \cdot \text{s}^{-1}$. Therefore, the conversion coefficients are:

$$\left\{ \begin{array}{l} \left(\frac{D_g}{\dot{\Phi}} \right)_{\text{Co}} = 1.602 \times 10^{-19} \times \frac{28.1}{0.65 \times 10^{-3} \times 1.415 \times 10^{-3}} = 4.90 \times 10^{-12} \text{ Gy} \cdot \text{cm}^2 \\ \left(\frac{D_g}{\dot{\Phi}} \right)_{\text{Am}} = 1.6 \times 10^{-19} \times \frac{1.6}{0.65 \times 10^{-3} \times 1.415 \times 10^{-3}} = 0.28 \times 10^{-12} \text{ Gy} \cdot \text{cm}^2 \end{array} \right.$$

where $\rho_{\text{air}} V_{\text{air}}$ is the air mass, in kg, inside the cavity. The factor 1.602×10^{-19} enables the conversion from eV to J. The value of the absorbed dose in the gaseous volume for each source is as follows:

$$\begin{cases} (D_g)_{\text{Co}} = \left(\frac{D_g}{\Phi}\right)_{\text{Co}} \dot{\Phi} = 4.9 \times 10^{-12} \times 1.336 \times 10^6 \times 3600 = 23.56 \text{ mGy.h}^{-1} \\ (D_g)_{\text{Am}} = \left(\frac{D_g}{\Phi}\right)_{\text{Am}} \dot{\Phi} = 0.28 \times 10^{-12} \times 1.336 \times 10^6 \times 3600 = 1.39 \text{ mGy.h}^{-1} \end{cases}$$

Therefore, for a ^{241}Am source responsible for the same fluence as the ^{60}Co source, the rate displayed by a detector calibrated with the coefficient N' would be:

$$m_{\text{Am}} = \dot{H}^*(10)_{\text{Co}} \frac{(D_g)_{\text{Am}}}{(D_g)_{\text{Co}}} = 29.90 \times \frac{1.39}{23.56} = 1.76 \text{ mSv.h}^{-1}$$

However, with the “fluence – ambient dose equivalent” conversion coefficient from the ICRP (1996), for 60 keV photons, we derive $h_{\Phi}^*(10) = 0.51 \text{ pSv.cm}^2$ (table 2.II.2). The actual value of the ambient dose equivalent rate should be:

$$\begin{aligned} \dot{H}^*(10)_{\text{Am}} &= 3600 \times h_{\Phi}^*(10) \times \dot{\Phi} \\ &= 3600 \times 0.51 \times 10^{-12} \times 1.336 \times 10^6 = 2.45 \text{ mSv.h}^{-1} \end{aligned}$$

The deviation from the actual value is:

$$R(E) = \left[\frac{m_{\text{Am}} - \dot{H}^*(10)_{\text{Am}}}{\dot{H}^*(10)_{\text{Am}}} \right] \times 100 = \left[\frac{1.76 - 2.45}{2.45} \right] \times 100 = -28.2 \%$$

Depending on requirements of standards related to the energy response of radiation protection devices for ambient measurements, this underestimation, and accordingly the use of this survey meter to measure such an energy would not necessarily be tolerated. Note that the approach described in this application, broadened to the whole energy spectrum, enables to give the detector energy response to the operational quantity measured.

TABLE 2.II.2 – Physical quantity to protection- and operational- quantity conversion coefficients.

	$\left(\frac{E}{K_{\text{air}}}\right)$	$\left(\frac{H^*}{K_{\text{air}}}\right)$	$h_{\Phi}^*(10)$
$E_{\gamma} = 60 \text{ keV}$			0.51 pSv.cm ²
$E_{\gamma} = 1.25 \text{ MeV}$	1.0002 Sv.Gy ⁻¹	1.16 Sv.Gy ⁻¹	

2.III Calculation of a Dose Rate in a LiF Pellet

Abstract:

In the past few years, Haider *et al.* (1997), have improved Burlin intermediate cavity theory (association of a small cavity and a large cavity) mostly by taking into account the electrons backscattered in the rear face of the chamber. In the first part, the new cavity theory is applied to evaluate the mean absorbed dose in a LiF pellet surrounded by aluminum (“buffer layer”). In this theory, this mean dose can be determined from the absorbed dose at a point under the aluminum inlet face of the detector with an analytical expression. In the second part, the analytical result is verified with MCNP simulations.

Objectives:

- Application of the new cavity theory.
- Calculation of the mean absorbed dose in a sensitive volume from the absorbed dose at a point under the aluminum inlet face of the detector.
- Dose calculation at an interface.
- Correction for photon scattering calculated with MCNP.

Main characteristics:

The pellet is composed of a ${}^7\text{LiF}$ crystal of thickness $t = 2.7$ mm, surrounded by aluminum of thickness $d = 3.7$ mm of 1000 mg.cm^{-2} mass surface. This dosimeter is exposed to a parallel field of 1.25 MeV photons, of fluence rate of $10^6 (\gamma).\text{cm}^{-2}.\text{s}^{-1}$. For 1.25 MeV photons, the coefficients (NIST site) needed for the calculation are (in $\text{cm}^2.\text{g}^{-1}$):

$$\left(\frac{\mu_{\text{en}}}{\rho}\right)^{\text{Al}} = 0.025 \quad \left(\frac{\mu}{\rho}\right)^{\text{Al}} = 0.055 \quad \left(\frac{\bar{\mu}_{\text{en}}}{\rho}\right)_{\text{Al}}^{\text{LiF}} = 0.961 \quad \left(\frac{\bar{S}}{\rho}\right)_{\text{Al}}^{\text{LiF}} = 1.040$$

Densities of aluminum and LiF are, respectively, 2.698 and 2.635 g.cm^{-3} . The backscattering coefficient of secondary electrons in the aluminum wall is $b_m = 0.26$ (Frujinoiu, 2001).

Part 1: Calculation of the Mean dose in a LiF Pellet Using the New Cavity Theory

(a) Calculation of the absorbed dose rate in aluminum at the Al/LiF interface

Firstly, let us check that electronic equilibrium condition holds true under the aluminum thickness. For the photon energy of this application, Compton effect is predominant. The maximum energy of electrons set in motion through this process is:

$$E_{C_{\text{max}}} = \frac{4E_{\gamma}^2}{4E_{\gamma} + 1} = \frac{4 \times (1.25)^2}{4 \times 1.25 + 1} = 1.041 \text{ MeV}$$

The use of Katz and Penfold formula enables to yield the range of secondary electrons set in motion in aluminum of mass surface 1000 mg.cm^{-2} .

$$R = 412 \times (1.041)^n \quad \text{with } n = 1.265 - 0.0954 \ln(1.041)$$

$$\Rightarrow R = 433 \text{ mg.cm}^{-2}$$

As $R < d$, the electronic equilibrium is held under the aluminum layer and the absorbed dose rate is quite close to the collision kerma rate.

$$\dot{D}_{\text{Al}}(10) = \dot{K}_{\text{Al}}^{\text{col}}(10) = 5.76 \times 10^{-4} \frac{\dot{\Phi}}{k_{\text{wall}}} E_{\gamma} \left(\frac{\mu_{\text{en}}}{\rho} \right)^{\text{Al}}$$

with k_{wall} defined as the product of the inverse of the transmission and of the correction factor for photon scattering k_{sc} in the aluminum wall:

$$k_{\text{wall}} = k_{\text{sc}} \exp \left(\left(\frac{\mu}{\rho} \right)^{\text{Al}} \rho_{\text{Al}} d \right)$$

Although the term with the exponential can be calculated, the correction factor can only be thoroughly obtained *via* numerical simulation. An MCNP calculation provides $k_{\text{sc}} = 0.926$ (details in the next part). The dose rate under the aluminum wall is:

$$\dot{D}_{\text{Al}}(10) = \frac{5.76 \times 10^{-4} \times 10^6 \times 0.0256 \times 1.25}{0.926 \times \exp(0.0550 \times 1)} = 18.83 \text{ mGy.h}^{-1}$$

(b) Calculation of the absorbed dose rate in the LiF pellet

In order to assess the absorbed dose rate in the LiF pellet, one has to determine the ratio f of the mean absorbed dose in the LiF to the absorbed dose in aluminum at the Al/LiF interface. According to Frujinou (2001), this ratio is obtained using simplified formulas of Haider *et al.* (1997)'s intermediate cavity theory. This theory is derived from Burlin's theory by encompassing the backscattering phenomenon, proportional to the material atomic number Z , through the introduction of a coefficient b_m . The f ratio is calculated with contributions from the small and large cavities as follows:

$$f = \frac{D_{\text{LiF}}}{D_{\text{Al}}} = d_1 \left(\frac{\bar{S}}{\rho} \right)_{\text{Al}}^{\text{LiF}} + (1 - d_1) \left(\frac{\bar{\mu}_{\text{en}}}{\rho} \right)_{\text{Al}}^{\text{LiF}}$$

with:

$$d_1 = \frac{1 - b_m - (1 - 2b_m) \exp(-\beta g) - b_m \exp(-2\beta g)}{\beta g}$$

The variable β corresponds to the mass attenuation coefficient for the secondary electron flux in the LiF pellet. This variable is expressed as a function of electrons energy, according to formulas of Paliwal and Almond (1976):

$$\left\{ \begin{array}{l} \beta_{\text{LiF}} = \frac{14}{T_{\text{max}}^{1.09}} \text{ for } 0.23 < T_{\text{max}} < 2.27 \text{ MeV} \\ \beta_{\text{LiF}} = \frac{37.9}{T_{\text{max}}^{1.61}} \text{ for } 8 < T_{\text{max}} < 20 \text{ MeV} \end{array} \right.$$

In this case, the maximum energy is 1.04 MeV, which leads to parameter β equal to:

$$\beta = \frac{14}{(1.04)^{1.09}} = 13.4 \text{ cm}^2 \text{g}^{-1}$$

The term g stands for the mean path length of secondary electrons crossing the LiF cavity. This quantity is commonly estimated from the cavity volume V and surface S with the formula $4V/S$. However, a more accurate evaluation from the angular differential scattering cross section of Compton electrons (Horowitz *et al.*, 1983) will be performed in this case.

$$g = \int_0^{\pi/2} \frac{t}{\cos\theta} P(\theta) d\theta = 1.539 t$$

where $P(\theta)$ is the Klein–Nishina angular distribution probability function for 1.25 MeV Compton scattered photons. For the LiF thickness of this application, the mean path length in the LiF pellet is derived:

$$g = 1.539 \times 0.267 = 0.411 \text{ g.cm}^{-2}$$

Numerical application for parameter d_1 provides the following result:

$$\begin{aligned} d_1 &= \frac{1 - 0.26 - (1 - (2 \times 0.26)) \exp(-13.4 \times 0.411) - 0.26 \exp(-2 \times 13.4 \times 0.411)}{13.4 \times 0.411} \\ &= 0.134 \end{aligned}$$

This finding allows to infer that the LiF pellet operates 13.4% as a small cavity and 86.6% as a large cavity. Finally, f is equal to:

$$f = 0.134 \times 1.040 + 0.866 \times 0.961 = 0.971$$

The dose rate in the cavity is:

$$\dot{D}_{\text{LiF}} = f \dot{D}_{\text{Al}}(10) = 0.971 \times 18.83 = 18.29 \text{ mGy.h}^{-1}$$

Part 2: Numerical Simulation Checking

(a) Determination of factor f

The numerical model is based on the work of Ogunleye *et al.* (1980). The LiF pellet is a cylinder of 1.7 mm radius and 2.7 mm thickness (with a density of

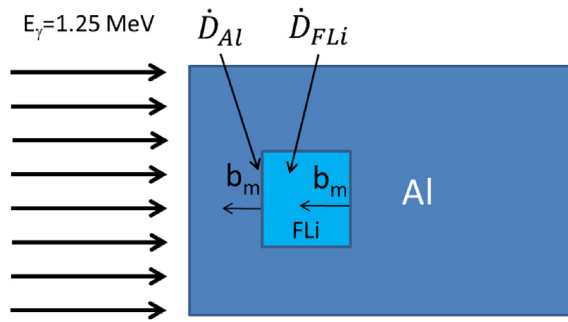


FIG. 2.III.1 – Layout of the LiF pellet inside its aluminum shell.

2.635 g.cm^{-3}). It is modeled inside an aluminum shell of 3.7 mm thickness inlet face (density 2.698 g.cm^{-3}) and of 4.4 cm global thickness, *i.e.*, equal to 12 times 0.37 cm. A parallel beam of 6 cm section radius of 1.25 MeV photons irradiates the materials (see figure 2.III.1).

In the proposed method, electron transport is only turned on below a 3.7 mm depth in the aluminum outlet face (see figure 2.III.2). Beyond this depth, electrons are inhibited by MCNP. Accordingly, we can assume that backscattered electrons do not affect the LiF dose. Only photons continue to be transported (instruction “imp: e” in the input file). Furthermore, this method enables to drastically decrease the calculation time compared to a simulation with an allowed transport of electrons in the whole aluminum shell.

The MCNP input file 2.III.1 is used for the mean dose calculation in the LiF pellet.

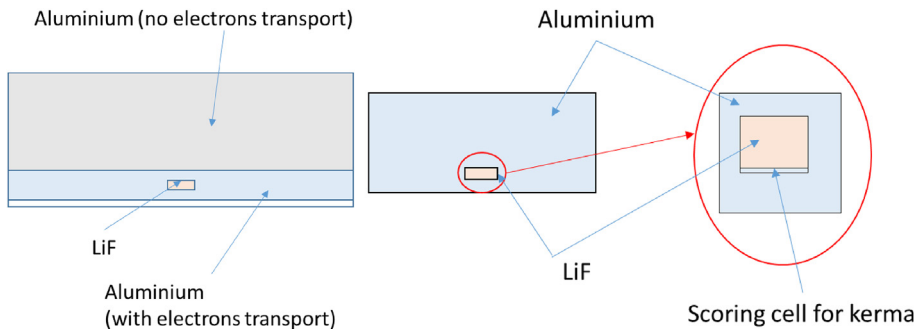


FIG. 2.III.2 – (left side) Calculation of the mean dose in the LiF pellet; (right side) calculation of the dose $\dot{D}_{Al}(10)$ at a point under the aluminum wall.

```

LiF simulation
c cell block
10 1 -2.698 -10 15 $ aluminum
15 2 -2.635 -15 $ LiF
20 3 -2.698 -20 $ scattering Aluminum
25 0 -25 21 10
30 0 25

10 RCC 0 0 0 0 0 1.01 6
15 RCC 0 0 .37 0 0 .27 .17
20 RCC 0 0 1.01 0 0 3.39 6
21 RCC 0 0 0 0 0 4.44 6
25 RCC 0 0 -.1 0 0 4.5 6

mode p e
imp:p 1 1 1 1 0
imp:e 1 1 0 0 0
sdef par=p pos 0 0 -.05 axs 0 0 1 ext 0 rad=d1 vec 0 0 1 dir 1 erg 1.25
PHYS:E 2 0 0 0 0 1 1 1 1 0 0 J J 0.917 0.001
PHYS:P 2 0 0 0 0 J 0
Si1 0 6
spl -21 1
M1 13000 1 estep 50
M2 3000 1 9000 1 estep 50
M3 13000 1
*F28:e 15
stop F28 .006

```

File 2.III.1

The MCNP input file used for the kerma calculation at the aluminum maximum depth is the following:

```

Kerma
c cell block
10 1 -2.698 -10 15 12 $ aluminum
12 1 -2.698 -12
15 2 -2.635 -15 $ LiF
20 3 -2.698 -20 $ scattering aluminum
25 0 -25 10 12 15 20
30 0 25

10 RCC 0 0 0 0 0 .64 6
12 RCC 0 0 .36 0 0 .01 .17
15 RCC 0 0 .37 0 0 .27 .17
20 RCC 0 0 .64 0 0 4.44 6
25 RCC 0 0 -.1 0 0 7 6

```

```

mode p
imp:p 1 1 1 1 1 0
sdef par=p pos 0 0 -.05 axs 0 0 1 ext 0 rad=d1 vec 0 0 1 dir 1 erg 1.25
PHYS:P 2 0 0 0 0 J 0
Si1 0 6
sp1 -21 1
M1 13000 1 estep 50
M2 3000 1 9000 1 estep 50
M3 13000 1
*F6:p 12
stop F26 .0004

```

File 2.III.2

The mean deposited energy $\bar{\epsilon}$ in the LiF is provided by the result of the tally *F28 = 1.857×10^{-5} MeV with a 0.58% relative uncertainty. The dose per unit fluence result is normalized as follows:

$$\frac{D_{\text{LiF}}}{\Phi} = \frac{\bar{\epsilon}}{\Phi_{\text{MCNP}} m_{\text{LiF}}} = \frac{\bar{\epsilon}}{10^{-3}(1/\pi R^2) \pi r^2 z \rho}$$

The coefficient 10^{-3} is used for the kg/g conversion. The normalized dose rate in mGy.h^{-1} is:

$$\begin{aligned} \dot{D}_{\text{LiF}} &= \left(\frac{D_{\text{LiF}}}{\Phi} \right) \dot{\Phi} = 3600 \times \frac{(\bar{\epsilon} \times 10^6)}{(1/\pi R^2) \pi r^2 z \rho} \times \dot{\Phi} \\ \dot{D}_{\text{LiF}} &= 3600 \times 10^6 \times \frac{1.857 \times 10^{-5} \times 1.602 \times 10^{-19}}{8.842 \times 10^{-3} \times 6.459 \times 10^{-5}} \times 1 \times 10^6 \\ &= 0.018747 \text{ Gy.h}^{-1} \quad (18.747 \text{ mGy.h}^{-1}) \end{aligned}$$

The coefficient 1.602×10^{-19} stands for the Joule to eV conversion. With the relative error of the MCNP result, the final value is: $\dot{D}_{\text{LiF}} \pm \sigma_{\dot{D}_{\text{LiF}}} = 18.747 \pm 0.109 \text{ mGy.h}^{-1}$. The second MCNP file enables to assess the kerma K in aluminum. This quantity derives from the result of the tally *F6 = 4.767×10^{-26} jerk.g $^{-1}$ with a 0.04% relative error. Let us recall that 1 jerk = 1 GJ and 1 jerk.g $^{-1}$ = 1 GJ.g $^{-1}$ = 1000 GJ.kg $^{-1}$ = 10^{12} Gy. The MCNP calculation accuracy is improved for the kerma result compared with the \dot{D}_{LiF} calculation since only photons are transported, leading to an improved statistical convergence.

$$\frac{K}{\Phi} = \frac{4.767 \times 10^{-26} \times 1 \times 10^{12}}{1/\pi R^2} = \frac{4.767 \times 10^{-26} \times 1 \times 10^{12}}{8.842 \times 10^{-3}} = 5.391 \text{ pGy.cm}^2$$

For this geometry, the kerma rate calculation under the aluminum wall leads to:

$$\dot{K} = \dot{D}_{Al}(10) = \left(\frac{K}{\Phi}\right) \cdot \dot{\Phi} = 5.391 \times 10^{-12} \times 1 \times 10^6 \times 1000 \times 3600 = 19.408 \text{ mGy}^{-1}$$

With the MCNP calculation relative error, the result is: $\dot{K} \pm \sigma_{\dot{K}} = 19.408 \pm 0.008 \text{ mGy} \cdot \text{h}^{-1}$. Finally, the f ratio along with its uncertainty obtained by uncertainties propagation is:

$$\begin{aligned} f \pm \sigma_f &= \frac{\dot{D}_{LiF}}{\dot{D}_{al}(10)} \pm \sqrt{\left(\frac{\partial f}{\partial \dot{D}_{LiF}}\right)^2 \sigma_{\dot{D}_{LiF}}^2 + \left(\frac{\partial f}{\partial \dot{D}_{al}}\right)^2 \sigma_{\dot{D}_{Al}}^2} \\ &= \frac{\dot{D}_{LiF}}{\dot{D}_{al}(10)} \pm \sqrt{\left(\frac{1}{\dot{D}_{Al}}\right)^2 \sigma_{\dot{D}_{LiF}}^2 + \left(\frac{\dot{D}_{LiF}}{\dot{D}_{Al}^2}\right)^2 \sigma_{\dot{D}_{Al}}^2} \end{aligned}$$

$$f \pm \sigma_f = \frac{18.747}{19.408} \pm \sqrt{\frac{0.109^2}{19.408^2} + \left(\frac{18.747}{19.408^2}\right)^2 \times (0.008)^2} = 0.966 \pm 0.006$$

(b) Determination of the correction for photon scattering

As seen before, a correction factor for scattering photons k_{sc} is needed to enhance the accuracy of the model. Accordingly, another geometry is modeled, in which the aluminum width is reduced to match the lateral dimensions of the LiF pellet for minimizing the photon scattering (see figure 2.III.3).

The MCNP input file matching this configuration is:

```

Build up
c cell block
10 1 -2.698 -10
11 1 -2.698 -11
15 2 -2.635 -15
20 1 -2.698 -20
25 0 -25 20 10 15 11
30 0 25

10 RCC 0 0 0 0 0 .36 .17
11 RCC 0 0 .36 0 0 .01 .17
15 RCC 0 0 .37 0 0 .27 .17
20 RCC 0 0 .64 0 0 .37 .17
25 RCC 0 0 -.1 0 0 1.5 .17

mode p e
imp:p,e 1 1 1 1 1 0
sdef par=p pos 0 0 -.05 axs 0 0 1 ext 0 rad=d1 vec 0 0 1 dir 1 erg 1.25
Si1 0 .17
    
```

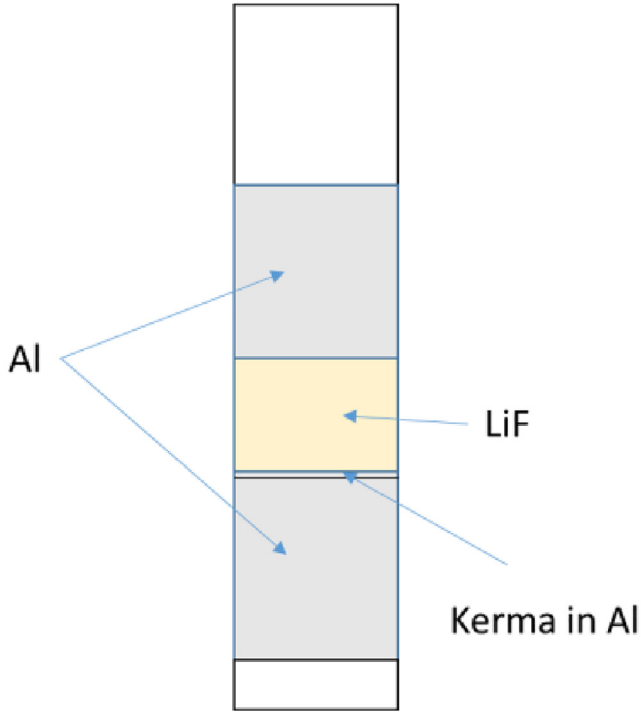


FIG. 2.III.3 – Geometry used for the calculation of k_{sc} .

```

sp1 -21 1
M1 13000 1 estep 50
M2 3000 1 9000 1 estep 50
*F6:p 11
ctme 3000

```

File 2.III.3

With this pattern and the formalism used above for K , the result is $\dot{D}'_{Al}(10) = 17.971 \text{ mGy}\cdot\text{h}^{-1}$. Thus, the correction factor for photon scattering is:

$$k_{sc} = \frac{\dot{D}'_{Al}(10)}{\dot{D}_{Al}(10)} = \frac{17.971}{19.409} = 0.926$$

2.IV Measurement of the Operational Quantity $H'(0.07, 0^\circ)$ for a β Spectrum with an Extrapolation Chamber

Abstract:

In a first part, the directional dose equivalent at a zero angle of incidence, $H'(0.07, 0^\circ)$, is evaluated for a reference $^{90}\text{Sr} + ^{90}\text{Y}$ source, using an extrapolation chamber, model 23392 PTW. This device is recommended by the ISO 6980 standard for the measurement of absorbed dose under $70 \mu\text{m}$ of tissue, $D_t(0.07)$ for β radiation. For this chamber model, a micrometer screw on a piston enables to adjust the depth of the sensitive volume of the chamber. This feature allows to determine the slope of the ionization current *versus* the depth of the chamber. A check of the slope value with a numerical simulation is performed in a second part.

Objectives:

- Calculation of the dose at the entrance window for an extrapolation chamber.
- Calculation of the theoretical current generated in the sensitive volume using the energy deposition tally.

Part 1: Determination of the Directional dose Equivalent at a Zero Angle of Incidence: $H'(0.07, 0^\circ)$

A $^{90}\text{Sr}/^{90}\text{Y}$ β source is located at 30 cm from the entrance window of an extrapolation chamber PTW model 23392 (see figure 2.IV.1). We propose, firstly, to assess the absolute dose rate under $7 \text{ mg}\cdot\text{cm}^{-2}$ of tissue as a function of the ionization current and secondly, to evaluate the directional dose equivalent rate at a zero angle of incidence.

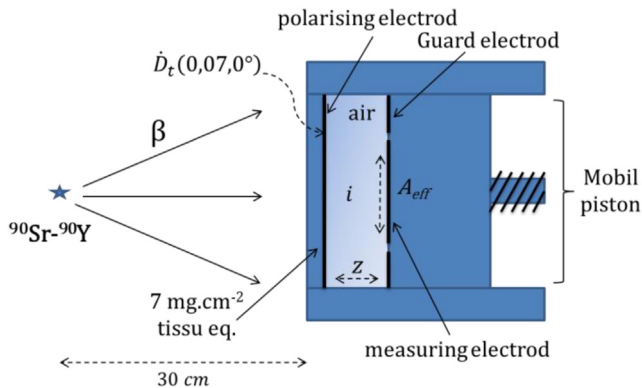


FIG. 2.IV.1 – Layout of the extrapolation chamber and $^{90}\text{Sr}/^{90}\text{Y}$ source.

The characteristics related to the $^{90}\text{Sr}/^{90}\text{Y}$ source are:

- Mean energy: 967 keV.
- Maximum energy: 2.28 MeV.
- Half-life: 28.8 years.
- Nominal activity: 1.857 GBq.

The characteristics related to the PTW 23392 chamber are:

- Cavity of adjustable depth filled with dry air ($\rho_a = 1.293 \times 10^{-3} \text{g.cm}^{-3}$, $\bar{W} = 33.97 \text{eV}$).
- Tissue-equivalent entrance window of thickness 7mg.cm^{-2} .
- Electric field $E = 10 \text{V.mm}^{-1}$ (10^4V.m^{-1}).
- Recommended cavity depth: $0.5 < z < 2 \text{mm}$.
- The charge measured using an electrometer placed on the collecting electrode is $\Delta Q = 6.393 \times 10^{-11} \text{C}$ for a 2 mm cavity depth.
- Current measurements at depths $z_1 = 0.5 \text{mm}$ and $z_2 = 2 \text{mm}$ are, respectively, $i_1 = 1.22 \text{pA}$ and $i_2 = 3.93 \text{pA}$ (Antonio *et al.*, 2012).
- Vacuum permittivity $\epsilon_0 = 8.854 \text{pF.m}^{-1}$ and relative permittivity of air $\epsilon_r \approx 1$.
- $\left(\frac{\bar{S}}{\rho}\right)_a^t = 1.110$ for the mean $^{90}\text{Sr}/^{90}\text{Y}$ β spectrum in the wall.

In contrast to the small cavity expression relating the dose rate under the entrance window to the current intensity, in this case, the absorbed dose rate depends on a variable sensitive volume whose expression is given below:

$$dV_a = A_{\text{eff}} dz$$

with A_{eff} the effective area of the collective electrode, to be calculated. This approach enables to express the absorbed dose rate *versus* the derivative of the current as a function of the cavity depth. The boundary condition for which $z = 0$ (virtual cavity of zero depth) guarantees that Bragg–Gray conditions hold true for all electrons of the β spectrum, particularly that of low energy. For this model, the absorbed dose rate under 7mg.cm^{-2} of tissue as a function of current is given by the following expression (Lecante and Bordy, 2006):

$$\dot{D}_t(0.07, 0^\circ) = 3.6 \times 10^9 \frac{\bar{W}}{\rho_a A_{\text{eff}}} \left(\frac{\bar{S}}{\rho}\right)_a^t k' \left[\frac{d(ki)}{dz} \right]_{z=0} \quad (1)$$

Term k is the product of correction factors which are dependent on the chamber depth, such as the correction of losses due to ion recombination, the correction due to the divergence of the field in the collection volume, the correction due to the electrostatic attraction field created by the entrance window of the chamber. Term k' is the product of correction factors that are independent of the chamber depth: the correction due to the field radial non-uniformity in the collection volume, the correction of the effect of variations of the air humidity of the cavity on the ionization (Lecante and Bordy, 2006).

(a) Calculation of the current as a function of the cavity depth

The measured current varies linearly with the depth of the cavity. The slope of the line represents the current as a function of the cavity depth.

$$\left[\frac{d(ki)}{dz} \right]_{z=0} = \frac{\Delta i}{\Delta z} = \frac{(3.93 - 1.22) \times 10^{-12}}{(2 - 0.5) \times 10^{-3}} = 1.806 \times 10^{-9} \text{ A.m}^{-1} \quad (1.806 \text{ pA.mm}^{-1})$$

Note that values of i_1 and i_2 take into account the product of correction factors k .

(b) Calculation of the effective area of the collecting electrode

In order to evaluate this area, the chamber electrode system is treated as a capacitor of capacitance C .

$$C = \frac{\Delta Q}{\Delta V} = \epsilon_o \epsilon_r \frac{A_{\text{eff}}}{z}$$

By replacing ΔV by Ez , we can write:

$$A_{\text{eff}} = \frac{\Delta Q}{\epsilon_o \epsilon_r E} = \frac{6.393 \times 10^{-11}}{8.854 \times 10^{-12} \times 1 \times 10^4} = 7.22 \times 10^{-4} \text{ m}^2$$

(c) Calculation of the dose rate under $70 \mu\text{m}$, $\dot{D}_t(0.07, 0^\circ)$

Finally, by converting the density in g.m^{-3} to unify units, and by neglecting the correction terms k' , the numerical application provides the result:

$$\begin{aligned} \dot{D}_t(0.07, 0^\circ) &= 3.6 \times 10^9 \frac{33.97}{1.293 \times 10^3 \times 7.22 \times 10^{-4}} \times 1.110 \times 1.806 \times 10^{-9} \\ &= 262.6 \text{ mGy.h}^{-1} \end{aligned}$$

The calculated slope is dependent on the initial activity of the source. In order to overcome this constraint, a calibration factor F_D which defines the dose rate per current slope unit for the $^{90}\text{Sr}/^{90}\text{Y}$ source is used:

$$F_D = \dot{D}_t(0.07, 0^\circ) \left[\frac{d(ki)}{dz} \right]^{-1} = \frac{262.6}{1.806} = 145.4 \text{ mGy.h}^{-1}/\text{pA.mm}^{-1}$$

Since the quality factor is equal to 1 for electrons, the reference measurement of the directional dose equivalent at a zero angle is straightforward:

$$H'(0.07, 0^\circ) = Q D_t(0.07, 0^\circ) = D_t(0.07, 0^\circ) \text{ in Sv} \Rightarrow H'(0.07, 0^\circ) = 262.6 \text{ mSv.h}^{-1}$$

Likewise, we can define a calibration factor describing the dose equivalent rate per current slope unit: $F_H = 145.4 \text{ mSv.h}^{-1}/\text{pA.mm}^{-1}$.

Part 2: Evaluation of the Current Slope as a Function of the Chamber Depth with Numerical Simulation

In this part, the extrapolation chamber is modeled with the $^{90}\text{Sr}/^{90}\text{Y}$ source located at 30 cm in order to numerically assess the current slope *versus* the chamber depth (in $\text{pA}\cdot\text{mm}^{-1}$). The modeled chamber has a PMMA wall and a tissue-equivalent entrance window of thickness $7\text{ mg}\cdot\text{cm}^{-2}$ and of 1.5 cm radius. The MCNP model of the chamber is shown in the left side of figure 2.IV.2. The source β spectrum data come from the RADAR website (<http://www.doseinfo-radar.com/RADARHome.html>). As represented in the right side of figure 2.IV.2, the spectrum includes the ^{90}Sr source component as well as the ^{90}Y source component.

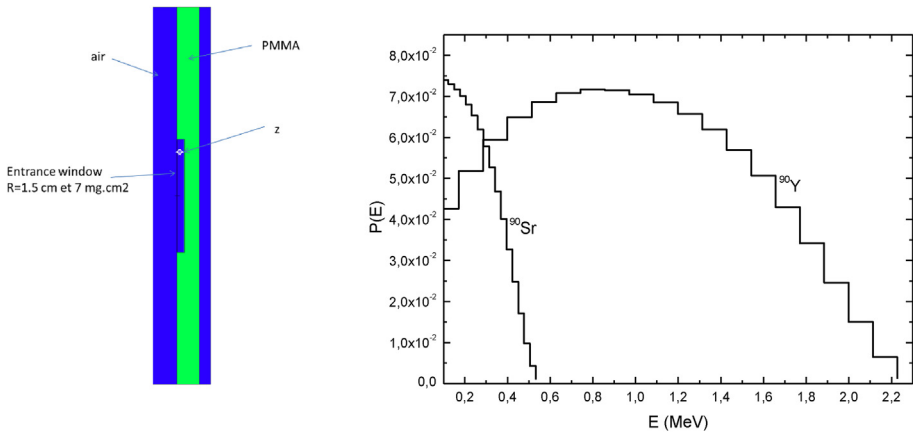


FIG. 2.IV.2 – (left side) Numerical model of the extrapolation chamber, (right side) β spectrum of the $^{90}\text{Sr}/^{90}\text{Y}$ source, sampled and set in the input file.

The source is located at 30 cm from the chamber and is considered as point-like. No filter is interposed between the source and the chamber. The input file 2.IV.1 is given as an example for $z = 1.5\text{ mm}$.

```

Extrapolation chamber
10 1 -1.293e-3 -10 $ chamber
20 2 -1.19 10 -20 $ PMMA
30 1 -1.293e-3 20 -30 $ air
35 0 30

10 RCC 0 0 0 0 0.15 1.5 $ cavity z=0.15 cm R=1.5 cm
20 RCC 0 0 -5.88e-3 0 0 .6 5
30 RCC 0 0 -31 0 0 31.9 5

imp:e,p 1 1 1 0
mode e p
c SDEF par=e pos 0 0 -20 erg d2

```

```
sdef par=e erg fpos d2 pos d1
si1 l 0 0 -30 0 0 -30 $ Sr and Y source position
spl d 1 1 $ same intensity for Sr-90 and Y-90
ds2 s 3 4
c Sr-90
# si3 sp3
0 0
0.0137 7.79E-02
0.0410 7.60E-02
0.0683 7.50E-02
0.0956 7.40E-02
0.1229 7.30E-02
0.1502 7.17E-02
0.1775 7.01E-02
0.2048 6.80E-02
0.2321 6.53E-02
0.2594 6.19E-02
0.2867 5.78E-02
0.3140 5.27E-02
0.3413 4.68E-02
0.3686 4.01E-02
0.3959 3.27E-02
0.4232 2.48E-02
0.4505 1.71E-02
0.4778 9.75E-03
0.5051 4.28E-03
0.5324 1.01E-03
c Y-90
# si4 sp4
0 0
0.0571 4.26E-02
0.1713 5.18E-02
0.2855 5.94E-02
0.3997 6.49E-02
0.5139 6.86E-02
0.6281 7.08E-02
0.7423 7.17E-02
0.8565 7.15E-02
0.9707 7.04E-02
1.0849 6.85E-02
1.1991 6.57E-02
1.3133 6.19E-02
1.4275 5.69E-02
1.5417 5.07E-02
1.6559 4.30E-02
1.7701 3.42E-02
1.8843 2.46E-02
1.9985 1.50E-02
2.1127 6.43E-03
```

```

2.2269 1.13E-03
M1 6000 -0.000124 7000 -0.755268 8000 -0.231781 18000 -0.012827
M2 1000 -0.080538 6000 -0.599848 8000 -0.319614
*F28:e 10
stop F28 .01

```

File 2.IV.1

The MCNP calculation is performed with the *F8 tally providing a result in MeV units, with a relative statistical error of 1%. This tally evaluates the total energy deposition in the chamber gas, ε_t . The current, in pA, is derived from the below expression:

$$i = 10^{18} \frac{\varepsilon_t}{\bar{W}} e A f_e$$

where A is the activity (in Bq), \bar{W} is the mean energy to produce an ion pair in air ($\bar{W} = 34$ eV), f_e is the emission factor taking into account the equilibrium between yttrium and strontium ($f_e = 2$) and e is the electron charge. The term 10^{18} stems from the multiplication of the conversion from MeV to eV by the conversion factor from A to pA. Results are given in table 2.IV.1 for a 1.85 GBq source activity for different chamber depths.

The values of the current *versus* the chamber depth z listed in table 2.IV.1 are represented in figure 2.IV.3.

Then, the slope is determined using the least-squares method.

$$a = \frac{\text{cov}(z, i)}{\text{var}(z)} = \frac{\sum_{j=1}^{j=n} (z_j - \bar{z})(i_j - \bar{i})}{\sum_{j=1}^{j=n} (z_j - \bar{z})^2} = 2.24 \text{ pA} \cdot \text{mm}^{-1}$$

The slope standard deviation estimator is defined with $n = 4$ in this case:

$$\hat{\sigma}_a = \frac{1}{\sqrt{n-2}} \sqrt{\frac{\sum_{j=1}^{j=n} (i_j - \bar{i})^2}{\sum_{j=1}^{j=n} (z_j - \bar{z})^2}} = 0.08$$

The slope calculated with the numerical method is $a \pm \hat{\sigma}_a = 2.24 \pm 0.08 \text{ pA} \cdot \text{mm}^{-1}$, whereas that experimentally obtained is $1.81 \text{ pA} \cdot \text{mm}^{-1}$. This deviation is partially due to the product of correction factors k in equation (1).

TAB. 2.IV.1 – MCNP calculation results of the theoretical intensity *versus* the chamber depth.

z (mm)	ε_t	i (pA)
0.7	9.54E-08	1.66
1	1.33E-07	2.32
1.5	1.96E-07	3.42
2	2.63E-07	4.58

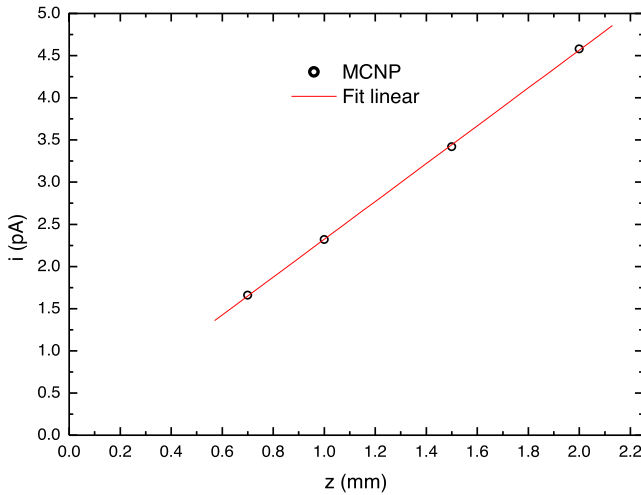


FIG. 2.IV.3 – Plot of the values calculated with MCNP and given in table 2.IV.1.

2.V Fast Monoenergetic Neutron Energy and Fluence Measurements with a Proton Recoil Telescope

Abstract:

This application is aimed at evaluating energy and fluence of monoenergetic neutrons with a proton recoil telescope. These neutrons emerge from a ^3H target impinged by a deuteron beam (150 keV) according to the reaction $^3\text{H}(d,n)^4\text{He}$. This method is highly recommended to carry out a reference measurement of the fluence and the energy of a fast neutron field for an external dosimetry purpose. In a next step, the ambient dose equivalent rate at the point at which the neutron beam interacts with the telescope radiator is then inferred. A comparison between results drawn from theoretical and numerical methods is performed.

Objectives:

- Theoretical calculation of the energy of fast neutrons undergoing elastic scattering in an organic radiator and evaluation of the associated uncertainty.
- MCNP simulation of a proton recoil telescope.
- Calculation of a detector efficiency.
- Calculation of the energy resolution.

Main characteristics:

The experimental set-up is composed of a hydrogenous radiator (composed of CH_2) of thickness $e = 200 \mu\text{m}$ and density 0.91 g.cm^{-3} , arranged on the collimated neutron beam axis. The neutron beam is collimated and its cross section on the radiator is

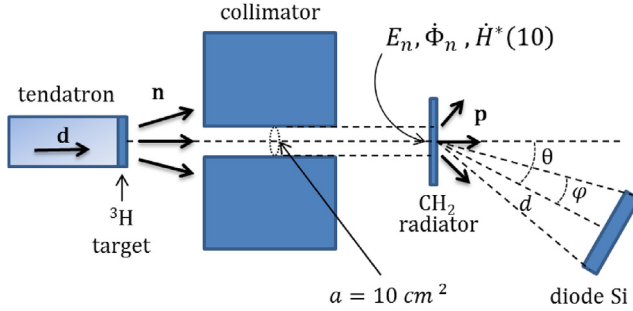


FIG. 2.V.1 – Proton recoil telescope set-up for the reference measurement of neutron fluence and energy.

$a = 10 \text{ cm}^2$. The neutron beam strikes the hydrogenous radiator, and the recoil protons produced, with a cross section $\sigma_{(n,p)} = 0.691$ barn at the considered energy, pass through a silicon detector. The silicon detector, with a disk-shaped entrance surface of 4 cm radius, is placed at a distance $d = 1$ m forming an angle of 40° with the beam axis. Its energy resolution at the recoil protons energy is 3% at the given neutron energy and at the considered angle (see figure 2.V.1). The recoil proton energy measured with the detector is $E_p^d = 7.79 \pm 0.23$ MeV. The detection efficiency of the silicon detector is 100% and we assume that recoil protons lose, on average, 5% of their initial energy in the radiator. The amplifier output of the Si detector is processed by a multi-channel analyzer to record pulse height spectra of energy deposits. For the channel matching 7.79 ± 0.23 MeV, 10 000 counts are recorded during the 10 min of the accelerator duty cycle.

(a) Calculation of neutron energy

In the case of elastic scattering, the relationship between the incoming neutron energy and the energy of the recoil nucleus of number mass A is:

$$E_n = \frac{(1+A)^2}{4A} \left(\frac{1}{\cos^2\theta} \right) E_A$$

where θ is the scattering angle of the recoil nucleus.

If the target nucleus is the proton of hydrogen ($A = 1$), this expression can be reduced to:

$$E_n = \frac{E_p}{\cos^2\theta} \quad (1)$$

One has to take into consideration the uncertainty on the incident neutrons energy owing to the Coulomb scattering in the radiator. The propagation of uncertainty provides the following formula:

$$\sigma_{E_n}^2 = \left(\frac{\partial E_n}{\partial E_p} \right)^2 \sigma_{E_p}^2 + \left(\frac{\partial E_n}{\partial \theta} \right)^2 \sigma_\theta^2$$

By partially deriving expression (1) of E_n , it becomes:

$$\sigma_{E_n}^2 = \left(\frac{1}{\cos^2\theta} \right)^2 \sigma_{E_p}^2 + \left(\frac{E_p 2 \sin\theta}{\cos^3\theta} \right)^2 \sigma_\theta^2$$

Dividing by E_n^2 gives the following expression (2):

$$\left(\frac{\sigma_{E_n}}{E_n} \right)^2 = \left(\frac{\sigma_{E_p}}{E_p} \right)^2 + 4 \tan^2\theta \sigma_\theta^2 \quad (2)$$

The total uncertainty depends on the standard deviation of the recoil protons scattering angle in the radiator but also on the measurement angle. The recoil protons' energy produced in the radiator is first calculated to evaluate the energy of the scattered neutrons.

$$E_p = E_p^d + E_p^c = E_p^d + 0.05 E_p \Rightarrow E_p = \frac{E_p^d}{1 - 0.05} = \frac{7.79}{0.95} = 8.20 \text{ MeV} \quad (3)$$

with E_p^d being the proton energy measured with the silicon detector and E_p^c the proton energy lost in the radiator through Coulomb scattering. We derive from expression (1):

$$E_n = \frac{8.20}{\cos^2(40^\circ)} = 13.97 \text{ MeV} \quad (4)$$

The term σ_θ (in rad) can be derived from the formula of Lynch and Dahl (1991).

$$\sigma_\theta = \frac{13.6}{\beta pc} \sqrt{\frac{e}{X_o}} \left[1 + 0.038 \log\left(\frac{e}{X_o}\right) \right]$$

where e is the radiator thickness, β and pc are, respectively, the Lorentz factor and the momentum of the recoil proton and X_o the radiation length (in cm) for a material (Z , A) calculated as follows:

$$X_o = \frac{716.4 \bar{A}}{\rho \bar{Z} (\bar{Z} + 1) \ln\left(\frac{287}{\sqrt{\bar{Z}}}\right)}$$

Firstly, the \bar{A} and \bar{Z} values of CH_2 are determined:

$$\bar{A} = \frac{1 \times 12 + 2 \times 1}{3} = 4.7 \quad \text{and} \quad \bar{Z} = \frac{1 \times 6 + 2 \times 1}{3} = 2.7$$

This way:

$$X_o = \frac{716.4 \times 4.7}{0.91 \times 2.7 \times (2.7 + 1) \ln\left(\frac{287}{\sqrt{2.7}}\right)} = 71.7 \text{ cm}$$

The Lorentz factor and the momentum are calculated according to the energy found in expression (3) as follows:

$$\beta = \frac{v}{c} = \sqrt{1 - \left(\frac{m_p c^2}{E_p + m_p c^2} \right)^2} = \sqrt{1 - \left(\frac{939.6}{8.20 + 939.6} \right)^2} = 0.1$$

$$pc = \sqrt{E_p(E_p + 2m_p c^2)} = \sqrt{8.20 \times (8.20 + (2 \times 939.6))} = 124.4 \text{ MeV}$$

The standard deviation of the angle is:

$$\sigma_\theta = \frac{13.6}{0.1 \times 124.4} \sqrt{\frac{200 \times 10^{-4}}{71.7} \left[1 + 0.038 \log\left(\frac{200 \times 10^{-4}}{71.7}\right) \right]} = 15.7 \text{ mrad}$$

Thus, given the total uncertainty on the neutron energy, the energy resolution is:

$$\frac{\sigma_{E_n}}{E_n} = \sqrt{(0.03)^2 + 4 \tan^2(40^\circ) \times (0.0157)^2} = 0.04 \quad (5)$$

The neutron energy along with its associated uncertainty is $E_n \pm \sigma_{E_n} = 13.97 \pm 0.56 \text{ MeV}$, meaning that the neutron energy is given with a resolution of 560 keV. The theoretical energy resolution corresponding to the full width at half maximum (FWHM) of the peak following a Gaussian distribution is:

$$\text{FWHM} = 2.355 \sigma_{E_n} = 1.32 \text{ MeV}$$

Technically, for the energy resolution, it is necessary to take into account the quality of the Si detector and the accuracy of the energy discrimination of the multi-channel analyzer composing the electronic acquisition system.

(b) Calculation of the neutron fluence

The rate of protons is given as a function of the number of neutrons per unit time according to expression (6):

$$\dot{N}_p = \dot{N}_n (1 - \exp(-N_H \sigma_{n,n} e)) \quad (6)$$

with $\sigma_{n,n}$ the neutron total elastic scattering cross section at the energy calculated previously ($\cong 14 \text{ MeV}$, $\sigma_{(n,n)} = 0.691 \text{ barn}$) and N_H the number of atoms per cm^3 in the radiator. N_H is expressed as a function of the hydrogen mass fraction W_H , Avogadro constant η_A and the radiator density as follows:

$$\begin{aligned} N_H &= W_H \eta_A \rho = \left(\frac{2 \times 1}{(2 \times 1) + (12 \times 1)} \right) \times 6.02 \times 10^{23} \times 0.91 \\ &= 7.826 \times 10^{22} (\text{atoms}) \cdot \text{cm}^{-3} \end{aligned}$$

Thus, we deduce the elastic scattering mean free path:

$$\lambda_{n,n} = \frac{1}{\Sigma_{n,n}} = \frac{1}{N_{\text{H}} \sigma_{n,n}} = \frac{1}{7.826 \times 10^{22} \times 0.691 \times 10^{-24}} = 18.5 \text{ cm}$$

By assuming the radiator to be thin enough compared to the mean free path of neutrons before elastic scattering, it is possible to achieve a Taylor expansion of the exponential function. Then, equation (6) can be reduced as:

$$\dot{N}_p \approx \dot{N}_n N_{\text{H}} \sigma_{n,n} e$$

By considering that all recoil protons created pass through the radiator, the number of protons collected per unit time by the Si detector, \dot{N}_p^d , can be expressed as follows:

$$\dot{N}_p^d = \varepsilon_d \int_0^{\Omega_d} \dot{N}_n N_{\text{H}} \left(\frac{d\sigma_{n,n}}{d\Omega} \right) e d\Omega$$

where $d\sigma_{n,n}/d\Omega$ is the angular differential elastic cross section, Ω_d is the detection solid angle covered by the Si diode and ε_d is the efficiency of the detector for the detection of protons crossing its entrance surface. Solving this integral leads to an expression involving the total elastic cross section:

$$\dot{N}_p^d = \varepsilon_d \dot{N}_n N_{\text{H}} \sigma_{n,n} e \Omega_d \frac{\cos\Theta}{\pi} k_{\text{an}}$$

where k_{an} is a term standing for the anisotropy of the elastic scattering cross section in the laboratory frame (Bame *et al.*, 1957):

$$k_{\text{an}} = \frac{1 + \left(\frac{E_n}{90}\right)^2 \cos^2 2\theta}{1 + \left(\frac{2}{3}\right) \left(\frac{E_n}{90}\right)^2}$$

Accordingly, the efficiency corresponding to the number of protons detected per incoming neutron in the radiator is:

$$\varepsilon_{n \rightarrow p} = \frac{\dot{N}_p^d}{\dot{N}_n} = \varepsilon_d N_{\text{H}} \sigma_{n,n} e \Omega_d \frac{\cos\Theta}{\pi} k_{\text{an}}$$

As defined in figure 2.V.1, the solid angle covered by the detector is:

$$\Omega_d = 2\pi(1 - \cos\varphi) = 2\pi \left(1 - \frac{d}{\sqrt{d^2 + r^2}} \right) = 2\pi \left(1 - \frac{100}{\sqrt{100^2 + 4^2}} \right) = 0.005 \text{ sr}$$

k_{an} expression yields:

$$k_{\text{an}} = \frac{1 + \left(\frac{14}{90}\right)^2 \cos^2(2 \times 40)}{1 + \left(\frac{2}{3}\right) \times \left(\frac{14}{90}\right)^2} = 0.984$$

Therefore, by assuming a 100% detection efficiency for the Si diode for the incident protons, the detection efficiency for the recoil protons is:

$$\begin{aligned}\varepsilon_{n \rightarrow p} &= 1 \times 7.826 \times 10^{22} \times 0.691 \times 10^{-24} \times 0.005 \times 200 \times 10^{-4} \times \left(\frac{\cos(40)}{\pi} \right) \times 0.984 \\ &= 1.30 \times 10^{-6}\end{aligned}$$

The 10 000 counts recorded over the 10 min of the accelerator duty cycle, in the channel corresponding to 7.79 ± 0.23 MeV, represent a count rate $\dot{N}_p^d = 16.7$ (c).s⁻¹. Finally, the fluence rate at the entrance of the radiator is:

$$\dot{\Phi}_n = \frac{\dot{N}_n}{a} = \frac{\dot{N}_p^d}{\varepsilon_{n \rightarrow p} a} = \frac{16.7}{1.30 \times 10^{-6} \times 10} = 1.28 \times 10^6 \text{ (n).cm}^2\text{s}^{-1}$$

Thus, at the radiator location, the accelerator yields a neutron fluence of 1.28×10^6 (n).cm²s⁻¹ of which the energy is $E_n \pm \sigma_{E_n} = 13.97 \pm 0.56$ MeV. For a 14 MeV energy, the “fluence – ambient dose equivalent” conversion coefficient, from ICRP (1996), is $h_{\Phi}^*(10) = 520$ pSv.cm². The ambient dose equivalent rate at the calculation point is:

$$\dot{H}^*(10) = 3600 \times h_{\Phi}^*(10) \dot{\Phi}_n = 3600 \times 520 \times 10^{-12} \times 1.28 \times 10^6 = 2.4 \text{ Sv.h}^{-1}$$

(c) Telescope simulation with MCNP

We consider a parallel beam of 13.97 MeV neutrons of section radius $r = 1.784$ cm, that is to say a cross section of 10 cm², interacting with a polyethylene cylinder of 1.784 cm radius and 200 μm thickness modeling the radiator. An empty cylinder of 4 cm radius and 1 cm thickness is placed at 1 m and 40° from the radiator generatrix in order to simulate the sensitive volume of the diode. The MCNP model is shown in the top part of figure 2.V.2.

The distribution of the fluence of protons reaching the Si diode (represented by cell 15 in the input file 2.V.1) is calculated by means of the mean fluence estimator, *i.e.*, a tally F4, coupled with an energy card “e4” binning the spectrum in 200 equidistant intervals between 5 and 10 MeV. We must point out that for this case, the 7th entry of the “phys:n” card must be modified in order to turn on the light-ion recoil. The MCNP input file of the telescope simulation is provided below:

```
Telescope simulation
c cell block
10 1 -.92 -10 $ radiator in (CH2)n
15 0 -15      $ detector
20 0 10 15 -20
30 0 20
```

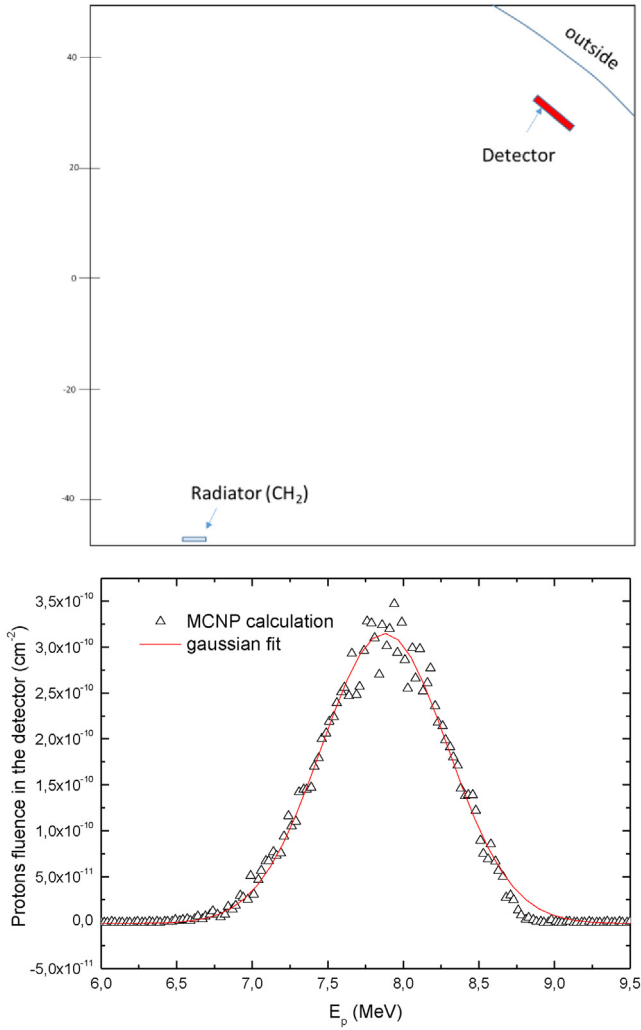


FIG. 2.V.2 – (top) Geometry modeled in MCNP, (bottom) fluence energy distribution as a function of protons energy.

```

10 RCC 0 0 -1E-2 0 0 1E-2 1.784
15 RCC 0 64.278761 76.6 0 .64279 .766 4
20 SO 110

imp:n,h 1 1 1 0
VOL j 50.26 j j $ volume of cell 15 must be input
c phys 7th entry coilf=n.m=1.001
PHYS:N 20 0 0 J J J 1.001 -1 J J J 0 0
mode n h
sdef par=n pos 0 0 -.05 axs 0 0 1 ext 0 rad=d1 vec 0 0 1 dir 1 erg 13.97
    
```

```

Si1 0 1.784
sp1 -21 1
ctme 3000
M1 1001 2 6012 1
F4:h 15
E4 5 200i 10

```

File 2.V.1

The resulting proton spectrum fitted with a Gaussian distribution is plotted in the bottom part of figure 2.V.2. The mean energy of protons is $E_p \pm \sigma_{E_p} = 7.87 \pm 0.41$ MeV. The theoretical energy resolution defined by the full width at half maximum of the peak following a Gaussian distribution is:

$$\text{FWHM} = 2.355 \sigma_{E_n} = 0.96 \text{ MeV}$$

In the MCNP output file, a population of 3253 protons is recorded, for 3.26×10^9 source neutrons. It means that the simulated proton detection efficiency of the Si diode for one neutron crossing the radiator is $\varepsilon_{n \rightarrow p} \cong 10^{-6}$. This last result reveals a good agreement between both approaches.

2.VI Fast Monoenergetic Neutron Time of Flight Energy Measurement

Abstract:

In this problem, the Time of Flight (ToF) technique is used to measure the energy of monoenergetic neutrons originating from the ${}^3\text{H}(p,n){}^3\text{He}$ reaction. Protons are produced with a 2 MV tandemtron operated in pulse mode with a MHz frequency. A BC501A liquid scintillator is placed at 2.5 m and 0° from the tritium target. In the scintillator, elastic scattering on hydrogen composing the xylene organic solvent leads to the emission of protons which excite the organic scintillator present as a solute. The latter transmits a light, proportional to the energy deposit, towards the photomultiplier. The resulting spectrum gathering several thousands of pulses is shown in figure 2.VI.1. In the first part, an analytical calculation of the ToF is detailed for the experimental data. In the second part, this calculation is done for a d - d neutron spectrum simulated with MCNP.

Objectives:

- Theoretical calculation of the time-of-flight (ToF) and matching neutron energy.
- ToF technique with a coincident secondary particle.
- ToF uncertainty and energy resolution calculations.
- Calculation of the mean ToF with MCNP using a fusion spectrum.

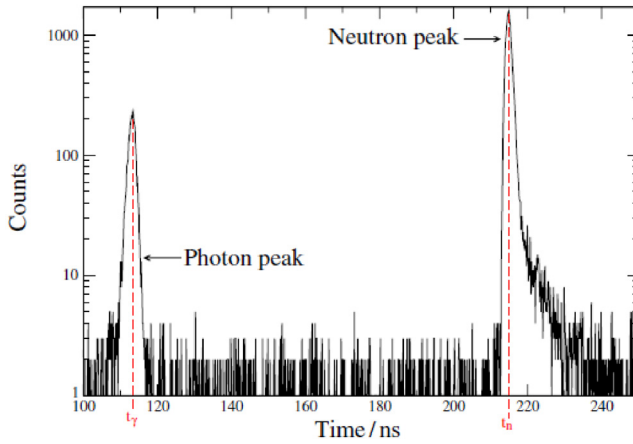


FIG. 2.VI.1 – Time of flight spectrum measured at 2.5 m from the neutron production target (from Cognet and Gressier, 2010).

Main characteristics:

- Neutrons ToF (Cognet and Gressier, 2010): $t_n = 214.10$ ns.
- ToF of coincident photons (from Cognet and Gressier, 2010): $t_\gamma = 114.58$ ns.
- Relative uncertainty in the distance: $\sigma_d/d = 0.075\%$.
- Relative uncertainty in the timing calibration factor for the channels: $\sigma_A/A = 0.72\%$.
- Uncertainty in the determination of the detection time of the photons: $\sigma_{t_\gamma} = 0.08$ ns.
- Uncertainty in the neutron measurement time: $\sigma_{t_n} = 0.4$ ns.

Part 1: ToF Calculation and Matching Neutron Energy

In this problem, the ToF is determined for a neutron travelling distance $d = 2.5$ m from the target to the detector.

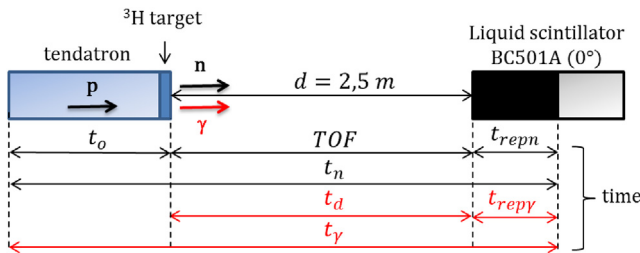


FIG. 2.VI.2 – Principle of the ToF apparatus used to measure the neutron energy at 0° incidence. The different time quantities used in the calculation are presented.

In the above figure, t_n represents the total time lapse between the proton emission, occurring during the pulse, and the neutron detection in the scintillator (see figure 2.VI.2). $t_{\text{rep } n}$ is the scintillator time response to count the neutron. Let t_o be the proton time between the source and the target. The neutron ToF is written as:

$$\text{ToF} = t_n - t_{\text{rep } n} - t_o$$

In this experimental approach, time t_o is not known accurately. To overcome this lack of information, a coincidence measurement of the photon emitted simultaneously with the neutron during the ${}^3\text{H}(p,n){}^3\text{He}$ reaction is achieved. The scintillator also detects the coincident photon and its time of flight is calculated as follows:

$$t_\gamma = t_d + t_{\text{rep } \gamma} + t_o \text{ with } t_d = \frac{d}{c}$$

where $t_{\text{rep } \gamma}$ is the scintillator photon time response. Photon and neutron time responses are identical as regards the BC501A scintillator. Therefore, t_o can be omitted for the ToF calculation:

$$\text{ToF} = t_n - t_\gamma + \frac{d}{c} \quad (1)$$

Figure 2.VI.2 provides $t_n = 215.1$ ns and $t_\gamma = 113.3$ ns. Thus, the neutron ToF is:

$$\text{ToF} = 214.10 - 114.58 + \left(\frac{2.5}{3 \times 10^8} \times 10^{-9} \right) = 107.85 \text{ ns}$$

The neutron energy is then calculated using expression (2):

$$E_n = m_n c^2 \left(\frac{1}{\sqrt{1 - \beta^2}} - 1 \right) = m_n c^2 \left(\frac{1}{\sqrt{1 - (d/(c \text{ToF}))^2}} - 1 \right) \quad (2)$$

$$E_n = 939.56 \times \left(\frac{1}{\sqrt{1 - (2.5/(3 \times 10^8 \times 107.85 \times 10^{-9}))^2}} - 1 \right) = 2.82 \text{ MeV}$$

The major uncertainty on the energy is that concerning the ToF measurement. Equation (1) can be expressed as a function of the time calibration coefficient A and of the signal acquisition channels c_n and c_γ respectively corresponding to the detection time of neutrons and photons:

$$\text{ToF} = A(c_n - c_\gamma) + \frac{d}{c}$$

The overall uncertainty in the ToF derives from the law of propagation of uncertainty:

$$\sigma_{\text{ToF}}^2 = \left(\frac{\sigma_d}{c}\right)^2 + \left(\text{ToF} - \frac{d}{c}\right)^2 \left(\frac{\sigma_A}{A}\right)^2 + \sigma_{t_n}^2 + \sigma_{t_p}^2$$

When expressing uncertainties in ns, the ToF uncertainty is:

$$\sigma_{\text{ToF}} = \sqrt{\left(\frac{0.075 \times 10^{-2} \times 2.5}{3 \times 10^8} \times 10^9\right)^2 + \left(107.85 - \left(\frac{2.5}{3 \times 10^8} \times 10^9\right)\right)^2 (0.72 \times 10^{-2})^2 + 0.4^2 + 0.08^2}$$

$$\sigma_T = 0.82 \text{ ns}$$

Hence, the overall uncertainty in the neutron energy is as follows:

$$\frac{\sigma_{E_n}}{E_n} = \frac{1-u}{u(1-\sqrt{u})} \sqrt{\left(\frac{\sigma_d}{d}\right)^2 + \left(\frac{\sigma_{\text{ToF}}}{\text{ToF}}\right)^2} \quad \text{with} \quad u = \frac{1}{\gamma^2} = 1 - \left(\frac{d}{c \text{ToF}}\right)^2$$

$$\Rightarrow u = 1 - \left(\frac{2.5}{3 \times 10^8 \times 107.85 \times 10^{-9}}\right)^2 = 0.994$$

$$\begin{aligned} \Rightarrow \frac{\sigma_{E_n}}{E_n} &= \frac{1-0.994}{0.994 \times (1-\sqrt{0.994})} \times \sqrt{(0.075 \times 10^{-2})^2 + \left(\frac{0.82}{107.85}\right)^2} = 0.0153 \\ &= 1.53\% \end{aligned}$$

Finally, the measured neutron energy is $E_n \pm \sigma_{E_n} = 2.82 \pm 0.43 \text{ MeV}$ against 2.8 MeV evaluated at the target exit, corresponding to a benchmark monoenergetic neutron field of the ISO 8529 standard. The theoretical energy resolution matching the peak full width at half maximum (FWHM) fitted with a Gaussian distribution is:

$$\text{FWHM} = 2.355 \sigma_{E_n} = 0.10 \text{ MeV}$$

Part 2: Numerical Study of the Neutron time of Flight Spectrum from a $d-d$ Fusion Reaction

In this part, the ToF of neutrons arising from the $d-d$ fusion reaction ${}^2\text{H}(d,n){}^3\text{He}$ is simulated. For this purpose, a particular source probability function is used “sp2 -4 -0.01 -2” where “-4” parameter stands for a Gaussian fusion spectrum and “-0.01 -2” parameters state a $d-d$ reaction at 10 keV. The entire input file is provided below:

```
TOF calculation
c cell block
10 0 -10
20 0 10 -20
30 0 20
```

```

10 RCC 0 0 -.5 0 0 1 4
20 RCC 0 0 -1 0 0 260 5

imp:p,n 1 1 0
mode p n
sdef par=n pos 0 0 0 erg D2
c Gaussian fusion spectrum at 10 keV (0.01 MeV)
SP2 -4 -.01 -2
ctme 15
F15:n 0 0 250 .1
T15 0 200i 50
F35:n 0 0 10 .1
E35 0 100i 10

```

File 2.VI.1

The neutron fluence as a function of time is calculated with tally 15 coupled with the t5 tally time card. The fluence spectrum in terms of energy is derived from tally 35. It should be specified that the MCNP unit for time is the *shake*, equivalent to 1×10^{-8} s. Thus, multiplying the results by a factor 10 enables to get the time in current unit ns. The fluence distribution throughout the time is represented in figure 2.VI.3a.

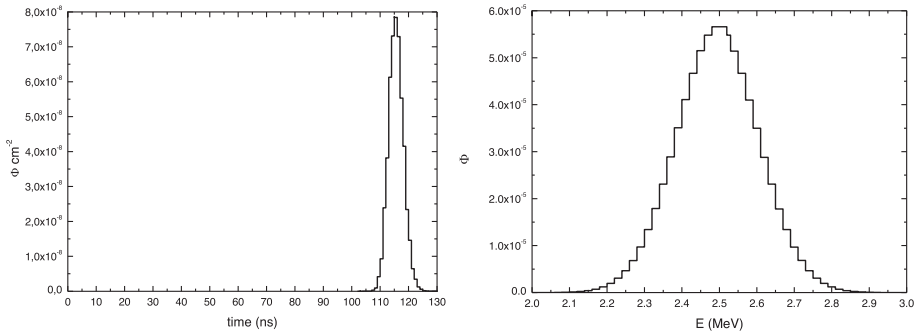


FIG. 2.VI.3 – (a) ToF spectrum simulated with MCNP for a $d-d$ reaction, (b) same expressed in terms of energy.

The neutron ToF for a distance of 2.5 m matches the maximum of the peak displayed in figure 2.VI.3, that is to say 115 ns. According to expression (2), the matching neutron energy is:

$$E_n = m_n c^2 \left(\frac{1}{\sqrt{1 - \beta^2}} - 1 \right) = m_n c^2 \left(\frac{1}{\sqrt{1 - (d/c \text{ToF})^2}} - 1 \right)$$

$$E_n = 939.56 \times \left(\frac{1}{\sqrt{1 - (2.5/(3 \times 10^8 \times 115 \times 10^{-9}))^2}} - 1 \right) = 2.47 \text{ MeV}$$

This calculation for all time bins of figure 2.VI.3a provides the theoretical energy resolution. The latter derives directly from tally 35, as shown in figure 2.VI.3b.

2.VII Measurement of a Realistic Neutron Spectrum Using Bonner Spheres Spectrometer

Abstract:

In this application, we propose to determine the neutron fluence- and ambient dose equivalent- rates for three energy regions (thermal – epithermal – fast) by employing a Bonner Sphere Spectrometer (BSS) located at 50 cm from an outgoing neutron flux produced by the CANEL/T400 facility (see figure 2.VII.1). In the first part, the response of each Bonner sphere is simulated with MCNP for the three energy regions. In the second part, the neutron fluence is calculated for each energy range through the least squares method. Note that the multi-Bonner spheres method is a reference to assess the overall fluence and the spectrum.

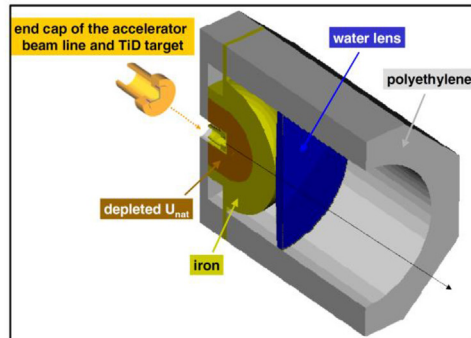


FIG. 2.VII.1 – (left side) Picture of the CANEL/T400 facility with a single Bonner sphere, (right side) layout of the CANEL apparatus as modeled in MCNP (from Lacoste *et al.*, 2011).

Objectives:

- Solving of an equation system through the least squares method.
- Study the principle of an unfolding algorithm to derive a spectrum from the signal provided by several detectors.
- Calculation of the matrix response of a BSS with MCNP.
- Study the principle of Bonner spheres to evaluate a reference neutron spectrum.
- Calculation of a mean “physical quantity-to-dosimetric quantity” conversion coefficient for an energy spectrum.

Main characteristics:

The measurement is achieved by employing a Bonner Sphere Spectrometer (BSS). BSS consists of a set of polyethylene spheres of different diameters. A thermal neutron detector is located at the center of each sphere. Fast neutrons impinging on a sphere are moderated during their transport in the polyethylene and arrive to the sphere’s center as thermal neutrons where they are detected by the central counter. For our case, we consider three polyethylene Bonner spheres of respective diameters 2, 4 and 8 in. The thermal neutron detector is a ^3He -filled spherical detector of diameter 3.2 cm located at the center of each of the polyethylene spheres. The ^3He gas pressure is 172 kPa. We provide in table 2.VII.1 the count rates \dot{m}_s (counts per second) measured by the BSS located at 50 cm from the water lens of the CANEL/T400 device.

TAB. 2.VII.1 – BSS count rate at 50 cm away from the water lens of the CANEL/T400 device.

Sphere	2 in.	4 in.	8 in.
\dot{m}_s	955.78	1183.63	483.18

Part 1: Numerical Simulation of the Bonner Spheres Matrix Response

In this first part, we propose to determine the response of these three spheres through MCNP calculations, for the three regions of neutron energy described in the introduction: thermal ($E_n < 0.5$ eV), epithermal (0.5 eV $< E_n < 50$ keV) and fast ($E_n > 50$ keV). This energy splitting allows to separate the 3 distinctive parts of the neutron spectrum produced by the CANEL/T400 facility, for a measurement made at 50 cm away from the water lens. This spectrum is displayed in figure 2.VII.2.

The hereinafter detailed example refers to the simulated response of the 8" Bonner sphere, of 20.32 cm diameter, exposed to a parallel neutron beam of 10.16 cm radius cross section. A similar method can be applied to the other spheres of 2" and 4" diameter.

The MCNP calculation, with the input file 2.VII.1, consists in evaluating the number of (n, p) reactions in the gaseous volume V of the ^3He proportional counter

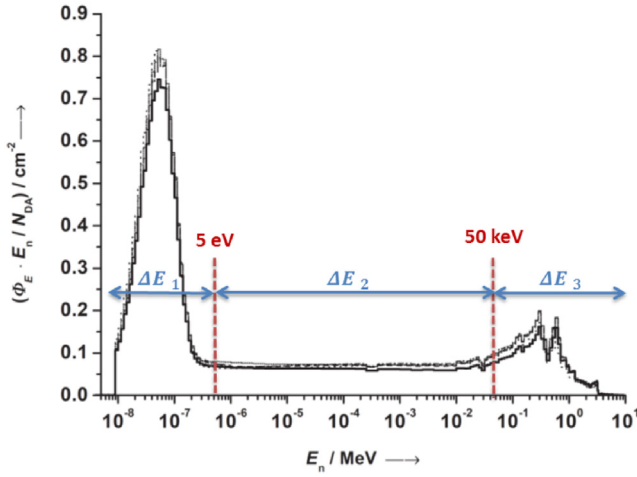


FIG. 2.VII.2 – Neutron fluence distribution at the end of the CANEL/T400 facility (from Lacoste *et al.*, 2011).

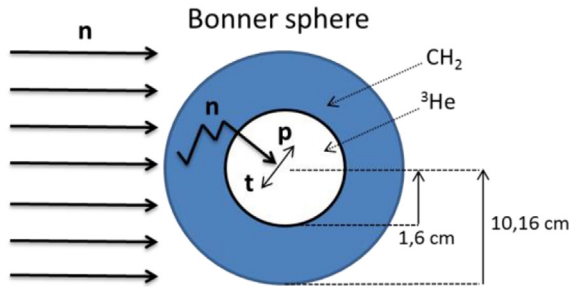


FIG. 2.VII.3 – Principle of the numerical model used to evaluate the 8" BSS response.

figure 2.VII.3). This calculation is achieved with a F4 tally in the cell modeling the gas volume, coupled with a “fm” tally multiplier card according to the instruction: “fm4 0.2364 1 103”. The parameter “0.2364” corresponds to the product of the ^3He atomic density, the gas volume and the beam cross section area a_s , that is to say the factor $n_{\text{He}} V a_s$, enabling to get a result per fluence unit. The atomic density of helium at 273 K is $n_{\text{He}} = 4.25 \times 10^{19} \text{ (atom).cm}^{-3}$ (Mares *et al.*, 1991). However, this density has to be expressed in $(\text{atom}).\text{cm}^{-3}$ barn in the input file. Accordingly, the atomic density is multiplied by a conversion factor equal to 10^{-24} to match the desired units. Finally, this first parameter is obtained as follows:

$$a_s n_{\text{He}} V = \pi \times (10.16)^2 \times 4.25 \times 10^{19} \times 10^{-24} \times \frac{4}{3} \times \pi \times (1.6)^3 = 0.2364$$

The second parameter, “1”, corresponds to the material number of helium in the MCNP input file. The parameter “103” stands for the ENDF/B reaction type (n,p) (see the MT column list from Colin, 2017). It is used to multiply the fluence by the cross section of the (n,p) reaction for each neutron entering the sensitive volume, depending on the energy group it belongs. Thus, we can deduce the k^{th} sphere response to a neutron of energy E_n :

$$R_k(E_n) = a_s n_{\text{He}} V \int_0^{E_n} \left(\frac{d\Phi_k}{dE} \right) \sigma_{(n,p)}(E) dE \quad (1)$$

The input file 2.VII.1 is used to evaluate the 8 in. sphere response to $E_n = 1 \text{ MeV}$.

```

BSS simulation
c cell block
10 1 4.2497e-5 -10      $ He-3
20 2 -.95      -20 10  $ CH2
30 0           -30 20
40 0 30

10 SO 1.6
20 SO 10.16
30 SO 50

imp:n 1 1 1 0
mode n
sdef par=n pos 0 0 -11 axs 0 0 1 ext 0 rad=d1 vec 0 0 1 dir 1 erg 1
Si1 0 10.16
spl -21 1
F4:n 10
FM4 .2364 1 103
PHYS:N 20 20 0 J J J 1 -1 J J J 0 0
m1 2003 1
m2 1001 2 6000 1
c MT2 S (a,b) THERMAL NEUTRON SCATTERING in polyethylene
mt2 poly.20t
stop F4 .01

```

File 2.VII.1

The calculation has to be made for different neutron energies to cover the full spectrum ranging from 0 to 10 MeV. These successive energy values are set in the “erg” parameter of the source definition card “sdef” of the MCNP input file 2.VII.1. For the 8” sphere ($k = 3$), the shape of the response derived from the MCNP simulation over the whole energy spectrum is presented in figure 2.VII.4. By fitting the curve, one can obtain the detector response in the energy group i from the area under the curve divided by the energy interval as follows:

$$R_{k,i} = \frac{1}{\Delta E_i} \int_{E_{\min}}^{E_{\max}} R_k(E_n) dE_n$$

The mean “fluence – ambient dose equivalent” conversion coefficient, $\bar{h}_\Phi^*(10)$, is calculated for each energy group ΔE_i according to the following formula:

$$[\bar{h}_\Phi^*(10)]_{\Delta E_i} = \frac{1}{\Phi} \int_{\Delta E_i} \left(\frac{d\Phi}{dE_n} \right) [h_\Phi^*(10)]_{E_n} dE_n$$

The responses $R_{k,i}$, in cm^2 , as well as the mean “fluence – ambient dose equivalent” conversion coefficients, in pSv.cm^2 , for the three BSS in the energy groups are listed in table 2.VII.2.

TAB. 2.VII.2 – Responses $R_{k,i}$ (in cm^2) calculated with MCNP and mean “fluence – ambient dose equivalent” conversion coefficients (in pSv.cm^2) for the three BSS in the three energy groups.

Energy interval	$R_{k,i}$			$\bar{h}_\Phi^*(10)$
	2 in.	4 in.	8 in.	
$E_n < 0.5 \text{ eV}$	2.045	1.447	0.263	13.04
$0.5 \text{ eV} < E_n < 50 \text{ keV}$	0.217	2.175	1.001	21.44
$E_n > 50 \text{ keV}$	0.003	0.227	0.953	495

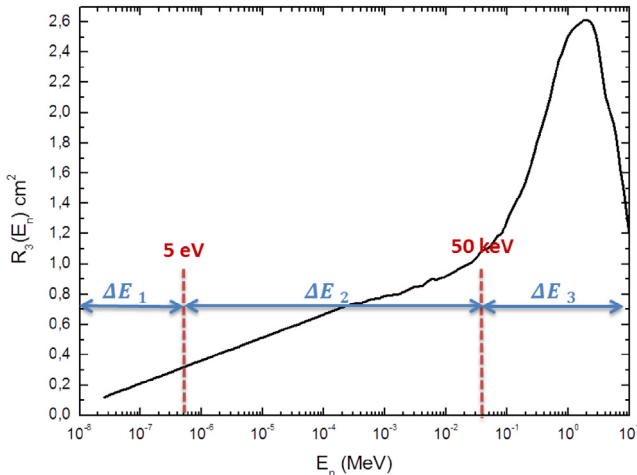


FIG. 2.VII.4 – Response function of the 8” BSS against the energy, simulated with MCNP. The three energy groups used for the sampling of the spectrum of the CANEL/T400 facility are superimposed for comparison.

Part 2: Calculation of Each Energy Group Fluence Using the Least Squares Method

The relationship between a count rate \dot{m}_k for a sphere k and the fluence rate $\dot{\Phi}_i = \dot{\Phi}_{E,i} \Delta E_i$ in each interval is derived from the following sum:

$$\dot{m}_k = \sum_{i=1}^{i=n} R_{k,i} \dot{\Phi}_{E,i} \Delta E_i = \sum_{i=1}^{i=n} R_{k,i} \dot{\Phi}_i \quad (2)$$

For three energy groups, $n = 3$ and the term $R_{k,i}$ is the response of sphere k for the energy interval ΔE_i . By expressing formula (1) for each sphere, we get the following matrix relationship:

$$\dot{\mathbf{M}} = \mathbf{R} \dot{\Phi} \quad (3)$$

The matrices presented below are filled according to the values from tables 2.VII.1 and 2.VII.2.

$$\dot{\mathbf{M}} = \begin{pmatrix} 955.78 \\ 1183.63 \\ 483.18 \end{pmatrix} \quad \mathbf{R} = \begin{pmatrix} 2.045 & 0.217 & 0.003 \\ 1.447 & 2.175 & 0.227 \\ 0.263 & 1.001 & 0.953 \end{pmatrix} \quad \dot{\Phi} = \begin{pmatrix} \dot{\Phi}_1 \\ \dot{\Phi}_2 \\ \dot{\Phi}_3 \end{pmatrix}$$

The system can be solved using an inverse matrix:

$$\dot{\Phi} = \mathbf{R}^{-1} \dot{\mathbf{M}}$$

This method allows obtaining a single result for the component of the vector $\dot{\Phi}$ but does not exclude negative values, *i.e.*, non-physical values. Therefore, we choose to apply a more robust approach, the least squares method, also known as the minimum χ^2 estimation. The latter consists in minimizing the χ^2 of fluence rates in energy intervals. This method is of special interest when the number of spheres and energy intervals is higher. This approach is advisable when the fluence does not change significantly in adjacent energy intervals. We should keep in mind that this approach, although tending to minimize the risk, does not exclude non-physical solutions. Other even more robust methods, essentially iterative, such as that implemented in the GRAVEL, MAXED and SANDII codes can be used (Matzke, 2002). In this case study, the χ^2 can be written with the following form:

$$\chi^2(\dot{\Phi}) = \sum_{k=1}^N \frac{1}{\sigma_s^2} \left(\sum_{i=1}^n R_{k,i} \dot{\Phi}_i - \dot{m}_k \right)^2$$

where $n = N = 3$, since there are equal numbers of spheres and energy bins. We can take advantage of the model linearity to express $\chi^2(\Phi)$ in a matrix format. It is shown that $\chi^2(\Phi)$ can be written as follows:

$$\chi^2(\dot{\Phi}) = (\dot{\mathbf{M}} - \mathbf{R} \dot{\Phi})^T \mathbf{W} (\dot{\mathbf{M}} - \mathbf{R} \dot{\Phi}) \quad (4)$$

\mathbf{W} being the weight matrix corresponding to the inverse of the covariance matrix \mathbf{C} related to the BSS measurements m_s . It can be calculated as follows:

$$\mathbf{W} = \mathbf{C}^{-1} = \left(\frac{1}{n-1} \mathbf{R}^T \mathbf{R} \right)^{-1}$$

The term n in the denominator represents the vector dimension, which is equal to 3 in this example. By differentiating the above expression (4) with respect to each $\dot{\Phi}(\Delta E_i)$, we get:

$$\text{grad } \chi^2(\dot{\Phi}) = 2\mathbf{R}^T \mathbf{W} \mathbf{R} \dot{\Phi} - 2\mathbf{R}^T \mathbf{W} \dot{\mathbf{M}}$$

The minimum $\dot{\Phi}_{\min}$ is reached for $\text{grad } \chi^2(\dot{\Phi}) = 0$, then, it becomes:

$$\dot{\Phi}_{\min} = (\mathbf{R}^T \mathbf{W} \mathbf{R})^{-1} \mathbf{R}^T \mathbf{W} \dot{\mathbf{M}}$$

The covariance matrix \mathbf{C} obtained from a calculation performed with Excel is the following:

$$\begin{aligned} \mathbf{C} &= \left(\frac{1}{3-1} \right) \mathbf{R}^T \mathbf{R} = \frac{1}{2} \begin{pmatrix} 2.045 & 1.447 & 0.263 \\ 0.217 & 2.175 & 1.001 \\ 0.003 & 0.227 & 0.953 \end{pmatrix} \begin{pmatrix} 2.045 & 0.217 & 0.003 \\ 1.447 & 2.175 & 0.227 \\ 0.263 & 1.001 & 0.953 \end{pmatrix} \\ &= \begin{pmatrix} 3.174 & 1.930 & 0.293 \\ 1.930 & 2.891 & 0.724 \\ 0.293 & 0.724 & 0.480 \end{pmatrix} \end{aligned}$$

Since its determinant is not equal to zero, the matrix is invertible. It can be inverted according to the classical method involving the determinant $|\mathbf{C}|$ and the transpose of the cofactor matrix $\text{com}(\mathbf{C})$:

$$\mathbf{W} = \mathbf{C}^{-1} = \frac{{}^T \text{com}(\mathbf{C})}{|\mathbf{C}|} = \begin{pmatrix} 0.566 & -0.468 & 0.360 \\ -0.468 & 0.943 & -1.137 \\ 0.360 & -1.137 & 3.579 \end{pmatrix}$$

The final calculation leads to:

$$\dot{\Phi}_{\min} = (\mathbf{R}^T \mathbf{W} \mathbf{R})^{-1} \mathbf{R}^T \mathbf{W} \dot{\mathbf{M}} = \begin{pmatrix} 442 \\ 236 \\ 137 \end{pmatrix}$$

From these results, table 2.VII.3 indicates the fluence rate and the ambient dose equivalent rate over the three energy groups.

The total ambient dose equivalent rate at 50 cm from the device is about 0.3 mSv.h^{-1} . We can point out the major contribution of the last energy group, although it presents a lower fluence rate component than the others.

TAB. 2.VII.3 – Fluence rates from the least squares minimization method and ambient dose equivalent rates for each energy group.

Energy interval	$\dot{\Phi}_i(\text{cm}^2.\text{s}^{-1})$	$\dot{H}^*(10) = \bar{h}_{\Phi}^*(10) \times \dot{\Phi}_i \times 3600(\mu\text{Sv.h}^{-1})$
$E_n < 0.5 \text{ eV}$	442	21
$0.5 \text{ eV} < E_n < 50 \text{ keV}$	236	18
$E_n > 50 \text{ keV}$	137	245
Total	815	284

Notes on the Bonner Spheres Spectrometer:

In practice, the BSS method is reliable for an evaluation of the total fluence on the entire neutron spectrum, from thermal to fast. Nevertheless, there is a broad uncertainty in the thermal part owing to the weak response of the BSS to low energies (see figure 2.VII.4). Concerning the spectroscopy, the performances of this method are necessarily constrained by the limited number of BSS (usually 12 BSS). A multi-type detector system may be preferable for its energy spectrum resolution quality, notably at fast energies. As an example, the ROSPEC system is composed of several SP type proton recoil detectors (see table 2.VII.4). These detectors operate in proportional counter mode and help assess the energy of protons originating from elastic scattering of fast neutrons on the hydrogen of the filling gas. An unfolding method, which can be similar to that described in the application, is applied to convert the proton recoil spectrum into the neutron spectrum.

In addition to proton recoil detectors, the ROSPEC system comprises a ^3He gas-filled counter whose external wall is coated with ^{10}B to cover epithermal neutrons (energy between 1 eV and 50 keV) and a ^3He gas-filled counter sensitive to thermal neutrons (energy ranging from 0.01 eV to 1 eV). For fast neutron spectroscopy, liquid scintillators, *e.g.*, BJ308 and BC501A, are widely used and can cover energies higher than 4.5 MeV (refer to application 2.VI) with a good efficiency (in the order of 30%) and an acceptable energy resolution. In mixed fields, their important sensitivity to gamma rays can be mitigated with an adequate n/γ discrimination, particularly by applying the pulse shape discrimination (PSD) method to process the signal.

TAB. 2.VII.4 – Features of the proton recoil proportional counters (SP chamber) used in the ROSPEC system to cover an energy range between 0.01 eV and 16 MeV (Ben Mosbah, 2017).

Detector	Radius (cm)	Gas	Pressure (kPa)	Energy range
^3He bare	2.54	$^3\text{He}/\text{Kr}$	83	0.01–1 eV
^3He boron	2.54	$^3\text{He}/\text{Kr}$	216	1 eV–0.05 MeV
Spherical SP2-1	2.54	H_2	76	0.05–0.25 MeV
Spherical SP2-4	2.54	H_2	400	0.15–0.75 MeV
Spherical SP2-10	2.54	H_2	1000	0.4–1.5 MeV
Spherical SP6	7.62	CH_4/Ar	500	1.2–5 MeV
Scintillator	2.8	–	–	4–16.6 MeV

2.VIII Absorbed Dose Measurement in a Water Calorimeter for a 170 MeV Proton Beam Used in Proton Therapy

Abstract:

This application is aiming at measuring the absorbed dose deposited by a proton beam of 170 MeV maximum energy, for proton therapy. An 8 cm × 8 cm × 8 cm proton box, corresponding to the Bragg curve plateau region in water, is scanned with a hermetic calorimeter. The latter is mounted in a sealed glass vessel, in which are placed NTC (Negative Temperature Coefficient) thermistors, filled with ultra-pure water at a temperature of 4 °C. The thermistors are coupled to a Wheatstone bridge, and an amplifier allows to link the resistance change induced by the temperature change with an amplified voltage change. The glass vessel is immersed in a cubic water phantom of dimensions 30 cm × 30 cm × 30 cm, as depicted in figure 2.VIII.1 (Gagnebin *et al.*, 2010).

In the first part, the absorbed dose to water is evaluated from the thermistors' temperature change. A subsidiary challenge will be to assess the fluence rate at the water phantom entrance face required for the proton beam to induce such a dose.

In the second part, we will evaluate the charge measured by an Exradin T1 ionization chamber located at the reference measurement point for the same proton beam. This procedure follows the protocol described in the reference IAEA (2000b).

Finally, in an independent third part, we will point out the difference in the holding time for the temperature variation, owing to the deposited dose, for both a graphite and a water calorimeter exposed to a ⁶⁰Co radiation field.

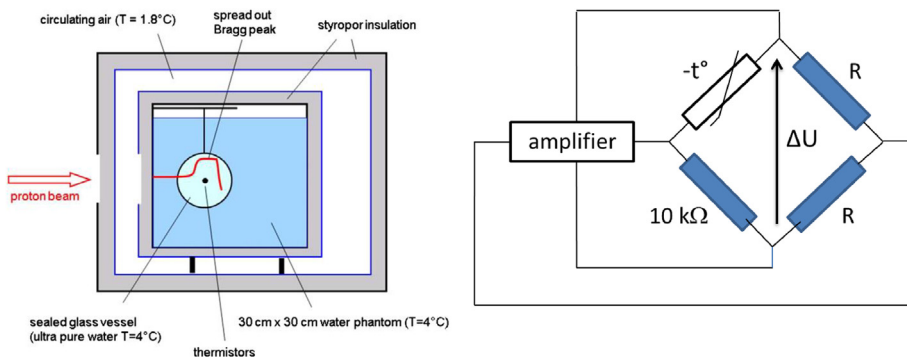


FIG. 2.VIII.1 – (left side) Sketch of the absorbed dose measurement under 15 cm of water in a calorimeter, (right side) Wheatstone bridge for the measurement of the temperature variation.

Objectives:

- Calculation of the absorbed dose from the temperature rise in a water calorimeter.
- Determination of the proton beam fluence as a function of the absorbed dose in depth.
- Study of the calibration process of an ionization chamber in air for the assessment of the proton dose to water.
- Evaluation of the holding time of the temperature variation in the calorimeter.

Main characteristics:*Thermistor and amplifier characteristics:*

- Resistance at $T_o = 4\text{ }^\circ\text{C}$: $R_o = 10\text{ k}\Omega$ (Gagnebin *et al.*, 2010).
- Resistance to temperature calibration curve parameter: $\beta = 3340\text{ K}^{-1}$.
- Resistance to voltage ratio: $F_C = 0.13\text{ }\Omega\cdot\text{V}^{-1}$.
- Voltage change measured at the output of the amplifier at the end of the proton beam irradiation: $\Delta U = 7.5\text{ V}$.
- The thermistors are located at 16.8 cm from the water phantom entrance face (Brede *et al.*, 2006).

Exradin T1 ionization chamber characteristics:

- Calibration factor in Gy/C providing, for reference conditions, the ratio between the readout charge of the ionization chamber for a ^{60}Co radiation field in air and the dose to water for the later at the same point: $N_{D_w, \text{Co}} = 7.67 \times 10^8\text{ Gy}\cdot\text{C}^{-1}$ (Vatnitskya *et al.*, 1999).
- Mean air ionization energy for ^{60}Co electrons: $\bar{W}_{\text{Co}} = 33.97\text{ eV}$ (Vynckier *et al.*, 1991).
- Mean air ionization energy for protons: $\bar{W}_{\text{Co}} = 35.18\text{ eV}$ (Vynckier *et al.*, 1991).
- Ratio of water and air mass stopping powers ^{60}Co electrons: $\left[\left(\bar{S}/\rho \right)_a^w \right]_{\text{Co}} = 1.134$ (Brede *et al.*, 2006).

Other useful data:

- Absorbed dose rate of the 170 MeV proton beam at the Bragg peak: $\tau = 10\text{ Gy}\cdot\text{min}^{-1}$.
- Reference depth for the measurements, at the middle of the Bragg peak (Gagnebin *et al.*, 2010): $R_m = 15\text{ cm}$.
- Proton range of the 10% level of the peak dose on the distal edge of the Bragg peak in water (Gagnebin *et al.*, 2010): $R_{10\%} = 18\text{ cm}$.
- Range of the most energetic proton (without modulator) in water (Gagnebin *et al.*, 2010): $R_{\text{max}} = 19.51\text{ cm}$.
- Water heat capacity at $4\text{ }^\circ\text{C}$ (Gagnebin *et al.*, 2010): $c_W = 4206\text{ J}\cdot\text{kg}^{-1}\cdot\text{K}^{-1}$.

The heat defect is provided in figure 2.VIII.2 for different ions and linear energy transfers. The solid line fits with two exponential functions. The dashed line gives

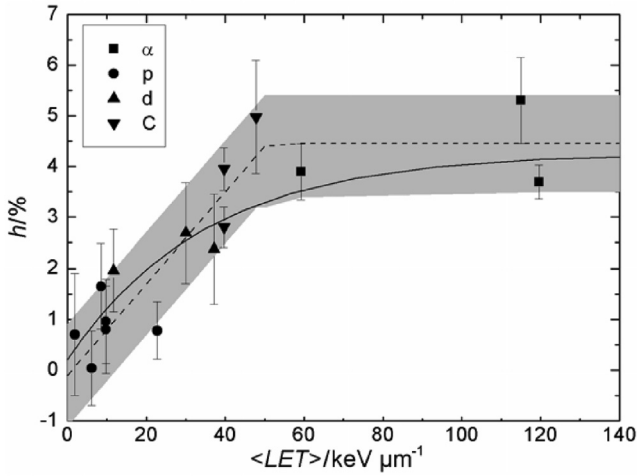


FIG. 2.VIII.2 – Measurement points and fitting of the heat defect h as a function of the linear energy transfer for different energies and particle types: ^{12}C ions (c), ^4He ions (a), deuterons (d) and protons (p), from Brede *et al.* (2006).

the mean value of the uncertainty zone described by the shaded area. The error bars associated with the points are the uncertainties on the mean values derived from different measurement campaigns (Brede *et al.*, 2006).

Part 1: Calculation of the Dose at the Thermistors

In the first place, we have to assess the temperature rise in the calorimeter, caused by the exposure to the proton beam.

(a) Calculation of the water temperature rise

Firstly, we calculate the thermistor resistance variation corresponding to a voltage change of 7.5 V. They are linked to each other by the proportionality coefficient F_C .

$$\Delta R = F_C \Delta U = 0.13 \times 7.5 \approx 1 \Omega$$

Then, we want to get the temperature change related to this resistance change. The thermistor resistance as a function of the temperature is given by the following expression:

$$R(T) = R_o \exp\left(\beta\left(\frac{1}{T} - \frac{1}{T_o}\right)\right) \quad (1)$$

Thus, from (1), we get the temperature as a function of the resistance:

$$T(R) = \left(\frac{\ln R - \ln R_o}{\beta} + \frac{1}{T_o}\right)^{-1}$$

The NTC thermistor resistance decreases when the temperature rises. Thus, the temperature rise related to the resistance decrease ΔR is:

$$\begin{aligned} T(R_o - \Delta R) &= \left(\frac{\ln(R_o - \Delta R) - \ln R_o}{\beta} + \frac{1}{T_o} \right)^{-1} \\ &= \left(\frac{\ln(9999) - (\ln 10\,000)}{3340} + \frac{1}{4 + 273.15} \right)^{-1} = 277.1523 \text{ K} \end{aligned}$$

Finally, the temperature variation is:

$$\Delta T = T(R_o - \Delta R) - T(R) = 277.1523 - 277.15 = 2.3 \text{ mK}$$

(b) Calculation of the dose at the thermistor in hyper-pure water

It is important to point out that in the field of radiotherapy, primary measurements for highly energetic proton beams are performed with water phantoms. Besides, the water calorimeter makes an excellent dosimeter to realize such a measurement (protocol from IAEA, 2000b). The dose to water as a function of the temperature change is provided by the following formula:

$$D_{W,p} = c_W \Delta T k \left(\frac{1}{1 - h} \right)$$

where k is the product of several correction factors, such as the heat transfer correction. These factors are very close to the unit and will therefore be omitted in the rest of this application. The term h corresponds to the heat defect and is conventionally defined as:

$$h = \frac{\varepsilon_a}{\varepsilon_a - \varepsilon_h}$$

where ε_a is the energy absorbed by the irradiated material and ε_h is the energy which appears as heat. An exothermic or an endothermic head defect correspond, respectively, to a negative or a positive value of h . The reader can draw an analogy at the nuclear level with the Q -value of the reaction taken into account in the local energy transfer balance, when nuclear reactions occur during the radiation exposure. The heat defect in water is almost entirely due to chemical reactions of free radicals produced, subsequent to the irradiation of water and its impurities. The curve provided in figure 2.VII.2 enables to evaluate this parameter. At the point where the thermistors are located, the latter witness the irradiation of proton beams of energies between 150 MeV and 170 MeV during successive scanings. Below these energies, the ranges in water are smaller than 15 cm. In order to evaluate the mean proton energy, we rely, as a first approximation, on the result of the proton effective energy, estimated to be $\bar{E}_p = 58.7 \text{ MeV}$, according to expression (2). At this mean energy, the linear mass stopping power is about $1 \text{ keV} \cdot \mu\text{m}^{-1}$ (PSTAR calculation).

We will consider a 1% heat defect, matching the upper limit of uncertainty interval (shaded area of figure 2.VIII.2). Finally, we obtain the absorbed dose to water:

$$D_{W,p} = 4206 \times 2.3 \cdot 10^{-3} \times \left(\frac{1}{1 - 0.01} \right) = 9.77 \text{ J} \cdot \text{kg}^{-1} \text{ (or Gy)}$$

Note that this dose is identical in the depth interval $R_{\text{max}} - 8 \text{ cm} < z < R_{\text{max}}$.

(c) Calculation of the 170 MeV proton fluence matching a 10 Gy dose

The maximum depth of the Bragg curve corresponds to the range of the most energetic protons, *i.e.*, that of 170 MeV protons. In application 1.VI, we estimated this maximum range in water to be 19.51 cm. We propose to calculate the proton beam fluence rate required at the entrance of the water phantom to induce a 10 Gy dose under this depth limit. In application 1.VI, we carried out a semi-empirical calculation of the absorbed dose per unit fluence, which lead to 3.69 nGy.cm² at the Bragg peak for 170 MeV protons. The inverse of this value weighted by the dose measured by the calorimeter provides the total fluence required:

$$\Phi = \left(\frac{D(R_{\text{max}})}{\Phi_0} \right)^{-1} D_{W,p} = \frac{10}{3.69 \times 10^{-9}} = 2.71 \times 10^9 \text{ (proton).cm}^{-2}$$

The absorbed dose rate is $\tau = 10 \text{ Gy} \cdot \text{min}^{-1}$. Accordingly, the proton beam fluence rate during the duty cycle is:

$$\dot{\Phi} = \frac{2.71 \times 10^9}{60} = 4.52 \times 10^7 \text{ (proton).cm}^{-2} \cdot \text{s}^{-1}$$

Note that this fluence rate is *a priori* the lowest among all scanning to be performed, with the aim of depositing a 10 Gy dose in the plateau region of the Bragg curve. Indeed, up to 8 cm upstream the 170 MeV proton range, the proton energy decreases with depth, and so does the Bragg peak. Accordingly, it is necessary to increase the proton fluence rate to reach the 10 Gy dose deposited in the whole plateau region of the Bragg curve.

Part 2: Calculation of the Charge Measured by an Ionization Chamber, Calibrated in ⁶⁰Co, Located in the Proton Beam at the Plateau Region of the Bragg Curve

The relationship between the absorbed dose to water and the absorbed dose measured by the ionization chamber is defined in the ICRU (1998b):

$$D_{W,p} = M_p N_{D_w,Co} k_{p,Co}$$

where $N_{D_w,Co}$ is the calibration factor in Gy.C⁻¹ providing, for reference conditions, the ratio between the ionization chamber charge reading in the air and the dose to water for a ⁶⁰Co beam at the same measurement point. M_p is the charge readout when the ionization chamber is located in the air, at the measurement point described in the previous part, with the same ⁶⁰Co beam. The term k is a dose

conversion factor between protons and the gamma rays emitted by ^{60}Co . According to Vatsnitskya *et al.* (1999), it can be defined by:

$$k_{p,\text{Co}} = \left[\left(\frac{\bar{S}}{\rho} \right)_a \right]_{\text{Co}}^p \left(\frac{\bar{W}_p}{\bar{W}_{\text{Co}_a}} \right)$$

The first term represents the ratio of the mean stopping powers of water and air for protons and secondary electrons set in motion by ^{60}Co . The second term corresponds to the ratio of mean air ionization energies for protons and the electrons produced by ^{60}Co . The first ratio can be determined by firstly evaluating the mean proton energy at the reference measurement point, located at the middle of the plateau region of the Bragg curve, *i.e.*, at 15 cm depth in the case study (Gagnebin *et al.*, 2010). This energy is also described as the effective energy and is obtained from the residual range. The latter corresponds to the subtraction of the reference measurement point R_m from the proton range at the 10% level of the peak dose on the distal edge of the Bragg peak $R_{10\%}$ (ICRU, 1998b), and is written below:

$$R_{\text{res}} = R_{10\%} - R_m = 18 - 15 = 3 \text{ cm}$$

The effective energy for water and proton beams of energy ranging between 20 MeV and 400 MeV can be calculated with the following empirical formula (Vynckier *et al.*, 1991):

$$\bar{E}_p = a(R_{\text{res}})^b + c^{R_{\text{res}}} \quad (2)$$

where $a = 30.676$, $b = 0.57305$ and $c = 1.0348$. Then, we can derive from the expression of Vynckier *et al.* (1994) the ratio of the mean stopping powers of water and air, for protons with this effective energy:

$$\left[\left(\frac{\bar{S}}{\rho} \right)_a \right]^p = d(\bar{E}_p)^f + g\bar{E}_p$$

with $d = 0.14687$, $f = -0.025218$ and $g = 1.00000619$. Finally, we get the numerical result for both quantities:

$$\bar{E}_p = 30.676 \times (3)^{0.57305} + 1.0348^3 = 58.7 \text{ MeV}$$

$$\left[\left(\frac{\bar{S}}{\rho} \right)_a \right]^p = 0.14687 \times (58.7)^{-0.025218} + 1.00000619^{58.7} = 1.1328$$

Then, we can derive the dose conversion coefficient:

$$k_{p,\text{Co}} = \frac{1.1328}{1.134} \times \frac{35.18}{33.97} = 1.034$$

After applying all correction factors related to the chamber (ion recombination correction factor, temperature and pressure correction, etc.), the ionization chamber charge readout within the proton beam should be:

$$M_p = \frac{D_{W,p}}{N_{D_w,Co} k_{p,Co}} = \frac{10}{7.67 \times 10^8 \times 1.034} = 1.26 \times 10^{-8} \text{ C}$$

Part 3: Difference in the Holding Time of the Temperature Variation between a Water Calorimeter and a Graphite Calorimeter for a ⁶⁰Co Beam (Ross and Klassen, 1996)

For measuring the temperature change with an uncertainty smaller than 0.5%, Ross and Klassen (1996), propose to calculate the time required to realize the irradiation and the measurement with both a graphite and a water calorimeter. The effect of conductive heat transfer can be estimated using the general equation for heat transport, which is given by:

$$\frac{\partial T(z, t)}{\partial t} = \alpha \nabla^2 T(z, t) + \frac{1}{c} \frac{\partial D(z, t)}{\partial t} \tag{3}$$

with $\alpha_w = \kappa/\rho c_w$, where κ is the thermal conductivity, ρ is the density and c is the specific heat of the calorimetric material. If we assume that the absorbed dose is delivered in a very short time, the right term can be considered as negligible. Moreover, since the temperature gradient depends essentially on the water depth, *i.e.*, it is along z -axis, equation (3) can be simplified to:

$$\frac{\partial T(z, t)}{\partial t} \approx \alpha \frac{\partial^2 T(z, t)}{\partial z^2} \tag{4}$$

When considering an irradiation by a broad photon beam, the dose variation as a function of depth, can be written as:

$$D = D_o \exp(-\mu(z - z_o)) \tag{5}$$

where D_o is the dose at depth z_o , the location of the entrance window of the calorimeter. It corresponds to the maximum dose. Since we assume that the dose is delivered in a very short time, the temperature gradient also will be given by equation (5). Therefore, expression (4) becomes:

$$\frac{\partial^2 T(z, t)}{\partial z^2} \approx \mu^2 T \tag{6}$$

Using expressions (4) and (6) we can estimate how the temperature distribution will deviate from the dose distribution:

$$\frac{\partial T}{\partial t} \approx \alpha \mu^2 T \iff \Delta t \approx \frac{1}{\alpha \mu^2} \left(\frac{\Delta T}{T} \right)$$

The linear attenuation coefficient μ is approximately equal to 0.5 cm^{-1} for graphite and water for ^{60}Co . The α coefficient is, respectively, equal to $0.8 \text{ cm}^2 \cdot \text{s}^{-1}$ and $1.41 \times 10^{-3} \text{ cm}^2 \cdot \text{s}^{-1}$ for graphite and water. As the result, for a measurement uncertainty $\Delta T/T = 0.005$, the values of Δt are:

$$\Delta t_g \approx \frac{1}{0.8 \times (0.5)^2} \times 0.005 = 2.5 \text{ s}$$

$$\Delta t_w \approx \frac{1}{1.41 \times 10^{-3} \times (0.5)^2} \times 0.005 \sim 23 \text{ min}$$

Therefore, for typical dose rates used in radiotherapy, a time of 2.5 s is not sufficient to perform an irradiation and a measurement, hence the necessity to thermally insulate as much as possible the absorbent material in the graphite calorimeter. However, it is not the case for water, whose temperature remains stable longer after irradiation.

2.IX Calibration of a Neutron Survey Meter with a ^{252}Cf Source

Abstract:

This application is aimed at describing the calibration of a neutron survey meter. In the first section, the device is calibrated in term of $\mu\text{Sv} \cdot \text{h}^{-1} / \text{c} \cdot \text{s}^{-1}$ with a ^{252}Cf source using the shadow cone method described in the ISO standard 8529-2 (ISO, 2000). The device is a spherical ^3He -filled proportional counter surrounded by a polyethylene layer, identical to the 8" Bonner sphere studied in the application 2.VII.

In the second section, the survey meter is used to measure a typical workplace neutron field, emitted by a PuF_4 solution considered as a point-like source. At the end, the reliability of the ^{252}Cf calibration is checked with respect to the deviation between the readout of the calibrated survey meter and the actual dose equivalent rate of the PuF_4 solution.

Objectives:

- Application of the shadow cone method described in the ISO 8529-2 standard.
- Calculation of the efficiency and energy response of a Bonner sphere using MCNP.
- Evaluation of a calibration coefficient for a proportional counter.
- Check of the calibration reliability depending on the characteristics of the workplace radiation field.

Main characteristics:

The dimensions of the irradiation room, in which the calibration bench is located, are taken as the minimum dimensions for a scatter contribution to reach 40%.

According to the ISO standard 8529-2 (appendix B), for a ^{252}Cf source and a large Bonner sphere in a semi-cubic room, the room dimensions must be: $L = W = 2H = 4.4$ m. The walls of the facility are modeled in MCNP as a significant thickness of ordinary concrete of density 2.3 g.cm^{-3} . The calibration bench is located at 1 m above the ground, at the center of the room.

Other data necessary for this application are given below:

- CH_2 sphere radius: $r_d = 10.16$ cm (8" diameter).
- ^3He sphere radius: $r_{\text{He}} = 1.6$ cm.
- Distance from the source to the detector center: 100 cm.
- Neutron “fluence – ambient dose equivalent” conversion coefficient for the bare ^{252}Cf source: $h_{\Phi}^* = 385 \text{ pSv.cm}^2$ (Antoni and Bourgois, 2017a).
- ^{252}Cf source activity: $A_{\text{Cf}} = 1 \text{ GBq}$.
- Neutron yield: $B_A = 0.116 \text{ (n).s}^{-1}.\text{Bq}^{-1}$ (Antoni and Bourgois, 2017a).
- Electronic loss coefficient, essentially due to the application of a low threshold for the n/γ discrimination (there is no dead time because of a weak count rate): $k_e = 0.7$ (Allinei, 1992).
- Anisotropy factor at 90° : $F(\theta) = 1$ (Ogheard, 2012).
- Total air scattering correction factor for the fluence and the ^{252}Cf source: $A = 1.4\%$ (ISO, 2000).
- Linear air attenuation coefficient for ^{252}Cf : $\bar{\Sigma} = 1.055 \times 10^{-4} \text{ cm}^{-1}$ (ISO, 2000).

Part 1: Calibration of the Bonner Sphere with a ^{252}Cf Source

Measurements with and without a shadow cone are performed in order to estimate the contribution from neutrons scattered by the air and the room walls. The shadow cone approved by the ISO standard 8529-2 is built up of two adjacent truncated cones. The calibration factor linking the count rate with the ambient dose equivalent rate is expressed as follows:

$$N_H = \frac{\dot{H}^*(10)}{m_n} = \frac{\dot{H}^*(10)}{m_t - m_s} = \frac{F_1(d) F_1(\theta)}{F_A(d)} \left[\frac{h_{\Phi}^* \dot{\Phi}}{m_t - m_s} \right] \quad (1)$$

with

- m_n the net measurement.
- m_t the detector reading measured without shadow cone.
- m_s the detector reading with a shadow cone.
- In the following example, the quantities m_t and m_s are simulated using the method described in the section 2.VII. These values are obviously measured for an in-field calibration.
- $\dot{\Phi}$ the fluence rate at the center of the detector.
- $F_1(\theta)$ the anisotropy factor, equal to 1 in this case since the source is considered as a point-like source.
- $F_A(d)$ the neutron emission attenuation factor in the air, corresponding to the exponential of the product of d and the macroscopic cross section $\bar{\Sigma}$.

- $F_1(d)$ a geometrical correction factor accounting for the individual dimensions of the source and the detector. For a spherical detector, this factor is given by the expression of Alliney (1992):

$$F_1(d) = 1 + \delta \left\{ \frac{2d^2}{r_d^2} \left[1 - \sqrt{1 - \left(\frac{r_d}{d} \right)^2} \right] - 1 \right\}$$

The recommended value for δ is 0.5 (ISO, 2000). In this case, we have $d/r_d > 2$, and the above expression can be reduced as:

$$F_1(d) = 1 + \delta \left(\frac{r_d}{2d} \right)^2 = 1 + 0.5 \times \left(\frac{10.16}{2 \times 100} \right)^2 = 1.0013 \cong 1$$

This term, very close to 1, will be vanished in subsequent calculations. As a result, the general formula (1) of the calibration coefficient can be expressed more specifically as follows:

$$N_H = \frac{h_{\Phi}^* A_{Cf} B_A}{4 \pi d^2 (m_t - m_s)} \exp(-\bar{\Sigma} d) \quad (2)$$

The MCNP simulation consists in evaluating the number of (n,p) reactions occurring on ${}^3\text{He}$ per source neutron, which matches the detector efficiency ε . Then, by weighting the MCNP result by the neutron emission, $A_{Cf} B_A$, and the electronic loss coefficient k_e , we get the final result in counts per second, for the studied source.

$$m_{t,s} = k_e A_{Cf} B_A \varepsilon_{t,s} = k_e A_{Cf} B_A n_{\text{He}} V \int_0^E \left(\frac{d\Phi}{dE} \right)_{t,s} \sigma_{(n,p)}(E) dE \quad (3)$$

where n_{He} is the ${}^3\text{He}$ atomic density, V is the chamber gas volume, $(d\Phi/dE)_{t,s}$ is the energy distribution of the neutron fluence in the gas volume, for the measurement without or with a shadow cone, stated respectively by subscripts t and s , and $\sigma_{(n,p)}(E)$ is the (n,p) reaction cross section at the neutron energy E .

(a) Measurement without shadow cone for the ${}^{252}\text{Cf}$ source

In order to determine the Bonner sphere efficiency, the neutron fluence is initially calculated with MCNP, using a F4 tally. This quantity is then weighted by a multiplication card “fm”, allowing to directly assess the efficiency ε_t in expression (3). The parametrization of this card in the input file 2.IX.1 is “fm4 7.2913e-4 1 103”. The first entry corresponds to the ${}^3\text{He}$ atomic density in the chamber volume V . For a temperature of 273 K at the considered gas pressure, this density is $n_{\text{He}} = 4.249 \times 10^{19}$ (atom).cm $^{-3}$. Since the cross sections are expressed in barn in

the MCNP libraries, this density has to be multiplied by a factor accounting for the conversion from barn to cm^2 , *i.e.*, 10^{-24} cm^2 . From this calculation, we get:

$$n_{\text{He}} V = 4.249 \times 10^{19} \times 10^{-24} \times \frac{4}{3} \times \pi \times (1.6)^3 = 7.2913 \times 10^{-4} \text{ (a).cm}^{-1}$$

Parameter “1” stands for the material number of ^3He in the materials definition and the parameter “103” is stated for weighting the fluence by the (n,p) reaction cross section in the corresponding energy bin, for all neutrons entering the sensitive volume of the sphere. The ^{252}Cf neutron spectrum resulting from spontaneous fission is modeled by a Watt spectrum whose distribution is:

$$p(E) = c \exp\left(-\frac{E}{a}\right) \sinh\sqrt{bE}$$

Parameters for the ^{252}Cf source are $a = 1.025 \text{ MeV}$ and $b = 2.926 \text{ MeV}^{-1}$ (from Briesmeister, 2000). The input file below is provided for a 100 cm distance between the source and the detector center:

```

neutron dosimetry simulation
c cell block
10 1 4.2497e-5 -10 $ He3
20 2 -.95 -20 10 $ CH2
30 3 -1.3e-3 -30 20 $ air
40 4 -2.35 -40 30 $ ordinary concrete
50 0 40

10 Sx 50 1.6
20 Sx 50 10.16
30 RPP -220 220 -220 220 -110 110
40 RPP -270 270 -270 270 -160 160

imp:n 1 1 1 1 0
mode n
sdef par=n pos -50 0 0 erg d1
c Watt spectrum a=1.025 b=2.926
spl -3 1.025 2.926
F4:n 10
FM4 7.2913e-4 1 103
m1 2003 1 $ He3
m2 1001 2 6000 1 $ CH2
m3 7014 .781 8016 .212 7015 .007 $ air
c concrete
M4 14000 -20.68 13027 -.363 8016 -50.853 20000 -21.645 12000 -.198 19000 -.088 &
11023 -.0384 16000 -.139 6000 -4.52 22000 -.0155 15031 -.0208 25055 -.0192 &

```

```

1001 -.701 26054 -.0418 26056 -.6588 26057 -.0157 26058 -.0024 24052 -.00057
mt2 poly.20t
stop F4 .01

```

File 2.IX.1

The efficiency evaluated with MCNP is given by the F4 tally result: $\varepsilon_t = 3.046 \times 10^{-5} \text{c.n}^{-1}$. When multiplying this result by the neutron emission and the electronic loss coefficient, we get the detector readout without shadow cone for a 1 GBq source:

$$m_t = k_e A_{\text{Cf}} B_A \varepsilon_t = 0.7 \times 10^9 \times 0.116 \times 3.046 \times 10^{-5} = 2473 \text{c.s}^{-1}$$

(b) Measurement with a shadow cone for the ^{252}Cf source

The shadow cone MCNP model is described in the ISO standard 8529-2 (appendix E). It is built up of two truncated cones; the iron-based one of length $d_2 = 20$ cm and the borated polyethylene-based one (CH_2 with 5% of boron) of length $d_3 = 30$ cm. The distance between the source and the first truncated cone is $d_1 = 5$ cm (Kim *et al.*, 2015). The shadow cone angle is chosen so that the projection of its solid angle is greater than the radius of the detector, while at the same time being smaller than two times the solid angle of the detector. In this case study, we choose r_4 to be 1.5 times the Bonner sphere radius ($r_4 = 1.5 \times 10.16 = 15.24$ cm). The Bonner sphere is located at 100 cm away from the source. When applying Thales' theorem, it becomes $r_1 = 0.76$ cm, $r_2 = 3.81$ cm and $r_3 = 8.38$ cm. The whole system is represented in figure 2.IX.1.

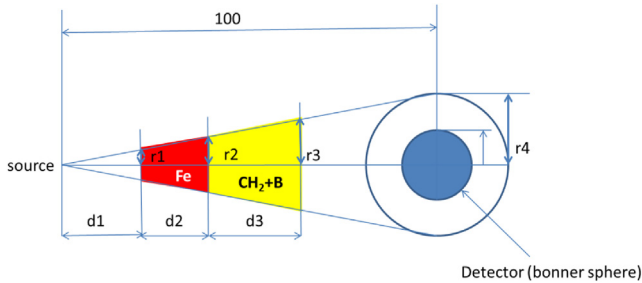


FIG. 2.IX.1 – MCNP model of the shadow cone recommended by the ISO standard 8529-2.

A truncated cone can be modeled with MCNP by applying a pre-defined closed surface, also called *macrobody*, of type “trc”. Its set of parameters is “trc $x y z h_x h_y h_z r_1 r_2$ ”, where x , y and z are coordinates of the cone basis center, h_x , h_y and h_z , are

coordinates of the steering vector defining the cone axis and r_1 and r_2 are the first and the second radius of the truncated cone. The input file 2.IX.2 for the efficiency evaluation with the shadow cone described above is the following.

```
Shadow cone simulation
c cell block
10 1 4.2497e-5 -10 $ He-3
20 2 -.95 -20 10 $ CH2
30 3 -1.3e-3 -30 20 50 60 $ air
40 4 -2.35 -40 30 $ concrete
50 5 -7.8 -50 $ Fe cone
60 6 -.95 -60 $ CH2 B cone
100 0 40

10 Sx 50 1.6
20 Sx 50 10.16
30 RPP -220 220 -220 220 -110 110
40 RPP -270 270 -270 270 -160 160
50 TRC -45 0 0 20 0 0 .762 3.81
60 TRC -24.999999 0 0 30 0 0 3.81 8.38

imp:n 1 1 1 1 1 1 0
mode n
sdef par=n pos -50 0 0 erg d1
sp1 -3 1.025 2.926 $ Cf-252 Watt spectrum
F4:n 10
FM4 7.2913e-4 1 103
PHYS:N 100 100 0 J J J 1 -1 J J J 0 0
m1 2003 1 $ 6000 1 8016 2o
m2 1001 2 6000 1
m3 7014 .781 8016 .212 7015 .007 $ air
M4 14000 -20.68 13027 -.363 8016 -50.853 20000 -21.645 12000 -.198 19000 -.088 &
11023 -.0384 16000 -.139 6000 -4.52 22000 -.0155 15031 -.0208 25055 -.0192 &
1001 -.701 26054 -.0418 26056 -.6588 26057 -.0157 26058 -.0024 24052 -.00057
M5 26000 1
M6 1001 -0.136501 1002 -0.000031 5010 -0.009215 &
5011 -0.040785 6000 -0.813468
mt2 poly.20t
mt6 poly.20t
stop F4 .015
```

File 2.IX.2

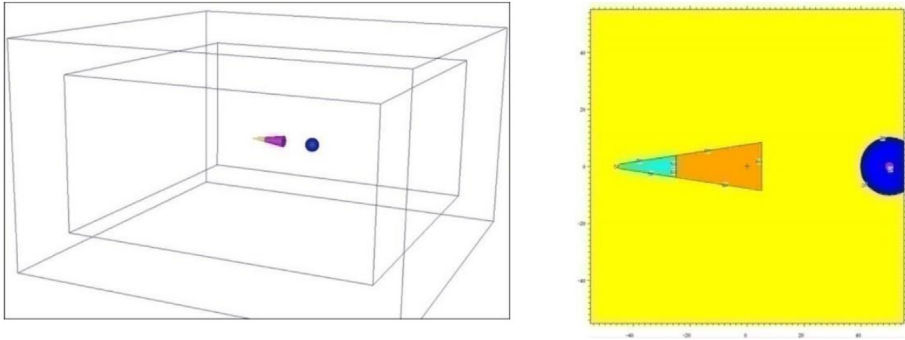


FIG. 2.IX.2 – MCNP modeling of the radiological scene for the measurement with the shadow cone.

The modeled geometry is displayed in figure 2.IX.2.

The efficiency provided by this calculation is $\varepsilon_s = 1.232 \times 10^{-5} (\text{c}).\text{n}^{-1}$. When multiplying this result by the neutron emission and the electronic loss coefficient, we obtain the readout with a shadow cone for a 1 GBq source:

$$m_s = k_e A_{\text{Cf}} B_A \varepsilon_s = 0.7 \times 10^9 \times 0.116 \times 1.232 \times 10^{-5} = 1001 \text{ c.s}^{-1}$$

Therefore, we can derive the net readout m_n , without scattering:

$$m_n = m_t - m_s = 2473 - 1001 = 1472 \text{ c.s}^{-1}$$

Comparatively, we can evaluate the Bonner sphere theoretical response to the ^{252}Cf source, in vacuum (refer to the first part of application 2.VII reviewing the Bonner spheres). The fluence theoretical response is $R_{\text{th}} = 2.328 \text{ cm}^2$. Then, the theoretical net measurement of the sphere, without scattering and attenuation by the air, can be assessed with expression (4):

$$(m_n)_{\text{th}} = k_e R_{\text{th}} \frac{A_{\text{Cf}} B_A}{4 \pi d^2} = 0.7 \times 2.328 \times \frac{1.16 \times 10^8}{4 \pi (100)^2} = 1504 \text{ c.s}^{-1} \quad (4)$$

We find $(m_n)_{\text{th}} \approx m_n$, within 2%. Thus, we can infer that the described process is satisfactory.

(c) Calculation of the calibration coefficient in ambient dose equivalent

As defined in expression (2), the calibration coefficient can be calculated:

$$N_{\text{H}} = \frac{385 \times 1.16 \times 10^8}{4 \pi (100)^2 \times 1472} \exp(-1.055 \times 10^{-4} \times 100) = 243 \text{ pSv.}(c)^{-1}$$

It is also equivalent to:

$$N_H = 243 \times 3600 = 0.87 \mu\text{Sv.h}^{-1}/\text{c.s}^{-1}$$

Finally, for the ^{252}Cf source, the “detected counts – ambient dose equivalent rate” conversion coefficient is $0.87 \mu\text{Sv.h}^{-1}/\text{c.s}^{-1}$. The dose equivalent rate, without shadow cone, obtained for the previous source is:

$$\dot{H}^*(10) = m_l N_H = 2473 \times 0.87 \cdot 10^{-3} = 2.16 \text{ mSv.h}^{-1}$$

Part 2: Measurement of the Ambient dose Equivalent for a Typical Neutron Spectrum of a Radiation Workplace

Once the survey meter calibration is completed, the detector is exposed to a 100 g PuF_4 solution in the same conditions as before (same distance from the source and same concrete surroundings). The solution is assumed to be a point-like source, responsible for an emission rate $B = 10^6 \text{ n.s}^{-1}$ in $4\pi \text{ sr}$ (Stewart, 1991). We aim to evaluate the dose equivalent rate, at 1 m from this solution, with the Bonner sphere previously calibrated in ^{252}Cf . The subsequent step consists in determining the deviation between the measured value and the actual value of the ambient dose equivalent rate of the PuF_4 solution. The actual value is assessed with MCNP by simulating the ambient dose equivalent rate at 100 cm from the PuF_4 solution, without a Bonner sphere.

- (a) Measurement of the ambient dose equivalent for the PuF_4 solution with the ^{252}Cf calibrated Bonner sphere

The PuF_4 solution neutron spectrum, measured at the workplace (from IAEA, 2001) is shown in figure 2.IX.3.

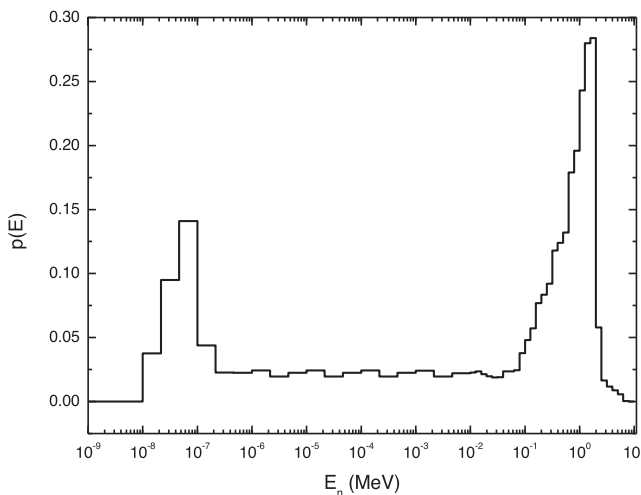


FIG. 2.IX.3 – PuF_4 solution workplace spectrum.

The input file 2.IX.3 is set for the calculation of the efficiency ε_t at 100 cm from the PuF₄ solution, without shadow cone.

```

Bonner sphere simulation with the PuF4 spectrum
c cell block
10  1  4.2497e-5  -10    $ He3
20  2  -.95      -20 10  $ CH2
30  3 -1.3e-3    -30 20  $ air
40  4 -2.35     -40 30  $ concrete
50  0  40

10 Sx 50 1.6
20 Sx 50 10.16
30 RPP -220 220 -220 220 -110 110
40 RPP -270 270 -270 270 -160 160

imp:n 1 1 1 1 0
mode n
sdef par=n pos -50 0 0 erg d2
c PuF4 spectrum
si2 h 1.00E-09 2.15E-09 4.64E-09 1.00E-08 2.15E-08 4.64E-08 1.00E-07 2.15E-07 &
4.64E-07 1.00E-06 2.15E-06 4.64E-06 1.00E-05 2.15E-05 4.64E-05 1.00E-04 &
2.15E-04 4.64E-04 1.00E-03 2.15E-03 4.64E-03 1.00E-02 1.25E-02 1.58E-02 &
1.99E-02 2.51E-02 3.16E-02 3.98E-02 5.01E-02 6.30E-02 7.94E-02 1.00E-01 &
1.25E-01 1.58E-01 1.99E-01 2.51E-01 3.16E-01 3.98E-01 5.01E-01 6.30E-01 &
7.94E-01 1.00E+00 1.25E+00 1.58E+00 1.99E+00 2.51E+00 3.16E+00 3.98E+00 &
5.01E+00 6.30E+00 7.94E+00
sp2 d 0.00E+00 0.00E+00 0.00E+00 3.76E-02 9.49E-02 1.41E-01 4.38E-02 &
2.27E-02 2.25E-02 2.43E-02 1.96E-02 2.25E-02 2.43E-02 1.96E-02 2.25E-02 &
2.43E-02 1.96E-02 2.25E-02 2.41E-02 1.95E-02 2.21E-02 2.27E-02 2.35E-02 &
2.13E-02 1.98E-02 1.89E-02 1.90E-02 2.35E-02 2.35E-02 2.45E-02 3.78E-02 &
4.81E-02 5.71E-02 7.69E-02 8.35E-02 9.21E-02 1.18E-01 1.24E-01 1.32E-01 &
1.79E-01 1.96E-01 2.43E-01 2.80E-01 2.84E-01 5.79E-02 1.64E-02 1.17E-02 &
8.84E-03 5.71E-03 4.62E-04 3.19E-05
F4:n 10
FM4 7.2913e-4 1 103
m1 2003 1 $ He-3
m2 1001 2 6000 1 $ CH2
m3 7014 .781 8016 .212 7015 .007 $ air
c m4 concrete
M4 14000 -20.68 13027 -.363 8016 -50.853 20000 -21.645 12000 -.198 19000 -.088 &
11023 -.0384 16000 -.139 6000 -4.52 22000 -.0155 15031 -.0208 25055 -.0192 &
1001 -.701 26054 -.0418 26056 -.6588 26057 -.0157 26058 -.0024 24052 -.00057
mt2 poly.20t
stop F4 .01

```

The spectrum plotted in figure 2.IX.3 is sampled in energy and emission probability, respectively, with the “si2” and “sp2” cards of the input file 2.IX.3. The efficiency got with the MCNP simulation is $\epsilon_t = 2.308 \times 10^{-5} \text{ (c).n}^{-1}$. When multiplying this result by the neutron emission and the electronic loss coefficient, we obtain the detector measurement without shadow cone for the 1 MBq source:

$$m_t = k_e B \epsilon_t = 0.7 \times 10^6 \times 2.308 \times 10^{-5} = 16 \text{ c.s}^{-1}$$

In order to obtain the readout, the value is multiplied by the calibration coefficient N_H calculated in the previous part.

$$\dot{H}^*(10) = m_t N_H = 16 \times 0.87.10^{-3} = 0.0139 \text{ mSv.h}^{-1} = 13.9 \mu\text{Sv.h}^{-1}$$

- (b) Calculation of the actual dose equivalent rate for the PuF₄ solution and comparison with the previous estimation

In this final step, the theoretical ambient dose equivalent rate due to the PuF₄ solution is assessed in the same manner. The calculation is performed with the fluence at a point estimator, *i.e.*, a F5 tally, weighted by the ICRP “fluence – ambient dose equivalent” conversion coefficients using the “de” and “df” cards. The result obtained corresponds to the ambient dose equivalent per source neutron, $H^*(10)/B$. The MCNP input file 2.IX.4 is set for this calculation:

```
PuF4 ambient dose equivalent calculation
c cell block
30 3 -1.3e-3 -30 $ air
40 4 -2.35 -40 30 $ concrete
50 0 40

30 RPP -220 220 -220 220 -110 110
40 RPP -270 270 -270 270 -160 160

imp:n 1 1 0
mode n
sdef par=n pos -50 0 0 erg d2
c PuF4 spectrum
si2 h 1.00E-09 2.15E-09 4.64E-09 1.00E-08 2.15E-08 4.64E-08 1.00E-07 2.15E-07 &
4.64E-07 1.00E-06 2.15E-06 4.64E-06 1.00E-05 2.15E-05 4.64E-05 1.00E-04 &
2.15E-04 4.64E-04 1.00E-03 2.15E-03 4.64E-03 1.00E-02 1.25E-02 1.58E-02 &
1.99E-02 2.51E-02 3.16E-02 3.98E-02 5.01E-02 6.30E-02 7.94E-02 1.00E-01 &
1.25E-01 1.58E-01 1.99E-01 2.51E-01 3.16E-01 3.98E-01 5.01E-01 6.30E-01 &
7.94E-01 1.00E+00 1.25E+00 1.58E+00 1.99E+00 2.51E+00 3.16E+00 3.98E+00 &
5.01E+00 6.30E+00 7.94E+00
sp2 d 0.00E+00 0.00E+00 0.00E+00 3.76E-02 9.49E-02 1.41E-01 4.38E-02 &
2.27E-02 2.25E-02 2.43E-02 1.96E-02 2.25E-02 2.43E-02 1.96E-02 2.25E-02 &
2.43E-02 1.96E-02 2.25E-02 2.41E-02 1.95E-02 2.21E-02 2.27E-02 2.35E-02 &
2.13E-02 1.98E-02 1.89E-02 1.90E-02 2.35E-02 2.35E-02 2.45E-02 3.78E-02 &
```

```

4.81E-02 5.71E-02 7.69E-02 8.35E-02 9.21E-02 1.18E-01 1.24E-01 1.32E-01 &
1.79E-01 1.96E-01 2.43E-01 2.80E-01 2.84E-01 5.79E-02 1.64E-02 1.17E-02 &
8.84E-03 5.71E-03 4.62E-04 3.19E-05
F5:n 50 0 0 .1
C H*(10) ICRP 74 coefficient for neutrons
DE5 1e-9 1e-8 2.53e-8 1e-7 2e-7 5e-7 1e-6 2e-6 5e-6 1e-5 2e-5 5e-5 1e-4 2e-4 &
5e-4 1e-3 2e-3 5e-3 1e-2 2e-2 3e-2 5e-2 7e-2 .1 .15 .2 .3 .5 .7 .9 1 1.2 2 &
3 4 5 6 7 8 9 10 12 14 15 16 18 20 30 50 75 100 125 150 175 201
DF5 6.6 9 10.6 12.9 13.5 13.6 13.3 12.9 12 11.3 10.6 9.9 9.4 8.9 &
8.3 7.9 7.7 8 10 5 16.6 23.7 41.1 60 88 132 170 233 322 375 400 416 425 420 &
412 408 405 400 405 409 420 440 480 520 540 555 570 600 515 400 330 285 260 &
245 250 260
m3 7014 .781 8016 .212 7015 .007 $ air
M4 14000 -20.68 13027 -.363 8016 -50.853 20000 -21.645 12000 -.198 19000 -.088 &
11023 -.0384 16000 -.139 6000 -4.52 22000 -.0155 15031 -.0208 25055 -.0192 &
1001 -.701 26054 -.0418 26056 -.6588 26057 -.0157 26058 -.0024 24052 -.00057
mt2 poly.20t
stop F5 .001

```

File 2.IX.4

The simulation provides $H^*(10)/B = 2.708 \times 10^{-3} \text{ pSv.n}^{-1}$. Therefore, the actual value of the ambient dose equivalent rate is:

$$\dot{H}^*(10) = \left(\frac{H^*(10)}{B} \right) B = 3600 \times 2.708 \times 10^{-6} \times 10^{-3} \times 10^6 = 9.74 \mu\text{Sv.h}^{-1}$$

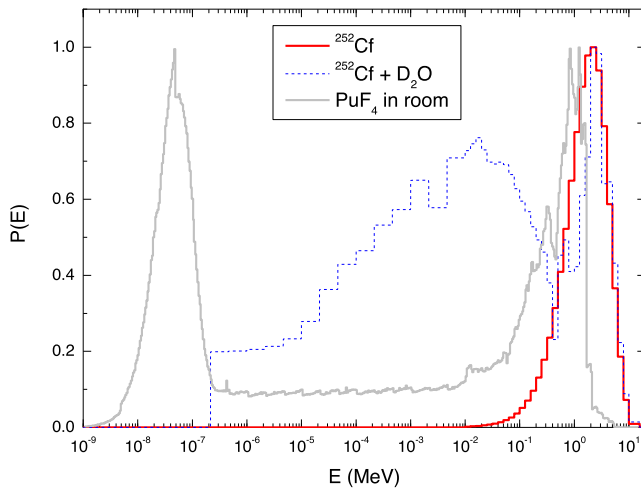


FIG. 2.IX.4 – ^{252}Cf , heavy-water moderated ^{252}Cf and PuF_4 spectra (from IAEA, 2001 data).

The deviation between the measurement with the Bonner sphere and the actual value of the ambient dose equivalent rate at this energy is about 43%. However, the IEC standard (1997), recommends an acceptability criterion of $\pm 30\%$ for the difference between the device measurement and the actual value of the operational quantity. Accordingly, the Bonner sphere calibration with a ^{252}Cf source would not allow the measurement of a typical workplace neutron spectrum emitted by a PuF_4 source.

Note: to carry out a workplace spectrum measurement of PuF_4 type, it would be more convenient to calibrate the Bonner sphere with a heavy-water moderated ^{252}Cf spectrum. The bare ^{252}Cf neutron spectrum is weakly populated in thermal and epithermal regions. When moderated with heavy water, these components are significant in the emission spectrum (see figure 2.IX.4). This enables to perform a calibration which is more representative of the typical workplace neutron spectra, in which thermal and epithermal neutrons are always present.

Chapter 3

Shielding and Activation Calculations for Several Types of Devices (Radioactive Sources, X-ray Generators, Accelerators...)

3.I Shielding Calculation for an AmBe Neutron Source

Abstract:

In this application, the thickness of a polyethylene shielding is determined to ensure a dose equivalent rate of $2 \mu\text{Sv/h}$ at 1 m of a 60 GBq AmBe source. The calculated thickness is derived from a semi-empirical model and checked by a numerical simulation.

Objectives:

- Semi-empirical and numerical calculations of a shielding for a neutron source.
- Use of neutron transmission coefficient.
- Neutron spectrum implementation in MCNP.
- Numerical calculation of dose equivalents for a mixed particle field composed of neutrons and photons.

This application deals with the concept of “dose equivalent index”, a semi-empirical tool useful in neutron source shielding calculations. Using a short number of operations, the latter enables to quickly calculate a shielding thickness. It takes into account the radiological impact of both neutrons and photons for a mixed field.

Part 1: Semi-Empirical Calculation of the Shielding

Behind a shielding, the ambient dose equivalent rate due to neutrons, $\dot{H}^*(10)_d$, is expressed as a function of the fluence rate $\dot{\Phi}$, the “fluence – ambient dose equivalent” conversion coefficient, and the transmission factor $T(\Sigma x, E)$.

$$\dot{H}^*(10)_d = \dot{\Phi} h_{\Phi}^*(10) T(\Sigma x, E) \tag{1}$$

Calculations must involve the primary neutron field but also secondary radiations arising from multiple nuclear reactions in the shielding. Special attention should be paid to the contribution of high-energy gamma emerging from radiative captures. The dose equivalent index, denoted $I(\Sigma x, E)$, is commonly used for neutrons. This index is obtained by multiplying the “fluence – ambient dose equivalent” conversion coefficient by the transmission factor (*cf.* Antoni and Bourgois, 2017a). It enables to assess directly the shielding thickness complying with the targeted external exposure limit, only from the neutron fluence of the primary field (or flux for an isotropic source). Thus, for an isotropic source emitting a neutron flux \dot{N}_n , expression (1) becomes:

$$I(\Sigma x, E) = h_{\Phi}^*(10) T(\Sigma x, E) \iff \dot{H}^*(10)_d = \dot{\Phi} I(\Sigma x, E) = \left(\frac{\dot{N}_n}{4\pi d^2} \right) I(\Sigma x, E) \tag{2}$$

For an Am-Be source, this index is obtained from figure 3.I.1 (from Antoni and Bourgois, 2017a). The AmBe source specific yield is $Y_n = 6.6 \times 10^{-5} \text{ (n).s}^{-1}.\text{Bq}^{-1}$ from Antoni and Bourgois (2017a). Thus, for a 60 GBq activity, the matching neutron flux is:

$$\dot{N}_n = A Y_n = 60 \times 10^9 \times 6.6 \times 10^{-5} = 4 \times 10^6 \text{ (n).s}^{-1}$$

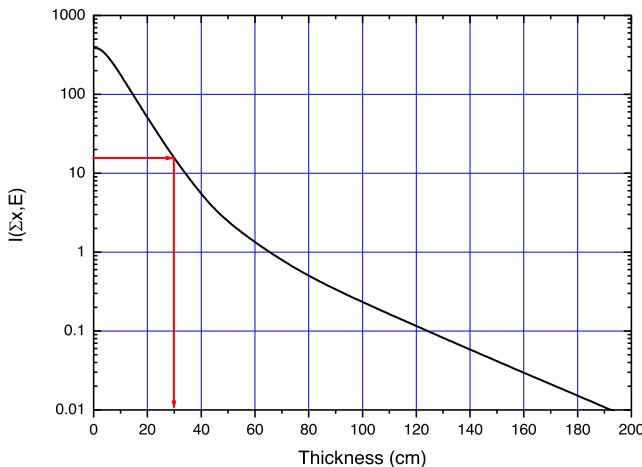


FIG. 3.I.1 – Transmission coefficient as a function of polyethylene thickness for an AmBe source (data from Antoni and Bourgois, 2017a).

The dose equivalent index is then expressed *versus* the terms of expression (2):

$$\dot{H}^*(10)_d = \left(\frac{\dot{N}_n}{4\pi d^2} \right) I(\Sigma x, E) \iff I(\Sigma x, E) = \left[\dot{H}^*(10) \right]_d \left(\frac{4\pi d^2}{\dot{N}_n} \right)$$

For the case study, the calculation leads to:

$$I(\Sigma x, E) = \left(\frac{2 \times 10^{-6}}{3600} \right) \times \left(\frac{4\pi \times 100^2}{4 \times 10^6} \right) = 1.74 \times 10^{-11} \text{ Sv.cm}^2 \text{ (17.4 pSv.cm}^2\text{)}$$

As seen in figure 3.I.1, a dose equivalent index of 17.4 pSv.cm² matches a shielding of 30 cm polyethylene thickness. This shielding ensures a dose equivalent rate of 2 μSv.h⁻¹ at 1 m from a 60 GBq Am-Be source.

In the next part, the modeling consists in evaluating the neutron and photon contributions of the ambient dose equivalent rate behind 30 cm of polyethylene.

Part 2: Numerical Solving with MCNP

The modeling of the scene requires the implementation of the neutron emission spectrum of the AmBe source. In the provided file, the spectrum is stated by means of a histogram of values with the “si1 h” card (energies histogram boundaries) coupled with the “sp1” card (emission probability for each energy bin). The spectrum is derived from Antoni and Bourgois (2017a). The assessment of the ambient dose equivalent rate is achieved according to the same procedure as in the previous application. The calculation is performed with a fluence point detector tally, *i.e.*, a type 5 tally, which evaluates the mean fluence for each energy bin defined in the “de15” card. Each result is afterwards weighted by the “fluence – ambient dose equivalent” conversion coefficient specified for each energy bin in the “df15” card. The sum over all energy bins provides the result of the ambient dose equivalent per source particle. In the proposed MCNP input file, the F5 tally assesses $(H_n^*(10)/N_n)$, while the F15 tally provides the same quantity for secondary photons: $(H_\gamma^*(10)/N_n)$.

Note the use of the specific “mt2 poly.20t” card. This card allows to use special data libraries, so-called $S(\alpha,\beta)$, which encompass a special thermal scattering treatment. For low energy neutrons, the default free gas model for scattering cross sections is not always well suited. Molecular effects or crystalline structure effects can affect the neutron scattering cross sections. These effects are included in the $S(\alpha,\beta)$ thermal neutron scattering (S stands for scattering, α is a momentum transfer variable and β is an energy transfer variable). For comparison, the black line of figure 3.I.2 states the total cross section of inelastic reactions on ¹²C as a pure chemical element, whereas the blue line refers to the same component in graphite form, specified *via* the $S(\alpha,\beta)$ library “grph.01t” instruction in the input file.

When considering only the cross section represented by the black curve, resonance peaks of blue and red curves between 0.01 and 0.1 eV are not taken into

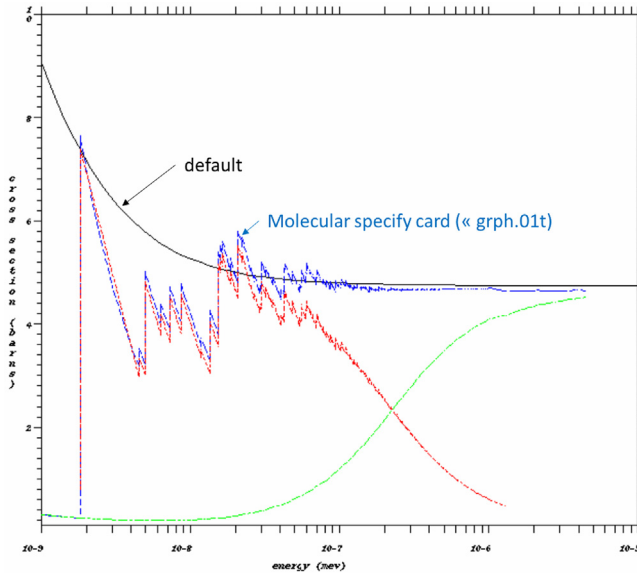


FIG. 3.I.2 – Cross sections of neutron inelastic reactions on ^{12}C : default and with the molecular specificity card “grph.01t”.

consideration. Thus, not calling in the molecular specificity card may cause an undervaluation of low energy absorptions. The input file 3.I.1 is used to simulate the case study:

```

Ambient equivalent dose for AmBe with 30 cm of polyethylene CH2
c cell block
10 1 -1.3e-3 -10 15 $ air calculation cells
15 2 -.92 -15 $ CH2
20 0 10 $ no transport outside

10 SO 300 $ Calculation in a sphere of radius R=300cm centered at origin
15 RPP -100 100 -100 100 1 31 $ CH2 slab S=200x200 30 cm thickness

imp:n,p 1 1 0 $ neutron, photon transport only in cells 10 and 15
M1 7014 .781 8016 .212 7015 .007 $ air
M2 1001 2 6012 1 $ (CH2)n
MT2 poly.20t $ THERMAL NEUTRON SCATTERING Hydrogen in Polyethylene
mode p n $ transport of neutrons and photons resulting of interactions
SDEF pos 0 0 0 par=n erg=d1
c AmBe spectrum energies
sil h 4.140E-07 1.100E-01 3.300E-01 5.400E-01 7.500E-01 9.700E-01

```

```

1.180E+00 1.400E+00 1.610E+00 1.820E+00 2.040E+00 2.250E+00
2.470E+00 2.680E+00 2.900E+00 3.110E+00 3.320E+00 3.540E+00
3.750E+00 3.970E+00 4.180E+00 4.390E+00 4.610E+00 4.820E+00
5.040E+00 5.250E+00 5.470E+00 5.680E+00 5.890E+00 6.110E+00
6.320E+00 6.540E+00 6.750E+00 6.960E+00 7.180E+00 7.390E+00
7.610E+00 7.820E+00 8.030E+00 8.250E+00 8.460E+00 8.680E+00
8.890E+00 9.110E+00 9.320E+00 9.530E+00 9.750E+00 9.960E+00
1.018E+01 1.039E+01 1.060E+01 1.082E+01 1.100E+01
c AmBe spectrum intensities
spl d 0.00 1.44E-02 3.34E-02 3.13E-02 2.81E-02 2.50E-02
2.14E-02 1.98E-02 1.75E-02 1.92E-02 2.23E-02 2.15E-02
2.25E-02 2.28E-02 2.95E-02 3.56E-02 3.69E-02 3.46E-02
3.07E-02 3.00E-02 2.69E-02 2.86E-02 3.18E-02 3.07E-02
3.33E-02 3.04E-02 2.74E-02 2.33E-02 2.06E-02 1.82E-02
1.77E-02 2.04E-02 1.83E-02 1.63E-02 1.67E-02 1.68E-02
1.88E-02 1.84E-02 1.69E-02 1.44E-02 9.68E-03 6.52E-03
4.26E-03 3.67E-03 3.81E-03 5.06E-03 6.25E-03 5.52E-03
4.68E-03 3.70E-03 2.78E-03 1.51E-03 3.63E-04
F5:n 0 0 100 .1 $ neutron fluence at 100 cm (z axis)
F15:p 0 0 100 .1 $ photon fluence at 100 cm (z axis)
c xxxxxxxxxxxxxxxxxxxxxxxxxxxxxxxxxxxxxxxxxxxxxxxxxxxxxxxxxxxxxxxxxxxxxxxxxxxxxxxxxxxxxxxxxxxxxxxxxxxxxxxxxxxxxxxxxxx
C H*(10)/phi psv.cm2 coefficient for neutrons DE energy DF conversion factor
DE5 1e-9 1e-8 2.53e-8 1e-7 2e-7 5e-7 1e-6 2e-6 5e-6 1e-5 2e-5 5e-5 1e-4 2e-4 &
5e-4 1e-3 2e-3 5e-3 1e-2 2e-2 3e-2 5e-2 7e-2 .1 .15 .2 .3 .5 .7 .9 1 1.2 2 &
3 4 5 6 7 8 9 10 12 14 15 16 18 20 30 50 75 100 125 150 175 201
DF5 6.6 9 10.6 12.9 13.5 13.6 13.3 12.9 12 11.3 10.6 9.9 9.4 8.9 &
8.3 7.9 7.7 8 10.5 16.6 23.7 41.1 60 88 132 170 233 322 375 400 416 425 420 &
412 408 405 400 405 409 420 440 480 520 540 555 570 600 515 400 330 285 260 &
245 250 260
c xxxxxxxxxxxxxxxxxxxxxxxxxxxxxxxxxxxxxxxxxxxxxxxxxxxxxxxxxxxxxxxxxxxxxxxxxxxxxxxxxxxxxxxxxxxxxxxxxxxxxxxxxxxxxxxxxxx
C H*(10)/phi psv.cm2 coefficient for photons
DE15 0.01 0.015 0.02 0.03 0.04 0.05 0.06 0.08 0.1 0.15 0.2 0.3 0.4 &
0.5 0.6 0.8 1 1.5 2 3 4 5 6 8 10
DF15 7.2 3.19 1.81 0.9 0.62 0.5 0.47 0.49 0.58 0.85 1.15 1.8 2.38 &
2.93 3.44 4.38 5.2 6.9 8.6 11.1 13.4 15.5 17.6 21.6 25.6
stop F5 .02

```

File 3.I.1

Tallies 5 and 15 results are stated under the “mean” label in the output file:

		tally 5			tally 15					
nps	mean	error	vov	slope	fom	mean	error	vov	slope	fom
304000	1.1594E-04	0.0198	0.0028	10.0	523	1.6263E-05	0.0063	0.0003	8.9	5092

The total dose equivalent, related to neutron and photon exposures is normalized to obtain the result in $\mu\text{Sv.h}^{-1}$. A 3.6×10^{-3} weighing factor is used to convert pSv.s^{-1} to $\mu\text{Sv.h}^{-1}$:

$$H_t^*(10) = 3.6 \times 10^{-3} \left[\left(\frac{H_\gamma^*(10)}{N_n} \right) + \left(\frac{H_n^*(10)}{N_n} \right) \right] \dot{N}_n$$

Finally, we get:

$$H^*(10) = 3.6 \times 10^{-3} \times (1.1594 \times 10^{-4} + 1.6263 \times 10^{-5}) \times 4 \times 10^6 = 1.9 \mu\text{Sv.h}^{-1}$$

This result is consistent with an ambient dose equivalent rate not exceeding $2 \mu\text{Sv.h}^{-1}$ to design the facility.

3.II Calculation of a ^{60}Co Photon Source Ambient Dose Equivalent Rate Behind a 4 m Water Shielding

Abstract:

In this problem, the ambient dose equivalent rate of a ^{60}Co photon source of 20 TBq is assessed behind a 4 m water shielding. The distance between the source and the calculation point is 4.2 m.

Objectives:

- Semi-empirical calculation of a shielding thickness for a ^{60}Co source.
- Use of the build-up factor for photons.
- Numerical calculation of a very thick shielding.
- Use of a variance reduction technique for numerical calculations.

Semi-empirical calculations of shielding often rely on conservative assumptions owing to the infinite height of the shielding to model the build-up factor. As a consequence, the resulting factor can give rise to an overestimation of operational quantities. The present work highlights build-up factor discrepancies observed between the accurate value obtained with Monte-Carlo simulation and the one used for the semi-empirical method.

Part 1: Semi-Empirical Calculation

For an isotropic source of photons, the ambient dose equivalent rate behind a shielding can be expressed as a function of \dot{H}_0^* , the ambient dose equivalent rate at 1 m from the unshielded source, according to the below expression:

$$\dot{H}^*(10) = \frac{\dot{H}_0^*}{d^2} B(\mu x, E) \exp\left(-\left(\frac{\mu}{\rho}\right) \rho x\right)$$

where d is the distance from the source to the observer (in m), x is the shielding thickness (in cm), ρ its density (in $\text{g}\cdot\text{cm}^{-3}$) and (μ/ρ) its mass attenuation coefficient (in $\text{cm}^2\cdot\text{g}^{-1}$). For a ^{60}Co point source, the ambient equivalent dose rate \dot{H}_0^* is $351 \mu\text{Sv}\cdot\text{h}^{-1}\cdot\text{GBq}^{-1}$ (refer to Antoni and Bourgois, 2017a). For a 20 TBq source, it becomes:

$$\dot{H}_0^* = 351 \times 2 \times 10^4 = 7.10^6 \mu\text{Sv}\cdot\text{h}^{-1}$$

Without a Monte-Carlo assessment, the build-up factor $B(\mu x, E)$ can only be approximated by an empirical formula. For instance, Berger’s formula holds for this factor:

$$B(\mu x, E) = 1 + a\mu x \exp(b\mu x)$$

Parameters a and b are accessible for water in figure 3.II.1. Mass attenuation coefficients (μ/ρ) are drawn from the NIST website (<https://physics.nist.gov/PhysRefData/XrayMassCoef/tab4.html>). ^{60}Co emits two photons of 1.17 and 1.33 MeV with a 100% emission intensity for each of them. Given the closeness of both energy values, a single energy of 1.25 MeV with a 200% emission intensity holds for the problem. For 1.25 MeV photons in water, the NIST website provides a mass attenuation value $\mu/\rho = 6.323 \times 10^{-2} \text{cm}^2\text{g}^{-1}$. For a 400 cm thickness of water, the number of mean free paths, which corresponds to the average number of interactions of the photon throughout the path, is:

$$\mu x = \left(\frac{\mu}{\rho}\right) \rho x = 6.323 \times 10^{-2} \times 1 \times 400 = 25$$

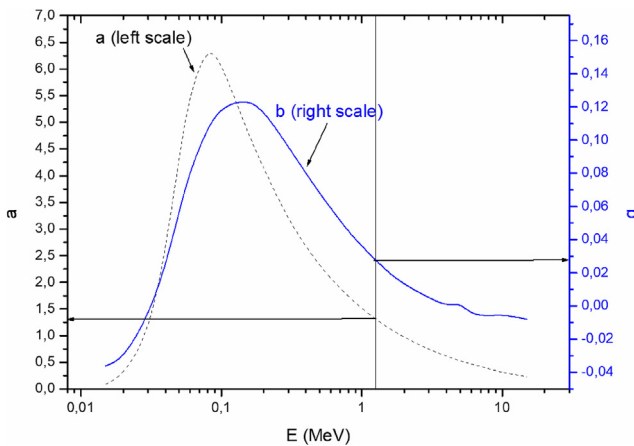


FIG. 3.II.1 – Berger’s parameters a and b as a function of energy for the build-up factor calculation in water.

Berger parameters read on figure 3.II.1 at 1.25 MeV are $a = 1.32$ and $b = 0.028$, which implies:

$$B(25, 1.25) = 1 + [1.32 \times 25 \exp(0.028 \times 25)] = 67$$

The build-up factor is greatly dependent on the shielding thickness, hence its broad value in this case: the thicker the shielding, the higher number of mean free paths and the greater the value of the build-up factor. For an observer located at 4.2 m from the shielded source, the ambient dose equivalent is:

$$\dot{H}^*(10) = \frac{7 \times 10^6}{4.2^2} \times 67 \times \exp(-25) = 3.7 \times 10^{-4} \mu\text{Sv.h}^{-1} (0.37 \text{ nSv.h}^{-1})$$

Although the semi-empirical method is easy to use, we must point out the conservative assumptions made, such as the infinite height of the shielding. This can lead to a large discrepancy with the actual value, especially in case of small lateral shielding. This deviation becomes even more substantial when the shielding is composed of miscellaneous materials with different densities. A better evaluation of the build-up factor, and consequently of the ambient dose equivalent, can be derived from a Monte-Carlo calculation. However, considering the thick water shielding of this application, the calculation can be prohibitive in terms of computing time. A further consequence is a risk for the tally to not reach statistical convergence. This issue entails the use of variance reduction techniques to improve the convergence and hence the computing time.

Part 2: First Numerical Approach with MCNP (Default Parameter in MCNP)

The radiological scene is modeled in the MCNP input file 3.II.1. The source coordinates are (0, 0, 0) and the observer is located at (0, 0, 420). A rectangular parallelepiped of dimensions $1000 \times 1000 \text{ cm}^2 \times 4 \text{ m}$ with the thickness perpendicular to the source-observer direction is simulated and a type 5 tally is used. As in the previous application, the ambient dose equivalent calculation derives from the fluence in different energy bins weighted by the “fluence – ambient dose equivalent” conversion coefficients.

```

Co-60 source with water shielding calculation
c cell block
10 1 -1.3e-3 -10      $ air cell
15 2 -1              -15    $ water cell
140 1 -1.3e-3 -200   $ air
200 0 10 15 200      $ outside

```

```

10 RPP -1000 1000 -1000 1000 -100 10 $ air
15 RPP -1000 1000 -1000 1000 10 410 $ water; surface=1000x1000 thickness=400 cm
200 RPP -1000 1000 -1000 1000 410 500 $ air

imp:p 1 1 1 0
M1 7014 .781 8016 .212 7015 .007 $ air
M2 1000 2 8000 1 $ water
mode p
SDEF pos 0 0 0 par=p erg=d1
SI1 L 1.17 1.33 $ 2 gamma-ray lines (MeV) of Co-60
SP1 1 1 $ Co-60 gamma rays relative intensities
F15:p 0 0 420 .1 $ photon fluence at 420 cm (z-axis)
C H* (10)/phi pSv.cm2 coefficient for photons
DE15 0.01 0.015 0.02 0.03 0.04 0.05 0.06 0.08 0.1 0.15 0.2 0.3 0.4 &
0.5 0.6 0.8 1 1.5 2 3 4 5 6 8 10
DF15 7.2 3.19 1.81 0.9 0.62 0.5 0.47 0.49 0.58 0.85 1.15 1.8 2.38 &
2.93 3.44 4.38 5.2 6.9 8.6 11.1 13.4 15.5 17.6 21.6 25.6
nps 6E9

```

File 3.II.1

The results in the output file are:

nps	mean	tally error	15 vov	slope	fom
5784574089	8.0698E-16	0.4047	0.5542	1.7	6.8E-04

For 5.8×10^9 particle histories, corresponding to a relatively high computing time of 150 h, the statistical error on the result is 40%. Since the acceptability for the error criterion of an F5 tally is roughly 5%, therefore, the result cannot be regarded as reliable. This observation is confirmed by the erratic behavior of the mean value, the statistical error and the variance of the variance (VOV) over computing time, *i.e.*, over the number of particle histories (see figure 3.II.2).

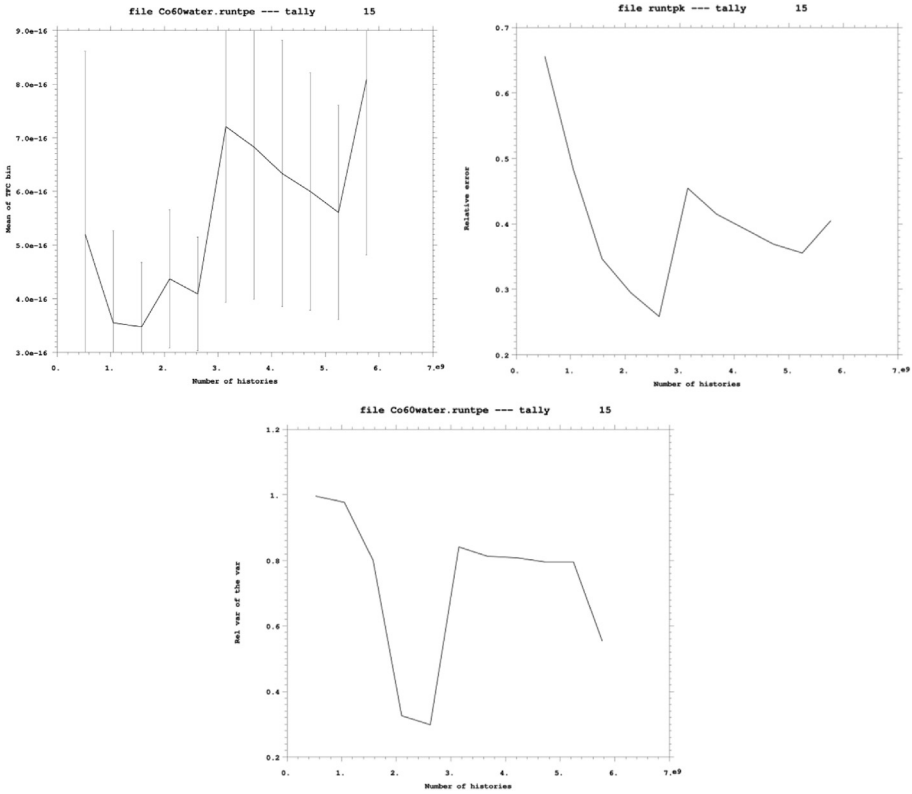


FIG. 3.II.2 – Evolution of the tally result, the relative error and the variance of the variance with the respect to the number of particle histories for the first MCNP input file.

Part 3: Second Numerical Solving with MCNP (Variance Reduction Technique)

At this stage, the weakness of the previous approach entails a variance reduction technique to obtain a statistically reliable value. In the case of thick shielding, the “Weight Windows Generator” card is greatly recommended. This generator is a quite simple statistical estimation of the mean score, so-called “importance”, for particles in the phase-space region. For applying the generator, a method consists in cutting out the shielding with a mesh grid composed of equal cells with small dimensions. In this application, the 4 m shielding is split into 25 slabs of 16 cm each. The “Weight Windows Generator” command is stated in the 3rd block by the use of the “wwg” card. The parameters to be set are the following:

- The first entry is the tally number of which we want to improve the convergence, in this tally “15”.
- The second entry is the number of the cell containing the photon source. In our model, the source is located in cell 10, so this parameter is “10”.
- The two first entries must be followed by the sequence “0 j j j j 0”.

In this way, a diagnosis will be carried out during the file execution in order to assign optimal statistical weight to each cell to improve tally 15 convergence when source particles are launched from cell 10. The diagnosis is produced by running the following input file 3.II.2.

```

Shielding for a Co-60 source
c cell block (Block 1)
10  1 -1.3e-3  -10  $ air cell
15  2      -1   -15  $   water
20  2      -1   -20  $   water
25  2      -1   -25  $   water
30  2      -1   -30  $   water
35  2      -1   -35  $   water
40  2      -1   -40  $   water
45  2      -1   -45  $   water
50  2      -1   -50  $   water
55  2      -1   -55  $   water
60  2      -1   -60  $   water
65  2      -1   -65  $   water
70  2      -1   -70  $   water
75  2      -1   -75  $   water
80  2      -1   -80  $   water
85  2      -1   -85  $   water
90  2      -1   -90  $   water
95  2      -1   -95  $   water
100 2      -1  -100  $   water
105 2      -1 -105  $   water
110 2      -1 -110  $   water
115 2      -1 -115  $   water
120 2      -1 -120  $   water
125 2      -1 -125  $   water
130 2      -1 -130  $   water
135 2      -1 -135  $   water
140 1 -1.3e-3 -200  $ air cell for calculation
200 0 10 15 20 25 30 35 40 45 50 55 60 65 70 75 80 85 90 95 100 105 &
110 115 120 125 130 135 200 $ outside

C geometry block (Block 2)
10  RPP      -1000    1000  -1000    1000  -100    10
15  RPP      -1000    1000  -1000    1000   10     26
20  RPP      -1000    1000  -1000    1000   26     42
25  RPP      -1000    1000  -1000    1000   42     58
30  RPP      -1000    1000  -1000    1000   58     74
35  RPP      -1000    1000  -1000    1000   74     90
40  RPP      -1000    1000  -1000    1000   90    106
45  RPP      -1000    1000  -1000    1000  106    122
50  RPP      -1000    1000  -1000    1000  122    138
55  RPP      -1000    1000  -1000    1000  138    154
60  RPP      -1000    1000  -1000    1000  154    170

```

```

65 RPP -1000 1000 -1000 1000 170 186
70 RPP -1000 1000 -1000 1000 186 202
75 RPP -1000 1000 -1000 1000 202 218
80 RPP -1000 1000 -1000 1000 218 234
85 RPP -1000 1000 -1000 1000 234 250
90 RPP -1000 1000 -1000 1000 250 266
95 RPP -1000 1000 -1000 1000 266 282
100 RPP -1000 1000 -1000 1000 282 298
105 RPP -1000 1000 -1000 1000 298 314
110 RPP -1000 1000 -1000 1000 314 330
115 RPP -1000 1000 -1000 1000 330 346
120 RPP -1000 1000 -1000 1000 346 362
125 RPP -1000 1000 -1000 1000 362 378
130 RPP -1000 1000 -1000 1000 378 394
135 RPP -1000 1000 -1000 1000 394 410
200 RPP -1000 1000 -1000 1000 410 500 $

C Block 3
imp:p 1 1 1 1 1 1 1 1 1 1 1 1 1 1 1 1 1 1 1 1 1 0
c weight windows generator
c WWG (tally number) (cell source) 0 j j j j j 0
WWG 15 10 0 j j j j 0
M1 7014 .781 8016 .212 7015 .007 $ air
M2 1000 2 8000 1
mode p
SDEF pos 0 0 0 par=p erg=d1
SI1 L 1.17 1.33 $ the 2 discrete energies (MeV) of Co-60
SP1 1 1 $ emission probability of each energy
F15:p 0 0 420 .1 $ photon fluence calculation at 300 cm (in z axis)
c xxxxxxxxxxxxxxxxxxxxxxxxxxxxxxxxxxxxxxxxxxxxxxxxxxxxxxxxxxxxxxxxxxxxxxx
c ICRP 74 H*(10)/phi psv.cm2 coefficient for photons
DE15 0.01 0.015 0.02 0.03 0.04 0.05 0.06 0.08 0.1 0.15 0.2 0.3 0.4 &
0.5 0.6 0.8 1 1.5 2 3 4 5 6 8 10
DF15 7.2 3.19 1.81 0.90.62 0.5 0.47 0.49 0.58 0.85 1.15 1.8 2.38 &
2.93 3.44 4.38 5.2 6.9 8.6 11.1 13.4 15.5 17.6 21.6 25.6
Ctme 5

```

File 3.II.2

At the end of an execution time of 5 min defined by the command “ctme 5”, a specific output file named “wwout” is created. For this case, this extra file is:

```

wwe:p 1.0000E+02
wnl:p 5.0000E-01 3.3108E-01 1.7703E-01 9.0161E-02 4.0648E-02
1.7258E-02 7.2003E-03 2.9740E-03 1.2316E-03 5.0556E-04
1.9262E-04 7.3564E-05 3.1546E-05 1.8956E-05 7.3541E-04

```


1photon activity in each cell										print table 126
cell	tracks entering	population	collisions	collisions *weight (per history)	number weighted energy	flux weighted energy	average track weight (relative)	average track mfp (cm)		
1	10	15664585	12828734	309514	2.3893E-02	1.0455E+00	1.0455E+00	9.8331E-01	1.2106E+04	
2	15	9440273	8009246	36258866	2.3912E+00	6.3712E-01	6.3712E-01	8.8250E-01	1.0669E+01	
3	20	7678375	8091835	43042315	1.4762E+00	3.4876E-01	3.4876E-01	4.4277E-01	8.0330E+00	
4	25	7176244	7817824	40966837	7.1415E-01	2.8134E-01	2.8134E-01	2.2310E-01	7.3675E+00	
5	30	7143668	7624563	39258231	3.0812E-01	2.5295E-01	2.5295E-01	1.0178E-01	7.0829E+00	
6	35	6243276	8245446	42707915	1.2589E-01	2.3840E-01	2.3840E-01	3.7506E-02	6.9376E+00	
7	40	6859949	7401009	37897908	5.0058E-02	2.2981E-01	2.2981E-01	1.7058E-02	6.8531E+00	
8	45	5790207	7707099	39845374	1.9626E-02	2.2404E-01	2.2404E-01	6.2592E-03	6.7964E+00	
9	50	6238483	6752209	34514326	7.6046E-03	2.2016E-01	2.2016E-01	2.8426E-03	6.7591E+00	
10	55	6174179	7752163	39626587	2.9255E-03	2.1722E-01	2.1722E-01	9.5143E-04	6.7308E+00	
11	60	5912529	7914175	40865577	1.1218E-03	2.1519E-01	2.1519E-01	3.4850E-04	6.7120E+00	
12	65	6297782	6846595	34956739	4.2879E-04	2.1346E-01	2.1346E-01	1.5812E-04	6.6954E+00	
13	70	6178368	7773304	39719633	1.6323E-04	2.1215E-01	2.1215E-01	5.2916E-05	6.6831E+00	
14	75	5880815	7878789	40682993	6.2110E-05	2.1099E-01	2.1099E-01	1.9374E-05	6.6715E+00	
15	80	6225358	6768965	34551676	2.3571E-05	2.1012E-01	2.1012E-01	8.7893E-06	6.6635E+00	
16	85	6073231	7644057	39089533	8.9320E-06	2.0936E-01	2.0936E-01	2.9417E-06	6.6565E+00	
17	90	5751168	7713121	39814237	3.3783E-06	2.0869E-01	2.0869E-01	1.0767E-06	6.6498E+00	
18	95	6063605	6598451	33666180	1.2766E-06	2.0831E-01	2.0831E-01	4.8849E-07	6.6463E+00	
19	100	5899534	7441192	38016384	4.8298E-07	2.0778E-01	2.0778E-01	1.6352E-07	6.6411E+00	
20	105	5587347	7500548	38698854	1.8234E-07	2.0744E-01	2.0744E-01	5.9783E-08	6.6379E+00	
21	110	5856884	6372913	32565580	6.8808E-08	2.0722E-01	2.0722E-01	2.7206E-08	6.6362E+00	
22	115	4782845	6413695	33092528	2.5955E-08	2.0693E-01	2.0693E-01	9.9530E-09	6.6331E+00	
23	120	5012627	5448105	27844449	9.7948E-09	2.0691E-01	2.0691E-01	4.5290E-09	6.6337E+00	
24	125	4078806	5471903	28266611	3.6933E-09	2.0683E-01	2.0683E-01	1.6585E-09	6.6332E+00	
25	130	4193971	4590344	23452310	1.3807E-09	2.0759E-01	2.0759E-01	7.5771E-10	6.6436E+00	
26	135	2048782	4038669	18441055	4.5352E-10	2.2245E-01	2.2245E-01	3.0665E-10	6.8260E+00	
27	140	299818	299789	7153	9.0151E-13	3.0921E-01	3.0921E-01	1.5690E-09	6.7062E+03	
total		164552709	188944743	898159365	5.1214E+00					

$$\begin{aligned}\dot{H}^*(10) &= 3600 \times 10^{-12} \times 10^9 \times A \Gamma \left(\frac{H^*}{N} \right) = 3.6 \times 20 \times 10^{12} \times 2 \times 2.24 \times 10^{-15} \\ &= 0.32 \text{ nSv.h}^{-1}\end{aligned}$$

The semi-empirical method provides a result 15% higher than that derived from the numerical simulation seen as reference value. This overestimation mainly stems in the infinite height of the shielding in the model of the build-up factor. This assumption causes a larger amount of Compton scatterings of photons in the shielding that arise dramatically the photon fluence at the observer point and consequently the operational quantity $H^*(10)$. However remember that without the use of the build-up factor, the result of the semi-empirical method would give a poor result: $0.0055 \text{ nSv.h}^{-1}$.

3.III Radiological Shielding for an X-ray Generator

Abstract:

The design of a radiological shielding for an X-ray generator is discussed in this problem. In the first part, a semi-empirical method is applied, and results are compared to a numerical approach in the second part.

Objectives:

- Semi-empirical calculation of a radiological shielding for an X-ray generator.
- Use of the transmission factor for an X-ray spectrum.
- Numerical simulation of an X-ray spectrum as a primary photon source.
- Application of a biasing technique to shielding calculations.

Main characteristics:

The X-ray device is operated with a 100 kV high-voltage and an intensity $i = 50 \mu\text{A}$. The accelerated electrons interact on a tungsten target with an anode angle of 45° . Filtration through 0.5 mm of aluminum is taken into account to cut the X-ray spectrum low-energy component. The field size of the X-ray beam is 400 cm^2 at 1 m. The radiation protection objective is to ensure an ambient dose equivalent limit of $0.5 \mu\text{Sv.h}^{-1}$ at 2 m from the target behind the shielding.

Part 1: Analytical Calculations

To calculate the ambient dose equivalent rate behind an X-ray shielding, the following formula depending on the transmission factor $T_m(x, E)$ for a material m can be used:

$$\dot{H}^*(10) = \left(\frac{\dot{H}_0^*(10)}{d^2} \right) T_m(x, E)$$

In this expression, the $\dot{H}^*(10)$ value is set according to the external exposure limit to comply with, *i.e.*, $0.5 \mu\text{Sv}\cdot\text{h}^{-1}$. The term \dot{H}_0^* is the ambient dose equivalent rate at 1 m from the unshielded source and d is the distance (in meters) between the source and the observer. Calculating the transmission factor according to expression (1) enables to determine the shielding thickness x .

$$T_m(x, E) = \frac{\dot{H}^*(10) d^2}{\dot{H}_0^*} \quad (1)$$

The source term used to design the facility with an X-ray device is the bremsstrahlung spectrum arising from the primary electrons interacting with the tungsten target (see figure 3.III.1). We can assume the absence of secondary neutrons produced through photonuclear reactions of which energy thresholds are generally higher than 5 MeV. For a 100 kV high voltage applied, the incident electrons on the tungsten target reach an energy of 100 keV. The bremsstrahlung spectrum extends from 0 to this end-point energy of 100 keV.

Few data, mostly based on Monte-Carlo calculations, allow to calculate the initial quantity $H_0^*(10)$. For instance, Antoni and Bourgois (2017a) propose H_0^* values for electron energies ranging over 50 to 900 kV and for different filtrations. The number of photons produced relies directly on the number of incident electrons. The latter is proportional to the generator intensity. Therefore, the ambient dose equivalent rate due to X-rays is proportional to the electron current of the generator. In the above-mentioned reference, for 100 kV and filtration through 0.5 mm of aluminum, the ambient dose equivalent rate at 1 m, as a function of the current intensity is $\dot{H}^*(10)/i = 19.4 \text{ mSv}\cdot\text{h}^{-1}\cdot\text{mA}^{-1}$ (Antoni and Bourgois, 2017a). At a $50 \mu\text{A}$ intensity at 1 m, we deduce:

$$\dot{H}_0^*(10) = 0.05 \times 19.4 \times 60 = 58.2 \text{ mSv}\cdot\text{h}^{-1}$$

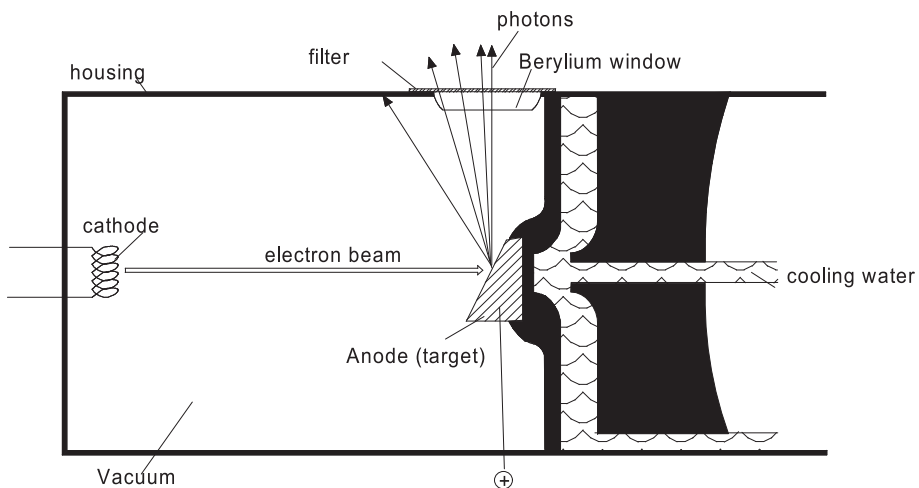


FIG. 3.III.1 – Layout of an X-ray generator, (from Antoni and Bourgois, 2017a).

In addition, those data provide the air kerma rate as a function of the primary electron intensity. Let us point out that this dosimetric quantity is widely used in the radiological field to characterize X-ray generator beams. In the same reference and for identical X-ray generator characteristics, the air kerma rate at 1 m, as a function of the current intensity is $\dot{K}_a(1)/i = 26 \text{ mGy}\cdot\text{h}^{-1}\cdot\text{mA}^{-1}$. Thus, for a $50 \mu\text{A}$ intensity at 1 m, we get:

$$\dot{K}_a(1) = 0.05 \times 26 \times 60 = 78 \text{ mGy}\cdot\text{h}^{-1}$$

The transmission factor can be calculated using the parametric equation developed by Archer *et al.* (1983). For a given couple of energy and material, this expression is a function of the thickness x and three parameters α , β and γ .

$$T_m(x, E) = \left[\left(1 + \frac{\beta}{\alpha} \right) \exp(\alpha\gamma x) - \left(\frac{\beta}{\alpha} \right) \right]^{-\frac{1}{\gamma}}$$

From the above equation, we get the shielding thickness x :

$$x = \frac{1}{\alpha\gamma} \ln \left[\frac{T_m(x, E)^{-\gamma} + \left(\frac{\beta}{\alpha} \right)}{1 + \left(\frac{\beta}{\alpha} \right)} \right] \quad (2)$$

Many publications report values for parameters α , β and γ . In particular, NCRP, 2005 provides transmission factors for medical generators with high voltages between 25 and 150 kV for different materials such as lead, concrete, steel, plaster and wood. More recently, Bourgois and Ménard (2018) calculated these transmission factors for high voltages ranging between 120 and 800 kV for lead and between 200 and 800 kV for concrete.

For a 100 kV high-voltage applied and a lead shielding, the corresponding parameters are: $\alpha = 2.5 \text{ mm}^{-1}$, $\beta = 15.28 \text{ mm}^{-1}$ and $\gamma = 0.7557$ (refer to NCRP, 2004 or Antoni and Bourgois, 2017a). The transmission factor complying with the limitation set can be calculated with equation (1) where $\dot{H}_0^*(10) = 58.2 \text{ mSv}\cdot\text{h}^{-1}$.

$$T_{\text{Pb}}(x, 100) = \frac{0.5 \times 10^{-6} \times 2^2}{58.2 \times 10^{-3}} = 3.5 \times 10^{-5}$$

The matching thickness obtained with expression (2) is:

$$x = \frac{1}{2.5 \times 0.7557} \ln \left[\frac{(3.5 \times 10^{-5})^{-0.7557} + \left(\frac{15.28}{2.5} \right)}{1 + \left(\frac{15.28}{2.5} \right)} \right] = 3 \text{ mm}$$

Thus, we can ensure, at most, an ambient dose equivalent rate of $0.5 \mu\text{Sv}\cdot\text{h}^{-1}$ at 2 m from the generator by interposing a 3 mm lead shielding.

Part 2: Numerical Solving

In this type of application, the simultaneous tracking of primary electrons and X-rays produced requires prohibitive computation times, particularly when high

Z and thick shieldings are involved. To overcome this limitation, we propose to break the calculation into two steps. In the first step, the bremsstrahlung spectrum is determined without shielding. Air kerma- and ambient dose equivalent-rates at 1 m from the target, without radiological protection, are also calculated. In the second step, the shielding is added and the ambient dose equivalent rate behind it is evaluated. In this case, the source term in the input file is the bremsstrahlung spectrum obtained in the previous step, and electrons are no longer transported.

- (a) Step 1: evaluations of the bremsstrahlung spectrum, the air kerma rate and the ambient dose equivalent rate at 1 m without shielding

The MCNP model geometry used in the first step is presented in figure 3.III.2. The housing is considered as completely opaque to secondary photons. Thus, the transport of these particles is disabled in this structural element. The housing is modeled with a zero importance for photons and electrons and described by cell 10 in the input file. Lateral dimensions of the aluminum filter are arbitrarily defined since only the spectrum component at 45° from the target is assessed. The electron beam is parallel and has a 0.3 cm section radius in the z direction (see figure 3.III.2).

The target, defined by the cell 1 in the input file, is a tungsten cylinder. It is modeled with a cylinder type enclosed surface preset in the MCNP code, known as RCC type macrobody. The definition of this surface is “ $rcc\ x_0\ y_0\ z_0\ a.\sin\theta\ a.\cos\theta\ r$ ”, where r is the radius, (x_0, y_0, z_0) are the coordinates of the cylinder base center, θ is the angle between the cylinder axis and the z direction and a is the cylinder height, matching the target thickness (see figure 3.III.2). The bremsstrahlung fluence spectrum is achieved using a point detector tally, *i.e.*, a type 5 tally, sorted into 100 energy bins of equidistant width ranging over 0–100 keV. This feature is handled by the card “E5 0 100i 0.1” associated with the F5 tally. The calculation point is located at 1 m from the target, on the y -axis (see figure 3.III.2). As for application 1.II, the ambient dose equivalent rate in each energy bin is likewise obtained by weighting the fluence spectrum by the “fluence – ambient dose equivalent” conversion coefficients from ICRP (1996). In the input file, this quantity is supported by tally 15. The air kerma assessment is derived from the same type of calculation, this time using the “fluence – ambient dose equivalent” conversion coefficients from ICRP (1996). Tally 25 calculates this quantity.

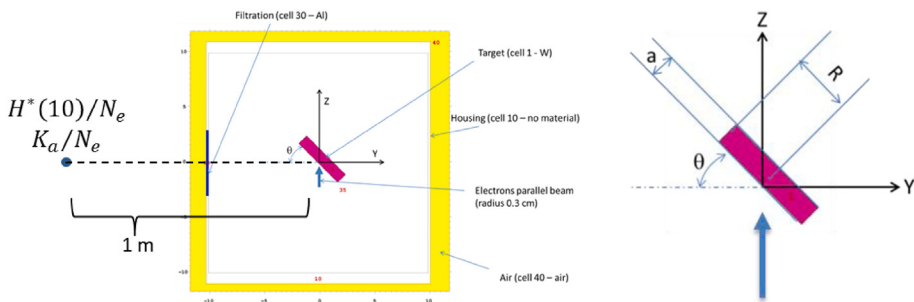


FIG. 3.III.2 – MCNP model used for step 1, without biological shielding.

```

X-ray generator
c ***** part 1 beam spectrum calculation ***
1 11 -19.3 -200 $ tungsten target
10 0 -220 210 #30 $ housing
30 13 -2.7 -220 210 -250 260 -270 280 -290 $ filtration through aluminum
35 0 -210 200 $ inside of X-ray generator
40 14 -1.293e-3 -91 220 $ air
9 0 91 $ outside

91 so 500
200 RCC 0 0 0 0 .707 .707 2.5
210 RCC 0 0 -10 0 0 20 10.
220 RCC 0 0 -11 0 0 22 10.05
250 PZ 3
260 PZ -3
270 PX 3
280 px -3
290 PY -8

imp:e 1 0 0 1 0 0
imp:p 1 0 1 1 1 0
mode p e
c source: electron parallel beam z direction
SDEF POS=0 0 -1 AXS=0 0 1 EXT=0 RAD=d1 PAR=e ERG=.1 &
VEC=0 0 1 DIR=1
SI1 0 .3
SP1 -21 1
m11 74000 1 $ W
m13 13000 1 $ filtration through aluminum
c Air - Density 0.00123 g/cm3
M14 006000 -0.000124 $ C
      007000 -0.755268 $ N
      008000 -0.231781 $ O
      018000 -0.012827 $ Ar
ctme 6000
F5:p 0 -100 0 .1 $ beam spectrum
C 100 intervals for the spectrum between 0 and 0.1 MeV
E5 0 100i .1
F15:p 0 -100 0 .1 $ equivalent dose at 1 m
c H*(10)/phi pSv.cm2 coefficient
DE15 .01 .015 .02 .03 .04 .05 .06 .08 .1 .15 .2 .3 .4 .5 .6 &
      .8 1 1.5 2 3 4 5 6 8 10
DF15 0.061 .83 1.05 .81 .64 .55 .51 .53 .61 .89 1.2 1.8 2.38 2.93 3.44 &
      4.38 5.2 6.9 8.6 11.1 13.4 15.5 17.6 21.6 25.6
F35:p 0 -100 0 .1 $ kerma at 1 m
c K/phi pSv.cm2 coefficient for photons
DE35 0.01 0.015 0.02 0.03 0.04 0.05 0.06 0.08 0.1 0.15 0.2 0.3 0.4 0.5 &
      0.6 0.8 1 1.5 2 3 4 5 6 8 10

```

DF35	7.43	3.12	1.68	0.721	0.429	0.323	0.289	0.307	0.371	0.599	0.856	&		
	1.38	1.89	2.38	2.84	3.69	4.47	6.14	7.55	9.96	12.1	14.1	16.1	20.1	24

File 3.III.1

The bremsstrahlung fluence spectrum is printed in the output file, in the same form as that described hereafter. The first column stands for the intervals upper energies in MeV, the second column gathers the photon fluence (X).cm² per primary beam electron, and the third column includes the tally statistical error.

tally type 5	particle flux at a point detector. units 1/cm**2	
detector located at x,y,z = 0.00000E+00-1.00000E+02 0.00000E+00		
energy		
0.00000E+00	0.00000E+00	0.0000
9.9010E-04	0.00000E+00	0.0000
1.9802E-03	0.00000E+00	0.0000
.		
.		
.		
9.6040E-02	5.82330E-11	0.0417
9.7030E-02	4.72500E-11	0.0454
9.8020E-02	3.00925E-11	0.0521
9.9010E-02	1.86723E-11	0.0670
1.0000E-01	7.56700E-12	0.0916
total	6.97931E-08	0.0015

Figure 3.III.3 displays the X-ray spectrum as a function of the photon energy.

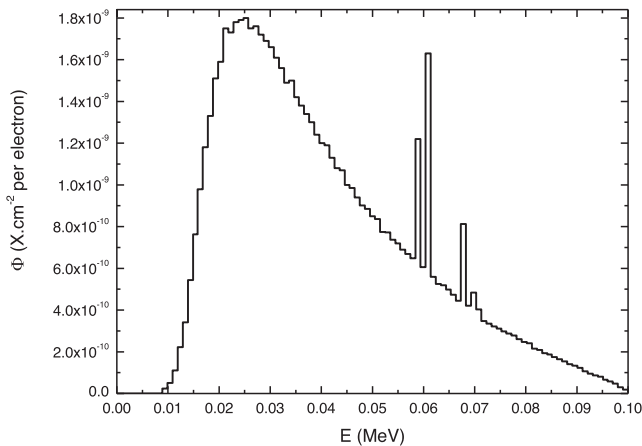


FIG. 3.III.3 – Bremsstrahlung spectrum obtained for 100 keV electrons impinging on a tungsten conversion target followed by a 0.5 mm aluminum screening.

One can note the presence of typical tungsten monoenergetic fluorescence rays in the bremsstrahlung spectrum. The tally results are printed at the end of the file:

nps	tally 5				fom	tally 15				fom	tally 35				fom
	mean	error	vov	slope		mean	error	vov	slope		mean	error	vov	slope	
8192000	7.0066E-08	0.0053	0.0464	2.0	689	4.9994E-08	0.0059	0.1006	2.1	354	6.1370E-08	0.0063	0.1765	1.9	513
93608108	6.9793E-08	0.0015	0.0182	2.8	740	4.9747E-08	0.0016	0.0564	2.8	636	6.1387E-08	0.0018	0.0940	2.6	507

Tally 15 provides the photon ambient dose equivalent in pSv per source electron: $H^*(10)/N_e = 4.9747 \times 10^{-8}$ pSv.(e) $^{-1}$. For 50 μ A, the matching electron flux is:

$$\dot{N}_e = \frac{i}{q} = \frac{50 \times 10^{-6}}{1.602 \times 10^{-19}} = 3.125 \times 10^{14} \text{ (e}^{-}\text{) s}^{-1}$$

Therefore, we deduce the ambient dose equivalent rate in mSv.h $^{-1}$ at 1 m from the target:

$$\begin{aligned} \dot{H}^*(10) &= 3600 \times 1000 \times 10^{-12} \dot{N}_e \left(\frac{H^*(10)}{N_e} \right) \\ &= 3.6 \times 10^{-6} \times 3.125 \times 10^{14} \times 4.97 \times 10^{-8} = 56 \text{ mSv.h}^{-1} \end{aligned}$$

Tally 35 gives the air kerma in pGy per source electron: $K_a/N_e = 6.14 \times 10^{-8}$ pGy.(e) $^{-1}$. Thus, the air kerma rate, in mGy.h $^{-1}$, at 1 m is:

$$\begin{aligned} \dot{K}_a &= 3600 \times 1000 \times 10^{-12} \dot{N}_e \left(\frac{K_a}{N_e} \right) = 3.6 \times 10^{-6} \times 3.125 \times 10^{14} \times 6.14 \times 10^{-8} \\ &= 69 \text{ mGy.h}^{-1} \end{aligned}$$

- (b) Step 2: determination of ambient equivalent dose rate and kerma, at 2 m from the target, behind the lead shielding

In the second step, two simulations are ran. It is first necessary to calculate a normalization coefficient allowing converting the ambient dose equivalent for a bremsstrahlung photon spectrum into the ambient dose equivalent that would be obtained for a 50 μ A intensity of primary electrons. The following file is used to reach this factor. The source is modeled as point-like source and isotropically emits the bremsstrahlung spectrum X, ($N_{E,X}$) drawn from the previous step. Tallies 5 and 15 provide, respectively, the ambient dose equivalent and the kerma per photon emitted by the new source, 2 m away from it.

```

c ***** X-ray generator transmission *****
c L. Bourgois 05 2016
1 0 -900
5 0 900

900 SO 500

imp:p 1 0
mode p
sdef pos=0 0 0 par=p erg=d2
c previously calculated spectrum (step 1)
# SI2 SP2
c 3456789012345678901234567890123456789012345678901234567890123456789
SI2 H 0.00E+00 9.90E-04 1.98E-03 2.97E-03 3.96E-03 4.95E-03 5.94E-03 &
6.93E-03 7.92E-03 8.91E-03 9.90E-03 1.09E-02 1.19E-02 1.29E-02 &
1.39E-02 1.49E-02 1.58E-02 1.68E-02 1.78E-02 1.88E-02 1.98E-02 &
2.08E-02 2.18E-02 2.28E-02 2.38E-02 2.48E-02 2.57E-02 2.67E-02 &
2.77E-02 2.87E-02 2.97E-02 3.07E-02 3.17E-02 3.27E-02 3.37E-02 &
3.47E-02 3.56E-02 3.66E-02 3.76E-02 3.86E-02 3.96E-02 4.06E-02 &
4.16E-02 4.26E-02 4.36E-02 4.46E-02 4.55E-02 4.65E-02 4.75E-02 &
4.85E-02 4.95E-02 5.05E-02 5.15E-02 5.25E-02 5.35E-02 5.45E-02 &
5.54E-02 5.64E-02 5.74E-02 5.84E-02 5.94E-02 6.04E-02 6.14E-02 &
6.24E-02 6.34E-02 6.44E-02 6.53E-02 6.63E-02 6.73E-02 6.83E-02 &
6.93E-02 7.03E-02 7.13E-02 7.23E-02 7.33E-02 7.43E-02 7.52E-02 &
7.62E-02 7.72E-02 7.82E-02 7.92E-02 8.02E-02 8.12E-02 8.22E-02 &
8.32E-02 8.42E-02 8.51E-02 8.61E-02 8.71E-02 8.81E-02 9.60E-02 &
9.70E-02 9.80E-02 9.90E-02 1.00E-01
SP2 D 0 0 0 0 1.40E-45 3.63E-31 2.25E-25 &
5.83E-15 4.69E-13 2.37E-11 5.04E-11 1.11E-10 2.22E-10 3.41E-10 &
5.44E-10 7.63E-10 9.79E-10 1.18E-09 1.33E-09 1.51E-09 1.59E-09 &
1.75E-09 1.73E-09 1.78E-09 1.79E-09 1.80E-09 1.75E-09 1.76E-09 &
1.72E-09 1.69E-09 1.66E-09 1.61E-09 1.56E-09 1.49E-09 1.50E-09 &
1.42E-09 1.38E-09 1.34E-09 1.30E-09 1.24E-09 1.20E-09 1.19E-09 &
1.13E-09 1.08E-09 1.07E-09 1.00E-09 9.85E-10 9.40E-10 9.01E-10 &
8.85E-10 8.50E-10 8.36E-10 7.74E-10 7.72E-10 7.37E-10 7.19E-10 &
6.90E-10 6.69E-10 6.48E-10 1.22E-09 6.06E-10 1.63E-09 5.59E-10 &
5.25E-10 5.19E-10 4.98E-10 4.73E-10 4.45E-10 8.12E-10 4.21E-10 &
4.84E-10 4.03E-10 3.47E-10 3.35E-10 3.22E-10 3.11E-10 2.98E-10 &
2.87E-10 2.78E-10 2.60E-10 2.47E-10 2.41E-10 2.15E-10 2.09E-10 &
1.93E-10 1.87E-10 1.75E-10 1.64E-10 1.54E-10 1.41E-10 1.33E-10 &
1.23E-10 1.06E-10 9.55E-11 8.66E-11 8.08E-11 6.59E-11 5.82E-11 &
4.73E-11 3.01E-11 1.87E-11 7.57E-12
stop F5 .001
F5:p 0 0 200 .1

```

```

c ICRP 1996 H*(10)/phi (pSv.cm2) conversion coefficient for photons
DE5 .01 .015 .02 .03 .04 .05 .06 .08 .1 .15 .2 .3 .4 .5 .6 &
.8 1 1.5 2 3 4 5 6 8 10
DF5 0.061 .83 1.05 .81 .64 .55 .51 .53 .61 .89 1.2 1.8 2.38 2.93 3.44 &
4.38 5.2 6.9 8.6 11.1 13.4 15.5 17.6 21.6 25.6
F15:p 0 0 200 .1
c K/phi (pSv.cm2) conversion coefficient for photons
DE15 .01 .015 .02 .03 .04 .05 .06 .08 .1 .15 .2 .3 .4 .5 .6 &
.8 1 1.5 2 3 4 5 6 8 10
DF15 7.6 3.21 1.73 0.739 0.438 0.328 0.292 0.308 0.372 0.6 0.856 &
1.38 1.89 2.38 2.84 3.69 4.47 6.12 7.51 9.89 12 13.9 15.8 19.5 23.2

```

File 3.III.2

The results for both estimators are printed as follows:

nps	mean	tally 5				tally 15				
		error	vov	slope	fom	mean	error	vov	slope	fom
68000	1.4172E-06	0.0010	0.0000	10.0	2.3E+08	1.8033E-06	0.0039	0.0002	10.0	1.5E+07

Tally 5 handles the ambient dose equivalent for an X-ray spectrum photon. Using the ambient dose equivalent rate $\dot{H}^*(10) = 56 \text{ mSv.h}^{-1}$ obtained in the previous step for an intensity of $50 \mu\text{A}$, the normalization coefficient for the ambient dose equivalent is:

$$f_H = \frac{56}{1.42 \times 10^{-6}} = 3.95 \times 10^7 \text{ mSv.h}^{-1}/\text{pSv}(\gamma)^{-1}$$

The air kerma is given by tally 15 for an X-ray spectrum photon. By employing the air kerma drawn from the previous step for an intensity of $50 \mu\text{A}$, the normalization coefficient for the air kerma is:

$$f_K = \frac{69}{1.80 \times 10^{-6}} = 3.83 \times 10^7 \text{ mGy.h}^{-1}/\text{pGy}(\gamma)^{-1}$$

The previous file provides the basis for the second calculation and the modeling of the 3 mm thickness of lead found with the analytical calculation is added. The shielding is divided into 25 successive $120 \mu\text{m}$ thick cells in order to apply the variance reduction technique using the spatial distribution of particle importances (“weight windows generator”) used previously in application 3.II. The source is the same as in the previous file, but is this time collimated by a circular aperture of 0.113 cm radius (refer to cell 5 in the file) in order to produce an X-ray emission cone irradiating a 400 cm^2 disk at 1 m. Tallies 5 and 15 are located at 2 m on the z -axis (see figure 3.III.4).

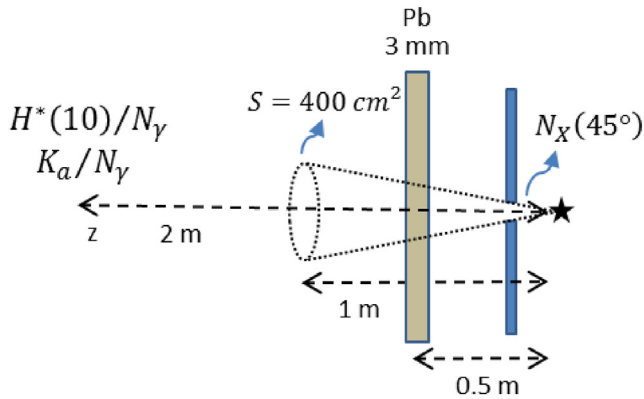


FIG. 3.III.4 – MCNP model for the final calculation of step 2 with the biological shielding.

The MCNP input file of the final calculation of the second step is given hereinafter.

```

c ***** calculation with 3 mm of lead *****
1 14 -1.293e-3 370 -110 -900 #5 imp:p=1
5 0 100 -104 101 -102 imp:p=0 $ cone emission (400 cm2 @ 1m)
10 1 -11.35 110 -120 -900 imp:p=1 $ lead
20 1 -11.35 120 -130 -900 imp:p=1 $ lead
30 1 -11.35 130 -140 -900 imp:p=1 $ lead
40 1 -11.35 140 -150 -900 imp:p=1 $ lead
50 1 -11.35 150 -160 -900 imp:p=1 $ lead
60 1 -11.35 160 -170 -900 imp:p=1 $ lead
70 1 -11.35 170 -180 -900 imp:p=1 $ lead
80 1 -11.35 180 -190 -900 imp:p=1 $ lead
90 1 -11.35 190 -200 -900 imp:p=1 $ lead
100 1 -11.35 200 -210 -900 imp:p=1 $ lead
110 1 -11.35 210 -220 -900 imp:p=1 $ lead
120 1 -11.35 220 -230 -900 imp:p=1 $ lead
130 1 -11.35 230 -240 -900 imp:p=1 $ lead
140 1 -11.35 240 -250 -900 imp:p=1 $ lead
150 1 -11.35 250 -260 -900 imp:p=1 $ lead
160 1 -11.35 260 -270 -900 imp:p=1 $ lead
170 1 -11.35 270 -280 -900 imp:p=1 $ lead
180 1 -11.35 280 -290 -900 imp:p=1 $ lead
190 1 -11.35 290 -300 -900 imp:p=1 $ lead
200 1 -11.35 300 -310 -900 imp:p=1 $ lead
210 1 -11.35 310 -320 -900 imp:p=1 $ lead
220 1 -11.35 320 -330 -900 imp:p=1 $ lead
230 1 -11.35 330 -340 -900 imp:p=1 $ lead
240 1 -11.35 340 -350 -900 imp:p=1 $ lead
250 1 -11.35 350 -360 -900 imp:p=1 $ lead

```

```

800 14 -1.293e-3 360 -400 -900 imp:p=1
999 0 -370:900:400          imp:p=0 $ outside

100 CZ .113
101 Pz 1
102 pz 1.0001
104 cz 500
110 PZ 50
120 PZ 50.012
130 pz 50.024
140 pz 50.036
150 pz 50.048
160 pz 50.06
170 pz 50.072
180 pz 50.084
190 pz 50.096
200 pz 50.108
210 pz 50.12
220 pz 50.132
230 pz 50.144
240 pz 50.156
250 pz 50.168
260 pz 50.18
270 pz 50.192
280 pz 50.204
290 pz 50.216
300 pz 50.228
310 pz 50.24
320 pz 50.252
330 pz 50.264
340 pz 50.276
350 pz 50.288
360 pz 50.3
370 pz -1
400 pz 500
900 cz 500

WWG 5 1 0 j j j j 0
stop F5 .02
mode p
sdef pos=0 0 0 par=p erg=d2
c SI2/SP2 X-ray spectrum calculated with the first MCNP file
SI2 H 0 9.90E-04 1.98E-03 2.97E-03 3.96E-03 4.95E-03 5.94E-03 &
6.93E-03 7.92E-03 8.91E-03 9.90E-03 1.09E-02 1.19E-02 1.29E-02 &
1.39E-02 1.49E-02 1.58E-02 1.68E-02 1.78E-02 1.88E-02 1.98E-02 &
2.08E-02 2.18E-02 2.28E-02 2.38E-02 2.48E-02 2.57E-02 2.67E-02 &
2.77E-02 2.87E-02 2.97E-02 3.07E-02 3.17E-02 3.27E-02 3.37E-02 &
3.47E-02 3.56E-02 3.66E-02 3.76E-02 3.86E-02 3.96E-02 4.06E-02 &
4.16E-02 4.26E-02 4.36E-02 4.46E-02 4.55E-02 4.65E-02 4.75E-02 &

```



```

4.85E-02 4.95E-02 5.05E-02 5.15E-02 5.25E-02 5.35E-02 5.45E-02 &
5.54E-02 5.64E-02 5.74E-02 5.84E-02 5.94E-02 6.04E-02 6.14E-02 &
6.24E-02 6.34E-02 6.44E-02 6.53E-02 6.63E-02 6.73E-02 6.83E-02 &
6.93E-02 7.03E-02 7.13E-02 7.23E-02 7.33E-02 7.43E-02 7.52E-02 &
7.62E-02 7.72E-02 7.82E-02 7.92E-02 8.02E-02 8.12E-02 8.22E-02 &
8.32E-02 8.42E-02 8.51E-02 8.61E-02 8.71E-02 8.81E-02 8.91E-02 &
9.01E-02 9.11E-02 9.21E-02 9.31E-02 9.41E-02 9.51E-02 9.60E-02 &
9.70E-02 9.80E-02 9.90E-02 1.00E-01
SP2 D 0 0 0.00E+00 0.00E+00 1.40E-45 3.63E-31 2.25E-25 &
5.83E-15 4.69E-13 2.37E-11 5.04E-11 1.11E-10 2.22E-10 3.41E-10 &
5.44E-10 7.63E-10 9.79E-10 1.18E-09 1.33E-09 1.51E-09 1.59E-09 &
1.75E-09 1.73E-09 1.78E-09 1.79E-09 1.80E-09 1.75E-09 1.76E-09 &
1.72E-09 1.69E-09 1.66E-09 1.61E-09 1.56E-09 1.49E-09 1.50E-09 &
1.42E-09 1.38E-09 1.34E-09 1.30E-09 1.24E-09 1.20E-09 1.19E-09 &
1.13E-09 1.08E-09 1.07E-09 1.00E-09 9.85E-10 9.40E-10 9.01E-10 &
8.85E-10 8.50E-10 8.36E-10 7.74E-10 7.72E-10 7.37E-10 7.19E-10 &
6.90E-10 6.69E-10 6.48E-10 1.22E-09 6.06E-10 1.63E-09 5.59E-10 &
5.25E-10 5.19E-10 4.98E-10 4.73E-10 4.45E-10 8.12E-10 4.21E-10 &
4.84E-10 4.03E-10 3.47E-10 3.35E-10 3.22E-10 3.11E-10 2.98E-10 &
2.87E-10 2.78E-10 2.60E-10 2.47E-10 2.41E-10 2.15E-10 2.09E-10 &
1.93E-10 1.87E-10 1.75E-10 1.64E-10 1.54E-10 1.41E-10 1.33E-10 &
1.23E-10 1.06E-10 9.55E-11 8.66E-11 8.08E-11 6.59E-11 5.82E-11 &
4.73E-11 3.01E-11 1.87E-11 7.57E-12
M1 82000 1 $ lead
M14 006000 -0.000124 $ C
007000 -0.755268 $ N
008000 -0.231781 $ O
018000 -0.012827 $ Ar
F5:p 0 0 200 .1
c H*(10)/phi (pSv.cm2) coefficient for photons
DE5 .01 .015 .02 .03 .04 .05 .06 .08 .1 .15 .2 .3 .4 .5 .6 &
.8 1 1.5 2 3 4 5 6 8 10
DF5 0.061 .83 1.05 .81 .64 .55 .51 .53 .61 .89 1.2 1.8 2.38 2.93 3.44 &
4.38 5.2 6.9 8.6 11.1 13.4 15.5 17.6 21.6 25.6
F15:p 0 0 200 .1
c K/phi (pSv.cm2) coefficient for photons
DE15 .01 .015 .02 .03 .04 .05 .06 .08 .1 .15 .2 .3 .4 .5 .6 &
.8 1 1.5 2 3 4 5 6 8 10
DF15 7.6 3.21 1.73 0.739 0.438 0.328 0.292 0.308 0.372 0.6 0.856 &
1.38 1.89 2.38 2.84 3.69 4.47 6.12 7.51 9.89 12 13.9 15.8 19.5 23.2
wwe:p 1.0000E+02
wnl:p 5.0000E-01 -1.0000E+00 8.7613E-03 1.9089E-03 9.7501E-04
5.7967E-04 3.7102E-04 2.4816E-04 1.7146E-04 1.2183E-04
8.8418E-05 6.5413E-05 4.9230E-05 3.7550E-05 2.9136E-05
2.2833E-05 1.8107E-05 1.4568E-05 1.1919E-05 9.9170E-06
8.4169E-06 7.2818E-06 6.5378E-06 6.1076E-06 6.0968E-06
7.0213E-06 1.0492E-05 0.0000E+00 -1.0000E+00

```

The ambient dose equivalent and air kerma results per emitted photon, with the lead shielding are the following:

nps	mean	tally error	5 vov	slope	fom	mean	tally error	15 vov	slope	fom
2953734	3.1079E-11	0.0141	0.0145	10.0	2809	1.8270E-11	0.0143	0.0147	10.0	2765

Final results for both these quantities are obtained by weighting the tally results by the normalization coefficients previously stated:

$$\dot{H}^*(10) = f_H \left(\frac{H^*(10)}{N_\gamma} \right) = 3.95 \times 10^7 \times 3.11 \times 10^{-11} = 1.2 \times 10^{-3} \text{ mSv.h}^{-1}$$

$$\dot{K}_a = f_K \left(\frac{K_a}{N_\gamma} \right) = 3.83 \times 10^7 \times 1.83 \times 10^{-11} = 7 \times 10^{-4} \text{ mGy.h}^{-1}$$

There is a deviation of more than a factor of 2 between the semi-empirical calculation ($0.5 \mu\text{Sv.h}^{-1}$) and the numerical calculation ($1.2 \mu\text{Sv.h}^{-1}$) for the ambient dose equivalent rate. This difference mainly stems in the assumptions made to reach the transmission factor. This factor is actually calculated for a given beam dimension and a certain filtration. The interest of Monte-Carlo calculation lies in the possibility to simulate fine structures of the radiological apparatus, notably the target/X-ray generator source set. Thus, it allows approaching realistic values of dosimetric quantities sought.

3.IV Evaluation of Ambient Dose Equivalent from Neutron Activation

Abstract:

The irradiation of a ^{59}Co sample with a monoenergetic neutron beam, resulting in the formation of ^{60}Co by activation is studied in this application. In a first part, the ^{60}Co activity is calculated analytically, as well as the resulting fluence and ambient dose equivalent rate at 1 m from the sample. In a second part, the same quantities are numerically evaluated and compared to that of the first part. The third part points out the possibility to assess fluence and dose equivalent rates for different irradiation scenarios and cooling steps, and therefore to perform the time profile of the external exposure.

Objectives:

- Analytical calculation of sample activation by neutrons, resulting fluence and ambient dose equivalent rates.
- Same as above with MCNP.
- MCNP calculations with the “act” activation card.
- Setting of an irradiation time profile with MCNP.
- Calculation of a prompt and delayed photon spectrum with MCNP during a continuous irradiation.
- Achievement of the time profile of the fluence rate for successive irradiation and cooling steps.

Main characteristics:

The ^{59}Co sample studied is a cylinder of 1 cm radius and 0.1 cm height. It is irradiated by a parallel beam of 1 MeV neutrons of cross section radius 1 cm, with a constant flux of 10^{10} n.s^{-1} . In this application, we only consider the formation of ^{60}Co through neutron radiative capture $^{59}\text{Co}(n,\gamma)^{60}\text{Co}$. The half-life of ^{60}Co is 5.27 years. The density of ^{59}Co is $\rho = 8.9 \text{ g.cm}^{-3}$.

Part 1: Induced Activity, Fluence and Ambient Equivalent Dose Rates for a 10 years Continuous Irradiation

A constant irradiation of the sample over 10 years is considered in this first part. The resulting ^{60}Co activity and associated fluence and ambient dose equivalent rates at 1 m from the sample are evaluated for cooling times of 1 and 5 years.

(a) Analytical calculation of the ^{60}Co activity

Let N_c be the number of ^{59}Co target nuclei irradiated by a neutron fluence rate $\dot{\Phi}_n$. The radiative capture cross section, $\sigma_{(n,\gamma)}$, leads to the production of a number N of ^{60}Co radioactive nuclei of decay constant λ . In the same time, ^{60}Co nuclei transmutation is likely to happen, through different absorption reactions of total cross section σ_t . If we assume the number of target nuclei to be constant over the irradiation time ($N_c = \text{constant}$), the formation of the N ^{60}Co nuclei can be described by the differential equation (1):

$$dN(t) = N_c \sigma_{(n,\gamma)} \dot{\Phi}_n dt - \lambda N(t) dt - \sigma_t \dot{\Phi}_n N(t) dt \quad (1)$$

The first right term stands for ^{60}Co production through neutron activation, the second term reflects the ^{60}Co nuclei transmutation into daughter nuclei while undergoing β decay and the third term features the ^{60}Co nuclei transmutation due to absorption reactions. It is worth noting that this equation is valid only if the decay chain of the daughter nucleus doesn't contain the target nuclei. The number of nuclei formed at the end of an irradiation time t_i is the solution of the above equation:

$$N(t_i) = \frac{N_c \sigma_{(n,\gamma)} \dot{\Phi}_n}{\lambda + \sigma_t \dot{\Phi}_n} [1 - \exp(-(\lambda + \sigma_t \dot{\Phi}_n) t_i)]$$

The transmutation reactions of the ^{60}Co have to be taken into account only for energies higher than 1 MeV (*e.g.*, the $(n,2n)$ reaction threshold is 8 MeV). As a consequence, the third term of equation (1) is equal to zero and the ^{60}Co residual activity at the end of irradiation can be described by:

$$A(t_i) = \lambda N(t_i) = N_c \sigma_{(n,\gamma)} \dot{\Phi}_n [1 - \exp(-\lambda t_i)]$$

The saturation activity corresponds to $t_i \rightarrow \infty$ and is defined by:

$$A_{\text{sat}} = N_c \sigma_{(n,\gamma)} \dot{\Phi}_n$$

The number of target nuclei N_c can be expressed as a function of the sample mass m . Thus, we derive from the previous expression:

$$A(t_i) = m \frac{\eta_A}{A} \sigma_{(n,\gamma)} \dot{\Phi}_n [1 - \exp(-\lambda t_i)]$$

The sample activity after a time t_d following the irradiation is:

$$A(t_i, t_d) = m \frac{\eta_A}{A} \sigma_{(n,\gamma)} \dot{\Phi}_n [1 - \exp(-\lambda t_i)] \exp(-\lambda t_d)$$

with η_A the Avogadro constant, $\eta_A = 6.02 \times 10^{23} \text{ mol}^{-1}$, $\sigma_{(n,\gamma)}$ the radiative capture cross section (data from the ENDF/B-VII.1 library, drawn from the website <http://www.nndc.bnl.gov/exfor/endlf02.jsp>). For 1 MeV neutrons, the cross section is equal to 6.44 mb. λ , the radioactive decay constant of ^{60}Co is $\lambda = \ln(2)/5.27 = 0.13 \text{ year}^{-1}$. m , the sample mass is:

$$m = \rho \pi r^2 h = 8.9 \times \pi \times 1^2 \times 0.1 = 2.79 \text{ g}$$

$\dot{\phi}_n$, the fluence rate at any point of the neutron parallel beam is (see section 1.I):

$$\dot{\phi}_n = \frac{\dot{N}_n}{\pi r^2} = \frac{10^{10}}{\pi \times 1^2} = 3.2 \times 10^9 \text{ (n) \cdot s}^{-1} \cdot \text{cm}^{-2}$$

For an irradiation time of 10 years and a cooling time of 1 year, the activity is:

$$A(10, 1) = 2.79 \times \frac{6.02 \times 10^{23}}{59} \times 0.00644 \times 10^{-24} \times 3.2 \times 10^9 \\ \times [1 - \exp(-0.13 \times 10)] \exp(-0.13 \times 1)$$

$$A(10, 1) = 3.74 \times 10^5 \text{ Bq (0.36 MBq)}$$

- (b) Analytical calculation of the fluence rate of ^{60}Co photons at 1 m from the sample

The gamma ray line emission probabilities are taken with a 2 digit precision in order to compare analytical and numerical models more closely: 99.98% for the

1.33 MeV line and 99.85% for the 1.17 MeV line (see <http://www.nucleide.org/Laraweb/>). We assume a point-like sample without self-attenuation effect for emitted gamma rays. The fluence rate of 1.33 MeV photons at 1 m from the sample for a cooling time of 1 year is:

$$\dot{\phi}_{1.33}(10, 1) = \frac{A(10, 1) \Gamma_{1.33}}{4\pi d^2} = \frac{3.74 \times 10^5 \times 0.9998}{4\pi \times 100^2} = 2.97 (\gamma) \text{ s}^{-1} \text{ cm}^{-2}$$

An analogous calculation for 1.17 MeV photons yields the same fluence rate. For a cooling time of 5 years, the fluence rates obtained for both 1.17 MeV and 1.33 MeV photons are $1.77 (\gamma) \cdot \text{s}^{-1} \cdot \text{cm}^{-2}$.

(c) Analytical calculation of the ambient equivalent dose rate at 1 m from the sample

The ^{60}Co ambient dose equivalent rate at 1 m against its activity is $\dot{H}_0^*(10)/A = 351 \mu\text{Sv} \cdot \text{h}^{-1} \cdot \text{GBq}^{-1}$ (refer to Antoni and Bourgois, 2017a). Thus, given the activity calculated previously, the ambient dose equivalent rate at 1 m is:

$$\begin{aligned} \dot{H}_0^*(10)_{1\text{year}} &= \left(\frac{\dot{H}_0^*(10)}{A} \right) A(10, 1) = 351 \times 3.74 \times 10^5 \times 10^{-9} \\ &= 0.131 \mu\text{Sv} \cdot \text{h}^{-1} \quad (131 \text{ nSv} \cdot \text{h}^{-1}) \end{aligned}$$

For the same irradiation time followed by 5 years of cooling, similar calculations provide a residual activity $A(10, 5) = 0.22 \text{ MBq}$ and an ambient dose equivalent rate at 1 m $\dot{H}_0^*(10)_{5\text{years}} = 78 \text{ nSv} \cdot \text{h}^{-1}$.

Part 2: Numerical Calculation of Fluences and Ambient Dose Equivalent Rates at 1 m from the Sample

MCNP offers the possibility to perform activation within the neutron transport run using the “act” card. In time mode, it enables the delayed gamma emission resulting from activation products created. Let us recall that in MCNP, the time unit is the “shake”, *i.e.*, 10^{-8} s. Therefore, an irradiation time of 10 years has to be transformed in the input file into $10 \times 365 \times 24 \times 3600 \times 1 \times 10^8 = 3.1536 \times 10^{16}$ shakes. Irradiation times are indicated with the “tme = d2” parameter in the source definition card (“sdef”). Parameter “d2” refers to the “si2 0 3.1536E + 16” instruction including the irradiation phase time. The different times at which the fluence- and dose equivalent- rates at 1 m are estimated are specified in the “t5” card associated with tally 5:

```
T5 0 3.46896E+16 3.47760E+16 4.7304E+16 4.73904E+16
```

It is important to mention that delayed gamma fluence cannot be calculated at a precise point in time. It is necessary to average this value over specific time windows. In the example above, these time periods are 10 days long (Δt_1 and Δt_2) and tally results are averaged over this duration. Thus, within the t5 “card”:

- The 2nd entry, 3.46896×10^{16} , corresponds to $T_{d1} = 11$ years, in shakes, *i.e.*, 10 years of irradiation and 1 year of cooling.
- The 3rd entry matches the 11 years above plus 10 days ($T_{d1} + \Delta t_1$).
- The 4th entry corresponds to $T_{d2} = 15$ years.
- The 5th entry represents 15 years plus 10 days ($T_{d2} + \Delta t_2$).

The fluence rates sought are those calculated in the second time interval (between 11 and 11 years plus 10 days, *i.e.*, Δt_1) and the fourth interval (ranging from 15 and 15 years plus 10 days, *i.e.*, Δt_2). A diagram representing the time pattern is available in figure 3.IV.1.

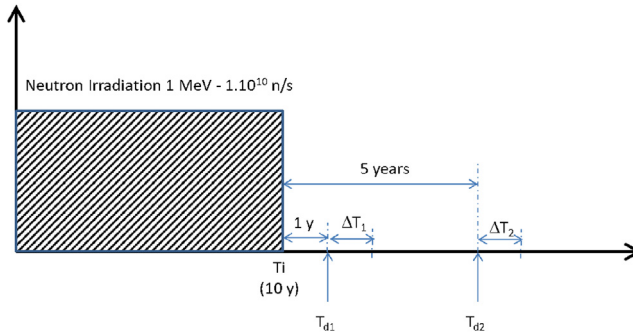


FIG. 3.IV.1 – Time diagram of irradiation, cooling phases and calculation time windows.

In the input file 3.IV.1, tallies 5 and 15 provide, respectively, the fluence and ambient dose equivalent per source neutron at 1 m from the sample, that is to say (Φ_γ/N_n) and ($H_0^*(10)/N_n$). In order to limit the output to ^{60}Co gamma ray lines, the “e5” energy card is added and set on an energy interval ranging from 1 to 1.5 MeV.

```

***** activation calculation *****
c cell block
10 1 -8.9 -10 $ Co-59 sample
20 0 10 -20 $ calculation cell
30 0 20 $ outsidet

c geometry block
10 RCC 0 0 0 0 0 .1 1 $ sample
20 RCC 0 0 -.5 0 0 150 16

imp:n 1 1 0
mode n p

```

```

m1 27059 1 $ Co-59
c ***** source definition *****
c parallel beam of 1 MeV neutrons, 1 cm radius, z direction
c 10 years irradiation in shakes
sdef par=n pos 0 0 -.10 axs 0 0 1 ext 0 rad=d1 vec 0 0 1 dir 1 erg 1 tme=D2
SI2 0 3.1536E+16 $ irradiation time
SP2 0 1
SI1 0 1 $ beam radius
SP1 -21 1
c ***** activation calculation ACT card *****
c FISSION= NONE => Create no delayed particles from fission events
c NONFISSION=p => Create delayed gamma from non-fission events
c DG=LINES => Sample delayed gamma using models based on
c           line-emission data.
ACT FISSION=none NONFISSION=p DG=LINES
c ***** F5: photon fluence at 1 meter from sample *****
F5:P 0 0 100 .5
c T5 time for the calculation results
c T5 0 T1 T1+DT1 T2 T2+DT1
T5 0 3.46896E+16 3.47760E+16 4.7304E+16 4.73904E+16
c E5 fluence calculation between 1 and 1.5 MeV interesting for Co-60
E5 1 100i 1.5
c ** F15 like F5 but equivalent dose conversion
c DE/DF coefficients
F15:P 0 0 100 .5
T15 3.46896E+16 3.47760E+16 4.7304E+16 4.73904E+16
c H*(10)/phi (pSv.cm2) conversion coefficient
DE15 .01 .015 .02 .03 .04 .05 .06 .08 .1 .15 .2 .3 .4 .5 .6 &
.8 1 1.5 2 3 4 5 6 8 10
DF15 0.061 .83 1.05 .81 .64 .55 .51 .53 .61 .89 1.2 1.8 2.38 2.93 3.44 &
4.38 5.2 6.9 8.6 11.1 13.4 15.5 17.6 21.6 25.6
ctme 100

```

File 3.IV.1

(a) Fluence rate at 1 m

Fluence values for delayed gamma rays between 1 and 1.5 MeV and for the different time windows set in the “t5” card for the calculation are available in the output file:

tally type 5	particle flux at a point detector.				units	1/cm**2
particle(s): photons						
detector located at x,y,z = 0.00000E+00 0.00000E+00 1.00000E+02						
time:	0.0000E+00	3.4690E+16	3.4776E+16	4.7304E+16	4.7390E+16	
energy						
1.1733E+00	0.00000E+00 0.0000	2.40949E-10 0.0002	8.20672E-13 0.0017	9.30016E-11 0.0003	4.87702E-13 0.0023	
1.3366E+00	0.00000E+00 0.0000	2.41483E-10 0.0002	8.26641E-13 0.0017	9.31877E-11 0.0002	4.88181E-13 0.0023	

The MCNP fluence for the two cooling phases of 10 days Δt_1 and Δt_2 and for both energy lines of ^{60}Co are given in table 3.IV.1.

Results have to be multiplied by a specific normalization coefficient \dot{N}'_n in neutrons per second. This factor is the ratio of the number of neutrons irradiating the sample (in other words the neutron flux multiplied by the irradiation time) to the time window duration (10 days for both intervals).

$$N'_n = \frac{\dot{N}_n t_i}{\Delta t_1} = \frac{\dot{N}_n t_i}{\Delta t_2} = \frac{1 \times 10^{10} \times 10 \times 365 \times 24 \times 3600}{10 \times 24 \times 3600} = 3.65 \times 10^{12} \text{ (n).s}^{-1} \quad (2)$$

For example, we can deduce the fluence for the first cooling phase Δt_1 and 1.17 MeV photons:

$$\dot{\phi}_{\Delta t_1} = N'_n \left(\frac{\Phi_\gamma}{N_n} \right)_{\Delta t_1} = 8.207 \times 10^{-13} \times 3.65 \times 10^{12} = 2.99 \text{ (}\gamma\text{).s}^{-1}\text{cm}^{-2}$$

The whole of fluence rates at 1 m for ^{60}Co gamma ray lines, for both time windows are summarized in table 3.IV.2, with analytical and numerical models.

One clearly infers a good agreement between both approaches.

(b) Ambient equivalent dose rate at 1 m

Ambient dose equivalent rate assessed by tally 15 for both time windows are:

detector located at x,y,z = 0.00000E+00 0.00000E+00 1.00000E+02							
time:	0.0000E+00	3.4690E+16	3.4776E+16	4.7304E+16	4.7390E+16		
	0.00000E+00 0.0000	1.63161E-08 0.0011	1.02965E-11 0.0013	1.16363E-09 0.0002	6.10044E-12 0.0016		

TAB. 3.IV.1 – MCNP fluence per source neutron for the two emission lines of ^{60}Co and both time windows.

^{60}Co energies	$\left(\frac{\Phi_\gamma}{N_n} \right)_{\Delta t_1}$	$\left(\frac{\Phi_\gamma}{N_n} \right)_{\Delta t_2}$
1.17	8.207×10^{-13}	4.877×10^{-13}
1.33	8.266×10^{-13}	4.882×10^{-13}

TAB. 3.IV.2 – Overview of the numerical and analytical results of the fluence rates for both ^{60}Co energies and both calculation time intervals.

^{60}Co energies	$\dot{\phi}_{\Delta t_1} \text{ (}\gamma\text{s}^{-1}\text{cm}^{-2}\text{)}$		$\dot{\phi}_{\Delta t_2} \text{ (}\gamma\text{s}^{-1}\text{cm}^{-2}\text{)}$	
	Numerical	Analytical	Numerical	Analytical
1.17	2.99	2.97	1.78	1.77
1.33	3.01	2.97	1.78	1.77

MCNP results are given in pSv.(n⁻¹) and have to be multiplied by the normalization factor previously described (2). For the first time window Δt_1 , after 1 year of cooling, the ambient dose equivalent rate is:

$$\begin{aligned}\dot{H}_0^*(10)_{\Delta t_1} &= N'_n \left(\frac{H_0^*(10)}{N_n} \right) = 3.65 \times 10^{12} \times 1.03 \times 10^{-11} \times 10^{-12} \\ &= 3.76 \times 10^{-11} \text{ Sv.s}^{-1}\end{aligned}$$

$$\Leftrightarrow \dot{H}_0^*(10)_{\Delta t_1} = 135 \text{ nSv.h}^{-1}$$

All ambient dose equivalent rate results at 1 m for both time windows for analytical and numerical methods are summarized in table 3.IV.3.

The deviation between the two methods is very small and mainly due to a slight change in the photon spectrum escaping the sample. This way, the mean “fluence – ambient dose equivalent” conversion coefficient undergoes a small change compared to that used in the section (b) of the first part.

TAB. 3.IV.3 – Overview of the numerical and analytical results of the ambient equivalent dose rates of ⁶⁰Co photons for both cooling times

$\dot{H}_0^*(10)_{\Delta t_1}$ (nSv.h ⁻¹)		$\dot{H}_0^*(10)_{\Delta t_2}$ (nSv.h ⁻¹)	
Numerical	Analytical	Numerical	Analytical
135	131	80	78

Part 3: Numerical Calculation of the Fluence Rate Profile for Successive Irradiation and Cooling Steps

It is possible to extend the MCNP method discussed above for fluence and dose equivalent rate calculations comprising multiple irradiation and cooling phases. In this part, we propose to calculate the fluence rate time profile at 1 m from the sample for three different irradiation phases interspersed with a cooling phase, as shown in figure 3.IV.2.

In the first place, we have to define the time parameters describing the different irradiation and cooling phases, to set them in the “sp” emission probability card of the source. To that end, ratio r_k of the number of neutrons irradiating the sample to the total number of neutrons is calculated for each irradiation phase. The total

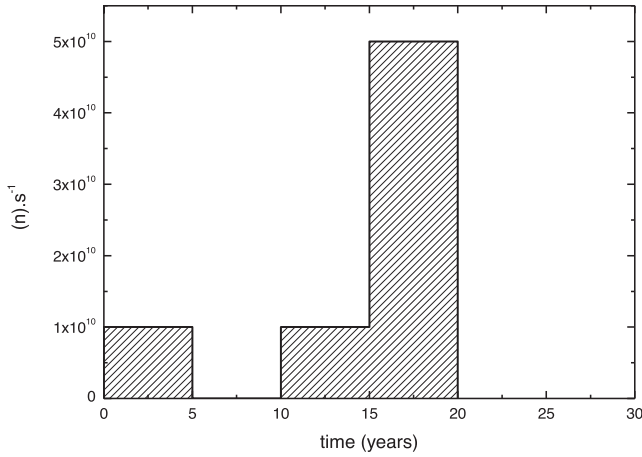


FIG. 3.IV.2 – Irradiation and cooling phases for the calculation in the 3rd part.

number of neutrons irradiating the sample can be described by the following formula:

$$N_t = c \sum_k (t_i)_k (\dot{N}_n)_k$$

Coefficient c is used for the time conversion from years to seconds and is equal to $3.1536 \times 10^7 \text{ s} \cdot (\text{year}^{-1})$. For the case study, we derive from the equation above:

$$\begin{aligned} N_t &= 3.1536 \times 10^7 \times [(5 \times 1 \times 10^{10}) + (5 \times 1 \times 10^{10}) + (5 \times 5 \times 10^{10})] \\ &= 3.1536 \times 10^7 \times 7 \times (5 \times 1 \times 10^{10}) = 1.103 \times 10^{19} \text{ (n)} \end{aligned}$$

For each irradiation phase k , the ratio r_k to parametrize in the “sp” card is:

$$r_k = \frac{c (t_i)_k (\dot{N}_n)_k}{N_t}$$

For the first irradiation phase, when factoring the N_t formula, we get the ratio:

$$r_1 = \frac{3.1536 \times 10^7 \times (5 \times 1 \times 10^{10})}{3.1536 \times 10^7 \times 7 \times (5 \times 1 \times 10^{10})} = \frac{1}{7} = 0.14$$

This calculation also leads to $1/7$ for r_2 and to $r_3 = 5/7 = 0.71$. The sum of the three ratios is necessarily equal to 1. Concerning the cooling phase from 5 to 10 years, the ratio is *de facto* equal to zero. These values are specified in the “sp2” card of the MCNP input file. The latter enables to provide the total photon fluence every $\Delta t = 0.5 \text{ year}$ (refer to the “t5” card parameters) in accordance with the irradiation and cooling time profile of figure 3.IV.2.

```

***** Activation with steps *****
c cell block
10 1 -8.9 -10 $ Co-59 sample
20 0 10 -20 $ photon fluence calculation cell
30 0 20 $ no transport outside

C geometry block
10 RCC 0 0 0 0 0 .1 1 $ sample
20 RCC 0 0 -.5 0 0 150 16

imp:n 1 1 0
mode n p
m1 27059 1 $ Co-59
c ***** source definition *****
c 1 MeV neutron parallel beam radius=1 cm z direction
c 10 years irradiation in shakes
sdef par=n pos 0 0 -.10 axs 0 0 1 ext 0 rad=d1 vec 0 0 1 dir 1 erg 1 tme=D2
c times 0 5 years 10 years 15 years 20 years
SI2 0 1.5768E+16 3.1536E+16 4.73E+16 6.31E+16
c the profile is 1/7 0 1/7 5/7
Sp2 0 .14 0 .14 .71
Si1 0 1
spl -21 1
ACT FISSION=none NONFISSION=p DG=LINES
F5:P 0 0 100 .5 $ fluence at 1 meter
c calculation each 0.5 year = 1.5768E15 shakes
T5 0 1.5768E+15 3.1536E+15 4.7304E+15 6.3072E+15 7.884E+15 9.4608E+15 &
1.10376E+16 1.26144E+16 1.41912E+16 1.5768E+16 1.73448E+16 1.89216E+16 &
2.04984E+16 2.20752E+16 2.3652E+16 2.52288E+16 2.68056E+16 2.83824E+16 &
2.99592E+16 3.1536E+16 3.31128E+16 3.46896E+16 3.62664E+16 3.78432E+16 &
3.942E+16 4.09968E+16 4.25736E+16 4.41504E+16 4.57272E+16 4.7304E+16 &
4.88808E+16 5.04576E+16 5.20344E+16 5.36112E+16 5.5188E+16 5.67648E+16 &
5.83416E+16 5.99184E+16 6.14952E+16 6.3072E+16 6.46488E+16 6.62256E+16 &
6.78024E+16 6.93792E+16 7.0956E+16 7.25328E+16 7.41096E+16 7.56864E+16 &
7.73E+16 7.88E+16 8.04E+16 8.20E+16 8.36E+16 8.51E+16 8.67E+16 8.83E+16 &
8.99E+16 9.15E+16 9.30E+16
1 100i 1.5
ctme 100

```

File 3.IV.2

A normalization coefficient N''_n corresponding to the ratio of the total number of neutrons irradiating the sample to the duration of the calculation time steps, *i.e.*, 0.5 year, has to be applied to the raw fluence results of the simulation:

$$N''_n = \frac{N_t}{\Delta t} = \frac{1.103 \times 10^{19}}{0.5 \times 365 \times 24 \times 3600} = 7 \times 10^{11} \text{ (n).s}^{-1}$$

The neutron flux as well as the photon fluence rate profile every 0.5 year for the global irradiation and cooling profile are plotted in figure 3.IV.3. We note that this profile accounts for delayed gamma rays resulting from ^{60}Co nuclei radioactive decay over time. Moreover, it takes into account, for a low fraction, prompt gamma rays originating from neutron interactions with ^{59}Co nuclei. This second component is besides equal to zero during cooling phases.

In the following input file, the fluence rate spectrum for the time window between 16.5 and 17 years is evaluated. This time interval is located at the middle of the third irradiation phase. “e5” and “t5” cards of the previous file have to be replaced by the instruction below:

```
T5 0 5.20344E+16 5.36112E+16 9.30E+16
E5 .1 500i 8
```

The “e5” line enables to calculate the fluence rate spectral distribution from 100 keV to 8 MeV for the chosen time window. This distribution is represented in figure 3.IV.4. We can notice the two ^{60}Co emission lines preceded by a Compton continuum up to approximately 1 MeV and an extremely low continuum due to prompt gamma rays up to 8 MeV.

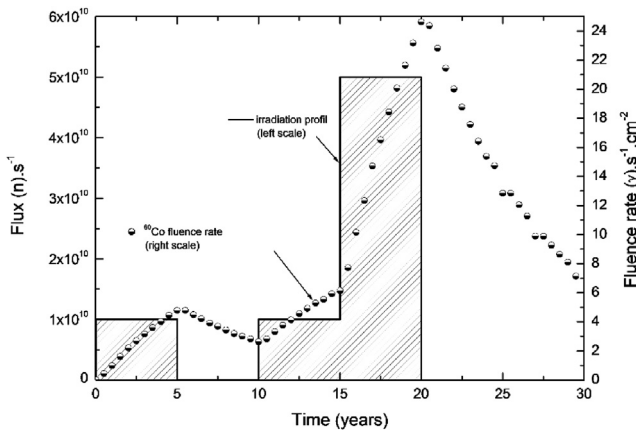


FIG. 3.IV.3 – Flux and fluence rate profiles at 1 m from the irradiated sample, with 0.5-year time steps.

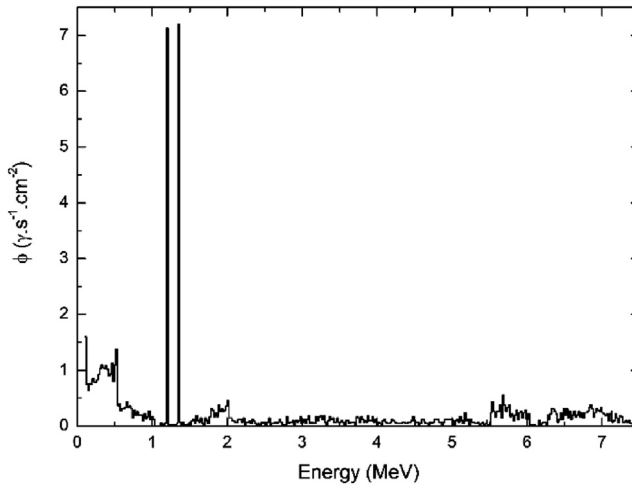


FIG. 3.IV.4 – Prompt and delayed photons fluence rate spectrum at 1 m from the irradiated sample, in the middle of the 3rd irradiation phase.

3.V Calculation of the Scattered Ambient Equivalent Dose Rate for an X-ray Generator Beam on a Water Phantom

Abstract:

In this application, the ambient equivalent dose rate resulting from the scattering of an X-ray generator beam on a water phantom is evaluated.

Objectives:

- Assess the ambient equivalent dose rate for an X-ray scattering field.
- MCNP and semi-empirical models of the scattered radiation and its related ambient dose equivalent.
- Variance reduction techniques with the use of the pseudo-particle and of the DXTRAN sphere.

Main characteristics:

The X-ray generator is operated under a 150 kV high voltage and a 1 mA intensity with a 3 mm aluminum filtration. The geometry used for the calculation is displayed in figure 3.V.1. The following characteristics are considered: $d_1 = 1$ m, $d_2 = 50$ cm and a $\theta = 45^\circ$ scattering angle of the beam on the phantom. The scattering object is a cylindrical water phantom of 10 cm radius and 40 cm height. The bremsstrahlung

beam area at the phantom surface is 200 cm^2 which corresponds to an 8 cm radius disk. We aim at assessing the scattered dose equivalent rate at the observer level.

Part 1: Semi-Empirical Calculation of the Ambient Equivalent Dose Rate Due to the Scattered Radiation

In order to evaluate the secondary beam ambient dose equivalent rate \dot{H}_{sec}^* (10) due to photon scattering on geometries like that presented in figure 3.V.1, some authors (Antoni and Bourgois, 2017a; NCRP, 2004) use the following equation derived from a semi-empirical model:

$$\dot{H}_{\text{sec}}^*(10) = \frac{\Gamma_R \alpha S}{d_1^2 d_2^2}$$

where Γ_R is the ambient dose equivalent rate due to the primary beam, at 1 m from the source, without phantom. Let d_1 be the shortest distance between the X-ray generator and the front face of the phantom (see figure 3.V.1). Thus, the ambient dose equivalent rate at the phantom surface due to the primary photon beam is given by Γ_R/d_1^2 , where d_2 is the distance between the center of the phantom and the observer. Both distances are given in meters. S is the beam area at the phantom

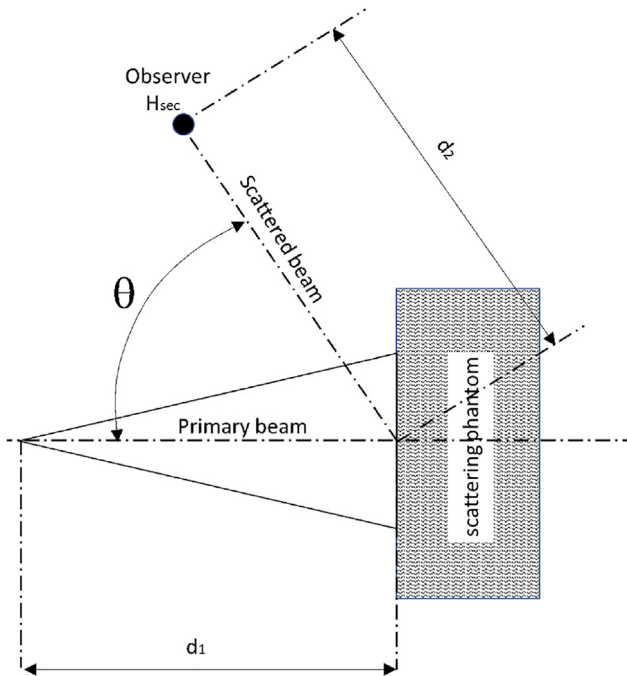


FIG. 3.V.1 – Calculation geometry.

surface and α is the scatter fraction. The product αS is dimensionless, hence α having the reciprocal dimensions of S . This equation is valid only for a sufficiently small beam area at the phantom surface with respect to distance d_2 , so the diffuse source can be regarded as a point with respect to the observer. The scatter fraction α depends on the scattering angle θ , the energy of the primary photon incident on the phantom and the material of the phantom. The values for the scatter fraction α are available in the literature (NCRP, 2005; Simpkin and Dixon, 1998; NCRP, 1976). In this application, we rely on the recent publication of Bourgois and Ménard (2017) gathering calculations for high voltages of X-ray generator ranging from 50 to 800 kV, with various filters, several phantom materials (water, TNT, concrete, iron) at different scattering angles. Figure 3.V.2a (data from Bourgois and Ménard, 2017) represents the scatter fraction α as a function of the scattering angle θ for a 150 kV X-ray generator with a 3 mm aluminum filtration. Figure 3.V.2b provides us with Γ_R values for high voltages ranging from 50 to 900 kV with a 3 mm aluminum filtration (data from Antoni and Bourgois, 2017a).

In the case study, we consider $= 5.64 \times 10^{-6} \text{cm}^{-2}$ (figure 3.V.2a) for a scattering angle of 45° and an ambient dose equivalent rate at 1 m $\Gamma_R = 22 \text{mSv} \cdot \text{min}^{-1} \text{mA}^{-1}$ (figure 3.V.2b). The secondary dose equivalent rate at the observer for a 200cm^2 beam area at the phantom surface and a 1 mA current intensity is given by:

$$\begin{aligned} \dot{H}_{\text{sec}}^*(10) &= \frac{\Gamma_R \alpha S}{d_1^2 d_2^2} = \frac{1 \times 22 \times 5.64 \times 10^{-6} \times 200}{1^2 \times 0.5^2} \\ &= 9.9 \times 10^{-2} \text{mSv} \cdot \text{mm}^{-1} \quad (5.94 \text{mSv} \cdot \text{h}^{-1}) \end{aligned}$$

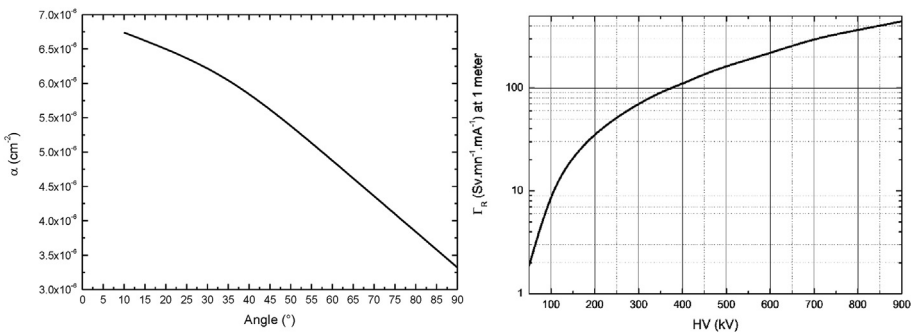


FIG. 3.V.2 – (a) Scatter fraction α as a function of the scattering angle θ for a 150 kV X-ray generator with a 3 mm aluminum filtration (according to Bourgois and Ménard, 2017), (b) ambient dose equivalent at 1 m from the source for high-voltages between 50 and 900 kV with a 3 mm aluminum filtration (data from Antoni and Bourgois, 2017a).

Although this component is substantially below that from the primary radiation ($22 \text{ mSv}\cdot\text{min}^{-1}$), it cannot be neglected. Indeed, it may require installing a lateral shielding around the generator, depending on the radiation protection objective.

Part 2: Numerical Calculation of the Ambient Equivalent Dose Rate of the Scattered Radiation

In section 3.III devoted to the calculation of the lead shielding thickness around a 100 kV X-ray generator, the evaluation of the ambient dose equivalent was done in two separate steps. Firstly, the bremsstrahlung spectrum was estimated. Secondly, this spectrum was used as a new source in a new MCNP file. However, under certain conditions, it is possible to assess the dosimetric quantity related to photons in a single step by coupling electron and photon transport. It is then necessary to apply one or several variance reduction techniques to enhance the statistical convergence. For instance, the photon and electron energies can be biased by restricting the transport to particles with an energy higher than the set threshold. In this case, the instruction is turned on through the “cut” card, set at 10 keV. Particles of lower energy are killed in order to constrain the track to particle energies useful for the tally convergence.

A spatial biasing can also be set up to force the transport of secondary photons towards areas of interest. This biasing is conducted using a virtual DXTRAN sphere (Breisemeister, 2000; Boothe, 1985). The latter is a deterministic transport method for increasing the sampling in a spherical region that would otherwise not be adequately sampled, owing to the weakness of the scattering probability toward the target region. Upon collision (or exiting the source) outside the sphere, DXTRAN creates a special “DXTRAN particle” or pseudo-particle and deterministically scatters it toward the DXTRAN sphere and transports it, without collision, to the surface of the DXTRAN sphere. The collision itself is otherwise treated normally, producing a non-DXTRAN particle that is sampled in the normal way, with no reduction in weight. However, the non-DXTRAN particle is killed if it enters the DXTRAN sphere.

With regard to the statistical weights, the real particle keeps with the weight before collision, for example w_o , while the pseudo-particle is assigned with a fraction of the statistical weight of the “real” particle: pw_o . This fraction matches the probability for the pseudo-particle to reach the DXTRAN sphere. The DXTRAN card formalism is as follows: “dxt : $p \ x_o \ y_o \ z_o \ r_i \ r_o$ ”. The first entry p corresponds to the type of particle tracked, $(x_o \ y_o \ z_o)$ are the sphere center coordinates, r_i is the inner radius and r_o is the outer radius of the sphere. Therefore, we can regard the DXTRAN sphere as two concentric spheres with pseudo-particles systematically reaching the outer sphere. As for the inner sphere, it enables to focus pseudo-particles on the solid angle formed by the initial collision point and this given inner sphere. The presence of this inner sphere has an effect on the probability p , defined with the following expression:

$$p = \frac{P(\mu)}{P(\eta)} \exp(-\Sigma_t l)$$

with $P(\mu)$ being the probability that the cosine of the angle between the collision direction and the scattering direction towards the DXTRAN sphere is equal to μ . $P(\eta)$ is the probability that the cosine of the angle between the axis running from the collision point to the sphere center and the scattering direction towards the DXTRAN sphere is equal to η . Note that the cosine η upper bound is limited by the outer sphere dimension. This ratio of probabilities can be seen as the probability for a pseudo-particle heading towards the DXTRAN sphere to be transported with a specific direction defined by η . The probability $P(\eta)$ of the pseudo-particle being scattered towards the inner sphere is 5 times higher than that for the rest of the outer sphere. Accordingly, pseudo-particles heading towards the inner sphere have a statistical weight 5 times lower than that heading towards the rest of the outer sphere (see figure 3.V.3). Finally, the exponential term stands for the deterministic transport of the pseudo-particle, undergoing no interaction on its straightaway path of length l until it reaches the surface of the outer sphere. Let w_o be the statistical weight of a particle before collision. The weight of the pseudo-particle when it reaches the outer sphere is:

$$w_{pp} = pw_o = w_o \frac{P(\mu)}{P(\eta)} \exp(-\Sigma_t l)$$

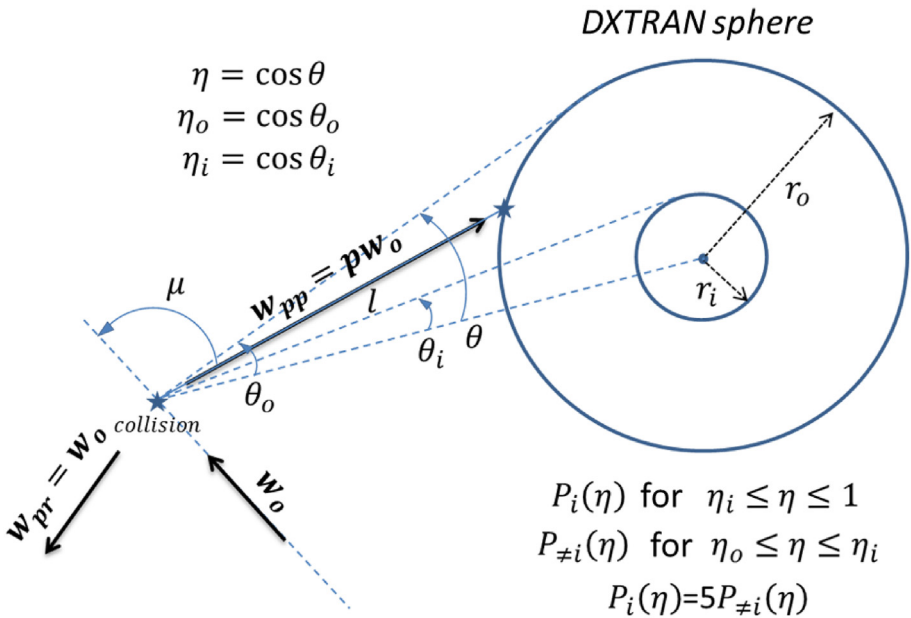


FIG. 3.V.3 – MCNP DXTRAN sphere principle.

Once it reaches the surface of the outer sphere, the pseudo-particle undergoes a classical transport and brings a normal tally contribution. This possibility to focus the particle launch towards an inner sphere is relevant, for instance when the DXTRAN sphere is centered on a point detector tally. In this case, most of pseudo-particles are directed to the area close to the tally and the rest undergoes interactions in a more distant region bounded by the outer sphere.

In the case study, in order to evaluate the scattered radiation at 45° from the water phantom, it is not convenient to enclose the tally in a DXTRAN sphere. The goal is instead to focus particles on the front face of the phantom, which is responsible for the scattering. Ideally, the outer sphere diameter has to be the same that the scattering surface diameter, *i.e.*, 16 cm. The outer sphere must also be centered at the middle of the inlet face of the phantom of 20 cm diameter. Inner and outer spheres have the same radius of 8 cm since in this case the primary bremsstrahlung flux is substantially the same for the whole area of the beam on the phantom surface. Thus, it is not necessary to focus pseudo-particles on the center of the object.

In the following MCNP input file 3.V.1, the electron primary beam interacts with the 45° inclined tungsten target to produce the bremsstrahlung beam. A 3 mm aluminum filter is considered (modeled by a layer surrounding the target). The photon beam is collimated by means of a $1\ \mu\text{m}$ thickness cylinder (refer to figure 3.V.4 and cell 30 definition). An F5 tally is used to assess the fluence at a point located at 45° from the phantom generatrix and at 50 cm from the center of its inlet face. By weighting the secondary photons energy spectrum at this point by the “fluence – ambient dose equivalent” conversion coefficients from ICRP (1996), one can obtain the ambient dose equivalent per source electron, $(H^*(10)/N_{e^-})$, in $\text{pSv}\cdot(\text{e}^-)^{-1}$.

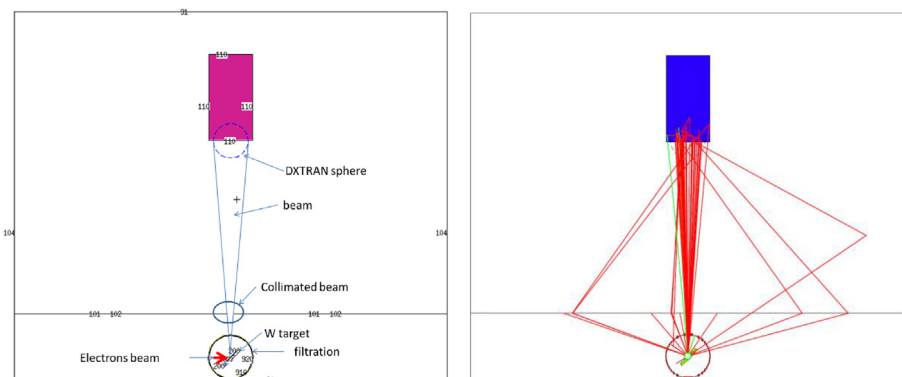


FIG. 3.V.4 – (a) Modeling of the radiological scene in MCNP (DXTRAN sphere in dotted line), (b) visualization of the transport of particles (electrons and bremsstrahlung photons) for 1000 electrons ran.

```

c ***** X-ray generator beam scatter on a phantom *****
10 11 -19.3 -200 $ X-ray generator
15 12 -2.7 -920 910 $ filtration
20 0 -91 #10 #15 #30 #40 $ calculation zone
30 0 100 -104 101 -102 $ emission cone
40 1 -1 -110 $ phantom
50 0 91

91 RCC 0 0 -10.31 0 0 170 100
100 CZ 1.59577
101 Pz 20
102 pz 20.0001
104 cZ 100
110 RCC 0 0 100 0 0 40 10
200 RCC 0 0 0 0 .707 -.707 5
910 SO 10
920 SO 10.3 $ 920-910 : filter thickness

imp:e 1 0 0 0 1 0
imp:p 1 1 1 0 1 0
mode e p
sdef pos=0 0 0 vec=0 1 0 dir=1 par=e erg=.15
M1 1001 2 8000 1
M11 74000 1
M12 13000 1
F5:p 0 -35.35 64.64 .1 $ 45°
C ICRP 74 H*(10) coefficient for photons
DE5 .01 .015 .02 .03 .04 .05 .06 .08 .1 .15 .2 .3 .4 .5 .6 &
.8 1 1.5 2 3 4 5 6 8 10
DF5 0.061 .83 1.05 .81 .64 .55 .51 .53 .61 .89 1.2 1.8 2.38 2.93 3.44 &
4.38 5.2 6.9 8.6 11.1 13.4 15.5 17.6 21.6 25.6
c F15:p 0 -35.35 64.64 .1 $ 45°
C ICRP 74 H*(10) coefficient for photons
c DE15 .01 .015 .02 .03 .04 .05 .06 .08 .1 .15 .2 .3 .4 .5 .6 &
c .8 1 1.5 2 3 4 5 6 8 10
c DF15 0.061 .83 1.05 .81 .64 .55 .51 .53 .61 .89 1.2 1.8 2.38 2.93 3.44 &
c 4.38 5.2 6.9 8.6 11.1 13.4 15.5 17.6 21.6 25.6
stop F5 .04
cut:p j .01 j j j
cut:e j .01 j j j
DXT:p 0 0 100 8 8

```

The output result is:

	tally	5			
nps	mean	error	vov	slope	fom
25000000	2.2407E-10	0.0263	0.0170	7.5	5.8E+00

The final calculation of the ambient dose equivalent rate (in mSv.h⁻¹) is achieved using the X-ray generator intensity i :

$$\dot{H}^*(10) = 3.6 \times 10^{-6} \left(\frac{H^*(10)}{N_{e^-}} \right) \frac{i}{e}$$

with $(H^*(10)/N_{e^-})$ being the MCNP result in pSv.(e⁻)⁻¹, i the current intensity, set at 1.10⁻³ A, e the electron elementary charge, *i.e.*, 1.602 × 10⁻¹⁹ C, and 3.6 × 10⁻⁶ the factor enabling the conversion from seconds to hours and from pSv to mSv. Finally, we get:

$$\dot{H}^*(10) = 3.6 \times 10^{-6} \times 2.24 \times 10^{-10} \times \left(\frac{1 \times 10^{-3}}{1.602 \times 10^{-19}} \right) = 5 \text{ mSv.h}^{-1}$$

The semi-empirical model provides a result 16% higher than the Monte-Carlo calculation. Given the complexity of the modeled scene and the simplicity of the semi-empirical approach, this deviation can be considered as satisfactory. Figure 3.V.4b represents electron transport, in green, and photon transport, in red, for a run of 1000 electrons. The right-figure clearly reveals the focus of pseudo-photons towards the DXTRAN sphere at the front face of the phantom, as well as the launch of real particles.

3.VI Calculation of Radiological Shielding for an Electron Accelerator with an X-ray Conversion Target

Abstract:

This application presents recommendations and technical information related to the design of radiological shielding for an electron accelerator. The accelerator operates at 20 MeV with a current of 100 nA. The electron beam is fully stopped in a target of high-Z material (tungsten). The facility works 20 h a month. The shielding is designed to reach an ambient dose equivalent smaller or equal to 80 μSv a month. For this case study, we assume that the source to observer distance, d , is 5 m (refer to figure 3.VI.1). Related issues of radiological exposure as air activation, skyshine and ozone production are also addressed.

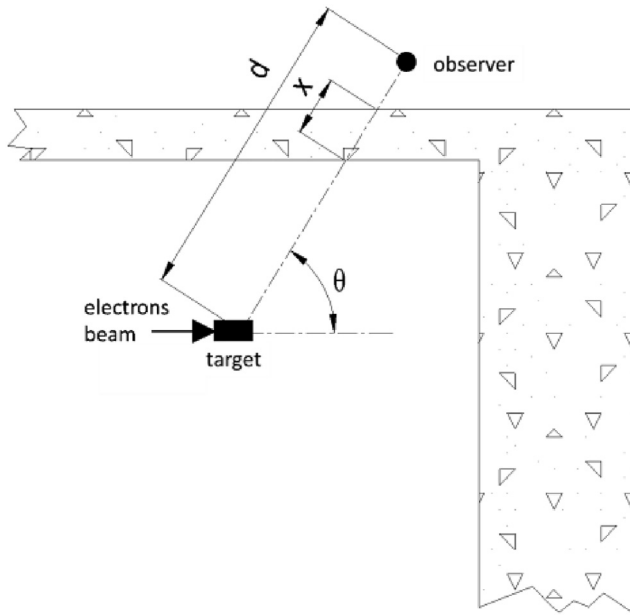


FIG. 3.VI.1 – Layout of the facility with the radiological shielding.

Warning:

For this application, an “ideal” accelerator is considered, assuming that only the 20 MeV electrons interactions with the target occur. All contributions to the source term should be taken into account to perform an exhaustive study. Accordingly, further calculations should be performed for all the beam losses, likely to produce secondary interactions with structural components (loss in a bending magnet, beam monitoring...).

Objectives:

- Complete study of source-terms for the irradiation facility.
- Calculation of the ambient equivalent dose rate due to bremsstrahlung produced by the interaction of electrons in tungsten.
- Assessment of the photonenergy.
- Calculation of the ambient equivalent dose rate due to neutrons produced by photonuclear reactions.
- Calculation of the shielding around an electron accelerator with high-Z target.
- Calculation of the external exposure component due to skyshine.
- Numerical calculation of the saturation activity in the air accelerator room.
- Air activity evolution as a function of time with an air change rate.
- Calculation of ozone concentration arising from photon interaction with air molecules.

In what follows, we will first define and characterize the “prompt source-term” related to the radiations emitted during the incoming of the electron beam in the target and the “delayed source-term” owing to the activation of the facility and the

ozone production. The first source-term leads to a shielding design and the second component results in collective protective equipment implementation such as the inclusion of a ventilation system with an adapted air change rate.

Part 1: Calculation of the Ambient Equivalent Dose Rate Due to the Interaction of Electrons with Tungsten

At 20 MeV, the prompt source-term consists of two radiative components. The interaction of the electron beam with the tungsten target produces bremsstrahlung with the emission of photons of energy smaller than or equal to that of incident electrons. When the photons energy is above the threshold for photonuclear reactions, photons can induce secondary neutrons.

(a) Semi-empirical model for the photon component

The ambient dose equivalent rate due to bremsstrahlung photons can be calculated with figure 3.VI.2. This figure represents $H^*(10)/i$, the ambient dose equivalent rate, at 1 m from the high-Z target per unit incident electron beam current

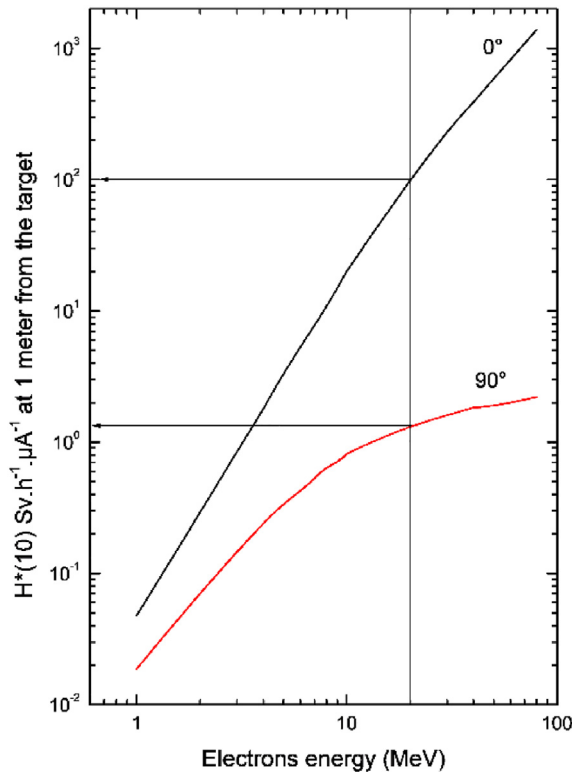


FIG. 3.VI.2 – Ambient dose equivalent rate at 1 m from a high-Z target, per μA , as a function of the primary electrons energy for the 0° and 90° directions (data from Antoni and Bourgois, 2017a).

(μA), as a function of incident primary electrons energy in forward (0°) and side-ward (90°) directions.

According to figure 3.VI.2, for a 20 MeV electron energy at 1 m from the target: $(H_\gamma^*(10)/i)_{0^\circ} = 100 \text{ Sv.h}^{-1} \cdot \mu\text{A}^{-1}$ at 0° and $(H_\gamma^*(10)/i)_{90^\circ} = 1.4 \text{ Sv.h}^{-1} \cdot \mu\text{A}^{-1}$ at 90° . For an operating point with a 100 nA current intensity, it arises:

$$\begin{aligned}\dot{H}_\gamma^*(10)_{0^\circ} &= 100 \times 100 \times 10^{-3} = 10 \text{ Sv.h}^{-1} \\ \dot{H}_\gamma^*(10)_{90^\circ} &= 1.4 \times 100 \times 10^{-3} = 0.14 \text{ Sv.h}^{-1}\end{aligned}$$

There are two decades of difference between the ambient dose equivalent rates in the two directions. This broad difference lies for part in the fact that bremsstrahlung photons are preferentially emitted in the same direction as the primary electrons interacting in the target.

(b) Analytical and semi-empirical model for the neutron component

Since bremsstrahlung photons can reach a 20 MeV energy, it is convenient to check if they are capable of inducing photonuclear reactions, at least (γ, n) reactions. For isotopes of tungsten, the (γ, n) reaction thresholds, drawn from the IAEA (2000a) reference, are given in table 3.VI.1.

Thus, (γ, n) reaction thresholds are reached for all tungsten isotopes. The energy of produced neutrons can be assessed with the Wattenberg (1947) formula written below.

$$E_n = \frac{A-1}{A} \left[E_\gamma - E_s - \frac{E_\gamma^2}{1862(A-1)} \right] + E_\gamma \cos \theta \sqrt{\frac{2(A-1)(E_\gamma - E_s)}{913 A^3}} \quad (1)$$

with A the atomic mass of the target, E_γ the incident photon energy, E_s the threshold energy and θ the photon-neutron emission angle. This analytical formula highlights that for high atomic masses, typically those of tungsten isotopes, the second term is negligible. Therefore, the neutron emission direction does not affect its energy. Note that the first term is quite close to $E_\gamma - E_s$. Thus, for the tungsten target, we assume it can be admitted that the maximum energy of the photoneutrons is equal to about $20 - 8 = 12 \text{ MeV}$.

TAB. 3.VI.1 – (γ, n) reaction thresholds in tungsten isotopes.

Isotope	(γ, n) reaction threshold (MeV)
^{182}W	8.07
^{183}W	6.19
^{184}W	7.41
^{186}W	7.19

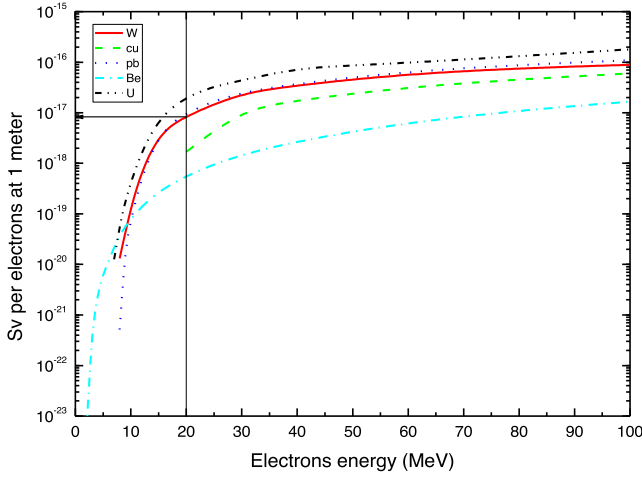


FIG. 3.VI.3 – Ambient equivalent dose as a function of the electron energy for different targets (from Antoni and Bourgeois, 2017a).

In order to evaluate the ambient dose equivalent related to these secondary neutrons, we may use figure 3.VI.3. This figure displays curves of the photoneutron ambient dose equivalent per electron of the primary beam, as a function of the electron energy, for different target materials.

For 20 MeV electrons interacting with tungsten, $H_n^*(10)/N_{e^-} = 8.2 \times 10^{-18}$ Sv.(e⁻)⁻¹; for 100 nA, the obtained rate is:

$$\begin{aligned} \dot{H}_n^*(10) &= \left(\frac{H_n^*(10)}{N_{e^-}} \right) \frac{i}{e} = 8.2 \times 10^{-18} \times \frac{100 \times 10^{-9}}{1.602 \times 10^{-19}} \\ &= 5.1 \times 10^{-6} \text{ Sv}\cdot\text{s}^{-1} \quad (18.4 \text{ mSv}\cdot\text{h}^{-1}) \end{aligned}$$

This value is weak compared to the ambient dose equivalent due to photons.

(c) Numerical calculation of the equivalent dose rate for the photon and neutron components

The modeling of the radiological scene consists, here, in simulating a tungsten cylinder of 1 cm in radius and length. Note that a 1 cm thickness is about two times the range of 20 MeV electrons in tungsten. Photoneutron production in MCNP requires the 4th entry “ispn” of the photon physics card “phys:p” to be different from zero. This value is set to -1, then photonuclear particle production is analog, i.e., computing a detailed description of physical phenomena involved throughout interactions. Mixed transport of electrons, photons and neutrons is very costly in terms of particle tracking and accordingly in calculation time with MCNP. Thus, an energy cut-off is handled by the “cut” card to transport only electrons and photons with energies greater than 100 keV. The input file enabling this mixed calculation is provided in file 3.VI.1.


```

Electron accelerator calculation
c cells
10 1 -19.3 -10 $ target
20 0 -20 10
30 0 20

10 RCC 0 0 0 0 0 1 1 $ twice the range
20 RCC 0 0 -1e-3 0 0 110 110

imp:e 1 0 0
imp:p,n 1 1 0
mode p n e
sdef par=e pos 0 0 1e-5 axs 0 0 1 ext 0 vec 0 0 1 dir 1 erg 20
PHYS:N 20 0 0 J J J 0 -1 J J J 0 0
PHYS:E 20 0 0 0 0 1 1 1 1 0 0 J J 0.917 0.001
c 4th entry of PHYS:p ispn=-1, then photonuclear particle production is analog
PHYS:P 20 0 0 -1 0 J 0
M1 74182 -.26 74183 -.14 74184 -.3 74186 -.3
F5:p 0 0 100 .1
E5 0 100i 20
F15:n 0 0 100 .1
E15 0 100i 20
F25:p 0 100 0 .1
E25 0 100i 20
F35:n 0 100 0 .1
E35 0 100i 20
F45:p 0 0 100 .1
F55:n 0 0 100 .1
F65:p 0 100 1 .1
F75:n 0 100 1 .1
C ICRP 74 H*(10)/phi conversion coefficient for neutrons
DE55 1e-9 1e-8 2.53e-8 1e-7 2e-7 5e-7 1e-6 2e-6 5e-6 1e-5 2e-5 5e-5 1e-4 2e-4 &
5e-4 1e-3 2e-3 5e-3 1e-2 2e-2 3e-2 5e-2 7e-2 .1 .15 .2 .3 .5 .7 .9 1 1.2 2 &
3 4 5 6 7 8 9 10 12 14 15 16 18 20 30 50 75 100 125 150 175 201
DF55 6.6 9 10.6 12.9 13.5 13.6 13.3 12.9 12 11.3 10.6 9.9 9.4 8.9 &
8.3 7.9 7.7 8 10.5 16.6 23.7 41.1 60 88 132 170 233 322 375 400 416 425 420 &
412 408 405 400 405 409 420 440 480 520 540 555 570 600 515 400 330 285 260 &
245 250 260
DE75 1e-9 1e-8 2.53e-8 1e-7 2e-7 5e-7 1e-6 2e-6 5e-6 1e-5 2e-5 5e-5 1e-4 2e-4 &
5e-4 1e-3 2e-3 5e-3 1e-2 2e-2 3e-2 5e-2 7e-2 .1 .15 .2 .3 .5 .7 .9 1 1.2 2 &
3 4 5 6 7 8 9 10 12 14 15 16 18 20 30 50 75 100 125 150 175 201
DF75 6.6 9 10.6 12.9 13.5 13.6 13.3 12.9 12 11.3 10.6 9.9 9.4 8.9 &
8.3 7.9 7.7 8 10.5 16.6 23.7 41.1 60 88 132 170 233 322 375 400 416 425 420 &
412 408 405 400 405 409 420 440 480 520 540 555 570 600 515 400 330 285 260 &
245 250 260
C conversion coefficient H*(10)/phi pSv.cm2 for photons
DE45 .01 .015 .02 .03 .04 .05 .06 .08 .1 .15 .2 .3 .4 .5 .6 &

```

```

.8 1 1.5 2 3 4 5 6 8 10 20
DF45 0.061 .83 1.05 .81 .64 .55 .51 .53 .61 .89 1.2 1.8 2.38 2.93 3.44 &
4.38 5.2 6.9 8.6 11.1 13.4 15.5 17.6 21.6 25.6 50
DE65 .01 .015 .02 .03 .04 .05 .06 .08 .1 .15 .2 .3 .4 .5 .6 &
.8 1 1.5 2 3 4 5 6 8 10 20
DF65 0.061 .83 1.05 .81 .64 .55 .51 .53 .61 .89 1.2 1.8 2.38 2.93 3.44 &
4.38 5.2 6.9 8.6 11.1 13.4 15.5 17.6 21.6 25.6 50
cut:p j .1 j j j
cut:e j .1 j j j
nps 62E6

```

File 3.VI.1

The “F5” tally enables to calculate the fluence at a point. Adding the “e5” card allows to build the energy fluence spectrum, that is to say the fluence in each energy bin specified, per source electron, Φ_E/N_{e^-} . For example, in the input file provided above, 100 energy bins are defined from 0 to 20 MeV with “e5 0 100i 20”. Furthermore, “de” and “df” cards are used to weight the secondary photon and neutron energy spectra by “fluence-to-ambient dose equivalent” conversion coefficients from ICRP (1996). This way, the result obtained is an ambient equivalent dose per source electron, i.e., $H^*(10)/N_{e^-}$ in $\text{pSv} \cdot (\text{e}^-)^{-1}$. Spectra as well as dose equivalents for photons and neutrons, at 1 m from the target are calculated in the 0° and 90° directions. Table 3.VI.2 summarizes the quantity matching each tally of the input file.

The ambient equivalent dose rate, in $\text{Sv} \cdot \text{h}^{-1}$ units, is calculated from the accelerator electron current i as follows:

$$\dot{H}^*(10) = 3.6 \times 10^{-9} \left(\frac{H^*(10)}{N_{e^-}} \right) \frac{i}{e}$$

TAB. 3.VI.2 – Quantities calculated for each tally mentioned in the MCNP file 3.VI.1.

Tally	Result type	Particles	Direction of the calculation point (1 m from target)
5	Energy fluence spectrum	Photons	0°
15	Energy fluence spectrum	Neutrons	0°
25	Energy fluence spectrum	Photons	90°
35	Energy fluence spectrum	Neutrons	90°
45	Dose equivalent	Photons	0°
55	Dose equivalent	Neutrons	0°
65	Dose equivalent	Photons	90°
75	Dose equivalent	Neutrons	90°

$H^*(10)/N_e$ is the MCNP result (pSv per electron), i the current expressed in ampere, e the electron elementary charge (1.602×10^{-19} C) and a factor enabling the conversion from seconds to hours and from pSv to Sv. The results obtained for the operational quantity for neutron and photon components are presented in table 3.VI.3.

Photon and neutron spectra calculated with tallies 5 to 35, in forward (0°) and sideward (90°) directions are displayed in figures 3.VI.4a and 3.VI.4b. For neutron spectra, as stated before with expression (1), the maximum energy of secondary neutrons is about 12 MeV and the spectra are invariant with emission directions. Conversely, a drop of the maximum energy and an overall reduction of the fluence are observed for the bremsstrahlung photons in the 90° direction.

TAB. 3.VI.3 – MCNP results of the ambient equivalent dose rate for the photon and neutron components at 0° and 90° .

MCNP results	
$\dot{H}_\gamma^*(10)_{0^\circ}$	9.94 Sv/h
$\dot{H}_\gamma^*(10)_{90^\circ}$	0.13 Sv/h
$\dot{H}_n^*(10)_{0^\circ}$	11.4 mSv/h
$\dot{H}_n^*(10)_{90^\circ}$	9.6 mSv/h

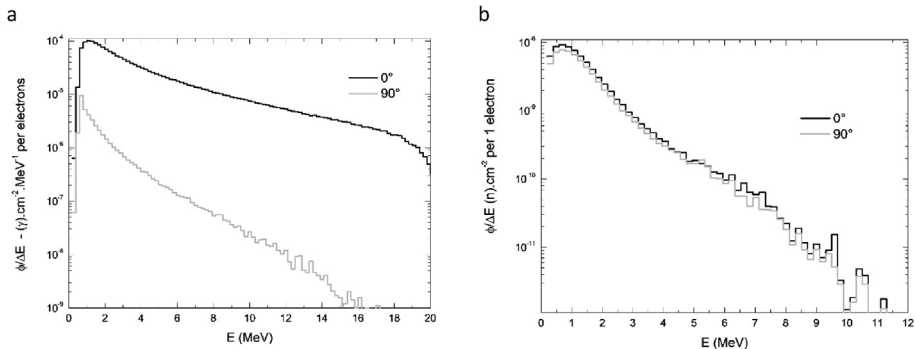


FIG. 3.VI.4 – Energy distribution of fluence for the photon (a) and neutron (b) components at 0° and 90° , simulated with MCNP.

Part 2: Calculation of Shielding for the Prompt Source-Term

When knowing the prompt source-term, one can assess the shielding thickness matching the targeted external exposure limit.

(a) Semi-empirical model for the primary barrier calculation

The primary barrier role is to ensure radiological protection in the electron incidence axis. Its thickness can be calculated using transmission factors. The total ambient dose equivalent rate, $\dot{H}_t^*(10)_{\text{obs}}$, behind the shielding, for a source-observer distance d , derives from expression (2):

$$\dot{H}_t^*(10)_{\text{obs}} = \frac{\dot{H}_\gamma^*(10)_{0^\circ}}{d^2} T_\gamma(\theta, x) + \frac{\dot{H}_n^*(10)}{d^2} T_n(x) \tag{2}$$

$\dot{H}_\gamma^*(10)_{0^\circ}$ is the photon ambient equivalent dose rate at 1 m previously calculated without shielding, d is the distance, in meters, between the target and the observer, and θ is the angle between the electron beam and the observer (see figure 3.VI.1). The term $T_\gamma(\theta, x)$ refers to the photon transmission coefficient for a shielding thickness x and can be drawn from figure 3.VI.5. The term $\dot{H}_n^*(10)$ stands for the neutron ambient equivalent dose rate at 1 m from the target, without shielding. Since the neutron field is isotropic, this value does not depend on θ . Finally, $T_n(x)$ is the neutron transmission coefficient for a shielding thickness x ; it is also invariant with θ . In a first approach, the neutron ambient dose equivalent can be omitted, owing to its low value compared to that of photons. The photon ambient dose equivalent rate of $10 \text{ Sv}\cdot\text{h}^{-1}$ previously calculated at 0° is equivalent to

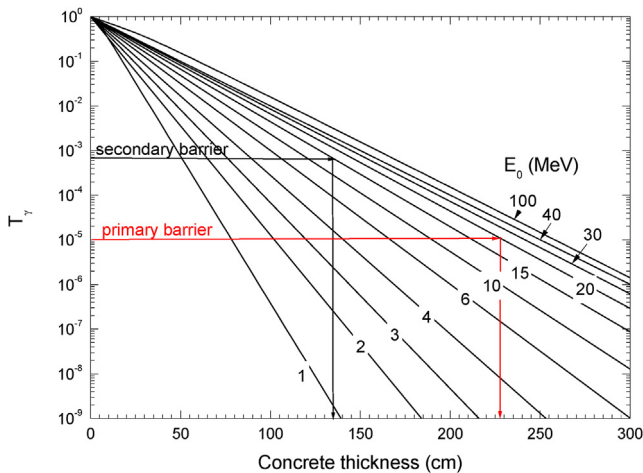


FIG. 3.VI.5 – Concrete thickness as a function of the transmission factor for electron accelerator energies E_0 ranging from 1 to 100 MeV (Antoni and Bourgois, 2017a).

200 Sv.month⁻¹ for 20 h of monthly operation. Thus, for a monthly exposition limit of 80 μSv expected in the initial objective, the matching transmission factor is:

$$T_\gamma(0^\circ, x) = d^2 \left(\frac{\dot{H}_t^*(10)_{\text{obs}}}{\dot{H}_\gamma^*(10)_{0^\circ}} \right) = 5^2 \times \frac{80 \times 10^{-6}}{200} = 10^{-5}$$

The graph shown in figure 3.VI.5 exhibits the concrete thickness transmission factor for the electron accelerator from 1 to 100 MeV. For a 10⁻⁵ transmission factor, the required concrete thickness for the primary barrier is 2.3 m.

At this stage, it is necessary to check if this shielding thickness ensures a negligible ambient dose equivalent rate due to neutrons. The neutron transmission coefficient is evaluated with the following exponentially decreasing function:

$$T_n(x) = \exp\left(-\frac{x\rho}{\rho\lambda}\right)$$

$\rho\lambda$ being the attenuation length expressed in kg.m⁻². The coefficient value, as a function of neutron energy, is found in NCRP (2003). The matching curve is plotted in figure 3.VI.6. For 12 MeV neutrons, the coefficient is 300 kg.m⁻².

The previous ambient dose equivalent rate for neutrons at 0°, 1.8 × 10⁻² Sv.h⁻¹, becomes 0.36 Sv.month⁻¹ for 20 h of monthly operation. Consequently, the resulting monthly ambient dose equivalent behind the protection is:

$$\begin{aligned} \dot{H}_n^*(10)_{\text{obs}} &= \frac{\dot{H}_n^*(10)}{d^2} \exp\left(-\frac{x\rho}{\rho\lambda}\right) = \frac{0.36}{5^2} \exp\left(-\frac{2.3 \times 2.35 \times 10^3}{300}\right) \\ &= 2.1 \times 10^{-10} \text{ Sv.month}^{-1} \end{aligned}$$

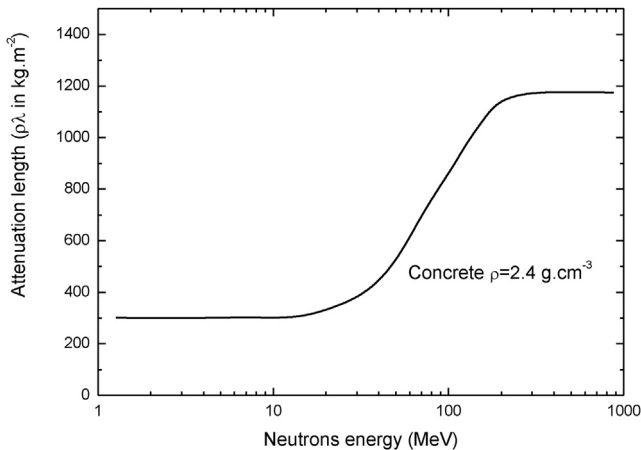


FIG. 3.VI.6 – Attenuation length for neutrons in ordinary concrete, according to NCRP 144.

Therefore, the neutron ambient dose equivalent can be neglected for such a thickness of shielding. More generally, this approach can be extended to studies concerning electron accelerators of less than 50 MeV. In these cases, the marginal neutron component of the prompt source-term can be omitted and the dimensioning of the shielding can be focused on the photon component.

(b) Secondary barrier calculation

The secondary barrier arranged laterally to the direction of incident electrons is dimensioned for the 90° component. The same as previously is done and the transmission coefficient is only determined for the photon component. The $0.14 \text{ Sv}\cdot\text{h}^{-1}$ photon ambient dose equivalent rate at 90° calculated before results in a rate of $2.8 \text{ Sv}\cdot\text{month}^{-1}$ for 20 h of monthly operation. It becomes the transmission coefficient:

$$T_\gamma(90^\circ, x) = d^2 \left(\frac{\dot{H}_t^*(10)_{\text{obs}}}{\dot{H}_\gamma^*(10)_{90^\circ}} \right) = 5^2 \times \left(\frac{80 \times 10^{-6}}{2.8} \right) = 7 \times 10^{-4} \quad (3)$$

The bremsstrahlung spectrum emitted at 90° from the target is lower in energy than that in the 0° direction (see MCNP calculated spectra of figure 3.VI.4a). In order to determine the concrete thickness of the secondary barrier in accordance with a penalizing approach, NCRP (1977), suggests to consider two thirds of the initial electron energy, *i.e.*, 13.3 MeV in this case. The thickness value matching the transmission coefficient at 15 MeV, read on figure 3.VI.5, is 140 cm. The ambient dose equivalent due to neutrons at the observer for this thickness is:

$$\dot{H}_{\text{neutron}}^* = \frac{0.36}{5^2} \exp\left(-\frac{1.4 \times 2.35 \times 10^3}{300}\right) = 2.5 \times 10^{-7} \text{ Sv}\cdot\text{month}^{-1}$$

Again, the monthly ambient dose equivalent for this component due to neutrons can be neglected.

(c) Numerical calculation of the ambient equivalent dose behind the radiological protections

The model used for the numerical simulation is similar to that detailed in the second part of problem 3.III devoted to the shielding calculation around an X-ray generator. The ambient equivalent dose behind the shielding is determined in two steps. The normalization factor f_H is calculated with a MCNP file in which the bremsstrahlung photon spectrum calculated in section (c) replaces the incident electron beam and the target. The file enabling the access to the factor for the bremsstrahlung spectrum at 0° is provided in file 3.VI.2.

```
Photon dose 0°
10 0 -10
20 0 10
10 SO 150
```

```

mode p
imp:p 1 0
sdef par=p pos 0 0 0 erg=d2
SI2 H 0.00E+00 1.98E-01 3.96E-01 5.94E-01 7.92E-01 9.90E-01 1.19E+00 1.39 &
1.58E+00 1.78E+00 1.98E+00 2.18E+00 2.38E+00 2.57E+00 2.77E+00 2.97E+00 &
3.17E+00 3.37E+00 3.56E+00 3.76E+00 3.96E+00 4.16E+00 4.36E+00 4.55E+00 &
4.75E+00 4.95E+00 5.15E+00 5.35E+00 5.54E+00 5.74E+00 5.94E+00 6.14E+00 &
6.34E+00 6.53E+00 6.73E+00 6.93E+00 7.13E+00 7.33E+00 7.52E+00 7.72E+00 &
7.92E+00 8.12E+00 8.32E+00 8.51E+00 8.71E+00 8.91E+00 9.11E+00 9.31E+00 &
9.51E+00 9.70E+00 9.90E+00 1.01E+01 1.03E+01 1.05E+01 1.07E+01 1.09E+01 &
1.11E+01 1.13E+01 1.15E+01 1.17E+01 1.19E+01 1.21E+01 1.23E+01 1.25E+01 &
1.27E+01 1.29E+01 1.31E+01 1.33E+01 1.35E+01 1.37E+01 1.39E+01 1.41E+01 &
1.43E+01 1.45E+01 1.47E+01 1.49E+01 1.51E+01 1.52E+01 1.54E+01 1.56E+01 &
1.58E+01 1.60E+01 1.62E+01 1.64E+01 1.66E+01 1.68E+01 1.70E+01 1.72E+01 &
1.74E+01 1.76E+01 1.78E+01 1.80E+01 1.82E+01 1.84E+01 1.86E+01 1.88E+01 &
1.90E+01 1.92E+01 1.94E+01 1.96E+01 1.98E+01 2.00E+01
SP2 D 0.00E+00 1.26E-07 2.67E-06 1.45E-05 1.88E-05 2.00E-05 1.93E-05 &
1.80E-05 1.66E-05 1.51E-05 1.38E-05 1.24E-05 1.15E-05 1.04E-05 9.66E-06 &
8.88E-06 8.26E-06 7.62E-06 7.07E-06 6.57E-06 6.15E-06 5.74E-06 5.32E-06 &
5.10E-06 4.81E-06 4.51E-06 4.26E-06 4.04E-06 3.82E-06 3.64E-06 3.45E-06 &
3.28E-06 3.10E-06 2.98E-06 2.84E-06 2.69E-06 2.60E-06 2.46E-06 2.37E-06 &
2.27E-06 2.14E-06 2.06E-06 2.03E-06 1.93E-06 1.84E-06 1.76E-06 1.69E-06 &
1.66E-06 1.59E-06 1.54E-06 1.47E-06 1.43E-06 1.37E-06 1.31E-06 1.27E-06 &
1.23E-06 1.19E-06 1.14E-06 1.10E-06 1.06E-06 1.04E-06 9.90E-07 9.46E-07 &
9.42E-07 8.97E-07 8.48E-07 8.36E-07 7.93E-07 7.98E-07 7.50E-07 7.37E-07 &
7.19E-07 6.97E-07 6.58E-07 6.54E-07 6.24E-07 6.04E-07 5.97E-07 5.82E-07 &
5.48E-07 5.26E-07 5.19E-07 4.88E-07 4.87E-07 4.68E-07 4.40E-07 4.36E-07 &
4.10E-07 4.09E-07 3.69E-07 3.43E-07 3.44E-07 3.30E-07 2.98E-07 2.57E-07 &
2.32E-07 2.18E-07 2.00E-07 1.59E-07 1.33E-07 9.64E-08 6.43E-08
F45:p 0 0 100 .1
DE45 .01 .015 .02 .03 .04 .05 .06 .08 .1 .15 .2 .3 .4 .5 .6 &
.8 1 1.5 2 3 4 5 6 8 10 20
DF45 0.061 .83 1.05 .81 .64 .55 .51 .53 .61 .89 1.2 1.8 2.38 2.93 3.44 &
4.38 5.2 6.9 8.6 11.1 13.4 15.5 17.6 21.6 25.6 50
stop F45 .0001

```

File 3.VI.2

Tally 45 provides here the ambient equivalent dose of 9.5201×10^{-5} for a bremsstrahlung photon at 0° , without shielding. By considering an ambient dose equivalent rate $\dot{H}_\gamma^*(10)_{0^\circ} = 9.94 \text{ Sv}\cdot\text{h}^{-1}$, obtained for $100 \mu\text{A}$ (see table 3.VI.3), the normalization factor is:

$$f_H = \frac{9.94}{9.5201 \times 10^{-5}} = 1.04 \times 10^5 \text{ Sv}\cdot\text{h}^{-1}/\text{pSv}\cdot(\gamma)^{-1}$$

Then, the 2.3 m thick concrete barrier is modeled in a second file. To improve tally 45 convergence, the variance-reduction technique based on a spatial mesh of

particle weight is used *via* the “wwg” card (see problem 3.II related to the calculation of a ^{60}Co photon source ambient dose equivalent rate behind a shielding). The file is shown below:

```

Primary barrier
c Block 1: cells
10 1 -1.3e-3 -10 $ air
15 2 -2.35 -15 $ concrete protection
20 2 -2.35 -20 $ concrete protection
25 2 -2.35 -25 $ concrete protection
30 2 -2.35 -30 $ concrete protection
35 2 -2.35 -35 $ concrete protection
40 2 -2.35 -40 $ concrete protection
45 2 -2.35 -45 $ concrete protection
50 2 -2.35 -50 $ concrete protection
55 2 -2.35 -55 $ concrete protection
60 2 -2.35 -60 $ concrete protection
65 2 -2.35 -65 $ concrete protection
70 2 -2.35 -70 $ concrete protection
75 2 -2.35 -75 $ concrete protection
80 2 -2.35 -80 $ concrete protection
85 2 -2.35 -85 $ concrete protection
90 1 -1.3e-3 -90 $ air
200 0 10 15 20 25 30 35 40 45 50 55 60 65 70 75 80 85 90 $ outside
10 RPP -1000 1000 -1000 1000 -10 200
15 RPP -1000 1000 -1000 1000 200 215
20 RPP -1000 1000 -1000 1000 215 230
25 RPP -1000 1000 -1000 1000 230 245
30 RPP -1000 1000 -1000 1000 245 260
35 RPP -1000 1000 -1000 1000 260 275
40 RPP -1000 1000 -1000 1000 275 290
45 RPP -1000 1000 -1000 1000 290 305
50 RPP -1000 1000 -1000 1000 305 320
55 RPP -1000 1000 -1000 1000 320 335
60 RPP -1000 1000 -1000 1000 335 350
65 RPP -1000 1000 -1000 1000 350 365
70 RPP -1000 1000 -1000 1000 365 380
75 RPP -1000 1000 -1000 1000 380 395
80 RPP -1000 1000 -1000 1000 395 410
85 RPP -1000 1000 -1000 1000 410 430
90 RPP -1000 1000 -1000 1000 430 510

imp:p 1 1 1 1 1 1 1 1 1 1 1 1 1 1 1 1 1 1 0
mode p
WWG 45 10 0 j j j j 0
M1 7014 .781 8016 .212 7015 .007 $ air
c M3 74182 -.26 74183 -.14 74184 -.3 74186 -.3
c standard concrete composition d=2.381

```



```

M2 14000 -20.68 13027 -.363 8016 -50.853 20000 -21.645 12000 -.198 19000 -.088 &
11023 -.0384 16000 -.139 6000 -4.52 22000 -.0155 15031 -.0208 25055 -.0192 &
1001 -.701 26054 -.0418 26056 -.6588 26057 -.0157 26058 -.0024 24052 -.00057
sdef par=p pos 0 0 0 erg d2
SI2 H 0.00E+00 1.98E-01 3.96E-01 5.94E-01 7.92E-01 9.90E-01 1.19E+00 1.39 &
1.58E+00 1.78E+00 1.98E+00 2.18E+00 2.38E+00 2.57E+00 2.77E+00 2.97E+00 &
3.17E+00 3.37E+00 3.56E+00 3.76E+00 3.96E+00 4.16E+00 4.36E+00 4.55E+00 &
4.75E+00 4.95E+00 5.15E+00 5.35E+00 5.54E+00 5.74E+00 5.94E+00 6.14E+00 &
6.34E+00 6.53E+00 6.73E+00 6.93E+00 7.13E+00 7.33E+00 7.52E+00 7.72E+00 &
7.92E+00 8.12E+00 8.32E+00 8.51E+00 8.71E+00 8.91E+00 9.11E+00 9.31E+00 &
9.51E+00 9.70E+00 9.90E+00 1.01E+01 1.03E+01 1.05E+01 1.07E+01 1.09E+01 &
1.11E+01 1.13E+01 1.15E+01 1.17E+01 1.19E+01 1.21E+01 1.23E+01 1.25E+01 &
1.27E+01 1.29E+01 1.31E+01 1.33E+01 1.35E+01 1.37E+01 1.39E+01 1.41E+01 &
1.43E+01 1.45E+01 1.47E+01 1.49E+01 1.51E+01 1.52E+01 1.54E+01 1.56E+01 &
1.58E+01 1.60E+01 1.62E+01 1.64E+01 1.66E+01 1.68E+01 1.70E+01 1.72E+01 &
1.74E+01 1.76E+01 1.78E+01 1.80E+01 1.82E+01 1.84E+01 1.86E+01 1.88E+01 &
1.90E+01 1.92E+01 1.94E+01 1.96E+01 1.98E+01 2.00E+01
SP2 D 0.00E+00 1.26E-07 2.67E-06 1.45E-05 1.88E-05 2.00E-05 1.93E-05 &
1.80E-05 1.66E-05 1.51E-05 1.38E-05 1.24E-05 1.15E-05 1.04E-05 9.66E-06 &
8.88E-06 8.26E-06 7.62E-06 7.07E-06 6.57E-06 6.15E-06 5.74E-06 5.32E-06 &
5.10E-06 4.81E-06 4.51E-06 4.26E-06 4.04E-06 3.82E-06 3.64E-06 3.45E-06 &
3.28E-06 3.10E-06 2.98E-06 2.84E-06 2.69E-06 2.60E-06 2.46E-06 2.37E-06 &
2.27E-06 2.14E-06 2.06E-06 2.03E-06 1.93E-06 1.84E-06 1.76E-06 1.69E-06 &
1.66E-06 1.59E-06 1.54E-06 1.47E-06 1.43E-06 1.37E-06 1.31E-06 1.27E-06 &
1.23E-06 1.19E-06 1.14E-06 1.10E-06 1.06E-06 1.04E-06 9.90E-07 9.46E-07 &
9.42E-07 8.97E-07 8.48E-07 8.36E-07 7.93E-07 7.98E-07 7.50E-07 7.37E-07 &
7.19E-07 6.97E-07 6.58E-07 6.54E-07 6.24E-07 6.04E-07 5.97E-07 5.82E-07 &
5.48E-07 5.26E-07 5.19E-07 4.88E-07 4.87E-07 4.68E-07 4.40E-07 4.36E-07 &
4.10E-07 4.09E-07 3.69E-07 3.43E-07 3.44E-07 3.30E-07 2.98E-07 2.57E-07 &
2.32E-07 2.18E-07 2.00E-07 1.59E-07 1.33E-07 9.64E-08 6.43E-08
F45:p 0 0 500 .1
DE45 .01 .015 .02 .03 .04 .05 .06 .08 .1 .15 .2 .3 .4 .5 .6 &
.8 1 1.5 2 3 4 5 6 8 10 20
DF45 0.061 .83 1.05 .81 .64 .55 .51 .53 .61 .89 1.2 1.8 2.38 2.93 3.44 &
4.38 5.2 6.9 8.6 11.1 13.4 15.5 17.6 21.6 25.6 50
stop F45 .02
wwe:p 1.0000E+02
wnl:p 5.0000E-01 2.5461E-01 1.0270E-01 3.3066E-02 1.1413E-02
4.2113E-03 1.6411E-03 6.6374E-04 2.7679E-04 1.1848E-04
5.2268E-05 2.3536E-05 1.0832E-05 5.1590E-06 2.5948E-06
1.4487E-06 2.4543E-04 -1.0000E+00

```

The result obtained for tally 45 is:

tally	45					
nps		mean	error	vov	slope	fom
	17,408,000	3.5191E-11	0.0200	0.0161	4.2	7.3E+00

The final result for the ambient equivalent dose rate behind the primary barrier is:

$$\begin{aligned}\dot{H}_t^*(10)_{\text{obs}} &\cong f_H \left(\frac{H^*(10)}{N_\gamma} \right)_{0^\circ} = 1.04 \times 10^5 \times 3.52 \times 10^{-11} \\ &= 3.7 \times 10^{-6} \text{ Sv}\cdot\text{h}^{-1} \quad (3.7 \mu\text{Sv}\cdot\text{h}^{-1})\end{aligned}$$

For 20 h monthly operation, the ambient dose equivalent rate is $73 \mu\text{Sv}\cdot\text{month}^{-1}$. The semi-empirical calculation yields a 9% higher result than the numerical simulation. This difference partly stems from the assumption of a semi-infinite build-up factor, and probably to the composition difference of the simulated concrete.

The same calculation with the bremsstrahlung spectrum in the 90° direction and 1.4 m of concrete leads to a monthly rate of $20 \mu\text{Sv}\cdot\text{month}^{-1}$. This value is four times lower than that obtained semi-empirically. This large deviation can be explained by the NCRP that recommends to only keeping two thirds of the incident electron energy and the choice to read the transmission coefficient curve for 15 MeV electrons, due to the lack of the exact energy. Actually, for a monthly rate of $20 \mu\text{Sv}\cdot\text{month}^{-1}$, the transmission coefficient numerically calculated with expression (3) would be:

$$T_\gamma(90^\circ, x) = d^2 \left(\frac{\dot{H}_t^*(10)_{\text{obs}}}{\dot{H}_\gamma^*(10)_{90^\circ}} \right) = 5^2 \times \left(\frac{20 \times 10^{-6}}{2.8} \right) = 1.92 \times 10^{-4} \sim 2 \times 10^{-4}$$

This value is quite different than that of 7×10^{-4} found at paragraph (b). However, on the transmission coefficient curves, the value $T = 2 \times 10^{-4}$ and a 1.4 m concrete thickness are associated to the 10 MeV incident electron curve (see figure 3.VI.7), which is far from the 13 MeV energy recommended by NCRP. We must point out that the exponential fitting of transmission coefficients can lead to significant deviation between the semi-empirical model and the Monte-Carlo simulation. Nevertheless, the semi-empirical model is a protective approach.

Part 3: Skyshine Calculation

In some cases, owing to the weight stress, the roof thickness above the source may not be as thick as the primary or secondary shielding. Then, the ambient dose equivalent rate on the roof must be assessed to specify access restrictions if necessary. Radiation scattered through air may increase the exposure for an observer located beyond primary and secondary shielding. This additional component is

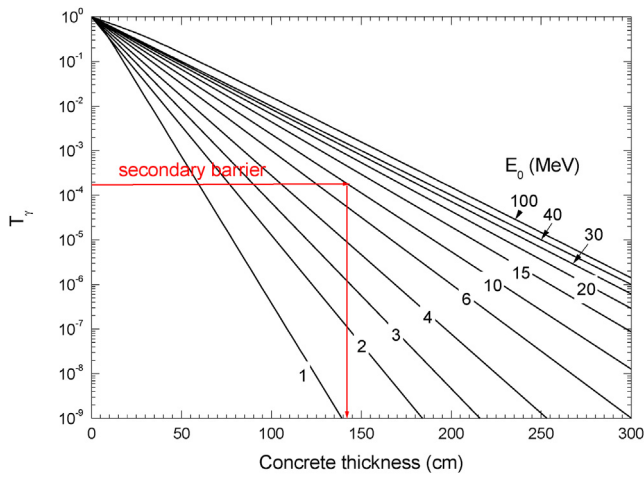


FIG. 3.VI.7 – Uncertainty on the transmission factor for the secondary barrier.

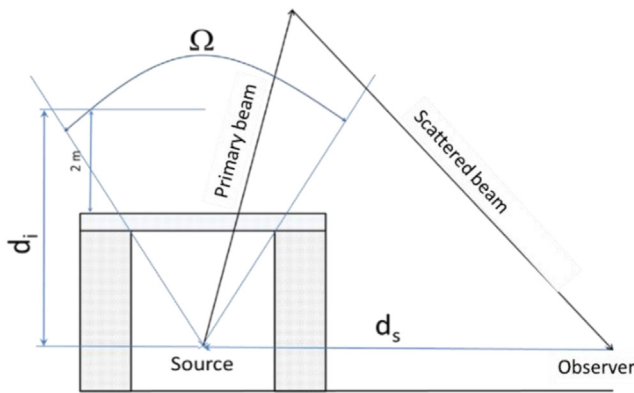


FIG. 3.VI.8 – Quantities for the skyshine assessment (Antoni and Bourgois, 2013).

denoted as “skyshine”. The quantities allowing its assessment are presented in figure 3.VI.8.

(a) Semi-empirical model of the skyshine for photons and neutrons

For an observer located beyond the facility boundaries, skyshine is evaluated using the NCRP (1977) semi-empirical formula. This former model is still recommended by ISO standards. The photon ambient dose equivalent rate due to skyshine, at the observer, in $\mu\text{Sv}\cdot\text{h}^{-1}$, is expressed as:

$$\dot{H}_\gamma^{\text{ef}} = 2.5 \times 10^4 \frac{T_{t,\gamma} \dot{H}_{0,\gamma} \Omega^{1.3}}{(d_i d_s)^2}$$

where d_s is the distance (in meters) between the source and the observer, d_i the distance (in meters) between the source and 2 m above the roof (see figure 3.VI.8), $T_{t,\gamma}$ is the photon transmission coefficient through the roof, $\dot{H}_{0,\gamma}$ is the dose equivalent rate ($\text{Sv}\cdot\text{h}^{-1}$) for photons at 1 m from the source and Ω is the emission solid angle (Sr) at the roof level, bounded by the irradiation room dimensions (refer to figure 3.VI.8). The neutron ambient dose equivalent rate due to skyshine, at the observer, in $\mu\text{Sv}\cdot\text{h}^{-1}$, is expressed as:

$$\dot{H}_n^{\text{ef}} = 5.4 \times 10^2 \frac{T_{t,n} \dot{H}_{0,n} \Omega}{2\pi}$$

where $T_{t,n}$ is the neutron transmission coefficient through the roof, $\dot{H}_{0,n}$ is the dose equivalent rate ($\text{Sv}\cdot\text{h}^{-1}$) for neutrons at 1 m from the source and Ω is the emission solid angle (sr) at the roof level, bounded by the irradiation room dimensions. This relationship does not depend on the distance between the source and the observer. The NCRP (1977) indicates that this expression is only reliable for distances not exceeding 20 m, and it specifies constant ambient dose equivalent rate in this area.

The irradiation room is box-shaped. Therefore, one has to calculate the solid angle Ω bounded by a $2p$ by $2q$ rectangle for an observer located at a distance h on the central line of this rectangle, according to figure 3.VI.9.

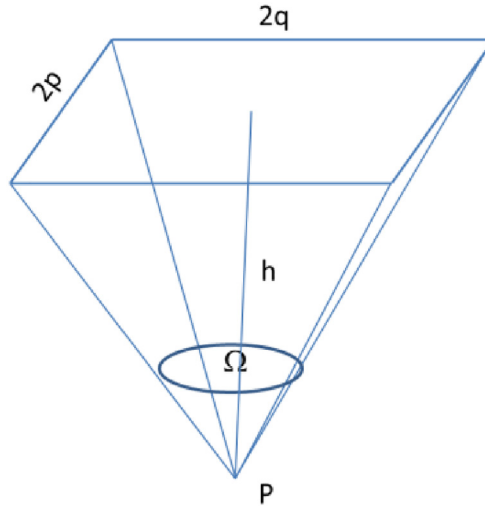


FIG. 3.VI.9 – Geometry for the calculation of the solid angle Ω .

The solid angle is expressed as a function of the different geometric variables:

$$\Omega = 4 \arcsin \left(\frac{pq}{\sqrt{q^2 + h^2} \sqrt{p^2 + h^2}} \right)$$

For this application, we assume a facility with no roof, involving zero attenuation. Accordingly, $T_{t,\gamma} = T_{t,n} = 1$. The dose equivalent rates \dot{H}_0 , and $\dot{H}_{0,n}$ are drawn from table 3.VI.3 and selected at 90° taking into account the geometric configuration considered. Matching values are, respectively, $0.13 \text{ Sv}\cdot\text{h}^{-1}$ and $0.01 \text{ Sv}\cdot\text{h}^{-1}$. The inner surface of the irradiation room is contained within a 7.2 m by 5.4 m rectangle, the distance between the target and the roof is 1.5 m. Thus, the calculation parameters are: $p = 3.6 \text{ m}$; $q = 2.7 \text{ m}$ and $h = 1.5 \text{ m}$. The corresponding solid angle is:

$$\Omega = 4 \arcsin \left(\frac{3.6 \times 2.7}{\sqrt{2.7^2 + 1.5^2} \sqrt{3.6^2 + 1.5^2}} \right) = 3.8 \text{ sr}$$

with $d_i = 1.5 + 2 = 3.5 \text{ m}$ (see figure 3.VI.8), the two contributions are:

$$\left\{ \begin{array}{l} \dot{H}_\gamma^{\text{ef}}(d_s) = \frac{2.5 \times 10^4 \times 1 \times 0.13 \times 3.8^{1.3}}{(3.5 \times d_s)^2} = \frac{1.5 \times 10^3}{d_s^2} \\ \dot{H}_n^{\text{ef}} = \frac{5.4 \times 10^2 \times 1 \times 0.01 \times 3.8}{2\pi} = 3.3 \mu\text{Sv}\cdot\text{h}^{-1} \quad \forall d_s < 20 \text{ m} \end{array} \right.$$

(b) Numerical simulation of the skyshine for photons and neutrons

For this calculation, the accelerator room, the tungsten target at the origin, and an environment of large dimensions composed of air, defined by a $2 \times 10^6 \text{ m}^3$ rectangular parallelepiped are simulated. Owing to its weak contribution to radiation attenuation, the roof is not simulated. The zero importance of cell 30 implies that the particle transport is turned off inside the accelerator room walls. The goal is here to simulate only skyshine radiation. The electron beam is located along the z -axis. In order to reach tally convergence, a DXTRAN sphere is added above the roof (refer to section 3.V). The sectional view of the configuration in the zy plane is shown in figure 3.VI.10. Ambient dose equivalent rate outside the accelerator room is calculated along the z -axis, at the tungsten target height every 5 m up to 100 m. Dose equivalent is assessed with F5 tallies weighted by “fluence – dose equivalent” conversion coefficients by means of “de” and “df” cards. In the input file 3.VI.4, the use of a unique set of “de0” and “df0” cards allows to weight all tallies.

File 3.VI.4 is devoted to the calculation of the equivalent doses of the photon component:

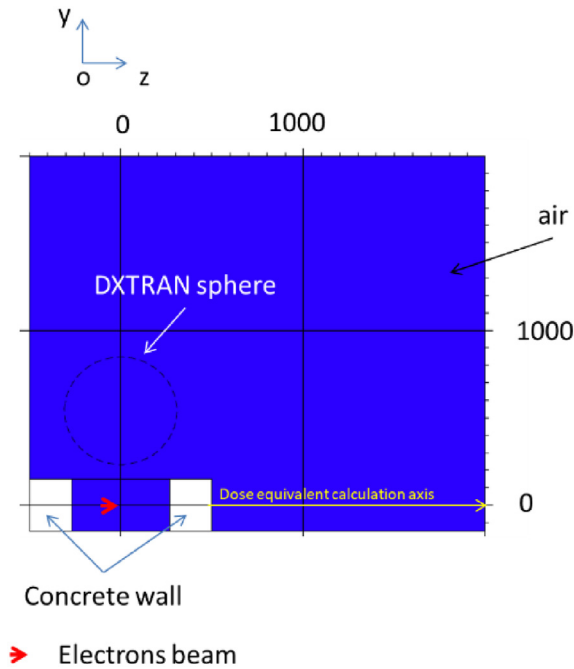


FIG. 3.VI.10 – Sectional view of the modeled geometry in the zy plane. The scene is constrained at 20 m in the y - and z -axis.

```

skyshine calculation
c cells
10 2 -19.3 -10 $ tungsten target
20 1 -1.2e-3 -20 10 $ air
30 0 -30 20 $ concrete
50 1 -1.2e-3 -50 30
100 0 50

10 RCC 0 0 0 0 0 2 1
20 RPP -360 360 -150 150 -270 270
30 RPP -500 500 -150 150 -500 500
50 RPP -10000 10000 -150 10000 -500 10000

vol j 1.1664E8 j j
imp:n,p 1 1 0 1 0
imp:e 1 0 0 0 0
mode n p e
m1 6000 -0.000124 7014 -0.755268 8016 -0.231781 18000 -0.012827
mx1:p 6012 j j 18040 $ photonuclear substitute material
m2 74182 -.3 74183 -.1 74184 -.3 74186 -.3
sdef par=e pos 0 0 1e-10 axs 0 0 1 ext 0 rad=d1 vec 0 0 1 dir 1 erg 20

```

```

c 4th entry of PHYS:p ispn=-1, then photonuclear particle production is analog
PHYS:P 100 0 0 -1 0 J 0
Si1 0 1
sp1 -21 1
ctme 10000
cut:p,e j .01
F5:p 0 0 510 0.1
F55:p 0 0 1000 0.1
F105:p 0 0 1500 0.1
F155:p 0 0 2000 0.1
F205:p 0 0 2500 0.1
F255:p 0 0 3000 0.1
F305:p 0 0 3500 0.1
F355:p 0 0 4000 0.1
F405:p 0 0 4500 0.1
F455:p 0 0 5000 0.1
F505:p 0 0 5500 0.1
F555:p 0 0 6000 0.1
F605:p 0 0 6500 0.1
F655:p 0 0 7000 0.1
F705:p 0 0 7500 0.1
F755:p 0 0 8000 0.1
F805:p 0 0 8500 0.1
F855:p 0 0 9000 0.1
F905:p 0 0 9500 0.1
F945:p 0 0 9900 0.1
C ICRP 74 H*(10)/phi pSv.cm2 coefficients for photons
DE0 .01 .015 .02 .03 .04 .05 .06 .08 .1 .15 .2 .3 .4 .5 .6 &
.8 1 1.5 2 3 4 5 6 8 10
DF0 0.061 .83 1.05 .81 .64 .55 .51 .53 .61 .89 1.2 1.8 2.38 2.93 3.44 &
4.38 5.2 6.9 8.6 11.1 13.4 15.5 17.6 21.6 25.6
DXT:p 0 540 0 308 308

```

File 3.VI.4

For the neutron dose equivalents assessment, some parts of the file are adjusted. The command line to set the minimum photon transport energy “cut:p,e j 0.01” is replaced by “cut:p,e j 5”. Since photonuclear production energy thresholds are high, it is not necessary to transport electrons and photons not exceeding 5 MeV to calculate dose equivalents due to neutrons. Moreover, type 5 tallies and “fluence – ambient dose equivalent” conversion coefficients defined by “de0” and “df0” cards are this time set for neutrons. Lastly, the DXTRAN card instruction “dxt:p 0 540 0 308 308” is replaced by “dxt:n 0 540 0 308 308”. The final ambient dose equivalent rate, in $\mu\text{Sv}\cdot\text{h}^{-1}$, is calculated from the current i of the electron accelerator as follows:

$$\dot{H}^*(10) = 3.6 \times 10^{-3} \left(\frac{H^*(10)}{N_{e^-}} \right) \frac{i}{e}$$

The quantity $H^*(10)/N_{e^-}$ being the MCNP result, in $\text{pSv} \cdot (\text{e}^-)^{-1}$, and $i = 100 \text{ nA}$ the operating current.

(c) Results of the numerical solving

The ambient dose equivalent rate as a function of the distance between the target is plotted in figure 3.VI.11a for photons and in figure 3.VI.12b for neutrons.

With respect to photons, one clearly infers that the semi-empirical method significantly overestimates the numerical results for distances lower than 15 m. However, from 20 to 50 m, this approach underestimates the MCNP results by a factor of 3. Beyond 50 m, this underestimation reaches a factor of 4. For neutrons, the semi-empirical formula provides a satisfactory assessment of the maximum ambient dose equivalent rate due to the skyshine. On the other hand, it does not take into account the decrease in the ambient dose equivalent with the distance.

For the numerical method, shading is observed when moving towards the wall of the irradiation room. Below 10 m, the ambient dose equivalent rate decreases with the distance to the wall. This shielding effect must be considered during radiation surveys undertaken around the facility. In other words, a wall contact measurement does not necessarily correspond to the maximum ambient dose equivalent rate. Thus, the radiation protection officer has to perform measurements at several locations far from walls.

We observe that the maximum ambient dose equivalent rate, located around 10 m, is $9 \mu\text{Sv} \cdot \text{h}^{-1}$ for photons and $3.5 \mu\text{Sv} \cdot \text{h}^{-1}$ for neutrons, which makes a total of $12.5 \mu\text{Sv} \cdot \text{h}^{-1}$, *i.e.*, $250 \mu\text{Sv} \cdot \text{month}^{-1}$ for the assumption of 20 h of monthly operation. This value is significantly higher than the initial objective of $80 \mu\text{Sv} \cdot \text{month}^{-1}$ limit. Therefore, a shielding has to be added for the roof to decrease the dose. The shielding thickness is determined from the photon transmission coefficient equal to $T = 80/250 = 0.3$. For this value, the irradiation room should be designed with a 23 cm thick concrete roof (see figure 3.VI.5). The neutron transmission coefficient matching this thickness is 10 (refer to part 2), which is consistent with the dose rate limit expected.

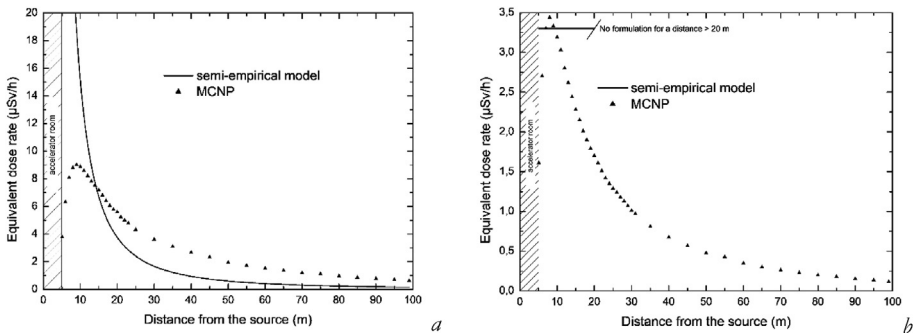


FIG. 3.VI.11 – Equivalent dose rate due to skyshine for (a) photons and (b) neutrons.

Part 4: Air Activation Calculation and Associated Consequences

Radiological protection issues make it of prior importance to quantify the structural elements- and the air- activation inside the accelerator room. Several physical processes can lead to a residual activity after the accelerator shut down. The main activation is due to photonuclear reactions caused by bremsstrahlung photons, arising from (γ, n) , (γ, p) , (γ, α) and (γ, t) reactions, depending on the chemical element and the photon energy. Neutrons from (γ, n) reactions can induce secondary nuclear reactions like (n, γ) and $(n, 2n)$. They are marginal when compared to reactions from photoneutrons produced in the target. In what follows, we will only focus on the air activation study. The structural elements activation requires a well description of their geometry as well as their constituting materials.

(a) Atmospheric photonuclear reactions

Since photonuclear reactions have thresholds, we firstly have to study those which can occur on air components at the highest photon energy. The atomic weight fractions of air are 0.0124% of carbon, 75.5% of nitrogen, 23.18% of oxygen and 1.3% of argon. The possible reactions and their associated thresholds are summarized in table 3.VI.4.

In MCNP, the photonuclear reactions-induced activity can be evaluated with the tally multiplication card “fm” associated with a type 4 tally providing the mean photon fluence in a cell, $\bar{\Phi}_\gamma/N_{e^-}$. The provided result is the saturation activity A_{sat}^i of radionuclide i , per source electron. The MCNP calculation yielding this activity can be formalized as follows:

$$A_{\text{sat}}^i = c \int_{E_\gamma} \sigma_{(\gamma, X), E_\gamma} \left(\frac{\bar{\Phi}_\gamma}{N_{e^-}} \right)_{E_\gamma} dE_\gamma$$

TAB. 3.VI.4 – Photonuclear reactions on isotopes composing the air, for maximum photon energy of 20 MeV.

Reaction	Threshold (MeV)	Daughter half-life
$^{12}\text{C}(\gamma, n)^{11}\text{C}$	18.72	20.36 min
$^{12}\text{C}(\gamma, p)^{11}\text{B}$	15.96	Stable
$^{12}\text{C}(\gamma, \alpha)^8\text{Be}$	7.37	7E-17 s
$^{14}\text{N}(\gamma, n)^{13}\text{N}$	10.55	10 min
$^{14}\text{N}(\gamma, p)^{13}\text{C}$	7.55	Stable
$^{14}\text{N}(\gamma, \alpha)^{10}\text{B}$	11.61	Stable
$^{16}\text{O}(\gamma, n)^{15}\text{O}$	15.66	2 min
$^{16}\text{O}(\gamma, p)^{15}\text{N}$	12.13	Stable
$^{16}\text{O}(\gamma, \alpha)^{12}\text{C}$	7.16	Stable
$^{40}\text{Ar}(\gamma, n)^{39}\text{Ar}$	9.87	Stable
$^{40}\text{Ar}(\gamma, p)^{39}\text{Cl}$	12.53	56 min
$^{40}\text{Ar}(\gamma, \alpha)^{36}\text{S}$	6.80	Stable

with $\sigma_{(\gamma, X), E_\gamma}$ the cross section of (γ, X) photonuclear reactions leading to the production of radionuclide i . The “fm” card parameters for the mean fluence calculation in a cell are:

```
F4 :p [cell number]
Fm4 k M Reaction(\gamma, X1) Reaction(\gamma, X2) Reaction(\gamma, X3) ...
```

k is the normalization constant depending on the desired result. In this case, this factor is determined to yield a saturation specific activity $A_{m, \text{sat}}(i)$. For instance, when considering ^{14}N nuclei, this constant is:

$$k = \frac{\eta}{A} \times 10^{-24} = \frac{6.02 \times 10^{23}}{14} \times 10^{-24} = 4.3 \times 10^{-2}$$

The 10^{-24} coefficient stems from the barn to cm^2 conversion and A is the atomic mass of target nuclei. The MCNP nomenclature of photonuclear reactions cross sections involves, in the “fm” command, the IPT value (particle type) of the secondary particle created through the reaction. These are given in the particle designator section of the user’s manual. IPT values for neutrons, protons and alpha particles are, respectively, 1, 9 and 34. The third parameter of the “fm” card is set to this value, for the desired reaction, followed by “001”. Thus, parameters for the three possible reactions are, respectively, 1001, 9001 and 34001. For photonuclear reactions allowed on ^{14}N , those three parameters must be set successively in the “fm” card, enabling to separately calculate the corresponding saturation activities. Finally, parameter M corresponds to a fictive material composed only of target nuclei for the reaction of interest. This parameter is also defined in the materials section of the input file. This material is only used for activity calculations and is not affected to any cell of the scene. In the same time, an “air” material is set in the cell modeling the internal air of the irradiation room to perform the particles transport and to sample the photonuclear reactions. As an example, the following input file presents instructions required to evaluate saturation activities of nuclides produced through reactions on ^{14}N . Calculations are performed in cell 20. The “real” air is defined by material “m1” and the virtual material composed of ^{14}N target nuclei is specified by “m4”.

```
c air composition
m1 6000 -0.000124 7014 -0.755268 8016 -0.231781 18000 -0.012827
mx1:p 6012 j j 18040 $ photonuclear substitute material
c nitrogen 14
m4 7014 1
c fluence in air cell number 20
FC24 nitrogen N-14 target
F24:p 20
FM24 4.3e-2 4 (1001) (9001) (34,001) $ (\gamma, n) (\gamma, p) and (\gamma, \alpha) reactions on N-14 target
```

The mix and match instruction, denoted as “mx1:p”, allows to substitute some photonuclear libraries by others. In the case study, the libraries used do not cover materials 6000 (all isotopes of natural carbon) and 18000 (all isotopes of natural argon). They are, respectively, replaced by 6012 (^{12}C) and 18040 (^{40}Ar) for which photonuclear libraries are implemented in the MCNP xsdir file.

(b) Neutron reactions in the air

A F8 tally in conjunction with the “ft res” option is used to assess the neutron activation of air due to photoneutrons produced in the target. For instance, instructions below are set to calculate the saturation activity in cell 20:

```
F8 :n 20
FT8 RES
```

Without any additional information, these command lines return all atoms created in cell 20 under the form “z zaaa”, representing 2200 values, including zero values. The use of a range of atomic numbers following the “res” card enables to target the desired result. Following instructions return only produced radionuclides of which the atomic number is lying between z1 and z2.

```
F8 :n [cell number]
FT8 RES Z1 Z2
```

When specifying the command “ft8 res z zaaa”, only the number of “z zaaa” atoms is printed. For instance, the “ft8 res 18041” instruction provides only the ^{41}Ar production once saturation is reached.

(c) Full calculation of the saturation activity with MCNP

This input file models the 20 MeV electrons interacting with the 2 cm long and 1 cm radius tungsten target. The target is located in the accelerator room of which the walls have the concrete thickness calculated in the previous part (see figure 3.VI.12). The air is contained inside a rectangular parallelepiped of dimensions $720\text{ cm} \times 300\text{ cm} \times 540\text{ cm} = 1.166 \times 10^8\text{ cm}^3$. Walls are included to account for neutron scattering in the irradiation room. However, photonuclear reactions in concrete are not simulated since only air activation is evaluated in this calculation. Since the energy threshold of photonuclear reaction is higher than 5 MeV, electrons and photons of energy lower than 5 MeV, pointless in the activity production, are inhibited. The “cut” card is used to define an energy cutoff with its last entry set to 5, *i.e.*, “cut:p,e j 5”. When using a F4 tally, the volume calculation has to be well defined. This calculation, by default, achieved by MCNP for simple geometries without “crushing” surface (refer to Antoni and Bourgois, 2013). In the following

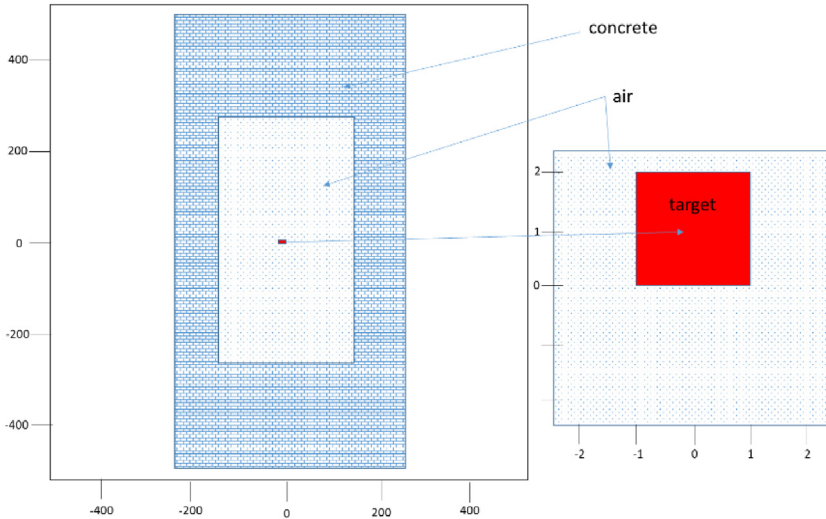


FIG. 3.VI.12 – Radiation scene modeled to calculate the saturation activity of the air inside the irradiation room.

simulated scene, the air cell volume encompasses a crushing surface: the target. Thus, the value of the volume has to be entered in a “vol” card.

The input file 3.VI.5 gives the complete calculation of the saturation activity of the pinpointed nuclides.

```

activation calculation
c cell block
10 2 -19.3 -10 $ tungsten target
20 1 -1.2e-3 -20 10 $ air
30 10 -2.35 -30 20 $ concrete
40 0 30

10 RCC 0 0 0 0 0 2 1
20 RPP -360 360 -150 150 -270 270
30 RPP -500 500 -250 259 -500 500

vol j 1.1664E8 j j
imp:n,p,e 1 1 1 0
mode n p e
m1 6000 -0.000124 7014 -0.755268 8016 -0.231781 18000 -0.012827
mx1:p 6012 j j 18040 $ photonuclear substitute material
m2 74182 -.3 74183 -.1 74184 -.3 74186 -.3
c standard concrete composition d=2.35
M10 14000 -20.68 13027 -.363 8016 -50.853 20000 -21.645 12000 -.198 &
19000 -.088 11023 -.0384 16000 -.139 6000 -4.52 22000 -.0155 15031 &
-.0208 25055 -.0192 1001 -.701 26054 -.0418 26056 -.6588 26057 &

```

```

-.0157 26058 -.0024 24052 -.00057
MX10:p 0 0 0 0 0 0 0 0 0 0 0 0 0 0 0 0 0 0 0 0 0 0 $ no photonuclear reaction in concrete
m3 6012 -1
m4 7014 -1
m5 8016 -1
m6 18040 -1
sdef par=e pos 0 0 1e-10 axs 0 0 1 ext 0 rad=d1 vec 0 0 1 dir 1 erg 20
c 4th entry of PHYS:p ispn=-1, then photonuclear particle production is analog
PHYS:P 100 0 0 -1 0 J 0
Si1 0 1
sp1 -21 1
FC14 C-12
F14:p 20
FM14 5e-2 3 (1001) (9001) (34001) $ ( $\gamma$ ,n) ( $\gamma$ ,p) and ( $\gamma$ , $\alpha$ ) reactions on C-12
FC24 N-14
F24:p 20
FM24 4.3e-2 4 (1001) (9001) (34001) $ ( $\gamma$ ,n) ( $\gamma$ ,p) and ( $\gamma$ , $\alpha$ ) reactions on N-14
FC34 O-16
F34:p 20
FM34 3.7625e-2 5 (1001) (9001) (34001) $ ( $\gamma$ ,n) ( $\gamma$ ,p) and ( $\gamma$ , $\alpha$ ) reactions on O-16
FC44 Ar-40
F44:p 20
FM44 1.505e-2 6 (1001) (9001) (34001) $ ( $\gamma$ ,n) ( $\gamma$ ,p) and ( $\gamma$ , $\alpha$ ) reactions on Ar-40
F8:n 20
FT8 RES
ctme 10000
cut:p,e j 5

```

File 3.VI.5

The results obtained for the activation of ^{14}N contained in air accelerator room *via* photonuclear reactions are listed in the output file as follows:

```

cible azote N-14
tally type 4 track length estimate of particle flux.
particle(s) : photons
volumes
cell: 20
1.16640E+08

```

cell 20			
multiplier bin:	4.30000E-02	4	1001
	4.11633E-13 0.000	4	
cell 20			
multiplier bin:	4.30000E-02	4	9001
	1.38743E-12 0.000	3	
cell 20			
multiplier bin:	4.30000E-02	4	34001
	1.04711E-14 0.0005		

The value obtained for reaction (1001) yields the saturation specific activity of ^{13}N per source electron $A_{m,\text{sat}}^{13\text{N}}/N_{e^-}$, that is, *via* the $^{14}\text{N}(\gamma,n)^{13}\text{N}$ reaction. By assuming the nitrogen of the air is only composed of ^{14}N , the ^{13}N saturation activity in the irradiation room air, per source electron, is:

$$\frac{A_{\text{sat}}^{13\text{N}}}{N_{e^-}} = \left(\frac{A_{m,\text{sat}}^{13\text{N}}}{N_{e^-}} \right) m_{^{14}\text{N}} = \left(\frac{A_{m,\text{sat}}^{13\text{N}}}{N_{e^-}} \right) \rho_{\text{air}} V_{\text{air}} (\%_{^{14}\text{N}})$$

$$\frac{A_{\text{sat}}^{13\text{N}}}{N_{e^-}} = 4.11 \times 10^{-13} \times 1.17 \times 10^8 \times 1.2 \times 10^{-3} \times 0.755 = 4.35 \times 10^{-8} \text{ Bq} \cdot (\text{e}^-)^{-1}$$

For 1 μA current intensity it arises:

$$A_{\text{sat}}^{13\text{N}} = \left(\frac{A_{\text{sat}}^{13\text{N}}}{N_{e^-}} \right) \frac{i}{e} = 4.3 \times 10^{-8} \times \frac{1 \times 10^{-6}}{1.6 \times 10^{-19}} = 2.72 \times 10^5 \text{ Bq}$$

The results for the other radionuclides are given in table 3.VI.5.

TAB. 3.VI.5 – Saturation activities for the radionuclides produced by photonuclear reactions in the air, per source electron for 1 μA electron beam.

Reaction	$\frac{A_{\text{sat}}}{N_{e^-}}$	$\frac{A_{\text{sat}}}{\mu} \text{ A}$
$^{12}\text{C}(\gamma,n)^{11}\text{C}$	6.54×10^{-14}	4.09×10^{-1}
$^{14}\text{N}(\gamma,n)^{13}\text{N}$	4.35×10^{-8}	2.72×10^5
$^{16}\text{O}(\gamma,n)^{15}\text{O}$	4.39×10^{-9}	2.74×10^4
$^{40}\text{Ar}(\gamma,p)^{39}\text{Cl}$	3.12×10^{-10}	1.95×10^3

For neutron activation, the results are printed with the following form (example given for the radionuclides with the form ZZAAA ranging from 18039 to 18043):

```

cell 20
user bin 1.80390E+04
           0.00000E+00 0.0000
cell 20
user bin 1.80400E+04
           0.00000E+00 0.0000
cell 20
user bin 1.80410E+04
           7.89893E-08 0.0716
cell 20
user bin 1.80420E+04
           0.00000E+00 0.0000
cell 20
user bin 1.80430E+04
           0.00000E+00 0.0000

```

Inside this list of radionuclides, the only non-zero value is related to the label 18041, *i.e.*, ^{41}Ar . This time, the result is given for the total air mass of cell 20, since it is obtained *via* the “ft res” instruction. For a $1\ \mu\text{A}$ current, it becomes:

$$A_{\text{sat}}^{41\text{Ar}} = \left(\frac{A_{\text{sat}}^{41\text{Ar}}}{N_{e^-}} \right) \frac{i}{e} = 7.9 \times 10^{-8} \times \frac{1 \times 10^{-6}}{1.6 \times 10^{-19}} = 4.94 \times 10^5 \text{ Bq}$$

^{14}C also has a saturation activity. It corresponds to $4 \times 10^{-5} \text{ Bq}$. (source electron) $^{-1}$, that is to say $2.5 \times 10^8 \text{ Bq} \cdot \mu\text{A}^{-1}$.

(d) Evolution of the air activity over time, without ventilation system

Let us recall that activity varies with irradiation, as a function of time like (see section 3.IV about ^{59}Co activation):

$$A(t_i) = A_{\text{sat}} [1 - \exp(-\lambda t_i)]$$

For a cooling time of t_d minutes after the electron beam interruption, the activity obeys an exponentially decreasing function:

$$A(t_i, t_d) = A(t_i) \exp(-\lambda t_d)$$

For instance, for a 4 h irradiation (240 min) and for the ^{14}N production, the exponential term of $A(t_i)$ tends towards 0. Thus, $A(t_i) = A_{\text{sat}}$ and the activity during the cooling time, per μA of beam, can be written as:

$$A^{13\text{N}}(240, t_d) = A_{\text{sat}}^{13\text{N}} \exp\left(-\left(\frac{\ln 2}{T_{1/2}}\right) t_d\right) = 2.72 \times 10^5 \exp(-6.93 \times 10^{-2} \times t_d)$$

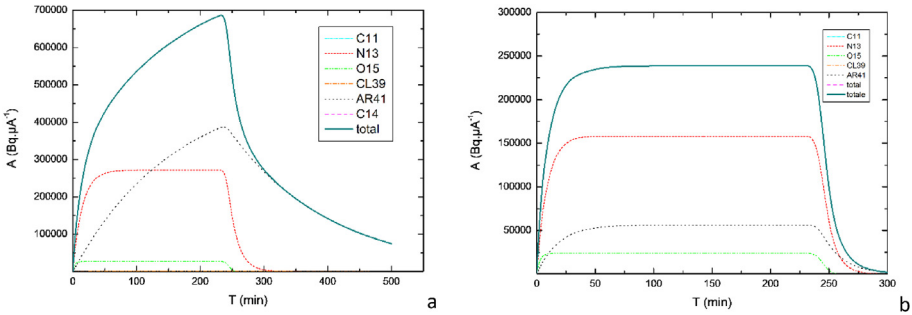


FIG. 3.VI.13 – Induced activities in the air over time for a 4 h irradiation (a) without ventilation system and (b) with ventilation system.

The activity profiles of radionuclides produced during the irradiation and cooling phases are shown in figure 3.VI.13a. During the irradiation phase, one can notice the ^{13}N activity saturation plateau starting around 50 min of irradiation, corresponding to roughly 5 half-lives of this radionuclide.

The activity profiles of figure 3.VI.13a are given for a confined facility. It is now proposed to study the impact of adding a ventilation system to the accelerator room.

(e) Evolution of the air activity over time, with ventilation

In the case of a ventilated accelerator room, the production of radionuclides, their disappearance through radioactive decay and the air change rate compete. The yield of radionuclide production in air through activation is covered by a differential equation of the same type as equation (1) of problem 3.IV, with the addition of a term taking into account the air change rate R inside the accelerator room:

$$dN(t) = N_c \sigma \dot{\Phi}(t) dt - \lambda N(t) dt - \sigma_t \dot{\Phi}(t) N(t) dt - R N(t) dt \quad (3)$$

The air change rate R is the ratio between the ventilation air flow rate of a containment enclosure and the volume of this containment enclosure. It is expressed as inverse of time units. It should be stated that the expression suggested above is reliable only if the intake flow is equal to the outtake flow, since it requires a constant number of air molecules in the volume. The solving of differential equation (3) leads to:

$$N(t_i) = \frac{N_c \dot{\Phi}}{\lambda + \sigma_t \dot{\Phi} + R} [1 - \exp(-(\lambda + \sigma_t \dot{\Phi} + R) t_i)]$$

By neglecting the transmutation of radionuclides *via* reactions and by replacing $N_c \sigma \dot{\Phi}$ by A_{sat} , the activity is then expressed by equation (4):

$$A(t_i) = \lambda N(t_i) = \frac{\lambda A_{\text{sat}}}{\lambda + R} [1 - \exp(-(\lambda + R) t_i)] \quad (4)$$

After a cooling time t_d , the activity can be written as:

$$A(t_i, t_d) = A(t_i) \exp(-(\lambda + R) t_d)$$

For the previous conditions, but with an air change rate of 3 h^{-1} , which corresponds to 0.05 min^{-1} , the ^{13}N activity shifts like:

$$A^{13\text{N}}(240, t_{\text{td}}) = \frac{\lambda A_{\text{sat}}^{13\text{N}}}{\lambda + R} \exp(-(\lambda + R) t_d) = 1.58 \times 10^5 \exp(-5.69 \times 10^{-2} t_{\text{td}}) \quad (5)$$

The activity evolution of radionuclides produced, with a ventilation system, is shown in figure 3.VI.13b. During the accelerator operation, we note that the air activity, with ventilation, reaches more quickly the saturation activity (plateau is exhibited in figure 3.VI.13b). Also, after the accelerator shutdown, the activity decreases faster with ventilation. This is linked to the $R + \lambda$ term of the exponential function, behaving like a “pseudo half-life” more rapidly inflecting the radioactive decay curve. We note that the saturation activity is different for both systems. Without ventilation, the saturation value is, indeed, $N_c \sigma \dot{\Phi}$, and with, it is $\lambda N_c \sigma \dot{\Phi} / (\lambda + R)$. This explains the difference in activity evolution during irradiation for ^{13}N and ^{41}Ar for systems with and without ventilation. After 4 h of irradiation and without ventilation, because of different half-lives (109 min for ^{41}Ar), the maximum activity of ^{13}N , which is not saturated, is larger than the saturation activity of ^{41}Ar . However, with ventilation system, both radionuclides quickly reach the saturation activity, but this time, the maximum activity is that of ^{13}N because of its lower half-life.

(e) Ambient equivalent dose due to the air activation

The effective dose received by a worker when entering the irradiation room right after the accelerator shutdown is calculated with the input file below. Here, only ^{13}N activity interests us, but the calculation can be extended to ^{41}Ar and ^{15}O . ^{13}N is an inert gas, thus it does not induce internal exposure though inhalation. Only external exposure due to its homogenous distribution in the irradiation room is assumed. This exposure is assessed through numerical simulation. Hereinafter, we propose to calculate the ambient dose equivalent rate received by a worker at the center of the irradiation room, modeled by a rectangular parallelepiped of dimensions $720 \text{ cm} \times 300 \text{ cm} \times 540 \text{ cm}$. This calculation is done using the point detector tally, *i.e.*, a type 5 tally, which evaluates the average fluence in each energy bin stated in the “de15” card. Each energy bin result is then weighted by the “fluence – ambient dose equivalent” conversion coefficient specified in the “df15” card. The sum over all energy bins yields the final ambient dose equivalent per source gamma.

```
cube calculation
c cell block
20 1 -1.2e-3 -20 $ air
40 0 20
```

```

20 RPP -360 360 -150 150 -270 270

imp:p 1 0
mode p
m1 6000 -0.000124 7000 -0.755268 8000 -0.231781 18000 -0.012827
sdef par=p pos 0 0 0 cel 20 erg .511 x=D1 y=d2 z=d3
Si1 -360 360
sp1 0 1
Si2 -150 150
sp2 0 1
Si3 -270 270
sp3 0 1
stop F15 1e-3
F15:p 0 0 0 .1
DE15 .01 .015 .02 .03 .04 .05 .06 .08 .1 .15 .2 .3 .4 .5 .6 &
.8 1 1.5 2 3 4 5 6 8 10
DF15 7.6 3.21 1.73 0.739 0.438 0.328 0.292 0.308 0.372 0.6 0.856 &
1.38 1.89 2.38 2.84 3.69 4.47 6.12 7.51 9.89 12 13.9 15.8 19.5 23.2

```

File 3.VI.6

The result for tally 15 is $H^*(10)/N_\gamma = 5.8 \times 10^{-6} \text{ pSv} \cdot (\gamma)^{-1}$. The decay of ^{13}N leads to the emission of two 511 keV photons. Thus, the ambient equivalent dose per hour per Becquerel is:

$$\begin{aligned} \left(\frac{\dot{H}^*(10)}{A} \right) &= 3.6 \times 10^{-9} \left(\frac{H^*(10)}{N_\gamma} \right) \Gamma_\gamma(^{13}\text{N}) = 3.6 \times 10^{-9} \times 5.8 \times 10^{-6} \times 2 \\ &= 4.2 \times 10^{-14} \text{ Sv} \cdot \text{h}^{-1} \cdot \text{Bq}^{-1} \end{aligned}$$

Let us calculate the ambient dose equivalent received by the worker for an intensity i and for the same irradiation time as before, that is to say a very larger time in comparison with the ^{13}N half-life. Expression (4) gives the activity per μA , so it is weighted by the intensity to get the activity during working conditions:

$$A(t_i, t_{\text{td}}) = \frac{A_{\text{sat}} i}{\lambda + R} \exp(-(\lambda + R) t_d)$$

The ambient equivalent dose rate at after given time of cooling is:

$$\dot{H}^*(10)_{\text{td}} = \left(\frac{\dot{H}^*(10)}{A} \right) A(t_i, t_{\text{td}}) = \left(\frac{\dot{H}^*(10)}{A} \right) \frac{\lambda A_{\text{sat}} i}{\lambda + R} \exp(-(\lambda + R) t_d)$$

For the case study the value of the term ahead of the exponential function is:

$$\left(\frac{\dot{H}^*(10)}{A} \right) \frac{\lambda A_{\text{sat}} i}{\lambda + R} = 4.2 \times 10^{-14} \times 1.58 \times 10^5 \times 0.1 = 6.7 \times 10^{-10} \text{ Sv} \cdot \text{h}^{-1}$$

When a worker enters the accelerator room right after the accelerator shut down, and stays there for a long period, the ambient dose equivalent received is:

$$H^*(10)_\infty = 6.7 \times 10^{-10} \int_0^\infty \exp(-(\lambda + R)t_d) dt_d = -\frac{6.7 \times 10^{-10}}{\lambda + R} [\exp(-(\lambda + R)t_d)]_0^\infty$$

$$\Leftrightarrow H^*(10)_\infty = \frac{6.7 \times 10^{-10}}{\lambda + R} = \frac{6.7 \times 10^{-10}}{\ln(2/10) + 0.05} = 5.6 \times 10^{-9} \text{ Sv}$$

To perform a more accurate assessment, the contributions from the structural elements of the facility, especially those composing the accelerator, for most of them made of steel, should be added to the overall assessment of delayed sources of exposure.

Part 5: Issue of the Ozone Production

In high dose rate facilities, nonradioactive toxic gases, of which the most toxic is ozone (O_3), can be produced by air radiolysis. The threshold limit value for ozone of 0.1 ppm ($0.2 \text{ mg} \cdot \text{m}^{-3}$) is commonly acknowledged in international standards. Furthermore, ozone is a powerful oxidizer causing a rapid corrosion of steel and copper elements. NCRP (2003) describes the buildup and destruction of ozone during irradiation using the following differential equation:

$$\frac{dN_o}{dt} = gI - \alpha N_o - \kappa I N_o - R N_o$$

where N_o is the number of ozone molecules per unit volume at time t (m^{-3}); I is the energy deposited in air per unit volume ($\text{eV} \cdot \text{m}^{-3} \cdot \text{s}^{-1}$); g is the number of ozone molecules formed per unit energy (eV^{-1}); α is the rate of decomposition of ozone molecules (s^{-1}); κ is the number of ozone molecules destroyed per unit energy and volume ($\text{eV}^{-1} \cdot \text{m}^{-1}$); R is the air change rate of the ventilation system (s^{-1}). Solving the differential equation enables the evolution of the number of ozone molecules as a function of time:

$$N_o(t_i) = \frac{gI}{\alpha + \kappa I + R} [1 - \exp(-(\alpha + \kappa I + R)t_i)]$$

NCRP (2003) provides usual values for g and α , which are respectively 0.074 eV^{-1} and $2.3 \times 10^{-4} \text{ s}^{-1}$. The low value of κ , about 1×10^{-16} , implies I to be commonly omitted. After irradiation time t_i , the amount of ozone molecules changes according to an exponential function depending only on the decomposition- and air change-rates:

$$N_o(t_i, t_r) = N_o(t_i) \exp(-(\alpha + R)t_d)$$

The last parameter needed is the energy deposited in air per unit volume I . In the case study, we assume that the energy deposit is only due to bremsstrahlung

photons. We can suppose, indeed, that the electron beam is fully contained in the vacuum tube of the accelerator, and consequently does not interact with the surrounding air. We propose, hereinafter, to calculate its value with MCNP, but it can be evaluated using data (see Antoni and Bourgois, 2017a). It is calculated with an F6 tally, corresponding to the energy deposit in $\text{MeV}\cdot\text{g}^{-1}$ per source electron (\bar{D}/N_e). The required input file is similar to that for the assessment of the air activation. Only tallies are different and photon neutrons are inhibited owing to their low energy deposit.

```

coefficient calculation for ozone
c cell block
10 2 -19.3 -10 $ tungsten target
20 1 -1.2e-3 -20 10 $ air
30 10 -2.35 -30 20 $ concrete
40 0 30

10 RCC 0 0 0 0 0 2 1
20 RPP -360 360 -150 150 -270 270
30 RPP -500 500 -250 259 -500 500

vol j 1.1664E8 j j
imp:p,e 1 1 1 0
mode p e
m1 6000 -0.000124 7000 -0.755268 8000 -0.231781 18000 -0.012827
m2 74182 -.3 74183 -.1 74184 -.3 74186 -.3
c standard concrete composition d=2.381
M10 14000 -20.68 13027 -.363 8016 -50.853 20000 -21.645 12000 -.198 &
19000 -.088 11023 -.0384 16000 -.139 6000 -4.52 22000 -.0155 15031 &
-.0208 25055 -.0192 1001 -.701 26054 -.0418 26056 -.6588 26057 &
-.0157 26058 -.0024 24052 -.00057
sdef par=e pos 0 0 1e-10 axs 0 0 1 ext 0 rad=d1 vec 0 0 1 dir 1 erg 20
Si1 0 1
spl -21 1
F6:p 20
stop F6 .005
cut:p,e j .1

```

File 3.VI.7

The result in the output file is:

```

tally 6
      nps      mean      error      vov      slope      fom
30496  1.9846E-07  0.0046  0.0001  10.0  49248

```

The calculated value is $(\bar{D}/N_{e^-}) = 2 \times 10^{-7} \text{MeV.g}^{-1} \cdot (\text{e}^-)^{-1}$. We can infer the energy deposited per unit volume using the below normalization:

$$I = 10^{12} \rho_{\text{air}} \left(\frac{\bar{D}}{N_{e^-}} \right) \frac{i}{e}$$

with the coefficient 10^{12} for the conversion from cm^3 to m^3 and from MeV to eV. For a beam current of $1 \mu\text{A}$, it becomes:

$$I = 10^{12} \times 1.3 \times 10^{-3} \times 2 \times 10^{-7} \frac{1 \times 10^{-6}}{1.602 \times 10^{-19}} = 1.6 \times 10^{15} \text{ eV.m}^{-3} \cdot \text{s}^{-1} \cdot \mu\text{A}^{-1}$$

The accelerator operates with a current intensity of 100 nA , so $I = 1.6 \times 10^{14} \text{ eV.m}^{-3} \cdot \text{s}^{-1}$. For a 4 h irradiation (*i.e.*, $1.44 \times 10^4 \text{ s}$) and an air change rate of 3 h^{-1} (*i.e.*, $8.33 \times 10^{-4} \text{ s}$), the number of ozone molecules after irradiation is:

$$\begin{aligned} N_o(4 \text{ h}) &= \frac{0.074 \times 2.2 \times 10^{14}}{(2.3 \times 10^{-4}) + (8.3 \times 10^{-4})} \\ &\quad \times [1 - \exp(-((2.3 \times 10^{-4}) + (8.3 \times 10^{-4})) \times 1.44 \times 10^4)] \\ &= 1.1 \cdot 10^{16} \text{ (mol).m}^{-3} \end{aligned}$$

As a result, the concentration of this toxic element is:

$$\begin{aligned} c_o(4 \text{ h}) &= \left(\frac{\eta_A}{\text{nA}} \right)^{-1} N_o(4 \text{ h}) = \frac{1.1 \cdot 10^{16}}{(6.02 \times 10^{23} / 3 \times 16)} \\ &= 8.8 \times 10^{-7} \text{ mg.m}^{-3} \quad (4.4 \times 10^{-7} \text{ ppm}) \end{aligned}$$

For these conditions, no countermeasure is needed (the limit is at 0.1 ppm). For accelerators with conversion targets, the ozone production is constraining in the case of an operating point with a current greater than 1 mA . However, when the electron beam interacts with the surrounding air, the ozone production problem exists in case of far lower intensities.

References

- Allineï P.G. (1992) Multisphere system neutron spectrometry applied to dosimetry for the personnel. Report CEA-R-5605.
- Allisy P.J., Kessler C., Burns D.T., Delaunay F., Leroy E. (2006) Comparison of the standards for air kerma of the LNE-LNHB and the BIPM for ^{60}Co gamma radiation. Bureau International des Poids et mesures.
- Antoni R., Bourgois L. (2013) *Physique appliquée à l'exposition externe: dosimétrie et radioprotection*. Springer, Paris.
- Antoni R., Bourgois L. (2017a) *Applied physics of external radiation exposure: dosimetry and radiation protection*. Springer International Publishing AG, Cham, Switzerland.
- Antoni R., Bourgois L. (2017b) Evaluation of the new electron-transport algorithm in MCNP6.1 for the simulation of dose point kernel in water, *Nucl. Inst. Methods Phys. Res. B* **412**, 102.
- Antoni R., Bourgois L. (2019) Microdosimetric spectra simulated with MCNP6.1 with INCL4/ABLA model for kerma and mean quality factor assessment, for neutrons between 100 keV to 19 MeV, *Radiat. Meas.* **128**, 106189.
- Antonio P.L., Carvalho V.S., Caldas L.V.E. (2012) Comparison of calibration results for an extrapolation chamber obtained with different ^{90}Sr + ^{90}Y secondary standard sources, *Appl. Radiat. Isot.* **70**, 388.
- Archer B.R., Thornby J.I., Bushong S.C. (1983) Diagnostic X-ray shielding design based on an empirical model of photon attenuation, *Health Phys.* **44**, 507.
- Attix F.H. (2007) *Introduction to radiological physics and radiation dosimetry*. Wiley VCH Verlag GmbH & Co. KGaA.
- Bame Jr. S.J., Haddad E., Perry Jr. J.E., Smith R.K. (1957) Absolute determination of monoenergetic neutron flux in the energy range 1 to 30 Mev, *Rev. Sci. Instrum.* **28**, 997.
- Behrens R. (2017) Conversion coefficients for $\text{H}'(3;\Omega)$ for photons, *J. Radiol. Prot.* **37**, 354.
- Ben Mosbah M. (2017) Spectrométrie des neutrons: étude de la réponse d'un ensemble de compteurs proportionnels. Thèse, Université Franche-Comté, 2007.
- Berger M.J. (1993) Penetration of proton beams through water I. Depth-dose distribution, spectra and LET distribution. Report NISTIR 5226, National Institute of standards and technology, Physics Laboratory, Gaithersburg, MD 20899.
- Boothe T.E. (1985) A sample problem for variance reduction in MCNP LANL, LA-10363-MS.
- Bortfeld T. (1997) An analytical approximation of the Bragg curve for therapeutic proton beams, *Med. Phys.* **24**, 2024.
- Bourgois L. (2011) Estimation de la dose extrémité due à une contamination par un radionucléide émetteur β^- : l'équivalent de dose est-il un bon estimateur de la grandeur de protection? *Radioprotection* **46**, 175.

- Bourgeois L., Ménard S. (2017) Évaluation par calcul Monte-Carlo des facteurs de diffusion en termes d'équivalent de dose, des rayonnements issus d'un générateur X, pour le calcul des équivalents de dose secondaires, Rapport CEA-R-6452 ISSN 0429 – 3460, DOI: [10.13140/RG.2.2.32475.05929](https://doi.org/10.13140/RG.2.2.32475.05929).
- Bourgeois L., Ménard S. (2018) Dose equivalent transmission data for shielding industrial X-ray facilities up to 800 kV, *J. Radiol. Prot.* **38**, 471.
- Brede H.J., Greif K.D., Hecker O., Heeg P., Heese J., Jones D.T., Kluge H., Schardt D. (2006) Absorbed dose to water determination with ionization chamber dosimetry and calorimetry in restricted neutron, photon, proton and heavy-ion radiation fields, *Phys. Med. Biol.* **51**, 3667.
- Briesmeister J.F. Ed. (2000) MCNPTM – A General Monte Carlo N-Particle Transport Code, Version 4C LA-13709-M.
- Cognet M.A., Gressier V. (2010) Development of a measurement reference standard for neutron energies between 1 MeV and 20 MeV using time of flight method at the AMANDE facility, *Metrologia* **47**, 377.
- Colin J.L. Ed. (2017) Listing of Available ACE Data Tables Formerly Appendix G of the MCNP Manual, Nuclear data team, XCP-5 LA-UR-17-20709.
- Cross W.G. (1997) Empirical expression for beta ray point source dose distributions, *Radiat. Prot. Dosim.* **69**, 85.
- Diethorn W. (1956) A methane proportional counter system for natural radiocarbon measurements. Thesis.
- Fawaz A. (2014) Design and Characterization of Next-Generation Tissue Equivalent Proportional Counters for Use in Low Energy Neutron Fields. Thesis, Faculty of Energy Systems and Nuclear Science, University of Ontario, Institute of Technology.
- Frujinoiu C. (2001) Reconsideration of the backscatter components in the intermediate cavity theory for photon beams, *Phys. Med. Biol.* **46**, 1205.
- Gagnebin S., Twerenbold D., Pedroni E., Meer D., Zenklusen S., Bula C. (2010) Experimental determination of the absorbed dose to water in a scanned proton beam using a water calorimeter and an ionization chamber, *Nucl. Instrum. Methods Phys. Res. B* **268**, 524.
- Gammel J.L. (1973) Fast neutron physics, Part II (J.B. Marion, J.L. Fowler, Eds).
- Haider J.A., Skarsgard L.D., Lam G.K.Y. (1997) A general cavity theory, *Phys. Med. Biol.* **42**, 491.
- Horowitz Y.S., Moscovitch M., Dubi A. (1983) Modified general cavity theory applied to the calculation of gamma dose in ⁶⁰Co thermoluminescence dosimetry, *Phys. Med. Biol.* **28**, 829.
- IAEA (2000a) Handbook on photonuclear data applications: cross sections and spectra IAEA, Vienna, 2000 IAEA-TECDOC-1178 ISSN 1011-4289. https://www-pub.iaea.org/mtcd/publications/pdf/te_1178_prn.pdf.
- IAEA (2000b) Absorbed dose determination in external beam radiotherapy, an international code of practice for dosimetry based on standards of absorbed dose to water. Technical Reports Series n° 398.
- IAEA (2001) Technical reports series n° 403 compendium of neutron spectra and detector responses for radiation protection purposes. Supplement to technical reports series n° 318.
- ICRP (1996) Conversion coefficients for use in radiological protection against external radiation. ICRP Publication 74.
- ICRP (2007) The 2007 recommendations of the international commission on radiological protection. ICRP Publication 103. Ann. ICRP 37 (2–4).
- ICRP (2010) Conversion coefficients for radiological protection quantities for external radiation exposures. ICRP Publication 116. Ann. ICRP 40 (2–5).
- ICRU (1983) Report 36, Microdosimetry. Bethesda, MD.
- ICRU (1986) Report 40, The quality factor in radiation protection. ICRU, Bethesda, MD.

- ICRU (1993) Report 49, Stopping powers and ranges for protons and alpha particles. Bethesda, MD.
- ICRU (1998a) Report 57, Conversion coefficients for use in radiological protection against external radiation. Bethesda, MD.
- ICRU (1998b) Clinical proton dosimetry, Part I: Beam production, beam delivery and measurement of absorbed dose. ICRU Report 59. Bethesda, MD.
- ICRU (2000) Report 63, Nuclear data for neutron and proton radiotherapy and for radiation protection. Bethesda.
- IEC 1525 ED. 1 (1997) Radiation protection instrumentation – X, gamma, high energy beta and neutron radiations – direct reading personal dose equivalent and/or dose equivalent rate monitors.
- ISO 8529-2 (2000) Reference neutron radiations – Part 2: Calibration fundamentals of radiation protection devices related to the basic quantities characterizing the radiation field.
- ISO 6980 (2006) Rayonnement bêta de référence.
- Katz L., Penfold A.S. (1952) Range energy relations for electrons and the determination on beta-ray end point energies by absorption, *Rev. Mod. Phys.* **24**, 28.
- Kim S.I., Kim B.H., Kim J.L., Lee J.I. (2015) A review of neutron scattering correction for the calibration of neutron survey meters using the shadow cone method, *Nucl. Eng. Technol.* **47**, 939.
- Knoll G.F. (1989) *Radiation detection and measurement*, 2nd edn. John Wiley & Sons.
- Lacoste V., Taylor G., Rottger S. (2011) Simulated workplace neutron fields, *Metrologia* **48**, S304.
- Lecante C., Bordy J.M. (2006) National standards of LNE-LNHB for dosimetry of beta particles in radiation protection CEA/LIST.
- Lee M., Nahum A.E., Webb S. (1993) An empirical method to build up a model of proton dose distribution for a radiotherapy treatment planning package, *Phys. Med. Biol.* **38**, 989.
- Leuthold G., Mares V., Schaube H. (1992) Calculation of the neutron ambient dose equivalent on the basis of the ICRP revised quality factor, *Radiat. Prot. Dosim.* **40**, 77.
- Loevinger R., Japha E.M., Brownwell G. (1956) L. Discrete radioisotope sources, *Radiation dosimetry* (G.J. Hine, G.L.L. Brownell, Eds). Academic Press, pp. 693–799.
- Lynch G.R., Dahl O.I. (1991) Approximations to multiple Coulomb scattering, *Nucl. Instrum. Methods Phys. Res. Sect. B: Beam Interact. Mater.* **58**, 6.
- Mares V., Schraube G., Schraube H. (1991) Calculated neutron response of a Bonner sphere spectrometer with ^3He counter, *Nucl. Instrum. Methods Phys. Res. A* **307**, 398.
- Matzke M. (2002) Propagation of uncertainties in unfolding procedures, *Nucl. Instrum. Methods Phys. Res. A* **476**, 230.
- McConn Jr. R.J., Gesh C.J., Pagh R.T., Rucker R.A., Williams III R.G. (2011) Compendium of material composition data for radiation transport modeling. PNNL-15870 Rev. 1.
- Menzel H.G., Buhler G., Schuhmacher H., Muth H., Dietze G., Guldbakke S. (1984) Ionisation distributions and A-150 plastic kerma for neutrons between 13.9 and 19.0 MeV measured with a low pressure proportional counter, *Phys. Med. Biol.* **29**, 1537.
- NCRP (1976) Report 49, National council on radiation protection and measurements structural shielding design and evaluation for medical use of X-rays and gamma-rays up to 10 MeV.
- NCRP (1977) Report 51, Radiation protection design guidelines for 0.1-100 MeV particle accelerator facilities.
- NCRP (2003) Radiation protection for particle accelerator facilities. NCRP Report 144.
- NCRP (2005) Structural shielding design for medical X-ray imaging facilities. NCRP Report 147.
- Numomiya T., Kim E., Kurosaw T., Taniguchi S., Nakamura T., Nakane Y., Sakamoto Y., Tanaka S. (2002) Measurement of lineal-energy distributions for neutrons of 8 keV to 65 MeV by using a tissue-equivalent proportional counter, *Radiat. Prot. Dosim.* **102**, 49.

- Ogheard F. (2012) Développement d'un système de mesure directe du débit d'émission de sources neutroniques. Université Paris Sud - Paris XI.
- Ogunleye O.T., Attix F.H., Paliwal B.R. (1980) Comparison of Burlin cavity theory with LiF TLD measurements for cobalt-60 gamma rays, *Phys. Med. Biol.* **25**, 203.
- Paliwal B.R., Almond P.R. (1976) Electron attenuation characteristics of LiF, *Health Phys.* **31**, 151.
- Pelowitz D.B. (Ed.) (2013) MCNP6 User's Manual Version 1.0 Manual Rev. 0 Editor: LA-CP-13-00634, Rev. 0.
- RADAR – The Radiation Dose Assessment Resource. <http://www.doseinfo-radar.com/>.
- Ravazzani A., Foglio A., Para R., Jaime M., Looman M., Marín Ferrer P., Peerani P., Schillebeeckx P. (2006) Characterisation of ^3He proportional counters, *Radiat. Meas.* **41**, 582.
- Ritts J.J., Solomito M., Stevens P.N. (1969) Calculation of neutron fluence-to-kerma factors for the human body, *Nucl. App. Technol.* **7**, 89.
- Rogers D.W.O., Bielajew A.F., Nahum A.E. (1985) Ion chamber response and Awall correction factors in a ^{60}Co beam by Monte Carlo simulation, *Phys. Med. Biol.* **30**, 429.
- Ross K., Klassen N.V. (1996) Water calorimetry for radiation dosimetry, *Phys. Med. Biol.* **41**, 1.
- Simpkin D.J., Dixon R.L. (1998) Secondary shielding barriers for diagnostic X-ray facilities: scatter and leakage revisited, *Health Phys.* **74**, 350.
- Stewart J.E. (1991) Principles of Total Neutron Counting, in Passive Nondestructive Assay of Nuclear Materials (PANDA). Nuclear Regulatory Commission NRCFIN- A7241, pp. 407–434.
- Thomas D.J., Burke M. (1985) W value measurement for ^{241}Am alpha particles in various gases, *Phys. Med. Biol.* **30**, 1215.
- Vatnitskya S. *et al.* (1999) Proton dosimetry intercomparison based on the ICRU report 59 protocol, *Radiother. Oncol.* **51**, 273.
- Vynckier S., Bonnett D.E., Jones D.T.L. (1991) Code of practice for clinical proton dosimetry, *Radiother. Oncol.* **20**, 53.
- Vynckier S., Bonnett D.E., Jones D.T.L. (1994) Supplement to the code of practice for clinical proton dosimetry, *Radiother. Oncol.* **32**, 174.
- Wattenberg A. (1947) Photo-neutron sources and the energy of the photo-neutrons, *Phys. Rev.* **71**, 497.